Development of Numerical Models to Advance the Understanding of Air Quality in Los Angeles

Thesis by

Elyse A. Pennington

In Partial Fulfillment of the Requirements for

the Degree of

Doctor of Philosophy

CALIFORNIA INSTITUTE OF TECHNOLOGY

Pasadena, California

2023

(Defended August 30, 2022)

Elyse A. Pennington
ORCID: 0000-0003-1736-2342

ACKNOWLEDGEMENTS

There are so many people I want to thank for their support during my PhD program. First and foremost, thank you to my advisor John H. Seinfeld, who has consistently had a positive influence on my research, coursework, and career goals. When I arrived at Caltech, I told John that I was interested in science policy, so he told me about modeling work because the science is applied and he knew that was in line with my interests. He has always advocated for my success by supporting endeavors like my minor in Environmental Science and Engineering, interning at the EPA, and reminding me not to worry about logistical aspects of my graduate experience and to just focus on the science. Second, I'd like to thank Yuan Wang. Yuan is incredibly smart and encouraging and significantly accelerated my PhD progress for the past two–three years. He has given me invaluable guidance ranging from important scientific questions to helping me debug my code. I'm very excited for his next role at Purdue and believe he will make a fantastic professor. Rick Flagan is another mentor who has been a major advocate for my interest in science policy. He was one of the first people to introduce me to CCST and we've had many conversations about the role of scientists in government, science communication tactics, and women in STEM. He also encouraged my use of Python, my favorite language. I'd also like to thank Paul Wennberg for always keeping an eye out for me (and all students) and reaching out to include me in his group meetings even though I'm not in his lab. I TA'ed with Paul twice and those experiences helped refresh my atmospheric chemistry knowledge, think pedagogically, and get to know Paul and other students better. Thank you to Mitchio Okumura for serving on my candidacy committee. Lastly, I'm grateful to all of the professors in the ChE and ESE departments who have taught my courses and/or engaged in interesting conversation.

I have had many mentors over the years who have guided me to where I am now. Lelia Hawkins was my advisor for my undergrad research, where I was first introduced to the world of atmospheric aerosols. Lelia is an incredible mentor who not only taught me about lab equipment and proper lab functions, but also exposed me to my first international travel experience in Paris. She was, and still is, very encouraging of my research and career, and cares deeply about the role of scientists in government and advocacy. My internship at EPA

dramatically impacted the trajectory of my PhD and I would not be here without the support of my team there. Havala Pye is one of the smartest people I've ever met and gave me a lot of great scientific advice and was always available to answer questions. Karl Seltzer was very generous with his time and knowledge, and had a lot of patience helping me navigate both scientific and logistical questions. Ben Murphy was one of the first people at EPA to help me run CMAQ and always had an encouragement to give. I'm grateful to Robert O. Green at JPL for hiring me as a summer intern, where I saw so many amazing satellites, rovers, and other inventions. My mentor David Thompson taught me so much about Python and supercomputing, which ultimately spurred my future research. My mentor Morgan Cable was helpful in navigating my internship and was so encouraging of my interests and future. I'd also like to thank all of the staff at the Caltech Y for providing a venue where I could engage with my interest in science policy through SASS, the Geneva trip, the Washington DC trip, and Friends dinners. In particular, Greg Fletcher has included me on many committees and been instrumental in organizing the many events at the Y. Other members of the Caltech Y staff, including Athena Castro and Agnes Tong, have provided immense support of these activities and always been a positive aspect of life at Caltech. I'd also like to thank all of the professors in the chemistry department at Harvey Mudd, who taught me a lot of chemistry, encouraged pursuing grad school, and always had a positive attitude with students.

I want to give a special thank you to the staff in ChE and ESE who make everything run smoothly. Allison Kinard handles so many tasks, knows the answers to any and all questions, and is also a lot of fun to talk to. Martha Hepworth helps keep the Seinfeld lab running and is so helpful with editing proposals, keeping track of money, and always being available to students. Nora Oshima takes care of everything in Linde and has such a kind, comforting attitude.

The members of the Seinfeld lab have been invaluably helpful, become my close friends, and made my grad school experience unforgettable. Brigitte was the first person to help me with CMAQ, and patiently helped as I struggled to install and debug it. Getting CMAQ to run

would've taken much longer if it had not been for her documentation and encouragement. Chris has been fun getting to know outside of the lab and I appreciate how often he would plan fun events, and also helped navigate the CCE and GPS divisions and defense requirements. Stephanie is a very fun person and we relate over many things, including attending Harvey Mudd, being in the ChE program, being in John's lab, having interest in science policy, and both working in the state government. I'm excited to live near her in Sacramento. Yuanlong is very talented at every single thing in the lab. He always offers to lend a hand and expects nothing in return because he is so generous. Sophia became a lifelong friend early on in grad school, and provided more support than anyone in terms of navigating ChE courses, lab culture, and Caltech culture. Reina has also become a lifelong friend and I really like that we can talk about both research and our personal lives. Ben is skilled at lab work, field work, and modeling work so he is always busy, but he always makes time to answer my questions about the instruments and LA air quality and does it with a positive attitude. Ryan is a good friend who is very driven, smart, and organized, but also one of the most fun and outgoing people I've ever met. Kat and Haroula are newer to the lab, but I've enjoyed getting to know them and their fun outlooks. Kelvin graduated before I arrived, but I've enjoyed seeing him at conferences where we've explored new cities together.

I'd like to thank multiple funding sources, including Samsung, ORISE, and the Rose Hills Foundation.

Grad school would not have been the same without the constant support and fun times with many friends. This includes, but is not limited to, Han, Zsofi, Megan, Ariana, Nate, Zach, Elizabeth, Ollie, Aishvarya, Vai, Lakshay, Paul, Hannah, Paulene, my ChE cohort, and the rest of the Wennberg lab and Linde Lab. My church, Reality LA, has been a very positive and enlightening part of my life.

Lastly, and most importantly, I'm incredibly grateful for my family. My mom and dad emphasized the importance of education since an early age, and supported my dedication to working so hard in school. My sisters, Margo and Blair, were my first friends ever and have

shaped me into who I am today. My grandpa, Bobby, first introduced me to Caltech through the Athenaeum, where I first decided I wanted to come to school here. My grandma was my second biggest supporter and was one of the most loving and generous people I've ever met. My biggest supporter is my mom, who is the most important person in my life. She has shaped so much of who I am and stuck up for me at every turn, and I would not be at this point in my life had it not been for her.

ABSTRACT

Atmospheric pollutants such as particulate matter (PM) and ozone (O_3) are harmful to human health and intensify climate change. Secondary organic aerosol (SOA) is a main component of PM and is formed via atmospheric oxidation reactions of thousands of gas- and aerosol-phase precursors. Regional-scale chemical transport models predict the formation of these pollutants by representing natural and human emissions of hundreds of species and their subsequent chemical and physical processing in the atmosphere. These models are useful in the absence of detailed measurements and allow researchers to investigate the impact of changing emissions and weather. Los Angeles has unique meteorology and anthropogenic emissions which lead to dangerous pollution events and make this region an important area to study SOA, PM, and O_3 formation. As vehicles have become cleaner and their emissions have declined, other sources of emissions have become increasingly important. One important category of emissions is volatile chemical products (VCPs), which are consumer and industrial products that have high volatile organic compound (VOC) emissions that have not been well-constrained or studied in relation to their SOA and O_3 formation potential. In this dissertation, I use the Community Multiscale Air Quality (CMAQ) model to represent the air quality of the Los Angeles Basin. First, a new chemical mechanism is developed to represent the formation of SOA from VCPs, implemented in the CMAQ model to simulate 2010 California, and the impact of VCPs on atmospheric pollutants is quantified. Next, we created contemporary inputs to CMAQ by simulating the meteorology, emissions, and land surface of the Los Angeles Basin in 2020. Lastly, the new inputs and chemistry are applied to CMAQ to understand current air quality issues in Los Angeles. We quantify the impact of VCPs on SOA, PM, O_3, and other pollutants in both 2010 and 2020. The apportionment of other emission sources and the impact of the COVID-19 pandemic are investigated, and pollutant concentrations are compared to measurements made throughout the Basin and specifically in Pasadena. This works demonstrates the importance of intentional policies to mitigate harmful air pollution events. Limiting NO_x emissions is not sufficient to limit the formation of ozone and PM, and there must be a simultaneous reduction of VOC emissions.

PUBLISHED CONTENT AND CONTRIBUTIONS

Pennington, E. A., Seltzer, K. M., Murphy, B. N., Qin, M., Seinfeld, J. H., & Pye, H. O. T. (2021). Modeling secondary organic aerosol formation from volatile chemical products. *Atmospheric Chemistry and Physics*, *21*(24), 18247–18261. https://doi.org/10.5194/acp-21-18247-2021.

EAP led model development, analyzed the data, and wrote the manuscript.

Pennington, E. A. (2020). *CMAQ Tutorial: Modifying a Chemical Mechanism in CMAQ*. Environmental Protection Agency. https://github.com/USEPA/CMAQ/blob/main/DOCS/Users_Guide/Tutorials/CMAQ_UG_tutorial_chemicalmechanism.md.

EAP wrote the tutorial.

Seltzer, K. M., Murphy, B. N., Pennington, E. A., Allen, C., Talgo, K., & Pye, H. O. T. (2021). Volatile Chemical Product Enhancements to Criteria Pollutants in the United States. *Environmental Science & Technology*. https://doi.org/10.1021/acs.est.1c04298.

EAP developed the VCP model and edited the manuscript.

Seltzer, K. M., Pennington, E., Rao, V., Murphy, B. N., Strum, M., Isaacs, K. K., & Pye, H. O. T. (2021). Reactive organic carbon emissions from volatile chemical products. *Atmospheric Chemistry and Physics*, *21*(6), 5079–5100. https://doi.org/10.5194/acp-21-5079-2021.

EAP calculated the impact of all VCPs on secondary organic aerosol (SOA) yields and edited the manuscript.

Yang, J., Wen, Y., Wang, Y., Zhang, S., Pinto, J. P., Pennington, E. A., Wang, Z., Wu, Y., Sander, S. P., Jiang, J. H., Hao, J., Yung, Y. L., & Seinfeld, J. H. (2021). From COVID-19 to future electrification: Assessing traffic impacts on air quality by a machine-learning model. *Proceedings of the National Academy of Sciences*, *118*(26). https://doi.org/10.1073/pnas.2102705118.

EAP participated in research discussions.

TABLE OF CONTENTS

LIST OF FIGURES

LIST OF TABLES

Chapter 1

INTRODUCTION

1.1 Motivation and Background

Poor air quality affects billions of people across the globe. Air quality describes the composition of the atmosphere, and we can understand the causes and effects of poor air quality events by investigating thousands of pollutants which interact via chemical and physical processes in the atmosphere. Some of these pollutants are gases — e.g., ozone (O_3), nitrogen oxides (NO_x), and volatile organic compounds (VOCs) — while others are particles — e.g., fine particulate matter ($PM_{2.5}$) and coarse particulate matter (PM_{10}). Particles are in the aerosol phase, meaning they are liquids or solids suspended stably in the air; this is colloquially known as smog. Particulate matter (PM) is particularly harmful, as it damages human health (Lim et al., 2012), reduces visibility (Hyslop, 2009), and influences the climate and global warming (Intergovernmental Panel on Climate Change, 2014). Gas-phase species also have harmful effects. Ozone is harmful to human health (Nuvolone et al., 2018) and restricts plant growth (Leisner & Ainsworth, 2012). Nitrogen oxides (NO_x = NO + NO_2) and VOCs react to form ozone and large organic species that react to form PM. It is critical that we understand the processes impacting these pollutants so that we can make educated decisions which reduce poor air quality events and their harmful effects.

Los Angeles (LA) is one of the most polluted cities in the United States, but the PM pollution in LA has been improving. Historically, vehicles were the main source of anthropogenic — or human-induced — emissions in LA. However, as catalytic converter technology advances and electric vehicles become more available, vehicles have become less important polluters (Khare & Gentner, 2018). Other sources of emissions, however, have not been reduced as quickly. One important emission

source is volatile chemical products (VCPs), a class of industrial and consumer products that emit reactive organic carbon (ROC), including VOCs and species with lower volatilities known as semivolatile organic compounds (SVOCs) and intermediate volatility organic compounds (IVOCs). Other important sources of anthropogenic emissions include off-road vehicles, oil and gas production, asphalt, agriculture, cooking, and road dust (Qin et al., 2021; Khare et al., 2020; McDonald et al., 2018; CARB, 2020).

As the sources and composition of anthropogenic emissions have evolved, so has the composition and chemistry of the atmosphere. As stated above, NO_x and VOCs react to form ozone and other oxidation products, typically large, oxidized organic species. As species become larger and more oxidized, their volatility decreases and they can condense to form secondary organic aerosol (SOA). SOA is a major component of total organic aerosol (OA; Jimenez et al., 2009) and total $PM_{2.5}$ (Zhang et al., 2007). As the composition of gas-phase precursor emissions evolves, so does the composition and chemical formation pathways of SOA. In addition, NO_x levels impact the formation of ozone, SOA, and other components of $PM_{2.5}$ by impacting atmospheric oxidizing capacity, for example, the concentration of the hydroxyl radical (OH; Seinfeld & Pandis, 2016). LA and many other urban areas have traditionally been considered "NO_x-saturated", meaning that there are high concentrations of NO_x, so reactions are more limited by VOC concentrations. But as NO_x emissions decline, LA has potentially begun to enter a NO_x-insensitive or even NO_x-limited regime (Laughner & Cohen, 2019). The NO_x regime has a large impact on the rate of pollutant formation. It is important to understand this so that informed policies can be developed to limit the occurrence of harmful air pollution events.

Regional-scale air quality modeling is used to understand the processes that are important in the formation and evolution of atmospheric pollutants. Chemical transport models (CTMs) represent the emissions, chemistry, and transport of hundreds or thousands of pollutants in a three-dimensional (3D) grid. Gridded

emissions from multiple sources and boundary conditions define the species that are introduced to the modeling system, while meteorological inputs define the transport occurring inside and between each grid cell. CTMs also typically represent processes such as bi-directional land-surface fluxes, lightning NO emissions, and deposition rates. Internal to the CTM is the chemical mechanism, describing photochemical, gas-phase, aerosol-phase, aqueous, and heterogeneous reactions. As stated above, there are thousands of species in the atmosphere undergoing complex chemical reactions, but it is computationally impossible to represent all of those processes. So, models must condense the chemistry by modeling "surrogate species" that can represent an entire class of compounds with similar properties, and which undergo simplified chemical reactions. The Community Multiscale Air Quality (CMAQ) model is the US Environmental Protection Agency's (EPA) 3D CTM that is widely used in the air quality modeling community and is used to inform regulatory standards (US EPA, 2020). The CMAQ model is used in our work.

Predicting air quality events using CTMs is difficult and many parts of the models can be improved. Due to the complexity of atmospheric chemistry, there is inherent difficulty in developing a simplified model that best represents the chemistry. Many models exist to represent gas-phase and heterogeneous chemistry (e.g., Carter, 2010; Yarwood et al., 2010; Goliff et al., 2013), and others are being developed (e.g., Keller & Evans, 2019). It is also difficult to model SOA chemistry because it is both nonlinear and not well-understood. Traditionally, researchers have modeled SOA formation from VOC oxidation (e.g., Odum et al., 1996; Carlton et al., 2010). It has become an active area of research to investigate the oxidation of SVOCs and IVOCs, which likely yield higher SOA than VOCs due to their lower volatility (e.g., Donahue et al., 2011; Murphy et al., 2017). It is well-documented that SOA tends to be underpredicted in CMAQ (Murphy et al., 2017; Appel et al., 2021). The modeled emissions impact predicted concentrations, but often have nonnegligible uncertainty (Qin et al., 2021). In addition to these modeling challenges, there are inherent difficulties when modeling a complex system. For example, the chemistry leading to

pollutant formation is highly nonlinear (Seinfeld & Pandis, 2016). The chemistry becomes even more complicated when considered in areas with different meteorology. Also, there is a lack of detailed measurement data that can be used to constrain model parameters. While pollutants like ozone, $PM_{2.5}$, and NO_2 are regularly monitored throughout the United States (US EPA, 2013), these sites are widely distributed and often there are only 0-1 sites in a given area. Measurements of radical species and specific VOCs are only obtained during field campaigns, which are limited to a small region and are very expensive to carry out. Even though the lack of in situ data makes it difficult to parameterize or evaluate models, it also underscores the importance of models. Models fill in the gaps in our understanding and allow us to make predictions about important air quality issues.

The goal of my dissertation work is to improve our understanding of atmospheric pollution using regional-scale modeling.

1.2 Organization of Thesis

Chapter 2 presents the work completed during my internship at the US EPA Office of Research and Development (ORD) and the following year upon my return to Caltech. I worked with the Atmospheric Chemistry and Aerosol Branch, which develops CMAQ. Specifically, I investigated the mechanism of SOA formation from VCPs, developed a condensed mechanism to represent this chemistry, and implemented the new model in CMAQ. This work was published in 2021 (Pennington et al., 2021).

Chapter 3 presents the methods employed to develop a model framework to represent all aspects of Los Angeles air quality in 2020. Many modeling studies have not developed complete meteorological simulations and emissions inventories to represent contemporary scenarios, so this work fills in an important gap in the literature. We explain models and their configurations used to develop the

meteorology, natural emissions, anthropogenic emissions, and boundary conditions that are used as input to CMAQ.

Chapter 4 presents the results of applying our modeling framework from Chapter 3 to predict air quality in Los Angeles in 2020. We investigate the impact of meteorology on pollutant transformation, the relative contribution of detailed emission sources, the impact of COVID-19 restrictions, and compare the predictions to measurements made throughout the Basin and in Pasadena. The work in chapters 3–4 is being drafted for publication.

Appendix A links to a page of the CMAQ documentation that I wrote. The documentation comprises a tutorial that teaches CMAQ users how to modify the chemical mechanism in CMAQ, with code examples. It also explains how to reflect these changes in Github. This tutorial was screened by the CMAQ team and made publicly available on their Github documentation site.

Appendices B–F each present a published, submitted, or drafted paper that I am an author on, excluding my first author works which are described in Chapters 2–4.

1.3 References

Appel, K. W., Bash, J. O., Fahey, K. M., Foley, K. M., Gilliam, R. C., Hogrefe, C., Hutzell, W. T., Kang, D., Mathur, R., Murphy, B. N., Napelenok, S. L., Nolte, C. G., Pleim, J. E., Pouliot, G. A., Pye, H. O. T., Ran, L., Roselle, S. J., Sarwar, G., Schwede, D. B., … Wong, D. C. (2021). The Community Multiscale Air Quality (CMAQ) model versions 5.3 and 5.3.1: System updates and evaluation. *Geoscientific Model Development*, *14*(5), 2867–2897. https://doi.org/10.5194/gmd-14-2867-2021

CARB. (2020). *Criteria Pollutant Emission Inventory Data | California Air Resources Board*. https://ww2.arb.ca.gov/criteria-pollutant-emission-inventory-data

Carlton, A. G., Bhave, P. V., Napelenok, S. L., Edney, E. O., Sarwar, G., Pinder, R. W., Pouliot, G. A., & Houyoux, M. (2010). Model Representation of Secondary Organic Aerosol in CMAQv4.7. *Environmental Science & Technology*, *44*(22), 8553–8560. https://doi.org/10.1021/es100636q

Carter, W. P. L. (2010). Development of the SAPRC-07 chemical mechanism. *Atmospheric Environment*, *44*(40), 5324–5335. https://doi.org/10.1016/j.atmosenv.2010.01.026

Donahue, N. M., Epstein, S. A., Pandis, S. N., & Robinson, A. L. (2011). A two-dimensional volatility basis set: 1. organic-aerosol mixing thermodynamics. *Atmospheric Chemistry and Physics*, *11*(7), 3303–3318. https://doi.org/10.5194/acp-11-3303-2011

Goliff, W. S., Stockwell, W. R., & Lawson, C. V. (2013). The regional atmospheric chemistry mechanism, version 2. *Atmospheric Environment*, *68*, 174–185. https://doi.org/10.1016/j.atmosenv.2012.11.038

Hyslop, N. P. (2009). Impaired visibility: The air pollution people see. *Atmospheric Environment*, *43*(1), 182–195. https://doi.org/10.1016/j.atmosenv.2008.09.067

Intergovernmental Panel on Climate Change (Ed.). (2014). Anthropogenic and Natural Radiative Forcing. In *Climate Change 2013 – The Physical Science Basis: Working Group I Contribution to the Fifth Assessment Report of the Intergovernmental Panel on Climate Change* (pp. 659–740). Cambridge University Press. https://doi.org/10.1017/CBO9781107415324.018

Jimenez, J. L., Canagaratna, M. R., Donahue, N. M., Prevot, A. S. H., Zhang, Q., Kroll, J. H., DeCarlo, P. F., Allan, J. D., Coe, H., Ng, N. L., Aiken, A. C., Docherty, K. S., Ulbrich, I. M., Grieshop, A. P., Robinson, A. L., Duplissy, J., Smith, J. D., Wilson, K. R., Lanz, V. A., … Worsnop, D. R. (2009). Evolution of Organic Aerosols in the Atmosphere. *Science*, *326*(5959), 1525–1529. https://doi.org/10.1126/science.1180353

Keller, C. A., & Evans, M. J. (2019). Application of random forest regression to the calculation of gas-phase chemistry within the GEOS-Chem chemistry model v10. *Geoscientific Model Development Discussions*, 1209–1225.

Khare, P., & Gentner, D. R. (2018). Considering the future of anthropogenic gas-phase organic compound emissions and the increasing influence of non-combustion sources on urban air quality. *Atmospheric Chemistry and Physics*, *18*(8), 5391–5413. https://doi.org/10.5194/acp-18-5391-2018

Khare, P., Machesky, J., Soto, R., He, M., Presto, A. A., & Gentner, D. R. (2020). Asphalt-related emissions are a major missing nontraditional source of secondary organic aerosol precursors. *Science Advances*, *6*(36), eabb9785. https://doi.org/10.1126/sciadv.abb9785

Laughner, J. L., & Cohen, R. C. (2019). Direct observation of changing NOx lifetime in North American cities. *Science*, *366*(6466), 723–727. https://doi.org/10.1126/science.aax6832

Leisner, C. P., & Ainsworth, E. A. (2012). Quantifying the effects of ozone on plant reproductive growth and development. *Global Change Biology*, *18*(2), 606–616. https://doi.org/10.1111/j.1365-2486.2011.02535.x

Lim, S. S., Vos, T., Flaxman, A. D., Danaei, G., Shibuya, K., Adair-Rohani, H., AlMazroa, M. A., Amann, M., Anderson, H. R., Andrews, K. G., Aryee, M., Atkinson, C., Bacchus, L. J., Bahalim, A. N., Balakrishnan, K., Balmes, J., Barker-Collo, S., Baxter, A., Bell, M. L., … Ezzati, M. (2012). A comparative risk assessment of burden of disease and injury attributable to 67 risk factors and risk factor clusters in 21 regions, 1990–2010: A systematic analysis for the Global Burden of Disease Study 2010. *The Lancet*, *380*(9859), 2224–2260. https://doi.org/10.1016/S0140-6736(12)61766-8

McDonald, B. C., Gouw, J. A. de, Gilman, J. B., Jathar, S. H., Akherati, A., Cappa, C. D., Jimenez, J. L., Lee-Taylor, J., Hayes, P. L., McKeen, S. A., Cui, Y. Y., Kim, S.-W., Gentner, D. R., Isaacman-VanWertz, G., Goldstein, A. H., Harley, R. A., Frost, G. J., Roberts, J. M., Ryerson, T. B., & Trainer, M. (2018). Volatile chemical products emerging as largest petrochemical source of urban organic emissions. *Science*, *359*(6377), 760–764. https://doi.org/10.1126/science.aaq0524

Murphy, B. N., Woody, M. C., Jimenez, J. L., Carlton, A. M. G., Hayes, P. L., Liu, S., Ng, N. L., Russell, L. M., Setyan, A., Xu, L., Young, J., Zaveri, R. A., Zhang, Q., & Pye, H. O. T. (2017). Semivolatile POA and parameterized total combustion SOA in CMAQv5.2: Impacts on source strength and partitioning. *Atmospheric Chemistry and Physics*, *17*(18), 11107–11133. https://doi.org/10.5194/acp-17-11107-2017

Nuvolone, D., Petri, D., & Voller, F. (2018). The effects of ozone on human health. *Environmental Science and Pollution Research*, *25*(9), 8074–8088. https://doi.org/10.1007/s11356-017-9239-3

Odum, J. R., Hoffmann, T., Bowman, F., Collins, D., Flagan, R. C., & Seinfeld, J. H. (1996). Gas/Particle Partitioning and Secondary Organic Aerosol Yields. *Environmental Science & Technology*, *30*(8), 2580–2585. https://doi.org/10.1021/es950943+

Pennington, E. A., Seltzer, K. M., Murphy, B. N., Qin, M., Seinfeld, J. H., & Pye, H. O. T. (2021). Modeling secondary organic aerosol formation from volatile chemical products. *Atmospheric Chemistry and Physics*, *21*(24), 18247–18261. https://doi.org/10.5194/acp-21-18247-2021

Qin, M., Murphy, B. N., Isaacs, K. K., McDonald, B. C., Lu, Q., McKeen, S. A., Koval, L., Robinson, A. L., Efstathiou, C., Allen, C., & Pye, H. O. T. (2021). Criteria pollutant impacts of volatile chemical products informed by near-field modelling. *Nature Sustainability*, *4*(2), 129–137. https://doi.org/10.1038/s41893-020-00614-1

Seinfeld, J. H., & Pandis, S. N. (2016). *Atmospheric Chemistry and Physics: From Air Pollution to Climate Change* (3rd ed.). John Wiley & Sons, Inc.

US EPA. (2020). *CMAQ*. Zenodo. https://doi.org/10.5281/zenodo.4081737

US EPA, O. (2013, August 1). *Air Quality System (AQS)* [Data and Tools]. US EPA. https://www.epa.gov/aqs

Yarwood, G., Jung, J., Whitten, G. Z., Heo, G., Mellberg, J., & Estes, M. (2010). *Updates to the Carbon Bond Mechanism for Version 6 (CB6)*. 9th Annual CMAS Conference, Chapel Hill, NC.

Zhang, Q., Jimenez, J. L., Canagaratna, M. R., Allan, J. D., Coe, H., Ulbrich, I., Alfarra, M. R., Takami, A., Middlebrook, A. M., Sun, Y. L., Dzepina, K., Dunlea, E., Docherty, K., DeCarlo, P. F., Salcedo, D., Onasch, T., Jayne, J. T., Miyoshi, T., Shimono, A., … Worsnop, D. R. (2007). Ubiquity and dominance of oxygenated species in organic aerosols in anthropogenically-influenced Northern Hemisphere midlatitudes. *Geophysical Research Letters*, *34*(13). https://doi.org/10.1029/2007GL029979

Chapter 2

MODELING SECONDARY ORGANIC AEROSOL FORMATION FROM VOLATILE CHEMICAL PRODUCTS

Pennington, E. A., Seltzer, K. M., Murphy, B. N., Qin, M., Seinfeld, J. H., & Pye, H. O. T. (2021). Modeling secondary organic aerosol formation from volatile chemical products. *Atmospheric Chemistry and Physics*, *21*(24), 18247–18261. https://doi.org/10.5194/acp-21-18247-2021.

2.0 Abstract

Volatile chemical products (VCPs) are commonly-used consumer and industrial items that are an important source of anthropogenic emissions. Organic compounds from VCPs evaporate on atmospherically relevant time scales and include many species that are secondary organic aerosol (SOA) precursors. However, the chemistry leading to SOA, particularly that of intermediate volatility organic compounds (IVOCs), has not been fully represented in regional-scale models such as the Community Multiscale Air Quality (CMAQ) model, which tend to underpredict SOA concentrations in urban areas. Here we develop a model to represent SOA formation from VCP emissions. The model incorporates a new VCP emissions inventory and employs three new classes of emissions: siloxanes, oxygenated IVOCs, and nonoxygenated IVOCs. VCPs are estimated to produce 1.67 μg m^{-3} of noontime SOA, doubling the current model predictions and reducing the SOA mass concentration bias from -75% to -58% when compared to observations in Los Angeles in 2010. While oxygenated and nonoxygenated intermediate volatility VCP species are emitted in similar quantities, SOA formation is dominated by the nonoxygenated IVOCs. Formaldehyde and SOA show similar relationships to temperature and bias signatures indicating common sources and/or chemistry. This work suggests that VCPs contribute up to half of anthropogenic SOA in Los Angeles and models must better represent SOA precursors from VCPs to predict the urban enhancement of SOA.

2.1 Introduction

Organic aerosol (OA) is a major component of fine particulate matter ($PM_{2.5}$) in urban areas throughout the world (Zhang et al., 2007). $PM_{2.5}$ influences human health (Lim et al., 2012), climate (Intergovernmental Panel on Climate Change, 2014), and visibility (Hyslop, 2009), so understanding OA composition is an important step in mitigating the adverse effects of $PM_{2.5}$. Secondary organic aerosol (SOA) is often the dominant component of OA (Jimenez et al., 2009) and is formed when gas-phase volatile organic compounds (VOCs) react with atmospheric oxidants to form products that condense into the aerosol phase, where they can undergo further reaction. SOA is formed via thousands of atmospheric reactions (Goldstein & Galbally, 2007), so understanding its sources remains a challenge.

Volatile chemical products (VCPs) are an important source of organic emissions that lead to SOA formation (McDonald et al., 2018; Qin et al., 2021). As vehicle exhaust becomes cleaner and mobile source emissions decline, the relative importance of VCP emissions increases (Khare & Gentner, 2018). Previous work suggests that during the 2010 California Nexus of Air Quality and Climate Change (CalNex) campaign in Southern California (Ryerson et al., 2013), VCPs contributed approximately 1.1 $\mu g\ m^{-3}$, or 41%, of observed SOA above background levels in the Los Angeles Basin (Qin et al., 2021).

Modeling the formation of SOA in three-dimensional (3D) chemical transport models (CTMs) is challenging due to the complexity of VOC chemistry and computational constraints of regional-scale modeling. Models have tended to underpredict SOA mass in urban locations for a variety of reasons. For one, the SOA formation potential of intermediate volatility organic compounds (IVOCs) and semivolatile organic compounds (SVOCs)—or S/IVOCs—is not well constrained. Observations made during the CalNex campaign demonstrate that S/IVOCs are important sources of SOA, making up 10% of total gas-phase organic compound concentrations (Zhao et al., 2014) while contributing up to 80% of above-background SOA mass (Hayes et al., 2015). Although it is often impossible to identify all

individual species contributing to ambient S/IVOCs, these compounds may be classified based on their properties (e.g., volatility). Volatility basis set (VBS) models (Donahue et al., 2011) are often used to represent S/IVOC chemistry and partitioning, and have improved model estimates of SOA (Woody et al., 2016; Hayes et al., 2015; Robinson et al., 2007). Murphy et al. (2017) integrated a VBS model into the Community Multiscale Air Quality (CMAQ) model version 5.2 to represent the multigenerational aging of semivolatile primary organic aerosol (POA) leading to the production of SOA. Other studies have parameterized VBS models to represent S/IVOCs from mobile emissions (Lu et al., 2020; Jathar et al., 2017), but none have parameterized SOA formation from VCP S/IVOCs emissions. Additionally, the emissions of S/IVOCs are not well constrained and are often not included in detailed emissions inventories (Zhao et al., 2015). However even when S/IVOCs are included in emissions inventories, they are often assigned to nonreactive or nonvolatile model surrogates that do not participate in model chemistry (T. Shah et al., 2020). Improving the representation of SOA chemistry in CMAQ will allow for more accurate exposure estimates in health studies and source apportionment for air quality management decisions.

Another source of error in CTMs is the lack of representation of oxygenated SOA precursors. Historically, mechanism development has focused on the oxidation chemistry of species emitted primarily from vehicles (e.g., BTEX: benzene, toluene, ethylbenzene, and xylene) or biogenic sources (e.g., isoprene, monoterpenes). While VCPs do emit some of these species, they also emit many oxygenated compounds (Seltzer et al., 2021; McDonald et al., 2018). The implications of a few important oxygenated precursors on air quality have recently been quantified (e.g., Janechek et al., 2017; Charan et al., 2020; L. Li & Cocker, 2018; W. Li et al., 2018), but many oxygenated precursors have not been studied in a laboratory setting. For the few oxygenated VCPs that have been studied in laboratory chambers, SOA yields were reported under unrealistic atmospheric conditions, e.g., high OH and aerosol seed concentrations (Charan et al., 2021). So, the SOA yields of these compounds have primarily been estimated using models such as the Statistical Oxidation Model

(SOM; Cappa & Wilson, 2012) or VBS (McDonald et al., 2018; R. U. Shah et al., 2020). These oxygenated species are not included as SOA precursors in most models, and their chemistry is needed to improve predictions of SOA mass.

In this work, we introduce a chemical mechanism to represent SOA formation from VCPs. Specifically, the potential of both oxygenated and nonoxygenated IVOCs to form SOA is developed and evaluated. We utilize a new VCP emissions inventory known as VCPy (Seltzer et al., 2021) to represent organic emissions from VCPs and to parameterize model species behavior in the chemical mechanism. The chemistry and emissions inventory are implemented in the CMAQ model version 5.3.2 to simulate air quality during the CalNex campaign in California in 2010. The model predictions are compared to measurements made in Pasadena during CalNex and the speciation of predicted SOA is examined.

2.2 Methods

2.2.1 VCPy emissions inventory implementation

VCPy is a modeling framework that estimates reactive organic carbon emissions from VCPs (Seltzer et al., 2021). Within this framework, the complete VCP sector is disaggregated into several product use categories (PUCs; e.g., cleaning products, personal care products, adhesives and sealants, paints and coatings). U.S. nationwide usage of each PUC is estimated, and survey data are then used to quantify the mass fraction of organic, inorganic, and water proportions, as well as speciate the organic fraction. Physiochemical properties of each organic component are used to estimate the characteristic evaporation timescale, which is then compared to an assigned use timescale to determine whether a compound is retained or evaporated from each PUC. In the initial implementation of VCPy (version 1.0), which is representative of 2016 conditions, the predicted nationwide and Los Angeles County VCP emission rates were 9.5 kg person^{-1} year^{-1} and 8.2 kg person^{-1} year^{-1}, respectively. These emission rates are consistent with the low end of values seen in a previous study that used a top-down approach to estimate VCP emissions (Qin et al., 2021). In our work,

product use is based on data from 2010 with composition specified using data from the early 2000s to overlap with the CalNex campaign.

Since the speciation of organic emissions from VCPy is explicit, the underlying chemical and physical properties of emissions are output from the framework. These properties, many of which are relevant to atmospheric oxidation and subsequent SOA formation, include the oxidation rate with the hydroxyl radical (k_{OH}), molecular weight (MW), effective saturation concentration (C*), and oxygen-to-carbon ratio (O:C). SOA mass yields, which are defined as the mass of SOA formed per mass of ROC precursor reacted, were assigned based on compound-specific structure and volatility (Seltzer et al., 2021).

A key step in implementing this inventory into CMAQ is ensuring that all compounds predicted to be emitted by VCPy are mapped to either an existing or a new model surrogate. Emissions of low-volatility organic vapors ($C^* < 10^{6.5}$ μg m^{-3}) from all sources are prime SOA precursors but traditionally discarded from the gas-phase chemical mechanism used in many CTMs (e.g., represented as nonvolatile (NVOL), nonreactive (NROG), or unspecified IVOC species that are not used in the chemical mechanism of CMAQ). As a result, these species do not participate in atmospheric chemistry and thus do not impact radical concentrations or SOA mass. In addition, oxygenated compounds are not currently included as SOA precursors in many mechanisms because of the historic focus on SOA formation from nonoxygenated vehicle exhaust and traditional VOCs like single-ring aromatics and biogenic hydrocarbons. The work of Qin et al. (2021) specifically identifies this loss of emitted reactive carbon mass as a reason for underestimated SOA from the personal care sector in the CMAQ model. To account for the SOA potential of this previously neglected organic mass, all compounds currently mapped to NROG, NVOL, and IVOC are reviewed, with most of this mass routed to one of three newly added categories of model surrogates: siloxanes (SILOX), oxygenated IVOCs (SOAOXY), or nonoxygenated IVOCs (IVOCP3, IVOCP4, IVOCP5, IVOCP6, IVOCP5ARO, and IVOCP6ARO). The updated mechanism (with SOA pathways described in

Section 2.2) with the newly implemented speciation mapping is henceforth described as SAPRC07TIC_AE7I_VCP and the complete list of assignment rules is provided in the SI Methods.

County-level VCPy emissions (Seltzer et al., 2021) were gridded at 4-km scale to fit the CalNex domain (Baker et al., 2015) using a variety of spatial surrogates. The spatial surrogates used depend on the category of VCP emissions being described: agricultural land is used as a proxy for all agricultural pesticide emissions, the density of oil and gas wells for the oil and gas solvent emissions, and population for all remaining VCP sources. While some categories of VCP emissions could feature more refined spatial surrogate proxies, the uncertainty associated with spatial allocation of sources may be lower than uncertainty in individual source strength. More specifically, if an entire VCP category could be matched to a single surrogate, allocation methods would still assume there is no variation in the strength of individuals within the population of that surrogate (Y. Li et al., 2021).

All VCP emissions feature a sinusoidal diurnal profile with a peak at noon, with no application of day-of-week or seasonal profiles. Since the simulation period used in this study is a single month, no seasonal changes would be observable over this time frame and previous work suggests little seasonal variability in VCP emissions (Gkatzelis et al., 2021). Other emission sectors (e.g., mobile sources, agriculture) are adjusted for seasonal impacts based on meteorological conditions and known activity data.

2.2.2 Parameterizing SOA formation from VCPs

To better represent the atmospheric chemistry of VCPs, SOA formation is added for the three new categories of emissions (siloxanes, oxygenated IVOCs, and nonoxygenated IVOCs) in the SAPRC07TIC_AE7I_VCP chemical mechanism within CMAQ (Table 2.1).

Cyclic volatile methylsiloxanes (cVMS), or siloxanes for short, are present in many personal care products, adhesives, and sealants. Collectively, siloxanes represent a

large fraction of VCP emissions (Seltzer et al., 2021). Decamethylcyclopentasiloxane (D_5-siloxane) is the most prevalent siloxane in urban atmospheres (D.-G. Wang et al., 2013) and laboratory studies have found D_5-siloxane SOA yields ranging from 0% (Charan et al., 2021) to 50% (Janechek et al., 2019). The explicit oxidation mechanism is unknown and the SOA yields of other siloxanes are not well understood (Coggon et al., 2018). Here, siloxanes are treated separately from other oxygenated VCP species due to their anomalously low OH oxidation rate (Table 2.1). The mechanism of SOA formation used here utilizes an existing two-product model from Janechek et al. (2019) that was parameterized using oxidation flow reactor (OFR) experiments and photooxidation chamber data from Wu & Johnston (2017). In this implementation, the OH oxidation rate constant for D_5-siloxane matches the rate reported in Janechek et al. (2017) and the hydroxyl radical is replenished after reaction.

Few laboratory chamber studies have investigated the oxidation processes of other oxygenated gas-phase species (e.g., Charan et al., 2020; L. Li & Cocker, 2018), so little experimental data exist about the SOA yields or oxidation products of oxygenated SOA precursors. Additionally, many models that predict the products of oxidation reactions (e.g., SOM and VBS) have not been parameterized or evaluated using oxygenated precursors. Without these models and laboratory studies, little is known about the oxidation products of these precursors, which limits our ability to develop a detailed model of their SOA formation. Therefore, all non-siloxane oxygenated IVOC emissions are represented by a single surrogate (SOAOXY) that undergoes a one-step gas-phase reaction with the hydroxyl radical to form a nonvolatile aerosol surrogate (AOIVOC). This simple mechanism reduces the reliance on many parameters that are not well-constrained. The MW, k_{OH}, C*, and SOA yield of this surrogate are calculated as a mass-weighted average of the oxygenated IVOC emissions from VCPs in Los Angeles County which are generally consistent with what would be calculated using nationwide information.

Nonoxygenated IVOC emissions are represented using the model described by Lu et al. (2020), which uses a VBS model and multigenerational aging scheme to represent the SOA from gasoline, diesel, and aircraft sources. Six surrogates are differentiated by structure (alkane vs. aromatic) and effective saturation concentration, and each is assigned a four-product yield distribution, generating SVOCs after one oxidation step. Many of the nonoxygenated IVOC species from mobile and VCP emission sources have similar structures (i.e., long and branched alkanes and aromatics), volatilities, and SOA yields (see Figure 2.S1), making the Lu et al. (2020) model a good representation of oxidation and SOA formation from nonoxygenated VCP IVOCs.

Table 2.1. Properties of the VCP surrogates added to CMAQ version 5.3.2.

	MW (g mol^{-1})	k_{OH} x 10^{11} (cm^3 $molec^{-1}$ sec^{-1})	α_i	C* (μg m^{-3})	SOA mass yield (at 10 μg m^{-3})	H_{vap} (kJ mol^{-1})	κ_{org}	H (M atm^{-1})	OM/ OC
SILOX	368.66[a]	0.155[b]	-	-	-	-	-	3.87 x 10^{2} [f]	-
SVSILOX1/ ASILOX1J	416.66[a]	-	0.14[c]	0.95[c]	0.13	131[d]	0.09[e]	2.97 x 10^{6} [f]	3.49[e]
SVSILOX2/ ASILOX2J	384.66[a]	-	0.82[c]	484[c]	0.017	101[d]	0.05[e]	7.99 x 10^{4} [f]	3.22[e]
SOAOXY[g]	170.95	2.54	-	-	-	-	-	2.85 x 10^{3} [f]	-
AOIVOCJ[g]	186.95	-	-	-	0.0628	-	0.09[e]	-	1.73[e]
IVOCP3[h]	296.6	2.65	[h]	10^{3}	0.43	52	-	2 x 10^{8}	-
IVOCP4[h]	254.9	2.25	[h]	10^{4}	0.43	41	-	2 x 10^{8}	-
IVOCP5[h]	219.4	1.89	[h]	10^{5}	0.35	30	-	2 x 10^{8}	-
IVOCP6[h]	184.4	1.55	[h]	10^{6}	0.15	19	-	2 x 10^{8}	-
IVOCP5ARO[h]	197.3	7.56	[h]	10^{5}	0.36	30	-	2 x 10^{8}	-
IVOCP6ARO[h]	162.3	3.05	[h]	10^{6}	0.25	19	-	2 x 10^{8}	-

[a]The gas-phase siloxane (SILOX) MW is the average of the MW of all VCPy siloxane and silane species weighted by Los Angeles County emission rates. The MW of the higher-volatility siloxane products (SVSILOX2/ASILOX2J) is approximated as the sum of the MW of SILOX and one oxygen. The MW of the

lower-volatility products (SVSILOX1/ASILOX1J) has an additional two oxygens to represent its significant decrease in volatility.

[b]The gas-phase siloxane (SILOX) k_{OH} is given in Janechek et al. (2017).

[c]The stoichiometric product yields (α_i) and C* of the siloxanes are given in Janechek et al. (2019).

[d]Enthalpy of vaporization (H_{vap}) values for the siloxanes are estimated according to the method in Epstein et al. (2010).

[e]All OM/OC ratios and hygroscopicity parameters (κ_{org}) are estimated using equations 5 and 12, respectively, in Pye et al. (2017).

[f]Henry's Law constants (H) at 298.15 K are estimated using the surrogate-based method in Hodzic et al. (2014).

[g]The MW, k_{OH}, C*, and SOA yield of SOAOXY (gas) and AOIVOCJ (aerosol) are calculated as a mass-weighted average of the oxygenated IVOC emissions from VCPs in Los Angeles County. Because AOIVOC is formed via a single reaction with a constant SOA yield, it is treated as nonvolatile and therefore is not assigned a C* or H_{vap}.

[h]All nonoxygenated IVOC surrogate properties—including four stoichiometric product yields (α_i) for each surrogate used in the multigenerational scheme—are described in Lu et al. (2020).

2.2.3 CMAQ model implementation

2.2.3.1 CalNex model configuration

The updated chemical mechanism and VCPy-derived emissions were implemented in CMAQ version 5.3.2 (US EPA Office of Research and Development, 2020). CMAQ version 5.3 and the subsequent minor releases are documented in Appel et al. (2021). The model was used to simulate air quality during the CalNex campaign from May 15 to June 15, 2010, with an additional 14-day spin-up period. Outside the VCP updates, the model configuration matches the implementation used in Qin et al. (2021) and Lu et al. (2020). The model domain has 4-km x 4-km horizontal resolution (325 x 225 grid cells) covering California and Nevada with 36 vertical levels reaching 50 mbar. Meteorological inputs are derived from the Weather Research and Forecasting (WRF) Advanced Research WRF core Model version 3.8.1 (Skamarock et al., 2008). Gas-phase chemistry is represented using SAPRC07TIC (Pye et al., 2013; Xie et al., 2013) with the addition of the VCP chemical mechanism summarized in Table 2.1. Aerosol-phase chemistry is simulated using an extended version of the AERO7 mechanism, depicted in Figure 2.1, including all AERO7

reactions plus those of the new VCP mechanism (boxed in red) and mobile IVOCs (boxed in red in the lower left) that participate in the multigenerational aging shown in the orange boxes (Lu et al., 2020). This diagram also includes a representation of the aqueous-phase cloud chemistry and removal used in the Asymmetric Convection Model (ACM) version 2 module (Binkowski & Roselle, 2003), which has been updated to include wet deposition properties for the new aerosol surrogates (Table 2.1).

All non-VCP anthropogenic emissions are based on the 2011 National Emissions Inventory (NEI) version 2 (US EPA, 2015). VCP emissions in the NEI are removed and replaced with VCPy predicted emissions using the Detailed Emissions Scaling, Isolation, and Diagnostic (DESID) module (Murphy et al., 2021). Mobile NO_x emissions were reduced by 25% in all simulations to better match observational data from the CalNex campaign (Qin et al., 2021). Mobile IVOC emissions and the semivolatile treatment of mobile POA were treated according to the methods described in Lu et al. (2020). The IVOCs are assigned to the appropriate IVOCP3/4/5/6/5ARO/6ARO surrogates that are also used to treat nonoxygenated IVOCs from VCPs. Wind-blown dust emissions are neglected in this study. Biogenic emissions are calculated online using the Biogenic Emission Inventory System (BEIS) version 3.6.1 (Bash et al., 2016) as are sea spray aerosol emissions.

2.2.3.2 Simulation cases

Three simulations were evaluated against the observations collected during the CalNex campaign. A “zero VCP” case removes all VCP emissions. The “CMAQv5.3.2” case is a standard CMAQ simulation with base emissions (i.e., VCP emissions from the NEI) and base chemistry (i.e., no new VCP chemistry). Finally, the “CMAQv5.3.2+VCP” case adds both the VCP chemistry described above (i.e., SAPRC07TIC_AE7I_VCP) and replaces all NEI VCP emissions with VCPy-derived VCP emissions. Comparisons between the “zero VCP” case and the “CMAQv5.3.2+VCP” case illustrate the complete impact of VCPy emissions on modeled SOA. In contrast, comparisons between the “CMAQv5.3.2” case and the

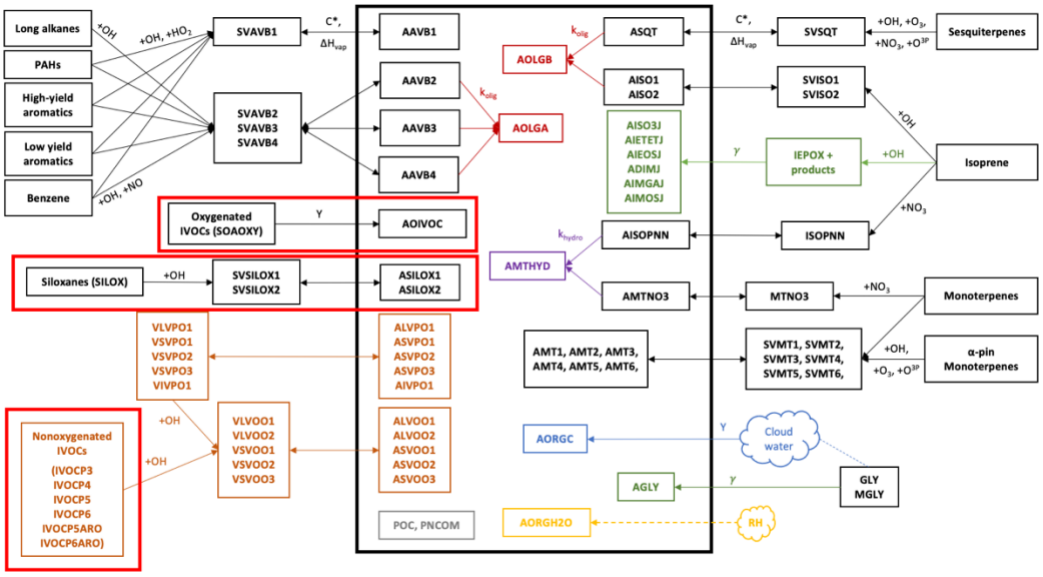

Figure 2.1: Treatment of OA chemistry in the CMAQv5.3.2+VCP model. The thick black box surrounds all aerosol-phase species. All smaller black boxes depict species undergoing gas-phase oxidation from VOCs to semivolatile or nonvolatile SOA species. Orange font depicts the VBS model for S/IVOCs. Red font depicts particle-phase accretion reactions while purple font depicts particle-phase hydrolysis reactions. Green font represents heterogeneous processes. Blue font shows cloud-processed aerosol and yellow font shows aerosol water associated with the organic phase. Gray boxes are nonvolatile primary organic aerosol (POA) species. Double-sided arrows represent reversible processes and one-sided arrows represent irreversible processes. Dashed lines represent processes that are dependent on relative humidity. The diagram includes the AERO7 mechanism plus the three VCP-forming pathways specific to this work (thick boxes in red). See AE7I Species Table (2016/2021) for species descriptions.

"CMAQv5.3.2+VCP" case illustrate the impact of the new representation of VCP emissions and chemistry against the current status of VCPs in CMAQ. Results from the CMAQv5.3.2 case are presented primarily in the SI.

2.2.3.3 Comparison with observations

Observational data are provided by a suite of instruments deployed during the 2010 CalNex campaign in Pasadena. There were two data collection sites in the CalNex campaign—Pasadena and Bakersfield—and model predictions are compared to measurements made at the Pasadena site, which is located in the Los Angeles Basin approximately 18 km downwind of the urban core (Ryerson et al., 2013). PM_1 (fine particulate matter with diameter < 1 μm) OA data were obtained with an aerosol mass spectrometer (AMS) and have been analyzed via positive matrix factorization (PMF) to determine its composition (Hayes et al., 2013). Formaldehyde (HCHO) data are provided in Warneke et al. (2011) and carbon monoxide (CO) data are available from Santoni et al. (2014). Ozone data throughout California were obtained from the EPA AQS monitoring network for 178 sites operating during the simulation period (US EPA, 2013). Hourly ozone concentrations were used to calculate daily maximum 8-hour average (MDA8) ozone concentrations.

2.3 Results & Discussion

2.3.1 VCP emissions and implications for SOA

VCP emissions were split almost equally between species that do and do not form SOA. The SAPRC07TIC_AE7I_VCP speciation mapping (Figure 2.2) indicates 56.4% (4.8×10^7 kg $year^{-1}$) of Los Angeles County VCP emitted mass does not form SOA. This mass includes small species commonly used as solvents, such as ethanol, acetone, and small alkanes. The remaining 43.6% (3.7×10^7 kg $year^{-1}$) of Los Angeles County emissions are assigned to model surrogates that form SOA. 3.5% of the total emissions are assigned to siloxanes, 7.8% to oxygenated IVOCs, 11.8% to nonoxygenated IVOCs, and 20.4% to traditional SOA precursors, such as VOC alkanes, toluene, and other aromatics. The volatility and SOA yields of species in each category are summarized in Figure 2.S1.

Figure 2.2 indicates that in traditional model processing, precursors to SOA are systematically discarded from chemistry calculations. As described in Section 2.1, low-volatility emissions (i.e., NROG, NVOL, and IVOC) do not participate in SOA or radical chemistry in traditional SAPRC07TIC_AE7I which is a key issue in

representing SOA mass. The inner ring of Figure 2.2 depicts the fraction of each category that was originally assigned to inactive species (NROG, NVOL, and IVOC; hatched) versus other existing surrogates (solid). 2.6 x 10^7 kg $year^{-1}$ (30.7%) of the total VCP emissions were originally assigned to these surrogates and did not participate in any atmospheric chemistry processes. Using the new speciation and mechanism, 1.8 x 10^7 kg $year^{-1}$ (21.2% of total VCP emissions) were reassigned to surrogates that form SOA in the model (hatched inner ring: red, blue, orange, and purple). The remaining 8.0 x 10^6 kg $year^{-1}$ (9.4% of total VCP emissions; inner ring hatched green) is comprised of species with SOA yields of zero and were not reassigned to SOA-forming surrogates.

Averaged over the duration of the CalNex campaign, VCPs are predicted to be a larger source of IVOCs than mobile sources, as shown by the increase in gas-phase IVOC mass in the CMAQv5.3.2+VCP case compared to the zero VCP case (Figure 2.S2). Across mobile and VCP sources during CalNex, CMAQ predicts 6.4 μg m^{-3} of the gas-phase IVOC mass is nonoxygenated and 2.6 μg m^{-3} of the IVOC mass is oxygenated (Figure 2.S2). The observed campaign-average total IVOC concentration was 10.5 μg m^{-3} (Zhao et al., 2014), with 6.3 μg m^{-3} attributed to hydrocarbon-like IVOCs and 4.2 μg m^{-3} attributed to oxygenated IVOCs. However, this observed estimate of oxygenated IVOCs is conservative (lower bound) based on the experimental method employed by Zhao et al. (2014). Thus, the predicted nonoxygenated IVOC mass, which includes contributions from both mobile and VCP sources, reproduces observations with high fidelity. CMAQ, which only considers IVOCs from VCP and mobile sectors, underpredicts the mass of oxygenated IVOCs by 38%, suggesting additional missing products of oxidation or emissions.

The new SOA systems combined with traditional SOA precursors in CMAQ resulted in an effective SOA yield for the VCP sector—defined as the emission-weighted average of the individual species' mass-based SOA yields—of 5.6% for Los Angeles County. This Los Angeles County yield is in good agreement with the work of Qin et al. (2021), that found a 5% yield led to SOA predictions consistent with ambient

observational constraints. The U.S. effective VCP SOA yield (5.3%) is only slightly lower than the yield expected for Los Angeles, due to differences stemming from the variability in the composition of VCP emissions nationwide versus in Los Angeles.

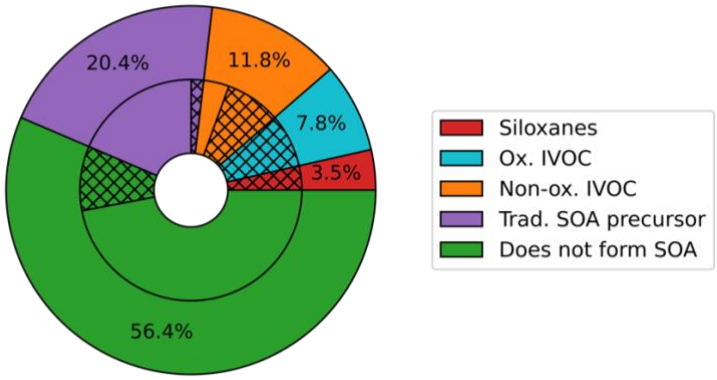

Figure 2.2: Percentage of the VCP emissions assigned to each category of CMAQ surrogates using the SAPRC07TIC_AE7I_VCP speciation profiles. The total rate of VCP emissions in Los Angeles County is 8.3 x 10^7 kg yr^{-1}. The outer ring depicts the percentage of total VCPy-derived emissions assigned to each of the three new VCP categories (siloxanes in red, oxygenated IVOCs in blue, and nonoxygenated IVOCs in orange), the traditional SOA precursors described by existing model surrogates (purple), and existing surrogates that do not form SOA (green). The inner ring gives an indication of the original assignments of each of the outer ring categories. Hatching indicates emissions originally assigned to model surrogates that do not participate in model chemistry: IVOC, NVOL, and NROG. Solid colors represent other surrogate assignments.

2.3.2 CMAQ results: SOA, ozone, and formaldehyde

Modeled PM_1 SOA increased considerably in response to the newly implemented VCP emissions and chemistry, bringing model predictions into closer agreement with observations. Daily maximum PM_1 SOA concentrations increased from 1.4 μg m^{-3} (-79% mean bias) in the zero VCP case to 2.8 μg m^{-3} (-58% mean bias) in the CMAQv5.3.2+VCP case, compared to the observed peak value of 6.6 μg m^{-3} (Figure 2.3a). The diurnal distributions resulted from photochemistry and the sinusoidal

distribution of VCP emissions that peak at 12:00 local time. Modeled PM_1 SOA concentrations improved for all mass loadings and all hours of the day, with the slope of modeled versus observed concentrations increasing from 0.23 in the zero VCP case to 0.43 in the CMAQv5.3.2+VCP case (Figure 2.4a). Results for the CMAQv5.3.2 case are given in Figs. 2.S3 and 2.S4. Modeled $PM_{2.5}$ SOA displayed similar behavior as PM_1 SOA; i.e., the organic fraction and secondary organic fraction of $PM_{2.5}$ was only marginally smaller than the corresponding fractions of PM_1 and followed the same diurnal pattern.

The difference between hourly averaged total (i.e., not size-resolved) SOA concentrations in the zero VCP and CMAQv5.3.2+VCP case are shown in Figure 2.3b and the contributions to that difference from categories of SOA surrogates are shown in Figure 2.3c. Of the three new categories of VCP emissions, nonoxygenated IVOC precursors formed the most SOA in CMAQ. The increased SOA from the nonoxygenated IVOC VCP precursors reached a peak concentration of 1.14 $\mu g\ m^{-3}$, equal to 69% of the total noontime difference. This can be explained by the high SOA yields of the individual species (Figure 2.S1) and the model surrogates.

SOA from oxygenated IVOC VCP precursors reached a peak concentration of 0.11 $\mu g\ m^{-3}$ (6.7% of the SOA difference). While oxygenated IVOC emissions were similar in abundance to nonoxygenated IVOC emissions (Figure 2.2), these species lead to less SOA formation due to their lower SOA yields (Figure 2.S1); higher degrees of oxygenation tend to promote fragmentation upon reaction with OH (Jimenez et al., 2009), producing smaller molecules with higher volatilities and lower potential to form SOA. It is possible that the net yield of modeled SOA from oxygenated IVOC precursors will increase as the results from more laboratory studies become available, or if a more detailed model is used. For example, particle-phase oligomerization reactions from oxygenated IVOC precursors would produce nonvolatile aerosol products, but this chemistry has not yet been investigated in an atmospheric chamber.

Siloxanes formed very little SOA, reaching a maximum of 21 ng m^{-3} (1.3% of the SOA difference) at noon. Despite having nonnegligible SOA yields (Figure 2.S1) and emission rates (Figure 2.2), siloxanes react with OH on long time scales (Table 2.1). As such, this results in low localized SOA mass, which is consistent with other modeling and laboratory studies that have predicted siloxanes to form SOA on the order of ng m^{-3} or less (Charan et al., 2021; Milani et al., 2021; Janechek et al., 2017). The low resultant SOA mass demonstrates that while gas-phase siloxanes serve as a useful tracer for personal care product and adhesive emissions from VCPs (Gkatzelis et al., 2021), particle-phase products from siloxane oxidation may not form quickly enough to serve as a reliable tracer for these emissions.

While traditional species accounted for the greatest fraction of VCP SOA precursor emissions that lead to SOA formation (Figure 2.2), they contributed only 23% (0.39 μg m^{-3}) of the increased noontime SOA in the CMAQv5.3.2+VCP case. These traditional SOA precursors form SOA less efficiently than the IVOC surrogates (Figure 2.S1), so they result in less SOA formation than IVOCs despite higher emissions.

While this work indicates oxygenated IVOCs form much less SOA than nonoxygenated IVOCs, more work is needed to determine if this result is robust across all emission sectors and in future conditions. Oxygenated IVOCs represent a class of emissions that has traditionally been discarded from regional models, but have become an important research focus with the rising importance of VCP emissions (Khare & Gentner, 2018). The contribution of oxygenated IVOCs and siloxanes to ambient conditions may be spatially variable and continue to evolve as product formulations shift towards exempt VOCs which tend to be oxygenated. Oxygenated IVOCs from other emissions sources, such as meat cooking or wood burning, could be abundant but were not considered here. Additionally, we do not know if SOA from these precursors has a health impact higher or lower than average $PM_{2.5}$.

The SOA from VCP IVOCs reached a daily maximum of 1.25 μg m^{-3} on average at noon (Figure 2.3c). IVOCs from mobile sources contributed an additional 1.1 μg m^{-3} at noon (Lu et al., 2020). Therefore this updated CMAQ model predicted a total IVOC-derived SOA concentration of 2.35 μg m^{-3}, equivalent to 35% of the total observed above-background PM_1 SOA concentration (6.6 μg m^{-3}). Previous work stated that 40-85% of above-background SOA concentrations in Pasadena are attributable to S/IVOCs (Hayes et al., 2015), suggesting that additional processes are still needed in the model. This will be discussed further in Section 3.3.

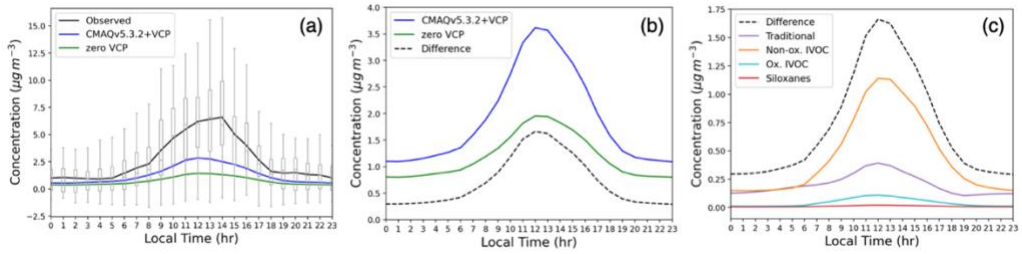

Figure 2.3: a) Average hourly concentrations of background-corrected PM_1 SOA observed and simulated by the zero VCP and CMAQv5.3.2+VCP modeling cases May 15–June 15. Box and whiskers show all hourly concentrations observed by AMS at the CalNex site. A constant background value was removed from all observed concentrations according to the method in Hayes et al. (2015). The background value of each simulation was determined by averaging the lower 50% of hourly concentrations from 00:00 LT to 04:00 LT and subtracting that from each curve. b) Average hourly concentration of total (not size-resolved) SOA for the two simulation cases and their difference (CMAQv5.3.2+VCP – zero VCP). c) Difference in hourly concentrations of total SOA by category.

Formaldehyde is one of the most abundant VOCs in the atmosphere and observations of this compound can serve many purposes. Biomass burning, vehicles, and other urban sources emit formaldehyde, and because of its short lifetime (~hours), it can serve as a proxy for local organic emissions. It is also formed in the atmosphere when VOCs undergo radical reactions, oxidize, and fragment, so it serves as an indicator

for SOA chemistry since it is formed by many of the same reactions that also lead to SOA formation (Seinfeld & Pandis, 2016). In addition, it is depleted by photolysis and is an important source of radical initiation reactions (Griffith et al., 2016). Formaldehyde can be retrieved directly by satellites (Levelt et al., 2018), which can be used to validate ground data, evaluate model predictions, and predict OA concentrations remotely (Liao et al., 2019). For all of these reasons, formaldehyde is a useful indicator of VOC chemistry in a model.

Predicted formaldehyde concentrations improved in response to the new VCP emissions and chemistry, indicating that model updates improve the representation of VOC chemistry beyond SOA in the model. Similar to predicted SOA, formaldehyde concentrations increased at all times, with the ratio of modeled to observed values increasing from 0.58 in the zero VCP case to 0.75 in the CMAQv5.3.2+VCP case (Figure 2.4b). The diurnal profile of hourly averaged formaldehyde concentrations is given in Figure 2.S3. This work focused primarily on improving the representation of SOA from VCPs, so radical chemistry for the new SOA precursors was treated using existing alkane-like behavior (surrogates ALK1/2/3/4/5). With a more detailed representation of VCP radical chemistry, predicted formaldehyde concentrations may improve further.

The bias in predicted ozone concentrations was also reduced by including VCP chemistry. The ratio of modeled to observed concentrations increased from 0.72 in the zero VCP case to 0.95 in the CMAQv5.3.2+VCP case (Figure 2.4c). Improved ozone is also seen for all operational AQS sites in the California modeling domain, with the modeled to observed ratio increasing from 0.63 in the zero VCP case to 0.70 in the CMAQv5.3.2+VCP case (Figure 2.S5). The diurnal profile of hourly averaged ozone concentrations is given in Figure 2.S3. This study focused on VCP behavior in relation to SOA formation and used existing model species to capture ozone formation. Future work focusing on the ozone chemistry of VCPs could change the magnitude and diurnal profile of predicted ozone.

SOA can be facilitated by increases in oxidant abundance and chemical pathways from precursors to semivolatile or low-volatility products. Average noontime total SOA mass increased from 1.96 μg m^{-3} in the zero VCP case to 3.62 μg m^{-3} in the CMAQv5.3.2+VCP case (Figure 2.3b), an increase of 84.7%. Ozone concentration can be used as an indicator of oxidant burden and oxidation rates due to its high responsiveness, while OH concentrations may be less responsive (Qin et al., 2021). The average noontime ozone concentration increased from 43.0 ppb in the zero VCP case to 49.2 ppb in the CMAQv5.3.2+VCP case (Figure 2.S3c), an increase of 14.4%. Assuming ozone can serve as a proxy for oxidation rates, the improved ozone concentration suggests that ~14.4% of increased model SOA concentrations are due to an increase in the oxidant burden and oxidation rates. The SOA mass increased by a larger percentage (84.7%), indicating emissions and chemistry updates combined were approximately 5 times [(84.7% - 14.4%) / 14.4%] more effective than enhanced oxidant levels alone in increasing SOA. This is consistent with the work of Qin et al. (2021), which found that the lack of key emitted precursors in models—rather than their associated radical chemistry—had the largest impact on $PM_{2.5}$ formation. Additionally, we note that the default CMAQ model (CMAQv5.3.2) with baseline chemistry and VCP emissions predicted about the same amount of SOA as the zero VCP case (Figure 2.S3a). In contrast, ozone increased in the default CMAQv5.3.2 model with VCPs (Figure 2.S3c). Since the oxidant burden increased noticeably in the CMAQv5.3.2 case but did not equate to a large increase in PM_1 SOA, results suggest the oxidant level alone does not have a large influence on enhancing SOA if the relevant precursor pathways are not also implemented.

The response of formaldehyde can similarly be compared to the change in oxidant burden due to VCPs. At noontime, average formaldehyde increased from 2.41 ppb in the zero VCP case to 2.80 ppb in the CMAQv5.3.2+VCP case, an increase of 16.2%. As above, we attribute ~14.4% of the increase in pollutant concentration to the increase in oxidation rates. While formaldehyde does contribute to the oxidant burden via photolysis and radical initiation, the contribution of formaldehyde to the

RO_x radical budget is likely small and on the order of 10% (e.g., Griffith et al., 2016; Kaiser et al., 2015; Luecken et al., 2018). Thus, the increase in formaldehyde concentrations between simulation cases is likely due primarily to the increase in oxidation rate. The increase in formaldehyde between simulation cases, therefore, cannot be largely attributed to the addition of S/IVOC emissions and their ability to form formaldehyde as a byproduct of oxidation. This is consistent with the work of Coggon et al. (2021), which showed that vehicle VOCs perturb formaldehyde to a larger degree than VCP VOCs do, suggesting that VCP emissions and fragmentation chemistry may not be directly responsible for formaldehyde, but rather modulate formaldehyde formation via changes in oxidant abundance.

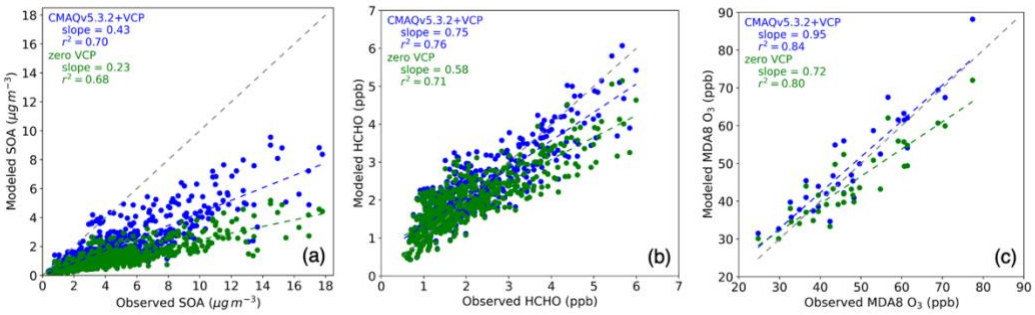

Figure 2.4: Modeled concentrations predicted by CMAQ zero VCP case (green) and CMAQv5.3.2+VCP case (blue) vs. observations from the CalNex Pasadena ground site. The line with a slope of 1 is indicated with a gray dashed line. a) Hourly PM_1 SOA. b) Hourly formaldehyde (HCHO). c) MDA8 O_3. Background values were not removed from any panels.

2.3.3 Features of remaining model bias

The residual PM_1 SOA bias in Pasadena is well-correlated with ambient temperature (Figure 2.5a). PM_1 SOA bias is defined as modeled hourly concentrations minus observed hourly concentrations. At cooler temperatures in the overnight hours, bias is low and fluctuates around zero. However, as temperature increases towards midday and SOA concentrations increase, the bias becomes more negative, indicating greater model underprediction.

SOA concentrations can be a function of temperature based on precursor emissions and chemistry throughout the day. Previous work demonstrated that observed OA in Los Angeles is positively correlated with temperature, and declining OA concentrations have been due largely to reductions of temperature-independent OA. Because this corresponds to a decline in anthropogenic emissions, they suggest that anthropogenically-derived OA is largely temperature-independent while biogenically-derived OA is largely temperature-dependent (Nussbaumer & Cohen, 2021). Modeled OA is positively correlated with temperature, consistent with the observed Los Angeles OA, and is driven by the larger, secondary portion of OA, rather than POA (Figure 2.S7). However, the improvement to predicted SOA between simulation cases was seen unequally at different temperatures, as indicated by the larger reduction in absolute model bias at higher temperatures (Figure 2.5a). This suggests that the SOA derived from VCP species have a temperature-dependent response, in addition to the biogenic emissions cited in Nussbaumer & Cohen (2021). In particular, because nonoxygenated IVOCs were the dominant source of increased SOA predicted by the CMAQv5.3.2+VCP simulation, this work suggests that S/IVOCs are an important source of temperature-dependent SOA in Los Angeles.

Because S/IVOCs have been shown to be a major constituent of modeled SOA and contribute to the correlation between SOA bias and temperature, other sources of S/IVOCs emissions may account for some of the remaining residual SOA bias in the model. For example, asphalt emissions are proposed to contribute 8-30% of total S/IVOC emissions in the South Coast Air Basin in Southern California and have SOA mass yields exceeding 10% (Khare et al., 2020). Their potential to form SOA is very large, and because asphalt emissions are highly temperature-dependent, the SOA increase would be seen largely during midday resulting in an improvement of high-temperature SOA bias. In addition, the underprediction of oxygenated gas-phase IVOCs (Section 3.1) suggests that additional sources of oxygenated IVOC precursors may be missing from the complete inventory. One possible explanation of the temperature-dependence of the SOA bias is that modeled SOA volatility is too

high. But, oxygenated SOA is nonvolatile and nonoxygenated IVOC SOA is continually processed to lower volatility through gas-phase OH oxidation.

Formaldehyde, CO, and POA are often used to understand the atmospheric evolution of SOA because they are products of the same anthropogenic activity and/or VOC oxidation chemistry that forms SOA. As such, they can be used to better understand the remaining sources of error in the model. POA is formed via combustion from vehicles, industrial processes, cooking, and biomass burning (Jathar et al., 2014; Huffman et al., 2009). CO and formaldehyde are emitted from many processes and formed as products of atmospheric VOC oxidation (Seinfeld & Pandis, 2016). These species are often used to understand the effect of dilution on SOA (Hayes et al., 2013). Dilution is caused both by atmospheric transport away from emission sources, as well as the change in planetary boundary layer (PBL) height over the diurnal cycle. VCPs do not emit POA, CO, or formaldehyde, so any changes observed in their simulated concentrations were caused by chemical and physical processing in the existing model.

The POA bias did not express the same temperature dependence as SOA, and thus POA is not affected in the same way in the model by the processes causing the temperature-dependence of SOA bias. Since VCPs do not emit POA and all other emission sources were consistent between simulation cases, the slight increase in POA concentrations between the zero VCP and CMAQv5.3.2+VCP cases (Figs. 2.5 and 2.S7) is due to increased partitioning of semivolatile POA into the particle-phase resulting from higher total OA mass loadings (the treatment of semivolatile POA in CMAQ is described in Murphy et al. (2017)). The POA bias can be exclusively attributed to errors in combustion source emissions inventories and meteorological effects. The combustion source inventories also include emissions of gaseous SOA precursors, which may be incorrectly modeled even if the POA emissions are accurate, especially for cooking and biomass burning sources. While the POA bias does decrease with increasing temperature, it is positive at all temperatures and does not have larger underpredictions at higher temperatures (Figure 2.5b). Due to the

inconsistency between POA and SOA behavior, errors influencing the emission and transport of POA can likely not be used to describe the temperature dependence of SOA bias. The POA bias also does not provide information about the error in vapor emissions from combustion sources—including S/IVOCs—and their temperature-dependence, and improving combustion emissions inventories may help to close the model-observation gap for SOA.

CO is often used to account for the effects of dilution by scaling SOA to CO enhancement ($\Delta CO = CO - CO_{background}$). Negligible changes in the CO concentration were found between simulation cases considered here (Figure 2.S3) and the model CO bias is uncorrelated with temperature (Figure 2.5d). The consistency of predicted CO concentration between cases implies that CO is not affected by the emissions changes to the VCP sector and thus cannot separate SOA formation efficiency from lack of emitted precursors. CO enhancement serves as an effective indicator and correction factor for mobile source emissions in urban areas (e.g., Hayes et al., 2013; Ensberg et al., 2014; Woody et al., 2016), but this work indicates that CO is not an effective tracer for distinguishing VCPs from other sources. The lack of correlation between CO and temperature also implies that errors in the modeled PBL height at different times of day (and potential impact on dilution of pollutant concentrations) is not an important driver of the SOA bias temperature-dependence.

In contrast to POA and CO, the formaldehyde bias demonstrated the same trend with temperature as SOA (Figure 2.5c). This suggests that formaldehyde is affected by emissions, chemistry, and dilution changes similarly to SOA. This is supported by the stronger correlation seen between SOA and formaldehyde compared to the correlation between SOA and POA or CO (Figure 2.S8). Therefore, formaldehyde may provide more information about the errors in modeling VOC chemistry and possibly SOA formation. It is possible that remaining formaldehyde bias is due to missing formaldehyde emissions. The VCP inventory includes near-zero emissions of formaldehyde, but formaldehyde is emitted from wooden furniture and emission rates increase with temperature (Y. Wang et al., 2021). This may account for some

of the temperature-dependence of formaldehyde bias, but likely not the entirety since the VCP emissions inventory has been evaluated with select ambient VOC measurements with low error (Seltzer et al., 2021). One possible explanation of the temperature-dependence of both the SOA and formaldehyde biases is missing sources of emissions and resulting chemistry. Previous work has shown that formaldehyde formation is particularly sensitive to the emissions/chemistry of alkenes (e.g., isoprene) and, to a lesser extent, alkanes and aromatics (Luecken et al., 2018), so these precursors likely indicate missing emissions as a source of error in our model. While the radical chemistry of these hydrocarbon precursors are included in the model, additional missing chemistry may be causing some of the error. Chemical processes that have not been included in the mechanism include autooxidation (Crounse et al., 2013)—which forms low-volatility SOA—and formaldehyde potentially formed from the fragmentation of S/IVOC precursors to SOA. The inclusion of these missing emissions and/or chemistry would further impact oxidant levels, which we have shown to be an important source of modeled SOA and formaldehyde. As stated above, the behavior of POA and CO bias suggest that errors in combustion emissions and PBL height cannot fully describe the temperature-dependence of SOA bias, and POA and CO are better indicators of mobile and industrial sources. Formaldehyde may instead serve as a better indicator of SOA production in urban areas where VCPs are important atmospheric constituents. While many factors may contribute to the temperature-dependence of SOA and formaldehyde bias, future work must investigate the importance of these factors and tracking the response of formaldehyde to these changes alongside SOA could provide insight.

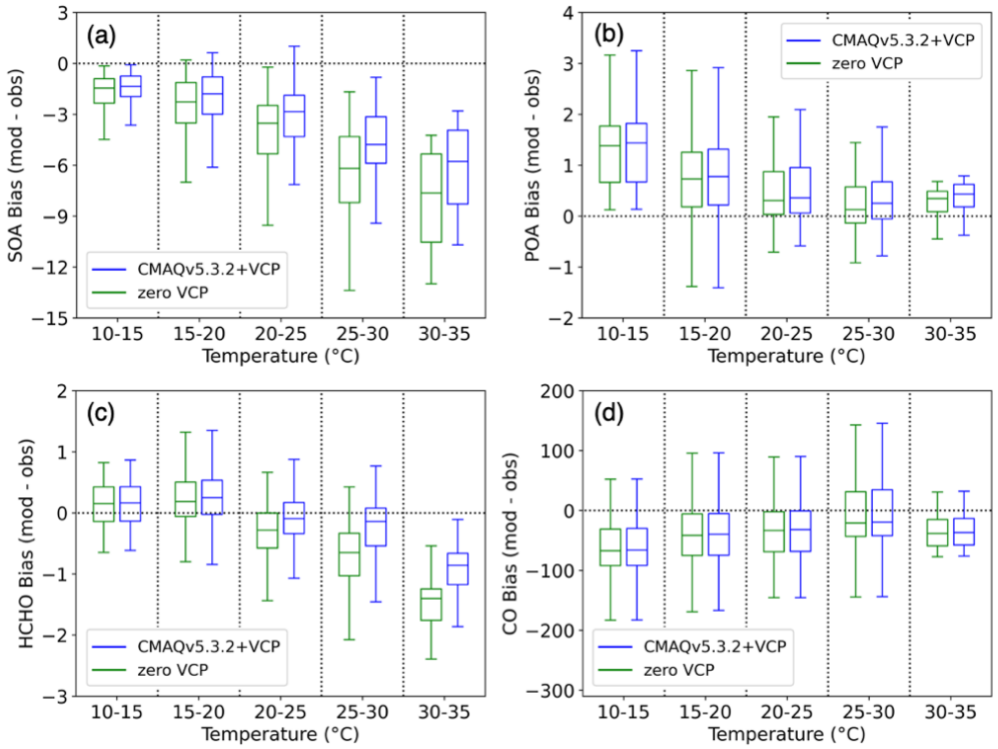

Figure 2.5: Bias (modeled - observed) of hourly concentrations vs. modeled temperature for the zero VCP case (green) and CMAQv5.3.2+VCP case (blue). Hourly concentrations are binned into five temperature ranges of 5°C each and the data in each bin is represented by a box-and-whisker plot. The horizontal midline depicts the median of the data, the edges of the box extend from the lower to upper quartile of the data, and the whiskers extend from the minimum to the maximum of the data. a) PM_1 SOA bias ($\mu g\ m^{-3}$). b) PM_1 POA bias ($\mu g\ m^{-3}$). c) Formaldehyde (HCHO) bias (ppb). d) CO bias (ppb).

2.4 Conclusions and future work

We have shown that VCPs are a major source of SOA in urban atmospheres by introducing updated emissions and VCP-relevant chemistry into CMAQ that better represents SOA precursors emitted from these sources. This includes three new categories of emissions: siloxanes, oxygenated IVOCs, and nonoxygenated IVOCs. VCP emissions from the VCPy framework (Seltzer et al., 2021) were used to parameterize the new chemistry, and the mapping of VCP emitted species to model

surrogates was reviewed and updated based on species structure, volatility, and estimated SOA yield.

The new model chemistry and emissions inventory doubles the predicted SOA concentrations above background levels, increasing the average daily maximum PM_1 SOA concentration by 1.4 μg m^{-3}, equating to a 21% decrease in the absolute mean bias. Most of the increased SOA mass was formed from nonoxygenated IVOC VCP precursors, followed by SOA formed from traditional VOC precursors and oxygenated IVOC precursors, with little SOA formed from siloxanes. Improvements were additionally seen in simulated formaldehyde and ozone concentrations.

Future work should consider how VCP emissions have evolved over time. VCPy version 1.0 requires information about VCP product composition and usage patterns from broad sources, including product surveys, economic statistics, and population distributions. These metrics change over time and will affect both the speciation and emission rates of organic compounds from VCPs. Diurnal and seasonal patterns of VCP emissions should also be updated to reflect more recent observations (Gkatzelis et al., 2021).

The remaining error in VCP-derived SOA predictions may reflect our lack of understanding about the oxidation pathways of low-volatility and/or oxygenated species. More information is needed about the structure, volatility, and reactivity of the products of atmospheric oxidation reactions, plus the impacts of wall loss and NO_x concentrations on SOA yields from experiments, so that models and parameterizations like the VBS can be developed. As this data become available, models can be improved to represent SOA formation from oxygenated precursors and S/IVOCs emitted from VCPs. In addition, the correlation between SOA concentration bias and temperature suggests residual model error is associated with missing sources of S/IVOC emissions, including emissions from asphalt (Khare et al., 2020), combustion sources, or other S/IVOCs that have large potential to form SOA. The formaldehyde bias demonstrates a similar relationship to temperature as the SOA bias, implying that investigations of formaldehyde could provide insight

into VOC chemistry leading to the formation of SOA from VCPs. Including S/IVOC emissions and their atmospheric chemistry will be important for future air quality models.

2.5 Data Availability

CalNex observations are publicly available at https://csl.noaa.gov/groups/csl7/measurements/2010calnex/. The full VCPy dataset is available by downloading VCPyv1.0 at https://doi.org/10.23719/1520157. The SAPRC07TIC_AE7I_VCP speciation profile, CMAQ chemical mechanism source code, and CMAQ output are posted at https://doi.org/10.23719/1522655 (U.S. EPA, 2021b).

2.6 References

AE7I Species Table. (2021). U.S. Environmental Protection Agency. https://github.com/USEPA/CMAQ/blob/72ec4e5681e1ed0b4917792a9a240b0302a303a7/CCTM/src/MECHS/mechanism_information/saprc07tic_ae7i_aq/AE7I_species_table.md (Original work published 2016)

Appel, K. W., Bash, J. O., Fahey, K. M., Foley, K. M., Gilliam, R. C., Hogrefe, C., Hutzell, W. T., Kang, D., Mathur, R., Murphy, B. N., Napelenok, S. L., Nolte, C. G., Pleim, J. E., Pouliot, G. A., Pye, H. O. T., Ran, L., Roselle, S. J., Sarwar, G., Schwede, D. B., … Wong, D. C. (2021). The Community Multiscale Air Quality (CMAQ) model versions 5.3 and 5.3.1: System updates and evaluation. *Geoscientific Model Development*, *14*(5), 2867–2897. https://doi.org/10.5194/gmd-14-2867-2021

Baker, K. R., Carlton, A. G., Kleindienst, T. E., Offenberg, J. H., Beaver, M. R., Gentner, D. R., Goldstein, A. H., Hayes, P. L., Jimenez, J. L., Gilman, J. B., Gouw, J. A. de, Woody, M. C., Pye, H. O. T., Kelly, J. T., Lewandowski, M., Jaoui, M., Stevens, P. S., Brune, W. H., Lin, Y.-H., … Surratt, J. D. (2015). Gas and aerosol carbon in California: Comparison of measurements and model predictions in Pasadena and Bakersfield. *Atmospheric Chemistry and Physics*, *15*(9), 5243–5258. https://doi.org/10.5194/acp-15-5243-2015

Bash, J. O., Baker, K. R., & Beaver, M. R. (2016). Evaluation of improved land use and canopy representation in BEIS v3.61 with biogenic VOC measurements in California. *Geoscientific Model Development*, *9*(6), 2191–2207. https://doi.org/10.5194/gmd-9-2191-2016

Binkowski, F. S., & Roselle, S. J. (2003). Models-3 Community Multiscale Air Quality (CMAQ) model aerosol component 1. Model description. *Journal of Geophysical Research: Atmospheres*, *108*(D6). https://doi.org/10.1029/2001JD001409

Cappa, C. D., & Wilson, K. R. (2012). Multi-generation gas-phase oxidation, equilibrium partitioning, and the formation and evolution of secondary organic aerosol. *Atmospheric Chemistry and Physics*, *12*(20), 9505–9528. https://doi.org/10.5194/acp-12-9505-2012

Charan, S. M., Buenconsejo, R. S., & Seinfeld, J. H. (2020). Secondary organic aerosol yields from the oxidation of benzyl alcohol. *Atmospheric Chemistry and Physics*, *20*(21), 13167–13190. https://doi.org/10.5194/acp-20-13167-2020

Charan, S. M., Huang, Y., Buenconsejo, R. S., Li, Q., Cocker III, D. R., & Seinfeld, J. H. (2021). Secondary Organic Aerosol Formation from the Oxidation of Decamethylcyclopentasiloxane at Atmospherically Relevant OH Concentrations. *Atmospheric Chemistry and Physics Discussions*, 1–17. https://doi.org/10.5194/acp-2021-353

Coggon, M. M., Gkatzelis, G. I., McDonald, B. C., Gilman, J. B., Schwantes, R. H., Abuhassan, N., Aikin, K. C., Arend, M. F., Berkoff, T. A., Brown, S. S., Campos, T. L., Dickerson, R. R., Gronoff, G., Hurley, J. F., Isaacman-VanWertz, G., Koss, A. R., Li, M., McKeen, S. A., Moshary, F., … Warneke, C. (2021). Volatile chemical product emissions enhance ozone and modulate urban chemistry. *Proceedings of the National Academy of Sciences*, *118*(32). https://doi.org/10.1073/pnas.2026653118

Coggon, M. M., McDonald, B. C., Vlasenko, A., Veres, P. R., Bernard, F., Koss, A. R., Yuan, B., Gilman, J. B., Peischl, J., Aikin, K. C., DuRant, J., Warneke, C., Li, S.-M., & de Gouw, J. A. (2018). Diurnal Variability and Emission Pattern of

Decamethylcyclopentasiloxane (D5) from the Application of Personal Care Products in Two North American Cities. *Environmental Science & Technology*, *52*(10), 5610–5618. https://doi.org/10.1021/acs.est.8b00506

Crounse, J. D., Nielsen, L. B., Jørgensen, S., Kjaergaard, H. G., & Wennberg, P. O. (2013). Autoxidation of Organic Compounds in the Atmosphere. *The Journal of Physical Chemistry Letters*, *4*(20), 3513–3520. https://doi.org/10.1021/jz4019207

Donahue, N. M., Epstein, S. A., Pandis, S. N., & Robinson, A. L. (2011). A two-dimensional volatility basis set: 1. organic-aerosol mixing thermodynamics. *Atmospheric Chemistry and Physics*, *11*(7), 3303–3318. https://doi.org/10.5194/acp-11-3303-2011

Ensberg, J. J., Hayes, P. L., Jimenez, J. L., Gilman, J. B., Kuster, W. C., de Gouw, J. A., Holloway, J. S., Gordon, T. D., Jathar, S., Robinson, A. L., & Seinfeld, J. H. (2014). Emission factor ratios, SOA mass yields, and the impact of vehicular emissions on SOA formation. *Atmospheric Chemistry and Physics*, *14*(5), 2383–2397. https://doi.org/10.5194/acp-14-2383-2014

Epstein, S. A., Riipinen, I., & Donahue, N. M. (2010). A Semiempirical Correlation between Enthalpy of Vaporization and Saturation Concentration for Organic Aerosol. *Environmental Science & Technology*, *44*(2), 743–748. https://doi.org/10.1021/es902497z

Gkatzelis, G. I., Coggon, M. M., McDonald, B. C., Peischl, J., Aikin, K. C., Gilman, J. B., Trainer, M., & Warneke, C. (2021). Identifying Volatile Chemical Product Tracer Compounds in U.S. Cities. *Environmental Science & Technology*, *55*(1), 188–199. https://doi.org/10.1021/acs.est.0c05467

Goldstein, A. H., & Galbally, I. E. (2007). Known and Unexplored Organic Constituents in the Earth's Atmosphere. *Environmental Science & Technology*, *41*(5), 1514–1521. https://doi.org/10.1021/es072476p

Griffith, S. M., Hansen, R. F., Dusanter, S., Michoud, V., Gilman, J. B., Kuster, W. C., Veres, P. R., Graus, M., Gouw, J. A. de, Roberts, J., Young, C., Washenfelder, R., Brown, S. S., Thalman, R., Waxman, E., Volkamer, R., Tsai, C., Stutz, J.,

Flynn, J. H., … Stevens, P. S. (2016). Measurements of hydroxyl and hydroperoxy radicals during CalNex-LA: Model comparisons and radical budgets. *Journal of Geophysical Research: Atmospheres*, *121*(8), 4211–4232. https://doi.org/10.1002/2015JD024358

Hayes, P. L., Carlton, A. G., Baker, K. R., Ahmadov, R., Washenfelder, R. A., Alvarez, S., Rappenglück, B., Gilman, J. B., Kuster, W. C., de Gouw, J. A., Zotter, P., Prévôt, A. S. H., Szidat, S., Kleindienst, T. E., Offenberg, J. H., Ma, P. K., & Jimenez, J. L. (2015). Modeling the formation and aging of secondary organic aerosols in Los Angeles during CalNex 2010. *Atmospheric Chemistry and Physics*, *15*(10), 5773–5801. https://doi.org/10.5194/acp-15-5773-2015

Hayes, P. L., Ortega, A. M., Cubison, M. J., Froyd, K. D., Zhao, Y., Cliff, S. S., Hu, W. W., Toohey, D. W., Flynn, J. H., Lefer, B. L., Grossberg, N., Alvarez, S., Rappenglück, B., Taylor, J. W., Allan, J. D., Holloway, J. S., Gilman, J. B., Kuster, W. C., Gouw, J. A. de, … Jimenez, J. L. (2013). Organic aerosol composition and sources in Pasadena, California, during the 2010 CalNex campaign. *Journal of Geophysical Research: Atmospheres*, *118*(16), 9233–9257. https://doi.org/10.1002/jgrd.50530

Hodzic, A., Aumont, B., Knote, C., Lee-Taylor, J., Madronich, S., & Tyndall, G. (2014). Volatility dependence of Henry's law constants of condensable organics: Application to estimate depositional loss of secondary organic aerosols. *Geophysical Research Letters*, *41*(13), 4795–4804. https://doi.org/10.1002/2014GL060649

Huffman, J. A., Docherty, K. S., Mohr, C., Cubison, M. J., Ulbrich, I. M., Ziemann, P. J., Onasch, T. B., & Jimenez, J. L. (2009). Chemically-Resolved Volatility Measurements of Organic Aerosol from Different Sources. *Environmental Science & Technology*, *43*(14), 5351–5357. https://doi.org/10.1021/es803539d

Hyslop, N. P. (2009). Impaired visibility: The air pollution people see. *Atmospheric Environment*, *43*(1), 182–195. https://doi.org/10.1016/j.atmosenv.2008.09.067

Intergovernmental Panel on Climate Change (Ed.). (2014). Anthropogenic and Natural Radiative Forcing. In *Climate Change 2013 – The Physical Science*

Basis: Working Group I Contribution to the Fifth Assessment Report of the Intergovernmental Panel on Climate Change (pp. 659–740). Cambridge University Press. https://doi.org/10.1017/CBO9781107415324.018

Janechek, N. J., Hansen, K. M., & Stanier, C. O. (2017). Comprehensive atmospheric modeling of reactive cyclic siloxanes and their oxidation products. *Atmospheric Chemistry and Physics*, *17*(13), 8357–8370. https://doi.org/10.5194/acp-17-8357-2017

Janechek, N. J., Marek, R. F., Bryngelson, N., Singh, A., Bullard, R. L., Brune, W. H., & Stanier, C. O. (2019). Physical properties of secondary photochemical aerosol from OH oxidation of a cyclic siloxane. *Atmospheric Chemistry and Physics*, *19*(3), 1649–1664. https://doi.org/10.5194/acp-19-1649-2019

Jathar, S. H., Gordon, T. D., Hennigan, C. J., Pye, H. O. T., Pouliot, G., Adams, P. J., Donahue, N. M., & Robinson, A. L. (2014). Unspeciated organic emissions from combustion sources and their influence on the secondary organic aerosol budget in the United States. *Proceedings of the National Academy of Sciences*, *111*(29), 10473–10478. https://doi.org/10.1073/pnas.1323740111

Jathar, S. H., Woody, M., Pye, H. O. T., Baker, K. R., & Robinson, A. L. (2017). Chemical transport model simulations of organic aerosol in southern California: Model evaluation and gasoline and diesel source contributions. *Atmospheric Chemistry and Physics*, *17*(6), 4305–4318. https://doi.org/10.5194/acp-17-4305-2017

Jimenez, J. L., Canagaratna, M. R., Donahue, N. M., Prevot, A. S. H., Zhang, Q., Kroll, J. H., DeCarlo, P. F., Allan, J. D., Coe, H., Ng, N. L., Aiken, A. C., Docherty, K. S., Ulbrich, I. M., Grieshop, A. P., Robinson, A. L., Duplissy, J., Smith, J. D., Wilson, K. R., Lanz, V. A., … Worsnop, D. R. (2009). Evolution of Organic Aerosols in the Atmosphere. *Science*, *326*(5959), 1525–1529. https://doi.org/10.1126/science.1180353

Kaiser, J., Wolfe, G. M., Bohn, B., Broch, S., Fuchs, H., Ganzeveld, L. N., Gomm, S., Häseler, R., Hofzumahaus, A., Holland, F., Jäger, J., Li, X., Lohse, I., Lu, K., Prévôt, A. S. H., Rohrer, F., Wegener, R., Wolf, R., Mentel, T. F., … Keutsch, F.

N. (2015). Evidence for an unidentified non-photochemical ground-level source of formaldehyde in the Po Valley with potential implications for ozone production. *Atmospheric Chemistry and Physics*, *15*(3), 1289–1298. https://doi.org/10.5194/acp-15-1289-2015

Khare, P., & Gentner, D. R. (2018). Considering the future of anthropogenic gas-phase organic compound emissions and the increasing influence of non-combustion sources on urban air quality. *Atmospheric Chemistry and Physics*, *18*(8), 5391–5413. https://doi.org/10.5194/acp-18-5391-2018

Khare, P., Machesky, J., Soto, R., He, M., Presto, A. A., & Gentner, D. R. (2020). Asphalt-related emissions are a major missing nontraditional source of secondary organic aerosol precursors. *Science Advances*, *6*(36), eabb9785. https://doi.org/10.1126/sciadv.abb9785

Levelt, P. F., Joiner, J., Tamminen, J., Veefkind, J. P., Bhartia, P. K., Stein Zweers, D. C., Duncan, B. N., Streets, D. G., Eskes, H., van der A, R., McLinden, C., Fioletov, V., Carn, S., de Laat, J., DeLand, M., Marchenko, S., McPeters, R., Ziemke, J., Fu, D., … Wargan, K. (2018). The Ozone Monitoring Instrument: Overview of 14 years in space. *Atmospheric Chemistry and Physics*, *18*(8), 5699–5745. https://doi.org/10.5194/acp-18-5699-2018

Li, L., & Cocker, D. R. (2018). Molecular structure impacts on secondary organic aerosol formation from glycol ethers. *Atmospheric Environment*, *180*, 206–215. https://doi.org/10.1016/j.atmosenv.2017.12.025

Li, W., Li, L., Chen, C., Kacarab, M., Peng, W., Price, D., Xu, J., & Cocker, D. R. (2018). Potential of select intermediate-volatility organic compounds and consumer products for secondary organic aerosol and ozone formation under relevant urban conditions. *Atmospheric Environment*, *178*, 109–117. https://doi.org/10.1016/j.atmosenv.2017.12.019

Li, Y., Rodier, C., Lea, J. D., Harvey, J., & Kleeman, M. J. (2021). Improving spatial surrogates for area source emissions inventories in California. *Atmospheric Environment*, *247*, 117665. https://doi.org/10.1016/j.atmosenv.2020.117665

Liao, J., Hanisco, T. F., Wolfe, G. M., St. Clair, J., Jimenez, J. L., Campuzano-Jost, P., Nault, B. A., Fried, A., Marais, E. A., Gonzalez Abad, G., Chance, K., Jethva, H. T., Ryerson, T. B., Warneke, C., & Wisthaler, A. (2019). Towards a satellite formaldehyde – in situ hybrid estimate for organic aerosol abundance. *Atmospheric Chemistry and Physics*, *19*(5), 2765–2785. https://doi.org/10.5194/acp-19-2765-2019

Lim, S. S., Vos, T., Flaxman, A. D., Danaei, G., Shibuya, K., Adair-Rohani, H., AlMazroa, M. A., Amann, M., Anderson, H. R., Andrews, K. G., Aryee, M., Atkinson, C., Bacchus, L. J., Bahalim, A. N., Balakrishnan, K., Balmes, J., Barker-Collo, S., Baxter, A., Bell, M. L., … Ezzati, M. (2012). A comparative risk assessment of burden of disease and injury attributable to 67 risk factors and risk factor clusters in 21 regions, 1990–2010: A systematic analysis for the Global Burden of Disease Study 2010. *The Lancet*, *380*(9859), 2224–2260. https://doi.org/10.1016/S0140-6736(12)61766-8

Lu, Q., Murphy, B. N., Qin, M., Adams, P. J., Zhao, Y., Pye, H. O. T., Efstathiou, C., Allen, C., & Robinson, A. L. (2020). Simulation of organic aerosol formation during the CalNex study: Updated mobile emissions and secondary organic aerosol parameterization for intermediate-volatility organic compounds. *Atmospheric Chemistry and Physics*, *20*(7), 4313–4332. https://doi.org/10.5194/acp-20-4313-2020

Luecken, D. J., Napelenok, S. L., Strum, M., Scheffe, R., & Phillips, S. (2018). Sensitivity of Ambient Atmospheric Formaldehyde and Ozone to Precursor Species and Source Types Across the United States. *Environmental Science & Technology*, *52*(8), 4668–4675. https://doi.org/10.1021/acs.est.7b05509

McDonald, B. C., Gouw, J. A. de, Gilman, J. B., Jathar, S. H., Akherati, A., Cappa, C. D., Jimenez, J. L., Lee-Taylor, J., Hayes, P. L., McKeen, S. A., Cui, Y. Y., Kim, S.-W., Gentner, D. R., Isaacman-VanWertz, G., Goldstein, A. H., Harley, R. A., Frost, G. J., Roberts, J. M., Ryerson, T. B., & Trainer, M. (2018). Volatile chemical products emerging as largest petrochemical source of urban organic

emissions. *Science*, *359*(6377), 760–764. https://doi.org/10.1126/science.aaq0524

Milani, A., Al-Naiema, I. M., & Stone, E. A. (2021). Detection of a secondary organic aerosol tracer derived from personal care products. *Atmospheric Environment*, *246*, 118078. https://doi.org/10.1016/j.atmosenv.2020.118078

Murphy, B. N., Nolte, C. G., Sidi, F., Bash, J. O., Appel, K. W., Jang, C., Kang, D., Kelly, J., Mathur, R., Napelenok, S., Pouliot, G., & Pye, H. O. T. (2021). The Detailed Emissions Scaling, Isolation, and Diagnostic (DESID) module in the Community Multiscale Air Quality (CMAQ) modeling system version 5.3.2. *Geoscientific Model Development*, *14*(6), 3407–3420. https://doi.org/10.5194/gmd-14-3407-2021

Murphy, B. N., Woody, M. C., Jimenez, J. L., Carlton, A. M. G., Hayes, P. L., Liu, S., Ng, N. L., Russell, L. M., Setyan, A., Xu, L., Young, J., Zaveri, R. A., Zhang, Q., & Pye, H. O. T. (2017). Semivolatile POA and parameterized total combustion SOA in CMAQv5.2: Impacts on source strength and partitioning. *Atmospheric Chemistry and Physics*, *17*(18), 11107–11133. https://doi.org/10.5194/acp-17-11107-2017

Nussbaumer, C. M., & Cohen, R. C. (2021). Impact of OA on the Temperature Dependence of PM 2.5 in the Los Angeles Basin. *Environmental Science & Technology*, *55*(6), 3549–3558. https://doi.org/10.1021/acs.est.0c07144

Pye, H. O. T., Murphy, B. N., Xu, L., Ng, N. L., Carlton, A. G., Guo, H., Weber, R., Vasilakos, P., Appel, K. W., Budisulistiorini, S. H., Surratt, J. D., Nenes, A., Hu, W., Jimenez, J. L., Isaacman-VanWertz, G., Misztal, P. K., & Goldstein, A. H. (2017). On the implications of aerosol liquid water and phase separation for organic aerosol mass. *Atmospheric Chemistry and Physics*, *17*(1), 343–369. https://doi.org/10.5194/acp-17-343-2017

Pye, H. O. T., Pinder, R. W., Piletic, I. R., Xie, Y., Capps, S. L., Lin, Y.-H., Surratt, J. D., Zhang, Z., Gold, A., Luecken, D. J., Hutzell, W. T., Jaoui, M., Offenberg, J. H., Kleindienst, T. E., Lewandowski, M., & Edney, E. O. (2013). Epoxide Pathways Improve Model Predictions of Isoprene Markers and Reveal Key Role

of Acidity in Aerosol Formation. *Environmental Science & Technology*, *47*(19), 11056–11064. https://doi.org/10.1021/es402106h

Qin, M., Murphy, B. N., Isaacs, K. K., McDonald, B. C., Lu, Q., McKeen, S. A., Koval, L., Robinson, A. L., Efstathiou, C., Allen, C., & Pye, H. O. T. (2021). Criteria pollutant impacts of volatile chemical products informed by near-field modelling. *Nature Sustainability*, *4*(2), 129–137. https://doi.org/10.1038/s41893-020-00614-1

Robinson, A. L., Donahue, N. M., Shrivastava, M. K., Weitkamp, E. A., Sage, A. M., Grieshop, A. P., Lane, T. E., Pierce, J. R., & Pandis, S. N. (2007). Rethinking Organic Aerosols: Semivolatile Emissions and Photochemical Aging. *Science*, *315*(5816), 1259–1262. https://doi.org/10.1126/science.1133061

Ryerson, T. B., Andrews, A. E., Angevine, W. M., Bates, T. S., Brock, C. A., Cairns, B., Cohen, R. C., Cooper, O. R., Gouw, J. A. de, Fehsenfeld, F. C., Ferrare, R. A., Fischer, M. L., Flagan, R. C., Goldstein, A. H., Hair, J. W., Hardesty, R. M., Hostetler, C. A., Jimenez, J. L., Langford, A. O., … Wofsy, S. C. (2013). The 2010 California Research at the Nexus of Air Quality and Climate Change (CalNex) field study. *Journal of Geophysical Research: Atmospheres*, *118*(11), 5830–5866. https://doi.org/10.1002/jgrd.50331

Santoni, G. W., Daube, B. C., Kort, E. A., Jiménez, R., Park, S., Pittman, J. V., Gottlieb, E., Xiang, B., Zahniser, M. S., Nelson, D. D., McManus, J. B., Peischl, J., Ryerson, T. B., Holloway, J. S., Andrews, A. E., Sweeney, C., Hall, B., Hintsa, E. J., Moore, F. L., … Wofsy, S. C. (2014). Evaluation of the airborne quantum cascade laser spectrometer (QCLS) measurements of the carbon and greenhouse gas suite – CO_2, CH_4, N_2O, and CO – during the CalNex and HIPPO campaigns. *Atmospheric Measurement Techniques*, *7*(6), 1509–1526. https://doi.org/10.5194/amt-7-1509-2014

Seinfeld, J. H., & Pandis, S. N. (2016). *Atmospheric Chemistry and Physics: From Air Pollution to Climate Change* (3rd ed.). John Wiley & Sons, Inc.

Seltzer, K. M., Pennington, E., Rao, V., Murphy, B. N., Strum, M., Isaacs, K. K., & Pye, H. O. T. (2021). Reactive organic carbon emissions from volatile chemical

products. *Atmospheric Chemistry and Physics*, *21*(6), 5079–5100. https://doi.org/10.5194/acp-21-5079-2021

Shah, R. U., Coggon, M. M., Gkatzelis, G. I., McDonald, B. C., Tasoglou, A., Huber, H., Gilman, J., Warneke, C., Robinson, A. L., & Presto, A. A. (2020). Urban Oxidation Flow Reactor Measurements Reveal Significant Secondary Organic Aerosol Contributions from Volatile Emissions of Emerging Importance. *Environmental Science & Technology*, *54*(2), 714–725. https://doi.org/10.1021/acs.est.9b06531

Shah, T., Shi, Y., Beardsley, R., & Yarwood, G. (2020). *Speciation Tool User's Guide Version 5.0*. Ramboll US Corporation.

Skamarock, W. C., Klemp, J. B., Dudhia, J., Gill, D. O., & Barker, D. (2008). *A Description of the Advanced Research WRF Version 3* (NCAR/TN-475+STR). University Corporation for Atmospheric Research. http://dx.doi.org/10.5065/D68S4MVH

US EPA, O. (2013, August 1). *Air Quality System (AQS)* [Data and Tools]. US EPA. https://www.epa.gov/aqs

US EPA, O. (2015, June 2). *National Emissions Inventory (NEI)* [Other Policies and Guidance]. US EPA. https://www.epa.gov/air-emissions-inventories/national-emissions-inventory-nei

US EPA Office of Research and Development. (2020). *CMAQ*. Zenodo. https://doi.org/10.5281/zenodo.4081737

Wang, D.-G., Norwood, W., Alaee, M., Byer, J. D., & Brimble, S. (2013). Review of recent advances in research on the toxicity, detection, occurrence and fate of cyclic volatile methyl siloxanes in the environment. *Chemosphere*, *93*(5), 711–725. https://doi.org/10.1016/j.chemosphere.2012.10.041

Wang, Y., Wang, H., Tan, Y., Liu, J., Wang, K., Ji, W., Sun, L., Yu, X., Zhao, J., Xu, B., & Xiong, J. (2021). Measurement of the key parameters of VOC emissions from wooden furniture, and the impact of temperature. *Atmospheric Environment*, 118510. https://doi.org/10.1016/j.atmosenv.2021.118510

Warneke, C., Veres, P., Holloway, J. S., Stutz, J., Tsai, C., Alvarez, S., Rappenglueck, B., Fehsenfeld, F. C., Graus, M., Gilman, J. B., & de Gouw, J. A. (2011). Airborne formaldehyde measurements using PTR-MS: Calibration, humidity dependence, inter-comparison and initial results. *Atmospheric Measurement Techniques*, *4*(10), 2345–2358. https://doi.org/10.5194/amt-4-2345-2011

Woody, M. C., Baker, K. R., Hayes, P. L., Jimenez, J. L., Koo, B., & Pye, H. O. T. (2016). Understanding sources of organic aerosol during CalNex-2010 using the CMAQ-VBS. *Atmospheric Chemistry and Physics*, *16*(6), 4081–4100. https://doi.org/10.5194/acp-16-4081-2016

Wu, Y., & Johnston, M. V. (2017). Aerosol Formation from OH Oxidation of the Volatile Cyclic Methyl Siloxane (cVMS) Decamethylcyclopentasiloxane. *Environmental Science & Technology*, *51*(8), 4445–4451. https://doi.org/10.1021/acs.est.7b00655

Xie, Y., Paulot, F., Carter, W. P. L., Nolte, C. G., Luecken, D. J., Hutzell, W. T., Wennberg, P. O., Cohen, R. C., & Pinder, R. W. (2013). Understanding the impact of recent advances in isoprene photooxidation on simulations of regional air quality. *Atmospheric Chemistry and Physics*, *13*(16), 8439–8455. https://doi.org/10.5194/acp-13-8439-2013

Zhang, Q., Jimenez, J. L., Canagaratna, M. R., Allan, J. D., Coe, H., Ulbrich, I., Alfarra, M. R., Takami, A., Middlebrook, A. M., Sun, Y. L., Dzepina, K., Dunlea, E., Docherty, K., DeCarlo, P. F., Salcedo, D., Onasch, T., Jayne, J. T., Miyoshi, T., Shimono, A., … Worsnop, D. R. (2007). Ubiquity and dominance of oxygenated species in organic aerosols in anthropogenically-influenced Northern Hemisphere midlatitudes. *Geophysical Research Letters*, *34*(13). https://doi.org/10.1029/2007GL029979

Zhao, Y., Hennigan, C. J., May, A. A., Tkacik, D. S., de Gouw, J. A., Gilman, J. B., Kuster, W. C., Borbon, A., & Robinson, A. L. (2014). Intermediate-Volatility Organic Compounds: A Large Source of Secondary Organic Aerosol.

Environmental Science & Technology, *48*(23), 13743–13750. https://doi.org/10.1021/es5035188

Zhao, Y., Nguyen, N. T., Presto, A. A., Hennigan, C. J., May, A. A., & Robinson, A. L. (2015). Intermediate Volatility Organic Compound Emissions from On-Road Diesel Vehicles: Chemical Composition, Emission Factors, and Estimated Secondary Organic Aerosol Production. *Environmental Science & Technology*, *49*(19), 11516–11526. https://doi.org/10.1021/acs.est.5b02841

2.7 Supporting Information

2.7.1 SAPRC07TIC_AE7I_VCP assignment rules

Note: Mapping for SOA and radical chemistry are independently treated. Therefore, double mapping may occur. Rules are based on contents of SMILES, k_{OH}, calculated log(C), number of oxygens (n_O), number of carbons (n_C), and estimated SOA yield.*

SOA Chemistry -

1. If SMILES string contains "Si" (i.e., it's a siloxane or silane), add it fully (fraction = 1.0) to **SILOX**.
2. If a species has a SPECIATE_ID = 9001-9032 (i.e., it's new), follow these rules to assign it fully (fraction = 1.0) to one of the new surrogates. IVOP3/4/5/6/5ARO/6ARO definitions are based on Lu et al. (2020). If a species is mapped to IVOC, NVOL, or NROG (US EPA, 2019), follow these rules to re-assign the existing fraction.
    a. If the species has an estimated SOA yield = 0.0%, assign it to **NONR**.
    b. If the species has $n_O > 0$ and an estimated SOA yield > 0.0%, assign it to **SOAOXY**.
    c. If the species has $n_O = 0$, an estimated SOA yield > 0.0%, and has log(C*) > 6.5, assign it to **SOAALK** (both aromatic and aliphatic species).
    d. If the species has $n_O = 0$, an estimated SOA yield > 0.0%, is aromatic, and has $5.5 < \log(C^*) < 6.5$, assign it to **IVOCP6ARO**.

e. If the species has $n_O = 0$, an estimated SOA yield > 0.0%, is aromatic, and has log(C*) < 5.5, assign it to **IVOCP5ARO**.
f. If the species has $n_O = 0$, an estimated SOA yield > 0.0%, is aliphatic, and has 5.5 < log(C*) < 6.5, assign it to **IVOCP6**.
g. If the species has $n_O = 0$, an estimated SOA yield > 0.0%, is aliphatic, and has 4.5 < log(C*) < 5.5, assign it to **IVOCP5**.
h. If the species has $n_O = 0$, an estimated SOA yield > 0.0%, is aliphatic, and has 3.5 < log(C*) < 4.5, assign it to **IVOCP4**.
i. If the species has $n_O = 0$, an estimated SOA yield > 0.0%, is aliphatic, and has log(C*) < 3.5, assign it to **IVOCP3**.

3. If an existing species is mapped to ALK4/5 and has an estimated SOA yield > 0.0%, assign it fully (fraction = 1.0) to **SOAALK**.
4. Four species are uniquely treated:
   a. Divinyl Benzene (SPECIATE_ID = 2081): assign fully (fraction = 1.0) to **ARO2MN**.
   b. Styrene (SPECIATE_ID = 698): assign fully (fraction = 1.0) to **ARO2MN**.
   c. Dimethyl Succinate (SPECIATE_ID = 420): assign fully (fraction = 1.0) to **SOAOXY**.
   d. Fragrances (SPECIATE_ID = 467): assign fully (fraction = 1.0) to **IVOCP6** and fully (fraction = 1.0) to **ALK5**.
5. Maintain all other original SAPRC07TC_AE7 assignments.
6. Replace all ARO2 assignments with ARO2MN to match CMAQ's EmissCtrl naming.

Radical Chemistry -

1. If SMILES string contains "Si" (i.e., it's a siloxane or silane), ignore. According to the SAPRC07 database (Carter, 2010), siloxanes have a negative MIR. No applicable surrogate available in SAPRC07.
2. If a species has a SPECIATE_ID = 9001-9032 (i.e., it's new), follow these rules to assign it fully (fraction = 1.0) to ALK1/2/3/4/5. If a species is mapped

to IVOC, NVOL, or NROG, follow these rules to re-assign the existing fraction. k_{OH} rules are based on definitions in CMAQ (US EPA Office of Research and Development, 2020).

a. If 1.35E-13 < k_{OH} < 3.38E-13 cm^3 $molec^{-1}$ sec^{-1}, assign to **ALK1**.
b. If 3.38E-13 < k_{OH} < 1.69E-12 cm^3 $molec^{-1}$ sec^{-1}, assign to **ALK2**.
c. If 1.69E-12 < k_{OH} < 3.38E-12 cm^3 $molec^{-1}$ sec^{-1}, assign to **ALK3**.
d. If 3.38E-12 < k_{OH} < 6.77E-12 cm^3 $molec^{-1}$ sec^{-1}, assign to **ALK4**.
e. If 6.77E-12 > k_{OH}, assign to **ALK5**.

3. Maintain all other original SAPRC07TC_AE7 assignments.

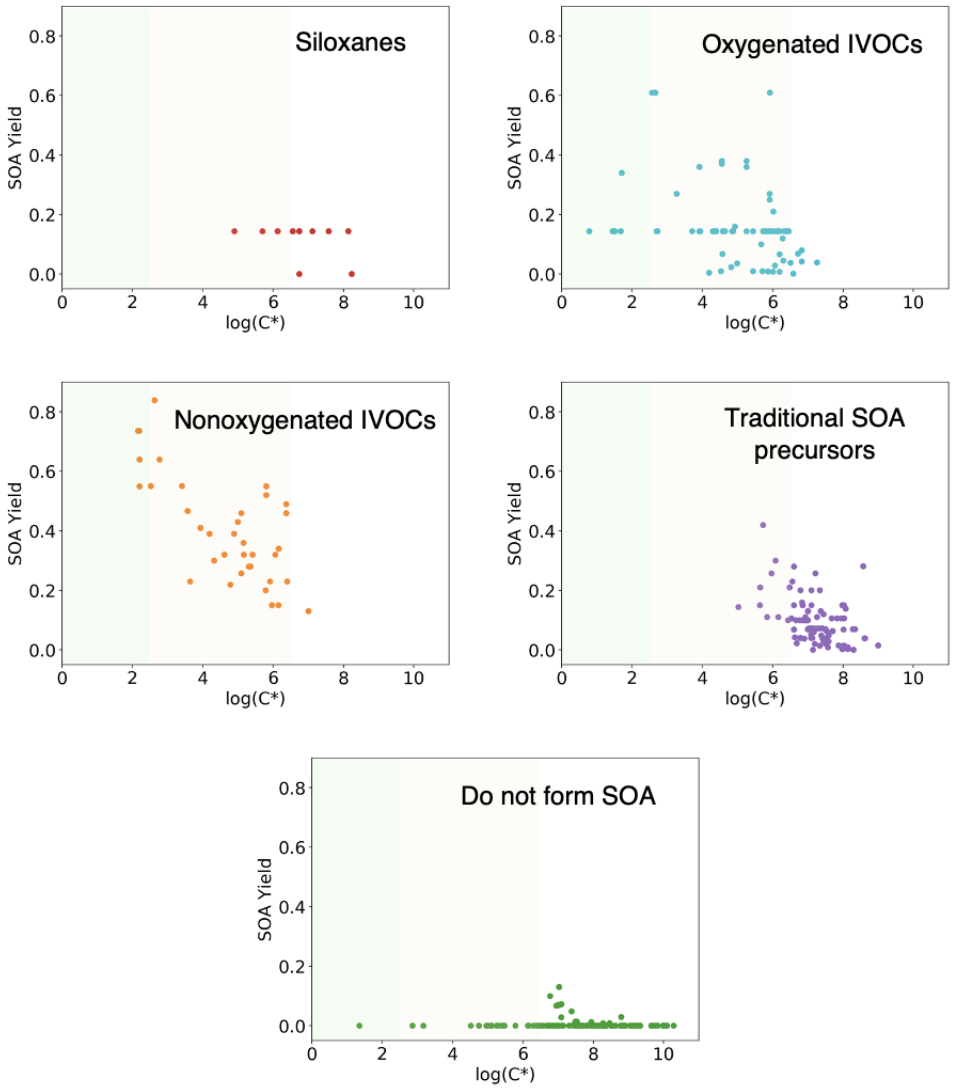

Figure 2.S1: SOA mass yield vs. log(C*) for 401 VCPy species categorized by their SAPRC07TC_AE7_VCP assignments. White shading indicates the range of VOCs with log(C*) > 6.5, orange shading indicates the range of IVOCs with 2.5 < log(C*) < 6.5, and green shading indicates the range of SVOCs with log(C*) < 2.5. SOA yield increases with decreasing volatility. The method of assigning SOA yields to each species is described in Seltzer et al. (2021) and the SOA yield data is provided in Presto et al. (2010), Tkacik et al. (2012), Cappa & Wilson (2012), McDonald et al. (2018), Ng et al. (2007), Hildebrandt et al. (2009), Janechek et al. (2019), Wu & Johnston (2017), Li & Cocker (2018), and Charan et al. (2020).

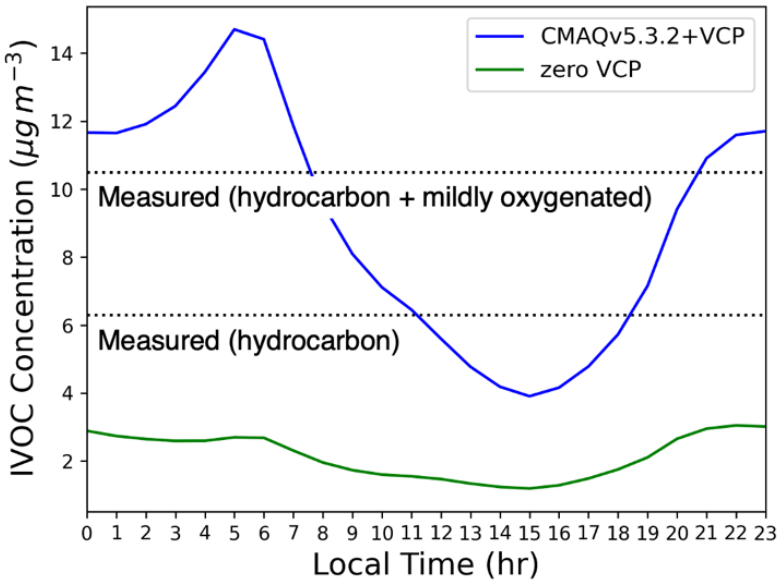

Figure 2.S2: Average hourly concentrations of gas-phase IVOCs (oxygenated + nonoxygenated) predicted by the model for the zero VCP (green) and CMAQv5.3.2 (blue) cases. Horizontal lines depict campaign-average values for hydrocarbon-like IVOCs (6.3 μg m^{-3}) and oxygenated + hydrocarbon-like IVOCs (10.5 μg m^{-3}) from Zhao et al. (2014).

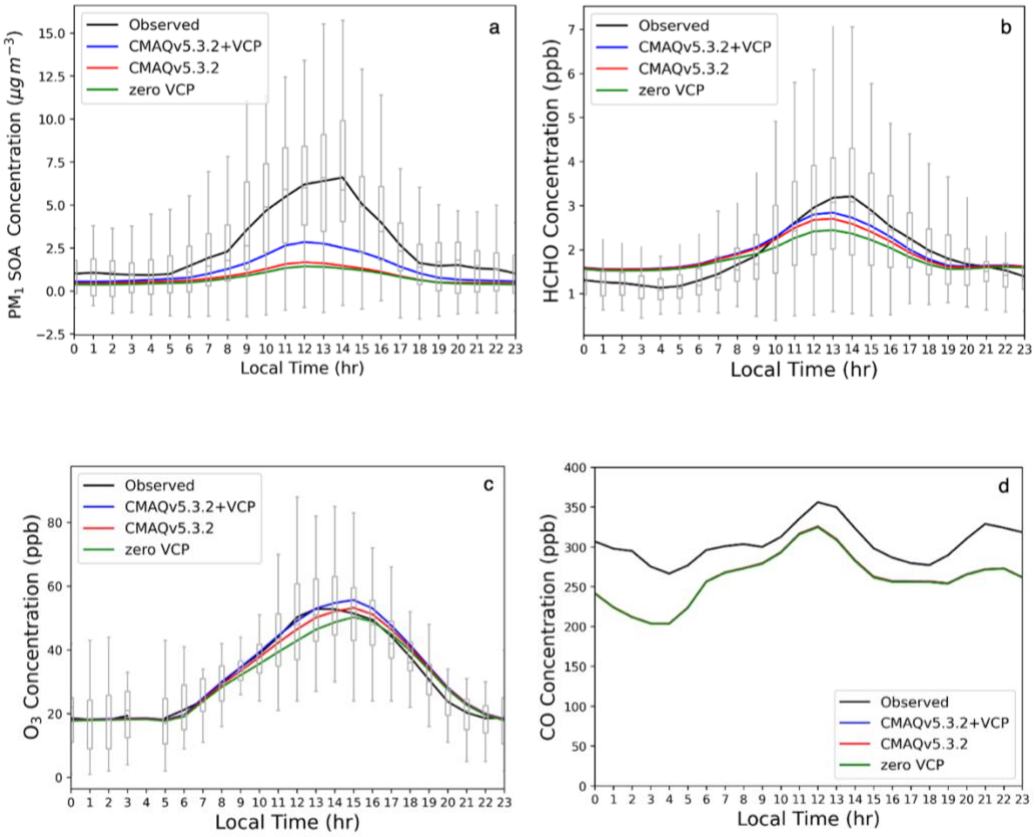

Figure 2.S3: Average hourly concentrations observed and simulated by all three modeling cases May 15–June 15. Box and whiskers show all hourly concentrations observed at the Pasadena CalNex site. a) Background-corrected PM_1 SOA. A constant background value was removed from all observed concentrations according to the method in Hayes et al. (2015). The background value of each simulation was determined by averaging the lower 50% of hourly concentrations from 00:00 LT to 04:00 LT and subtracting that from each curve. b) Formaldehyde (HCHO). Background values were not removed. c) Ozone (O_3). Background values were not removed. d) Carbon monoxide (CO). Background values were not removed. Box and whiskers were removed because they obscured the y-axis scale.

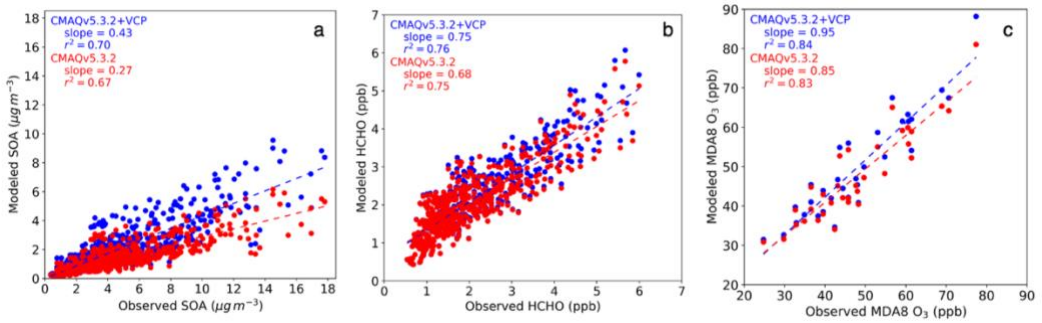

Figure 2.S4: Modeled concentrations predicted by CMAQv5.3.2 case (red) and CMAQv5.3.2+VCP case (blue) vs. observations from the CalNex Pasadena ground site. a) Hourly PM_1 SOA. b) Hourly formaldehyde (HCHO). c) MDA8 O_3. Background values were not removed from any panels.

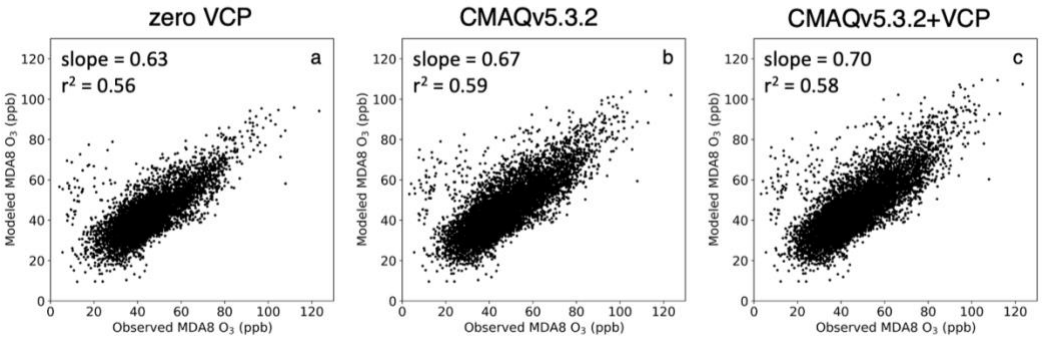

Figure 2.S5: Modeled vs. observed MDA8 O_3 concentration for 178 routine monitoring sites from the AQS monitoring network in California for the zero VCP case (a), CMAQv5.3.2 case (b), and CMAQv5.3.2+VCP case (c).

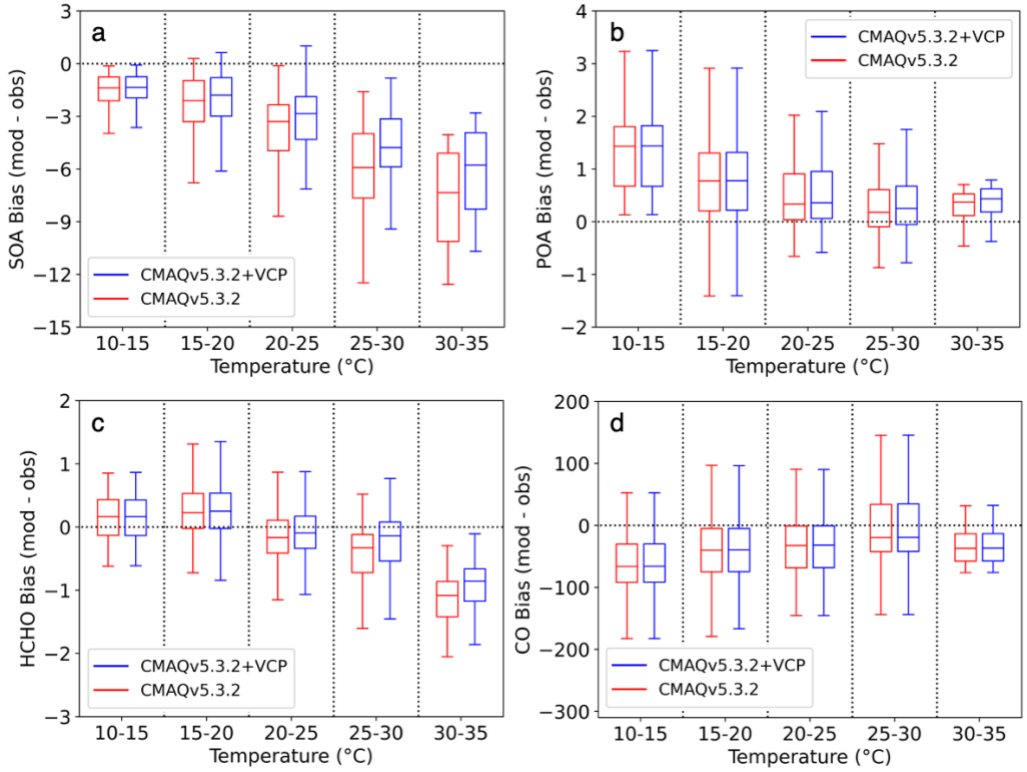

Figure 2.S6: Bias (modeled - observed) of hourly concentrations vs. hourly modeled temperature for the CMAQv5.3.2 case (red) and CMAQv5.3.2+VCP case (blue). a) PM_1 SOA bias (μg m^{-3}). b) PM_1 POA bias (μg m^{-3}). c) Formaldehyde (HCHO) bias (ppb). d) CO bias (ppb).

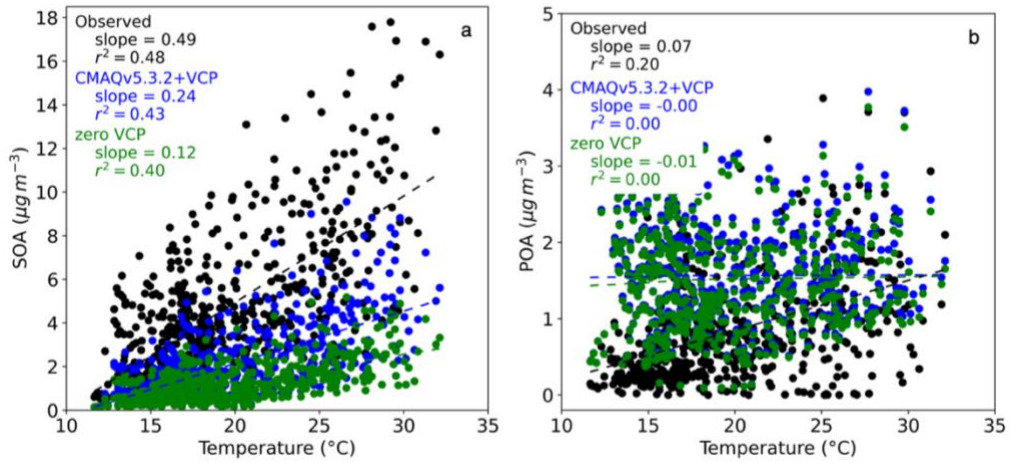

Figure 2.S7: PM_1 SOA (a) and PM_1 POA (b) vs. temperature for zero VCP case (green), CMAQv5.3.2+VCP case (blue), and CalNex observations (black). Background values were not removed from any concentrations.

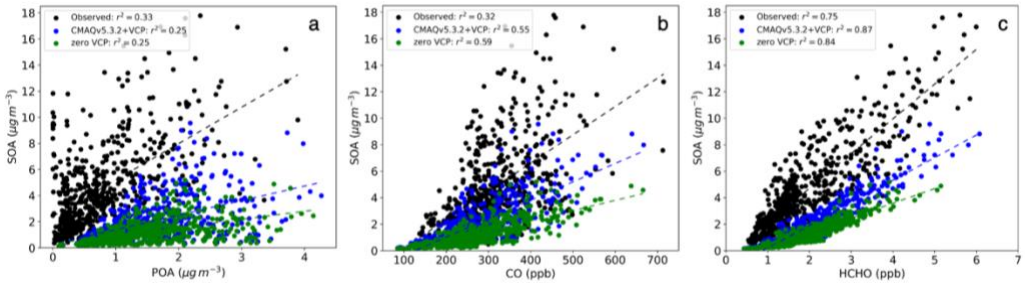

Figure 2.S8: PM_1 SOA vs. PM_1 POA (a), PM_1 SOA vs. CO (b), PM_1 SOA vs. HCHO (c) for zero VCP case (green), CMAQv5.3.2+VCP case (blue), and CalNex observations (black). Background values were not removed from any concentrations.

2.7.2 References

Cappa, C. D., & Wilson, K. R. (2012). Multi-generation gas-phase oxidation, equilibrium partitioning, and the formation and evolution of secondary organic aerosol. *Atmospheric Chemistry and Physics*, *12*(20), 9505–9528. https://doi.org/10.5194/acp-12-9505-2012

Carter, W. P. L. (2010). Development of the SAPRC-07 chemical mechanism. *Atmospheric Environment*, *44*(40), 5324–5335. https://doi.org/10.1016/j.atmosenv.2010.01.026

Charan, S. M., Buenconsejo, R. S., & Seinfeld, J. H. (2020). Secondary organic aerosol yields from the oxidation of benzyl alcohol. *Atmospheric Chemistry and Physics*, *20*(21), 13167–13190. https://doi.org/10.5194/acp-20-13167-2020

Hayes, P. L., Carlton, A. G., Baker, K. R., Ahmadov, R., Washenfelder, R. A., Alvarez, S., Rappenglück, B., Gilman, J. B., Kuster, W. C., de Gouw, J. A., Zotter, P., Prévôt, A. S. H., Szidat, S., Kleindienst, T. E., Offenberg, J. H., Ma, P. K., & Jimenez, J. L. (2015). Modeling the formation and aging of secondary organic aerosols in Los Angeles during CalNex 2010. *Atmospheric Chemistry and Physics*, *15*(10), 5773–5801. https://doi.org/10.5194/acp-15-5773-2015

Hildebrandt, L., Donahue, N. M., & Pandis, S. N. (2009). High formation of secondary organic aerosol from the photo-oxidation of toluene. *Atmospheric Chemistry and Physics*, *9*(9), 2973–2986. https://doi.org/10.5194/acp-9-2973-2009

Janechek, N. J., Marek, R. F., Bryngelson, N., Singh, A., Bullard, R. L., Brune, W. H., & Stanier, C. O. (2019). Physical properties of secondary photochemical aerosol from OH oxidation of a cyclic siloxane. *Atmospheric Chemistry and Physics*, *19*(3), 1649–1664. https://doi.org/10.5194/acp-19-1649-2019

Li, L., & Cocker, D. R. (2018). Molecular structure impacts on secondary organic aerosol formation from glycol ethers. *Atmospheric Environment*, *180*, 206–215. https://doi.org/10.1016/j.atmosenv.2017.12.025

Lu, Q., Murphy, B. N., Qin, M., Adams, P. J., Zhao, Y., Pye, H. O. T., Efstathiou, C., Allen, C., & Robinson, A. L. (2020). Simulation of organic aerosol formation during the CalNex study: Updated mobile emissions and secondary organic aerosol parameterization for intermediate-volatility organic compounds. *Atmospheric Chemistry and Physics*, *20*(7), 4313–4332. https://doi.org/10.5194/acp-20-4313-2020

McDonald, B. C., Gouw, J. A. de, Gilman, J. B., Jathar, S. H., Akherati, A., Cappa, C. D., Jimenez, J. L., Lee-Taylor, J., Hayes, P. L., McKeen, S. A., Cui, Y. Y., Kim, S.-W., Gentner, D. R., Isaacman-VanWertz, G., Goldstein, A. H., Harley, R. A., Frost, G. J., Roberts, J. M., Ryerson, T. B., & Trainer, M. (2018). Volatile chemical products emerging as largest petrochemical source of urban organic emissions. *Science*, *359*(6377), 760–764. https://doi.org/10.1126/science.aaq0524

Ng, N. L., Kroll, J. H., Chan, A. W. H., Chhabra, P. S., Flagan, R. C., & Seinfeld, J. H. (2007). Secondary organic aerosol formation from *m*-xylene, toluene, and benzene. *Atmospheric Chemistry and Physics*, *7*(14), 3909–3922. https://doi.org/10.5194/acp-7-3909-2007

Presto, A. A., Miracolo, M. A., Donahue, N. M., & Robinson, A. L. (2010). Secondary Organic Aerosol Formation from High-NOx Photo-Oxidation of Low Volatility Precursors: N-Alkanes. *Environmental Science & Technology*, *44*(6), 2029–2034. https://doi.org/10.1021/es903712r

Seltzer, K. M., Pennington, E., Rao, V., Murphy, B. N., Strum, M., Isaacs, K. K., & Pye, H. O. T. (2021). Reactive organic carbon emissions from volatile chemical products. *Atmospheric Chemistry and Physics*, *21*(6), 5079–5100. https://doi.org/10.5194/acp-21-5079-2021

Tkacik, D. S., Presto, A. A., Donahue, N. M., & Robinson, A. L. (2012). Secondary Organic Aerosol Formation from Intermediate-Volatility Organic Compounds: Cyclic, Linear, and Branched Alkanes. *Environmental Science & Technology*, *46*(16), 8773–8781. https://doi.org/10.1021/es301112c

US EPA, O. (2019, July 16). *SPECIATE 5.1 and 5.0 Addendum and Final Report* [Other Policies and Guidance]. US EPA. https://www.epa.gov/air-emissions-modeling/speciate-51-and-50-addendum-and-final-report

US EPA Office of Research and Development. (2020). *CMAQ*. Zenodo. https://doi.org/10.5281/zenodo.4081737

Wu, Y., & Johnston, M. V. (2017). Aerosol Formation from OH Oxidation of the Volatile Cyclic Methyl Siloxane (cVMS) Decamethylcyclopentasiloxane.

Environmental Science & Technology, *51*(8), 4445–4451. https://doi.org/10.1021/acs.est.7b00655

Zhao, Y., Hennigan, C. J., May, A. A., Tkacik, D. S., de Gouw, J. A., Gilman, J. B., Kuster, W. C., Borbon, A., & Robinson, A. L. (2014). Intermediate-Volatility Organic Compounds: A Large Source of Secondary Organic Aerosol. *Environmental Science & Technology*, *48*(23), 13743–13750. https://doi.org/10.1021/es5035188

Chapter 3

DEVELOPMENT OF A NEW MODEL FRAMEWORK FOR LOS ANGELES METEOROLOGY AND AIR QUALITY IN LOS ANGELES IN 2020

This work is in progress and will be completed and submitted for publication within the next few months.

3.0 Abstract

The Los Angeles Basin has high anthropogenic emissions and unique meteorological phenomena which makes it an important study location for understanding the chemistry of atmospheric pollutants and impact of mitigation policies. Chemical transport models (CTMs) provide regional-scale input by taking as input meteorology, emissions, and land surface information to represent complex chemical and physical processes. Here we develop those model inputs and new chemical frameworks to represent the Los Angeles Basin in 2020. We developed state-of-the-science inputs of meteorology, volatile chemical product (VCP) emissions, onroad vehicle emissions, biogenic emissions, and other anthropogenic emissions to be used in the Community Multiscale Air Quality (CMAQ) model with new chemistry to represent secondary organic aerosol (SOA) and ozone formation from VCPs and onroad vehicles. The application of these inputs are discussed in Chapter 4.

3.1 Background

The Los Angeles (LA) area is a highly-studied region for air quality research due to its high urban emissions and unique meteorology. The greater LA area is often referred to as the LA Basin because the sprawling urban area is surrounded by ocean to the west and mountains to the east, north, and south (Figure 3.1). This traps pollutants into a basin, where intense solar radiation leads to the formation of secondary pollutants such as ozone (O_3) and secondary organic aerosol (SOA). The precursors to these secondary species are gases and aerosol emitted from both human

and natural sources. Natural emissions from trees, soil, wildfires, and more are low in urban areas but can be transported from the ocean or from outside the basin. Anthropogenic emissions dominate the total mass of emitted material and include sources such as vehicles, cooking, oil and gas extraction, agriculture, and volatile chemical products (VCPs), which were introduced in Chapter 2.

Figure 3.1: Los Angeles Basin.

The composition of emissions have changed over time as vehicles have become cleaner, allowing other sources of emissions to become more important. In particular, VCPs are predicted to make up over half of anthropogenic emissions (Qin et al., 2021). Despite these changes, modeling studies which focus on Los Angeles typically model 2010 to overlap with the CalNex campaign (Ryerson et al., 2013). We lack detailed modeling studies of more recent years, and obtaining a model framework for contemporary LA is one of our goals.

The modeling period covers April, 2020, during the strict COVID-19 lockdown regulations in LA. Onroad vehicle miles traveled (VMT) declined significantly during this month as many people remained at home, and this altered the composition of anthropogenic emissions and resulting pollutant levels (Parker et al., 2020). However, this time period also overlapped with many weather patterns that are unusual to this spring period in LA, namely a rainy period and a very hot period. Untangling the relative impacts of decreased emissions versus meteorology is possible using the framework we develop here. Many studies in other parts of the

world investigated the impact of reduced vehicle emissions, specifically nitrogen oxide (NO_x) decreases, and found O_3 increases in many heavily polluted areas because of the O_3 dependence on NO_x reductions in a NO_x-saturated regime. In contrast, some regions saw O_3 decreases as NO_x decreased, representative of a NO_x-limited regime. Recent work suggests that LA may be transitioning from NO_x-saturated to NO_x-limited or NO_x-insensitive, and we aim to understand this at multiple locations throughout the basin (Laughner & Cohen, 2019; Parker et al., 2020).

In this work, we develop a model framework to represent the LA Basin in 2020. We develop CMAQ model inputs which represent meteorology, anthropogenic emissions, natural emissions, and land surface properties. This framework combines state-of-the-science models in all categories to provide the newest and most accurate representation of the LA atmosphere. The model configurations described here can be used by other researchers to develop similar simulations in other locations throughout the United States, and the model inputs and outputs used in this study will be publicly available in a future publication for use by others.

3.2 Model Development

The model framework is summarized in Figure 3.2 and described in detail below.

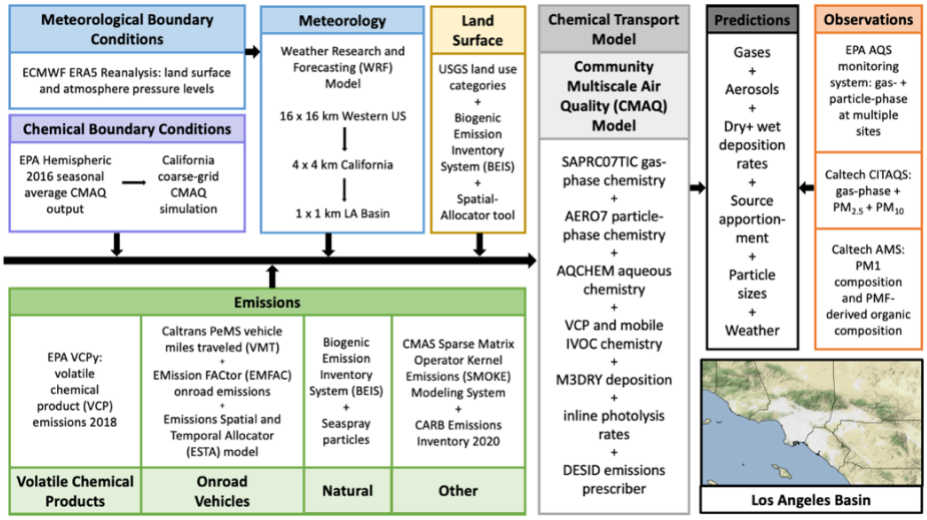

Figure 3.2: Model framework.

3.2.1 Meteorology

Meteorological simulations are performed using the Weather Research and Forecasting (WRF) Model (Skamarock et al., 2008). WRF is a numerical model that takes as input climatological data measured on a coarse-scale grid and predicts weather patterns on a finer scale using theoretical and empirical schemes. We use climatological data from the ERA5 Reanalysis Dataset (Hersbach et al., 2018), which contains hourly data on a 0.25° x 0.25° grid at the surface and on 37 pressure levels from 100 to 1 hPa. We configure WRF to use three nested domains to resample and simulate the meteorological variables from the input resolution to 16-km, 4-km, and then 1-km resolution (Figure 3.3). WRF simulates variables such as temperature, pressure, wind speed, precipitation rates, albedo, soil properties, and water content on a 3D grid, which are used in the chemical transport model (CTM) to calculate transport of pollutants, solar irradiation, and deposition.

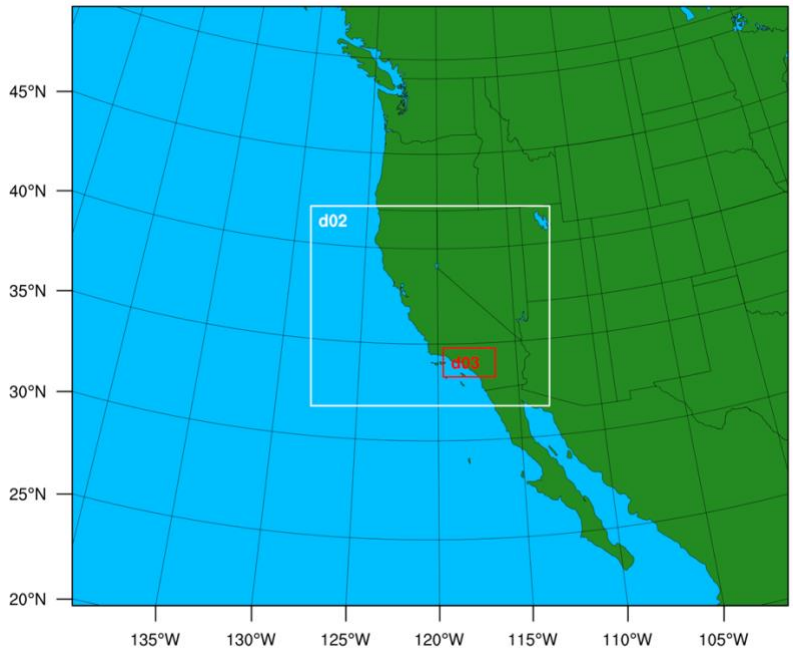

Figure 3.3: Three nested domains used in the WRF simulations. The outer domain has a resolution of 16 km x 16 km, the middle domain has a resolution of 4 km x 4 km, and the inner domain has a resolution of 1 km x 1km.

3.2.2 Chemical Transport Model (CTM)

3.2.2.1 Base model configuration

The Community Multiscale Air Quality (CMAQ) model is a CTM which predicts the hourly concentrations of atmospheric pollutants by simulating the emissions, transport, and chemical transformation of many species, as described in Chapter 1. We use CMAQ version 5.3.2 (US EPA Office of Research and Development, 2020), which is documented and evaluated in Appel et al. (2021). The gas-phase chemical mechanism used is SAPRC07TIC (Carter, 2010), the organic aerosol-phase chemical mechanism is AERO7 (Pye et al., 2013; Xie et al., 2013), the inorganic aerosol-phase chemical mechanism is ISORROPIA II (Fountoukis & Nenes, 2007), and the aqueous-phase chemical mechanism used is the Asymmetric Convection Model (ACM) version 2 (Binkowski & Roselle, 2003). The M3Dry module is the air-surface exchange module used to represent the dry deposition of gas- and particle-phase species (Pleim & Ran, 2011; Appel et al., 2021) and uses the Noah land surface model (Alapaty et al., 2008).

CMAQ includes the Detailed Emissions Scaling, Isolation, and Diagnostic (DESID) and Integrated Source Apportionment Method (ISAM) modules to aid in understanding the source apportionment of atmospheric pollutants. DESID allows for the separation of emissions inputs into multiple categories, the creation of chemical families, and complex scaling methods (Murphy et al., 2021). The scaling methods can be used to add, remove, or scale emissions of specified pollutants from individual emissions streams, which simplifies the process of modifying emissions and will be used in our source apportionment sensitivity simulations explained in Chapter 4. ISAM calculates the fractional contribution of multiple sources to concentrations of ozone and its precursors, all within a single simulation (Kwok et al., 2013; Kwok et al., 2015). For the concentrations of ozone, VOCs, and nitrogen-containing species, the ISAM module calculates the contribution from each emission source, initial conditions, boundary conditions, and transport. The DESID and ISAM modules were released with the newest version of CMAQ and will be used to

understand the contribution of various sources to ozone, NO_x, VOCs, and aerosol species, as described further in Chapter 4.

3.2.2.2 Chemical mechanism updates

The SAPRC07TIC_AE7I chemical mechanism was updated to include the emissions and chemistry of volatile chemical product (VCP) species and IVOCs from onroad mobile sources. The VCP emissions and chemistry treatment was described in Chapter 2 and Pennington et al. (2021). The onroad mobile IVOC chemistry was described in Q. Lu et al. (2020) and updated in the model by me. The SOA chemical mechanism is summarized in Figure 2.1.

3.2.3 Emissions

3.2.3.1 Onroad vehicles

Onroad mobile emissions have historically been the most important source of atmospheric pollution in the LA Basin, but this has evolved as vehicles have become cleaner (Khare & Gentner, 2018). Onroad vehicles can be separated into two categories, light duty and heavy duty, based on the weight of the vehicle. Light duty vehicles are smaller, tend to be passenger cars, and tend to use gasoline fuel. On the other hand, heavy duty vehicles are larger, tend to be used for transport, and tend to use diesel fuel. These categories are represented separately in the model because there has been historical interest in understanding what class of vehicles and fuel to target for emissions regulations (e.g., Bahreini et al., 2012; Ensberg et al., 2014; Gentner et al., 2017; Q. Lu et al., 2020). Additionally, because of the different uses of these types of vehicles, their driving and therefore emissions patterns differ spatially and temporally.

Onroad mobile emissions are represented by the EMission FACtor (EMFAC2017) emissions inventory and model projected to year 2020 (California Air Resources Board, 2018). The projection to year 2020 includes 2020-specific meteorological effects on emission rates. The Emissions Spatial and Temporal Allocator (ESTA) model uses 1 km x 1 km spatial surrogates and California Vehicle Activity Database

(CalVAD) temporal surrogates (Ritchie & Tok, 2016) to calculate hourly, gridded emissions on the LA domain. The speciation profiles used in ESTA include the surrogate NMOG (non-methane organic gases), but this surrogate is unused in SAPRC07TIC so these emissions are ultimately lost in the chemistry in CMAQ. To re-incorporate these emissions, the method of Q. Lu et al. (2020) was used to distribute the NMOG mass to nonoxygenated IVOC surrogates.

EMFAC and ESTA were not designed to capture the effect of COVID-19 policies on vehicle use, so we modified the onroad emissions to capture those changes. The California Performance Measurement System (PeMS) uses in-situ detectors distributed throughout California to measure vehicle usage metrics (Caltrans, 2020). One such metric is vehicle miles traveled (VMT), which measures the miles traveled by different vehicle types, e.g., light and heavy duty vehicles. VMT changed directly in response to COVID-19 policies and human behavior changes, so it can be used to reduce onroad emissions in response to the pandemic.

3.2.3.2 VCPs

VCP emissions are predicted using the VCPy model framework (Seltzer, Pennington, et al., 2021), described in Chapter 2 and Appendix D. VCPy version 1.1 (Seltzer, Murphy, et al., 2021) was used to calculate VOC emission rates for 2018 over the contiguous United States (CONUS) on a 4 km x 4 km grid, which we regridded to 1 km x 1 km to fit the LA domain grid. The year 2018 emissions are assumed to be representative of year 2020 emissions within the range of uncertainty present in VCPy, but sensitivity analyses will be performed to understand the impact of VCP emissions on air quality (Chapter 4).

3.2.3.3 Natural

Natural emissions are treated in-line in CMAQ using land surface descriptive files generated using the Spatial-Allocator tool (US EPA, 2017/2022). Gas-phase biogenic emissions and particle-phase seaspray emissions are modeled using the Biogenic Emission Inventory System (BEIS) version 3.6.1 (Bash et al., 2016).

3.2.3.4 Other emission sources

All other emissions are calculated using the California Air Resources Board (CARB) emissions inventory (CARB, 2020). The emissions inventory includes data from sources including offroad vehicles, agriculture, oil & gas production, industrial, and other sources. Annual emission rates were calculated for base year 2017 and scaled to year 2020 using the California Emissions Projection Analysis Model (CEPAM) growth and control data (CARB, 2020). The inventory is processed in the Sparse Matrix Operator Kernel Emissions (SMOKE) model version 4.8 (CMAS, 2020) using spatial and temporal surrogates from 2019. SMOKE calculates both gridded area source emissions as well as point source emissions from individual smokestacks.

3.2.4 Initial and boundary conditions

A nested modeling domain setup was used to represent the boundary conditions for the Los Angeles Basin. The Los Angeles Basin is represented by the innermost domain shown in Figure 3.3, has a resolution of 1 km x 1 km, and is the domain of interest for this project. The initial and boundary conditions for the LA domain were provided by a coarse-grid CMAQ simulation performed over a larger domain (Figure 3.4b). The outer domain covering California has a resolution of 4 km x 4 km and its air quality was simulated using the WRF and CMAQ scenarios described in Sections 3.2.1 and 3.2.2. The emissions for this domain match the emissions described in Jiang et al. (2021). Publicly-available seasonal average hemispheric CMAQ output was used as initial and boundary conditions for the California domain (Hogrefe et al., 2021). The CMAQ predictions from the coarse-grid California domain were used as initial and boundary conditions for the inner, finer-resolution LA domain.

3.3 Model Framework Evaluation

3.3.1 Observational data

Observational data were obtained from the EPA Air Quality System (AQS), a routine monitoring network which collects data throughout the modeling domain of temperature, relative humidity, wind speed, wind direction, O_3, NO, NO_2, CO, SO_2,

PM_{10}, $PM_{2.5}$, and select VOCs (US EPA, 2013). The monitoring site locations in the LA and California domains are shown in Figure 3.4a and b, respectively.

Figure 3.4: EPA AQS monitoring site locations (red markers) located in the a) LA modeling domain and b) California modeling domain. Black lines represent county lines.

Multiple statistics will be used to compare modeled data to observed data. These are mean bias (MB), normalized mean bias (NMB), root mean square error (RMSE) and r^2 (the square of the Pearson correlation coefficient), defined below. In these equations, M is modeled data, O is observed data, $\bar{M}$ is the mean of the modeled data, $\bar{O}$ is the mean of the observed data, and N is the number of data points.

$$MB = \frac{1}{N}\sum_{1}^{N}(M - O)$$

$$NMB = \frac{\sum_1^N (M - O)}{\sum_1^N O}\ x\ 100\%$$

$$RMSE = \sqrt{\frac{1}{N}\sum_{1}^{N}(M - O)^2}$$

$$r^2 = \frac{(\sum_1^N (M - \bar{M})(O - \bar{O}))^2}{\sum_1^N (M - \bar{M})^2 \sum_1^N (O - \bar{O})^2}$$

3.3.2 Meteorology

WRF predictions are illustrated spatially in Figure 3.5 and some important features emerge. The data in Figure 3.5 are either constant (terrain height, land use index) or averaged over the month of April, 2020 (surface temperature, relative humidity). The terrain height (Figure 3.5a) shows the mountainous regions that surround the LA Basin. Relative humidity (Figure 3.5d) is highest near the coast and decreases inland. Surface temperature (Figure 3.5c) is highest in the LA Basin at low elevation. The vertical temperature profile in the LA Basin often displays a unique quality which causes an inversion layer, in which temperature increases with height. This is atmospherically very stable and so little convection occurs, preventing the transport of pollutants up and out of the Basin. So, species are "trapped" in the Basin, allowing for long chemical aging to occur (R. Lu & Turco, 1995). Much of the Basin at low altitude and high temperature is urban (Figure 3.5b). The combination of the inversion layer and high urban emissions exacerbates the poor air quality in the LA Basin.

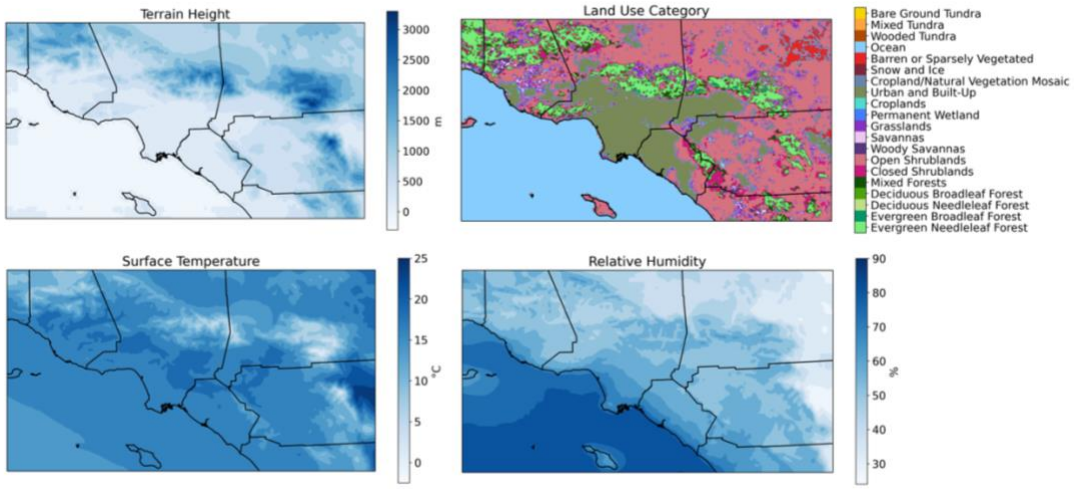

Figure 3.5: WRF predictions of a) terrain height (m), b) land use category, c) surface temperature (°C), and d) relative humidity (%), averaged over April, 2020.

April, 2020 demonstrates interesting meteorological patterns. Figure 3.6 shows domain-averaged surface temperature and column-total rain water mixing ratio—a proxy for precipitation—predicted by WRF. In the first third of April, temperatures were low and precipitation was high. As the month progressed, precipitation dropped off and temperatures rose. These meteorological patterns must be considered when understanding the contributions of various factors to pollutant concentrations.

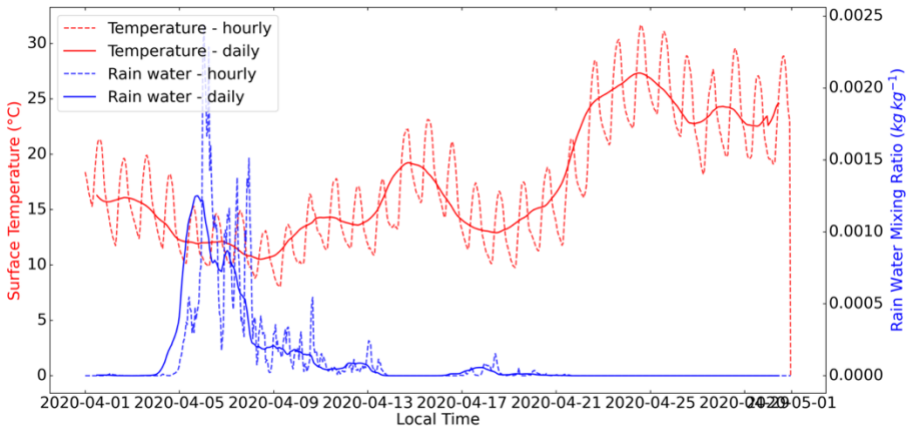

Figure 3.6: Hourly (dashed) and rolling daily average (solid) surface temperature (red) and column-total rain water mixing ratio (blue) predicted by WRF for the month of April, 2020, averaged over the LA domain.

The WRF predictions are compared to EPA AQS monitoring site observational data in Table 3.1. Temperature is well predicted, with very low bias (MB and NMB) and low scatter (low RMSE and high r^2). Relative humidity is fairly well-predicted, with low scatter (high r^2) but nonnegligible bias (MB and NMB). Errors in relative humidity will likely only affect the water content of aerosols and the resulting partitioning of aqueous aerosol, which will be investigated in Chapter 4. Wind speed and direction tends to not be predicted well, with high bias and high scatter. This will potentially affect the transport between grid cells, which we will investigate in Chapter 4. An important consideration when investigating these statistics is that they capture data over a long time period and over multiple different sites. So, some sites may have much less or much more error and/or scatter as these summarized statistics contain. So, the error at individual sites must be investigated

when making site-specific comparisons. Despite the range of sites contained in these statistics, temperature performs well, demonstrating the robustness of our temperature predictions. This is critical, as temperature has the largest impact on atmospheric chemistry and reaction rates.

Table 3.2: Statistical analysis of daily-averaged WRF predictions for the LA domain compared to EPA AQS monitoring site data.

	Temperature	**Relative Humidity**	**Wind Speed**	**Wind Direction**
MB	1.08 °C	-12.6%	0.87 m s^{-1}	-15.1°
NMB	6.65%	-19.2%	50.1%	-7.61%
RMSE	1.32 °C	14.8%	0.91 m s^{-1}	26.3°
r^2	0.98	0.85	0.30	0.31

3.3.3 Emissions

VMT data was summed for all PeMS monitoring sites in the LA domain—separated into heavy duty and light duty vehicles—and is shown in Figure 3.7a-b. VMT January through March (pre-pandemic) was relatively constant. These values were averaged and used as the baseline VMT, represented using the dashed black lines. In March, as COVID-19 policies were implemented, VMT decreased. It reached its lowest value in April and then slowly began to increase towards the baseline value. All weekly-averaged VMT values were divided by the baseline VMT to obtain scaling factors which are a proxy for vehicle emissions resulting from the decline in VMT and driving patterns (Figure 3.7c). The VMT scaling factors are not identical for light duty and heavy duty vehicles, consistent with the rationale for separating these vehicle types. There is a greater decrease in light duty VMT, since the pandemic primarily decreased the use of personal vehicles, with a lesser decrease of industrial transport vehicles' use.

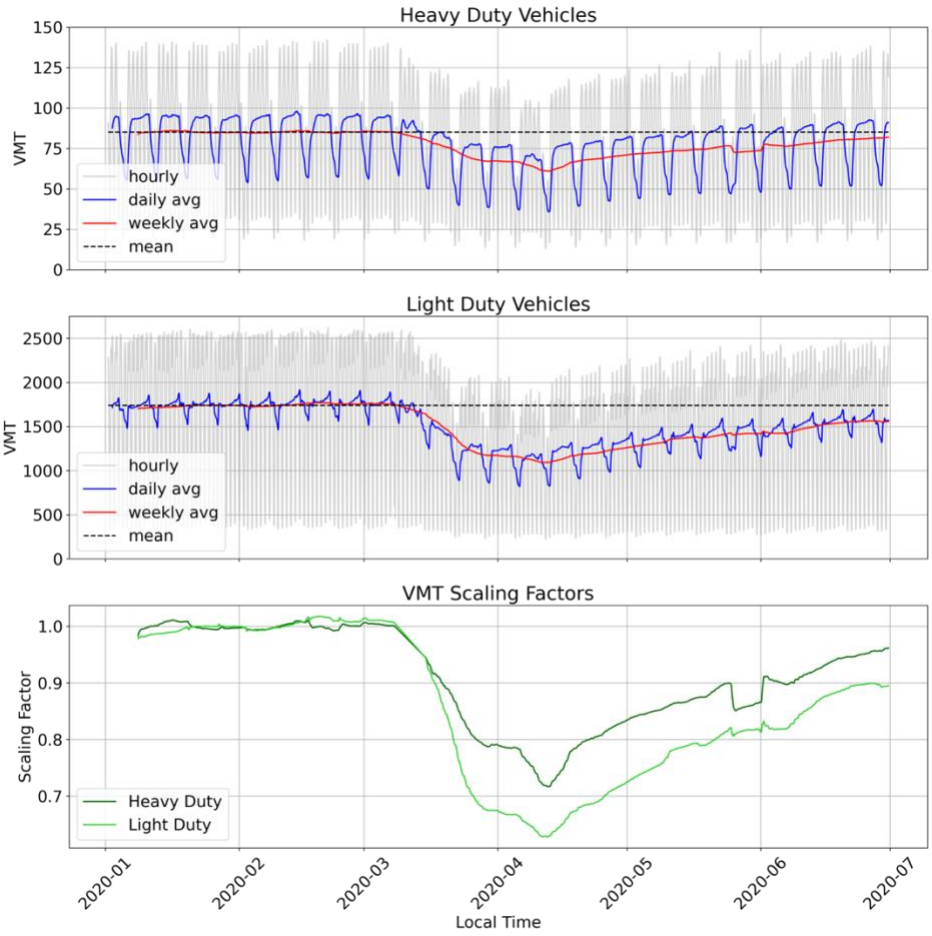

Figure 3.7: Hourly (gray), daily-averaged (blue), and weekly-averaged (red) VMT data for a) heavy duty vehicles and b) light duty vehicles. VMT averaged over January 1, 2020 to March 1, 2020 is represented by the dashed black line. c) Weekly-averaged VMT divided by the Jan.–Mar. mean for heavy duty (dark green) and light duty (light green).

The annual emission rates in California for area and point sources in the CARB emissions inventory are summarized in Figures 3.S1 and 3.S2, respectively. Areawide CO emissions are dominated by off-road vehicles, which also contribute significantly to NO_x emissions. Agriculture and food industries emit large amounts of NH_3 and PM. Boats are the primary emitters of NO_x and SO_x. with trains also emitting significant NO_x. There are high PM emissions from road dust and industrial sources. Industrial sources also emit high quantities of SO_x. Total organic gas (TOG)

emissions are primarily from waste sources. TOG includes methane emissions, which are not included in CMAQ because of methane's long chemical lifetime. Point source emissions are dominated by oil and gas production, with food, retail, and business contributing significant PM.

The emissions from all sources are compared in Figure 3.8. The emissions were summed over the LA domain and diurnally averaged. CO emissions are dominated by area sources, which is itself dominated by off-road vehicles (Figure 3.S1), followed by onroad light duty vehicles. NH_3 emissions are almost entirely from area sources, which is primarily due to agricultural and food sources (Figure 3.S1). NO_x emissions are primarily from area sources (off-road, boats, and trains, Figure 3.S1), with important contributions from light duty and heavy duty vehicles. PM emissions are dominated by overnight seaspray emissions occurring along the coastline, followed by daytime area source emissions deriving from road dust, industrial processes, and agriculture (Figure 3.S1). SO_2 emissions come mostly from area and point sources, which themselves come from oil and gas production, boats, and industrial processes (Figures 3.S1 and 3.S2). VOCs are emitted nearly equally from VCPs and biogenic sources, followed to a lesser extent by area sources (waste, industrial processes, oil and gas production, and agriculture, Figure 3.S1). All emissions, except seaspray, peak during midday due either to the importance of human behavior on or the temperature dependence of emissions. Seaspray emissions peak overnight because they are dependent on relative humidity and wind speed (Gantt et al., 2015). The emissions categories are displayed geographically in Figures 3.S3-3.S8. Light duty and heavy duty vehicles have the highest emissions along freeways and major roads. Biogenic emissions are highest over the mountains, while seaspray emissions occur only at the coastline. Because area sources comprise many kinds of emission sources, the spatial pattern of area sources is variable and spread out. Point source emissions are zero or near-zero everywhere except for specific point sources, as implied by the name. VCP emissions correlate with human population, and the striations over the ocean are near-zero resulting from the regridding process.

Multiple issues with natural source emissions must be addressed in the application of these models and emissions inventories. First, seaspray emissions are very high. It will be investigated whether these high emissions affect only coastal areas or reach inland. Sensitivity simulations will be performed to scale seaspray emissions. Second, biogenic VOC emissions are also very high. The high biogenic emissions are located primarily in the mountainous regions of the LA domain, while the VCP VOC emissions are located in urban areas with high human population. This results in a much smaller biogenic contribution of VOCs in urban areas, but this amount of biogenic VOCs summed over the domain is too large. Biogenic VOCs have traditionally represented only about 20% (CARB, 2020) of total VOC emissions in the Los Angeles area, so our future work will investigate the error in CMAQ's biogenic emissions module by performing sensitivity simulations to scale biogenic emissions.

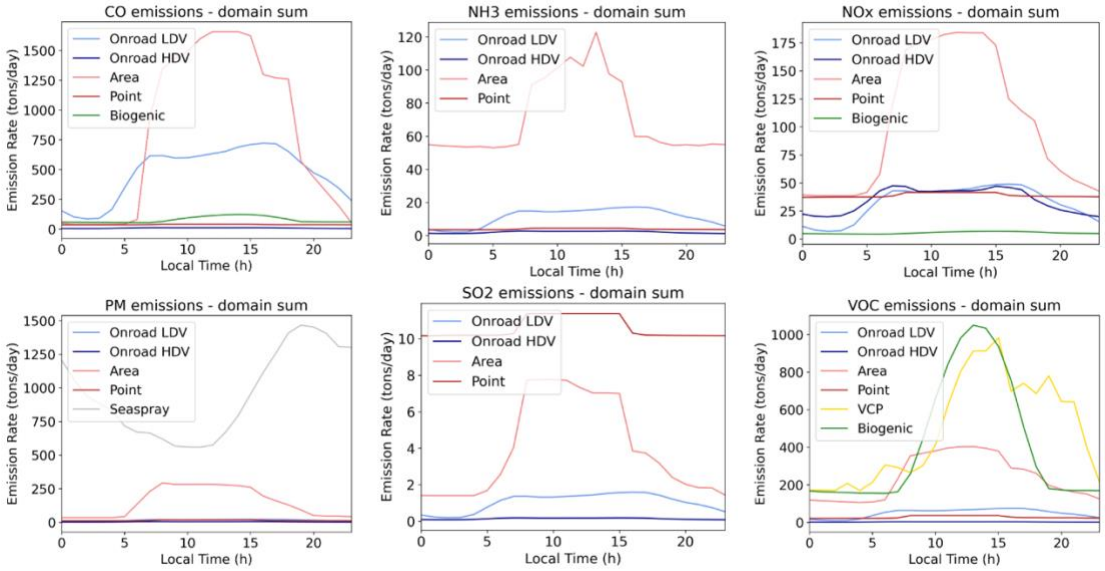

Figure 3.8: Diurnally averaged emission rates summed over the LA domain from all emission sources for a) CO, b) NH_3, c) NO_x, d) PM, e) SO_2, f) VOC.

The modeled emission rates can be approximately compared to the regional emission rates provided by CARB (CARB, 2020). While our domain does not completely align

with CARB's definitions of air regions, we can approximate our domain as covering the South Coast, Ventura, and Antelope Valley air districts. These air districts do not cover the small fractions of the San Diego or Santa Barbara air basins present in our domain, but does include a larger portion of Riverside County than is in our domain. Thus it is an approximate, order-of-magnitude comparison between our summed emission rates and the CARB emission rates summed over the South Coast, Ventura, and Antelope Valley air districts. These data are presented in Table 3.2, along with the percent difference between CARB's values and our study. CO emissions are underpredicted. CO does not impact PM mass in CMAQ, but it may have an impact on oxidants and O_3 and that will be investigated. NH_3 is only slightly underpredicted, and likely lies within the relatively high uncertainty of standard emissions inventories. NO_x is significantly underpredicted according to this comparison, but there are many likely explanations for that. For one, NO_x emissions were reduced by our VMT scaling method performed on onroad sources. Second, multiple studies have investigated LA's transition from a NO_x-abundant to a NO_x-limited regime, and these data may support that (e.g., Laughner & Cohen, 2019; Parker et al., 2020). The impact of NO_x will be investigated closely in our studies. PM is drastically overpredicted, likely due to the high seaspray emissions. The fifth row of Table 3.2 presents the emissions used in this study with seaspray emissions removed, and the new percent error is shown in the sixth row. In this case, PM emissions are underpredicted. This likely suggests that seaspray emissions should not be entirely removed, but reduced. Additionally, some of the PM emissions that CARB assumes to be nonvolatile are treated in CMAQ as semivolatile, so some of the PM mass is reallocated to VOC mass. SO_2 is underpredicted, which will not have a large impact on O_3 or OA, but may impact sulfate aerosol and will be investigated. Finally, VOC emissions are overpredicted. As explained above, the biogenic VOC emissions are likely too high. When these biogenic emissions are removed, the percent error is reduced so that VOC emissions are within the range of reasonable emissions uncertainty (rows 5-6 of Table 3.2). Some of this overprediction may be caused by the reallocation of some PM species to semivolatile VOCs.

Table 3.3: Comparison of emission rates (tons/day) summed over our modeling domain ("this study") and CARB air basins (South Coast, Ventura, and Antelope Valley). CARB's definition of reactive organic carbon (ROG) matches CMAQ's definition of VOC. CARB reports SO_x emissions while CMAQ reports SO_2 emissions.

	CO	**NH_3**	**NO_x**	**PM**	**SO_x, SO_2**	**ROG, VOC**
CARB (tons/day)	2156	98	403	428	20	661
This study (tons/day)	1324	88	215	1133	16	1220
Percent error	-39%	-10%	-47%	165%	-20%	85%
This study (no biog.) (tons/day)	-	-	-	181	-	805
Percent error*	-	-	-	-58%	-	22%

3.3.4 Initial and boundary conditions

The coarse-domain California simulation was performed and the predictions compared to EPA AQS monitoring site data (Table 3.3). O_3 and $PM_{2.5}$, the pollutants of most interest, are well-predicted based on their low MB, NMB, and RMSE. CO and NO_x are both underpredicted (MB and NMB) with moderately high scatter (RMSE), while PM_{10} is less underpredicted with high scatter (RMSE). These errors will be taken into account in the LA simulations, and the importance of the errors in the initial and boundary conditions will be investigated using the ISAM module.

Table 3.4: Statistical analysis of daily-averaged CMAQ predictions for the California domain compared to EPA AQS monitoring site data.

	O_3	**CO**	**NO_x**	**$PM_{2.5}$**	**PM_{10}**
MB	1.17 ppb	-103 ppb	-2.81 ppb	-0.29 μg m^{-3}	-2.36 μg m^{-3}
NMB	3.49%	-44.2%	-34.7%	-5.29%	-14.2%
RMSE	2.05 ppb	106 ppb	3.50 ppb	0.88 μg m^{-3}	4.77 μg m^{-3}
r^2	0.56	0.64	0.40	0.73	0.77

Further investigations of the impact of initial and boundary conditions will be performed in Chapter 4. First, the ISAM module will be used to determine the time-dependent fractions of O_3, NO_x, and VOC concentrations attributed to initial and boundary conditions. Second, a sensitivity simulation will be performed where the hemispheric boundary conditions are used for the LA domain simulations, and the results compared to the results using the initial and boundary conditions from the California domain.

3.4 Future Work

The technical framework developed here will be applied to understand the current state of air quality in the Los Angeles Basin. This chemical and meteorological evaluation is performed in Chapter 4.

3.5 References

Alapaty, K., Niyogi, D., Chen, F., Pyle, P., Chandrasekar, A., & Seaman, N. (2008). Development of the Flux-Adjusting Surface Data Assimilation System for Mesoscale Models. *Journal of Applied Meteorology and Climatology*, *47*(9), 2331–2350. https://doi.org/10.1175/2008JAMC1831.1

Appel, K. W., Bash, J. O., Fahey, K. M., Foley, K. M., Gilliam, R. C., Hogrefe, C., Hutzell, W. T., Kang, D., Mathur, R., Murphy, B. N., Napelenok, S. L., Nolte, C. G., Pleim, J. E., Pouliot, G. A., Pye, H. O. T., Ran, L., Roselle, S. J., Sarwar, G., Schwede, D. B., … Wong, D. C. (2021). The Community Multiscale Air Quality

(CMAQ) model versions 5.3 and 5.3.1: System updates and evaluation. *Geoscientific Model Development*, *14*(5), 2867–2897. https://doi.org/10.5194/gmd-14-2867-2021

Bahreini, R., Middlebrook, A. M., Gouw, J. A. de, Warneke, C., Trainer, M., Brock, C. A., Stark, H., Brown, S. S., Dube, W. P., Gilman, J. B., Hall, K., Holloway, J. S., Kuster, W. C., Perring, A. E., Prevot, A. S. H., Schwarz, J. P., Spackman, J. R., Szidat, S., Wagner, N. L., … Parrish, D. D. (2012). Gasoline emissions dominate over diesel in formation of secondary organic aerosol mass. *Geophysical Research Letters*, *39*(6). https://doi.org/10.1029/2011GL050718

Bash, J. O., Baker, K. R., & Beaver, M. R. (2016). Evaluation of improved land use and canopy representation in BEIS v3.61 with biogenic VOC measurements in California. *Geoscientific Model Development*, *9*(6), 2191–2207. https://doi.org/10.5194/gmd-9-2191-2016

Binkowski, F. S., & Roselle, S. J. (2003). Models-3 Community Multiscale Air Quality (CMAQ) model aerosol component 1. Model description. *Journal of Geophysical Research: Atmospheres*, *108*(D6). https://doi.org/10.1029/2001JD001409

California Air Resources Board. (2018). *EMFAC2017 Volume III Technical Documentation: V1.0.2*. https://ww3.arb.ca.gov/msei/downloads/emfac2017-volume-iii-technical-documentation.pdf

Caltrans. (2020). *Caltrans PeMS*. https://pems.dot.ca.gov/

CARB. (2020). *Criteria Pollutant Emission Inventory Data | California Air Resources Board*. https://ww2.arb.ca.gov/criteria-pollutant-emission-inventory-data

Carter, W. P. L. (2010). Development of the SAPRC-07 chemical mechanism. *Atmospheric Environment*, *44*(40), 5324–5335. https://doi.org/10.1016/j.atmosenv.2010.01.026

CMAS. (2020). *SMOKE (Sparse Matrix Operator Kerner Emissions) Modeling System*. CMAS: Community Modeling and Analysis System. https://www.cmascenter.org/smoke/index.cfm

Ensberg, J. J., Hayes, P. L., Jimenez, J. L., Gilman, J. B., Kuster, W. C., de Gouw, J. A., Holloway, J. S., Gordon, T. D., Jathar, S., Robinson, A. L., & Seinfeld, J. H. (2014). Emission factor ratios, SOA mass yields, and the impact of vehicular emissions on SOA formation. *Atmospheric Chemistry and Physics*, *14*(5), 2383–2397. https://doi.org/10.5194/acp-14-2383-2014

Fountoukis, C., & Nenes, A. (2007). ISORROPIA II: A computationally efficient thermodynamic equilibrium model for K^+–Ca^{2+}–Mg^{2+}–NH_4^+–Na^+–SO_4^{2}−–NO_3−–Cl−–H_2O aerosols. *Atmospheric Chemistry and Physics*, *7*(17), 4639–4659. https://doi.org/10.5194/acp-7-4639-2007

Gantt, B., Kelly, J. T., & Bash, J. O. (2015). Updating sea spray aerosol emissions in the Community Multiscale Air Quality (CMAQ) model version 5.0.2. *Geoscientific Model Development*, *8*(11), 3733–3746. https://doi.org/10.5194/gmd-8-3733-2015

Gentner, D. R., Jathar, S. H., Gordon, T. D., Bahreini, R., Day, D. A., El Haddad, I., Hayes, P. L., Pieber, S. M., Platt, S. M., de Gouw, J., Goldstein, A. H., Harley, R. A., Jimenez, J. L., Prévôt, A. S. H., & Robinson, A. L. (2017). Review of Urban Secondary Organic Aerosol Formation from Gasoline and Diesel Motor Vehicle Emissions. *Environmental Science & Technology*, *51*(3), 1074–1093. https://doi.org/10.1021/acs.est.6b04509

Hersbach, H., Bell, B., Berrisford, P., Biavati, G., Horányi, A., Muñoz Sabater, J., Nicolas, J., Peubey, C., Radu, R., Rozum, I., Schepers, D., Simmons, A., Soci, C., Dee, D., & Thépaut, J.-N. (2018). *ERA5 hourly data on pressure levels from 1979 to present*. Copernicus Climate Change Service (C3S) Climate Data Store (CDS). 10.24381/cds.bd0915c6

Hogrefe, C., Gilliam, R., Mathur, R., Henderson, B. H., Sarwar, G., Appel, K. W., Pouliot, G., Willison, J., Miller, R., Vukovich, J., Eyth, A., Talgo, K., Allen, C., & Foley, K. (2021). *CMAQv5.3.2 ozone simulations over the Northern Hemisphere: Model performance and sensitivity to model configuration*. https://drive.google.com/drive/folders/1A1ZzJE1t7OgwSezQNvy3rt9aATnXA0k2

Jiang, Z., Shi, H., Zhao, B., Gu, Y., Zhu, Y., Miyazaki, K., Lu, X., Zhang, Y., Bowman, K. W., Sekiya, T., & Liou, K.-N. (2021). Modeling the impact of COVID-19 on air quality in southern California: Implications for future control policies. *Atmospheric Chemistry and Physics*, *21*(11), 8693–8708. https://doi.org/10.5194/acp-21-8693-2021

Khare, P., & Gentner, D. R. (2018). Considering the future of anthropogenic gas-phase organic compound emissions and the increasing influence of non-combustion sources on urban air quality. *Atmospheric Chemistry and Physics*, *18*(8), 5391–5413. https://doi.org/10.5194/acp-18-5391-2018

Kwok, R. H. F., Baker, K. R., Napelenok, S. L., & Tonnesen, G. S. (2015). Photochemical grid model implementation and application of VOC, NO_x, and O_3 source apportionment. *Geoscientific Model Development*, *8*(1), 99–114. https://doi.org/10.5194/gmd-8-99-2015

Kwok, R. H. F., Napelenok, S. L., & Baker, K. R. (2013). Implementation and evaluation of PM2.5 source contribution analysis in a photochemical model. *Atmospheric Environment*, *80*, 398–407. https://doi.org/10.1016/j.atmosenv.2013.08.017

Laughner, J. L., & Cohen, R. C. (2019). Direct observation of changing NOx lifetime in North American cities. *Science*, *366*(6466), 723–727. https://doi.org/10.1126/science.aax6832

Lu, Q., Murphy, B. N., Qin, M., Adams, P. J., Zhao, Y., Pye, H. O. T., Efstathiou, C., Allen, C., & Robinson, A. L. (2020). Simulation of organic aerosol formation

during the CalNex study: Updated mobile emissions and secondary organic aerosol parameterization for intermediate-volatility organic compounds. *Atmospheric Chemistry and Physics*, *20*(7), 4313–4332. https://doi.org/10.5194/acp-20-4313-2020

Lu, R., & Turco, R. P. (1995). Air pollutant transport in a coastal environment—II. Three-dimensional simulations over Los Angeles basin. *Atmospheric Environment*, *29*(13), 1499–1518. https://doi.org/10.1016/1352-2310(95)00015-Q

Murphy, B. N., Nolte, C. G., Sidi, F., Bash, J. O., Appel, K. W., Jang, C., Kang, D., Kelly, J., Mathur, R., Napelenok, S., Pouliot, G., & Pye, H. O. T. (2021). The Detailed Emissions Scaling, Isolation, and Diagnostic (DESID) module in the Community Multiscale Air Quality (CMAQ) modeling system version 5.3.2. *Geoscientific Model Development*, *14*(6), 3407–3420. https://doi.org/10.5194/gmd-14-3407-2021

Parker, H. A., Hasheminassab, S., Crounse, J. D., Roehl, C. M., & Wennberg, P. O. (2020). Impacts of Traffic Reductions Associated With COVID-19 on Southern California Air Quality. *Geophysical Research Letters*, *47*(23), e2020GL090164. https://doi.org/10.1029/2020GL090164

Pennington, E. A., Seltzer, K. M., Murphy, B. N., Qin, M., Seinfeld, J. H., & Pye, H. O. T. (2021). Modeling secondary organic aerosol formation from volatile chemical products. *Atmospheric Chemistry and Physics*, *21*(24), 18247–18261. https://doi.org/10.5194/acp-21-18247-2021

Pleim, J., & Ran, L. (2011). Surface Flux Modeling for Air Quality Applications. *Atmosphere*, *2*(3), 271–302. https://doi.org/10.3390/atmos2030271

Pye, H. O. T., Pinder, R. W., Piletic, I. R., Xie, Y., Capps, S. L., Lin, Y.-H., Surratt, J. D., Zhang, Z., Gold, A., Luecken, D. J., Hutzell, W. T., Jaoui, M., Offenberg, J. H., Kleindienst, T. E., Lewandowski, M., & Edney, E. O. (2013). Epoxide Pathways Improve Model Predictions of Isoprene Markers and Reveal Key Role

of Acidity in Aerosol Formation. *Environmental Science & Technology*, *47*(19), 11056–11064. https://doi.org/10.1021/es402106h

Qin, M., Murphy, B. N., Isaacs, K. K., McDonald, B. C., Lu, Q., McKeen, S. A., Koval, L., Robinson, A. L., Efstathiou, C., Allen, C., & Pye, H. O. T. (2021). Criteria pollutant impacts of volatile chemical products informed by near-field modelling. *Nature Sustainability*, *4*(2), 129–137. https://doi.org/10.1038/s41893-020-00614-1

Ritchie, S., & Tok, Y. C. (2016). *Development of a New Methodology to Characterize Truck Body Types Along California Freeways* (No. 11–316; p. 176). California Air Resources Board. https://ww2.arb.ca.gov/sites/default/files/classic/research/apr/past/11-316.pdf

Ryerson, T. B., Andrews, A. E., Angevine, W. M., Bates, T. S., Brock, C. A., Cairns, B., Cohen, R. C., Cooper, O. R., Gouw, J. A. de, Fehsenfeld, F. C., Ferrare, R. A., Fischer, M. L., Flagan, R. C., Goldstein, A. H., Hair, J. W., Hardesty, R. M., Hostetler, C. A., Jimenez, J. L., Langford, A. O., … Wofsy, S. C. (2013). The 2010 California Research at the Nexus of Air Quality and Climate Change (CalNex) field study. *Journal of Geophysical Research: Atmospheres*, *118*(11), 5830–5866. https://doi.org/10.1002/jgrd.50331

Seltzer, K. M., Murphy, B. N., Pennington, E. A., Allen, C., Talgo, K., & Pye, H. O. T. (2021). Volatile Chemical Product Enhancements to Criteria Pollutants in the United States. *Environmental Science & Technology*. https://doi.org/10.1021/acs.est.1c04298

Seltzer, K. M., Pennington, E., Rao, V., Murphy, B. N., Strum, M., Isaacs, K. K., & Pye, H. O. T. (2021). Reactive organic carbon emissions from volatile chemical products. *Atmospheric Chemistry and Physics*, *21*(6), 5079–5100. https://doi.org/10.5194/acp-21-5079-2021

Skamarock, W. C., Klemp, J. B., Dudhia, J., Gill, D. O., & Barker, D. (2008). *A Description of the Advanced Research WRF Version 3* (NCAR/TN-475+STR).

University Corporation for Atmospheric Research. http://dx.doi.org/10.5065/D68S4MVH

US EPA. (2022). *Spatial Allocator v4.4 (June 2019 release)* [C++]. CMAS Center. https://github.com/CMASCenter/Spatial-Allocator/blob/14176784e03f7379d8c6a25f4ce7cfb2dd08128c/docs/User_Manual/README.md (Original work published 2017)

US EPA, O. (2013, August 1). *Air Quality System (AQS)* [Data and Tools]. US EPA. https://www.epa.gov/aqs

US EPA Office of Research and Development. (2020). *CMAQ*. Zenodo. https://doi.org/10.5281/zenodo.4081737

Xie, Y., Paulot, F., Carter, W. P. L., Nolte, C. G., Luecken, D. J., Hutzell, W. T., Wennberg, P. O., Cohen, R. C., & Pinder, R. W. (2013). Understanding the impact of recent advances in isoprene photooxidation on simulations of regional air quality. *Atmospheric Chemistry and Physics*, *13*(16), 8439–8455. https://doi.org/10.5194/acp-13-8439-2013

3.6 Supporting Information

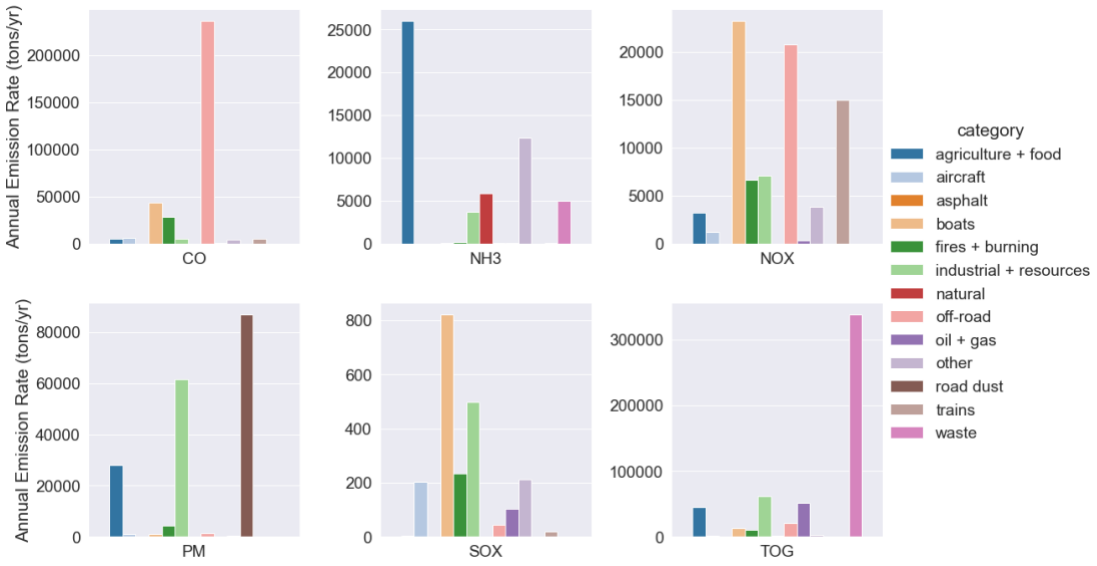

Figure 3.S1: Annual emission rates of pollutants in CARB area source emissions inventory.

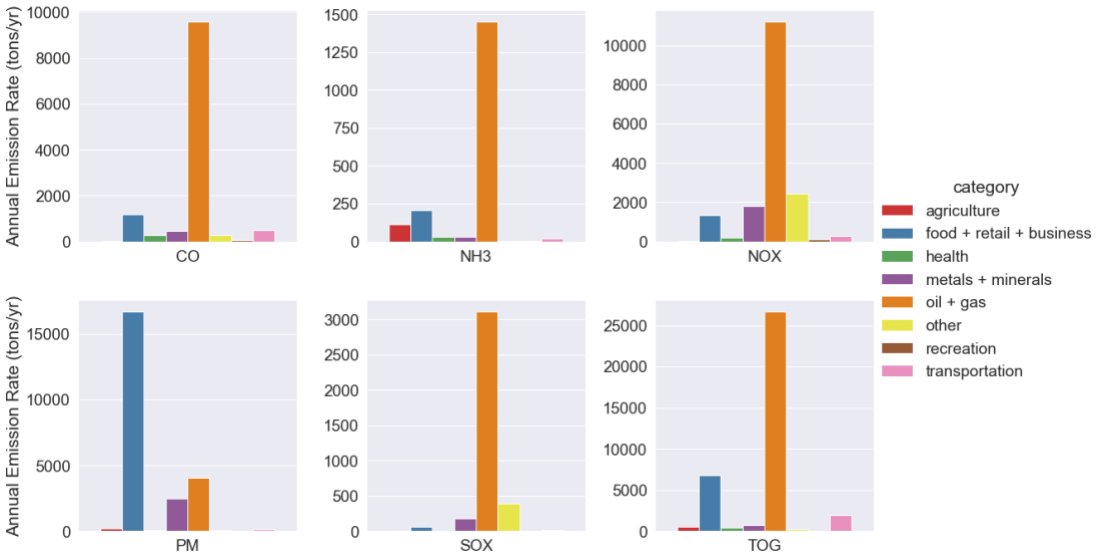

Figure 3.S2: Annual emission rates of pollutants in CARB point source emissions inventory.

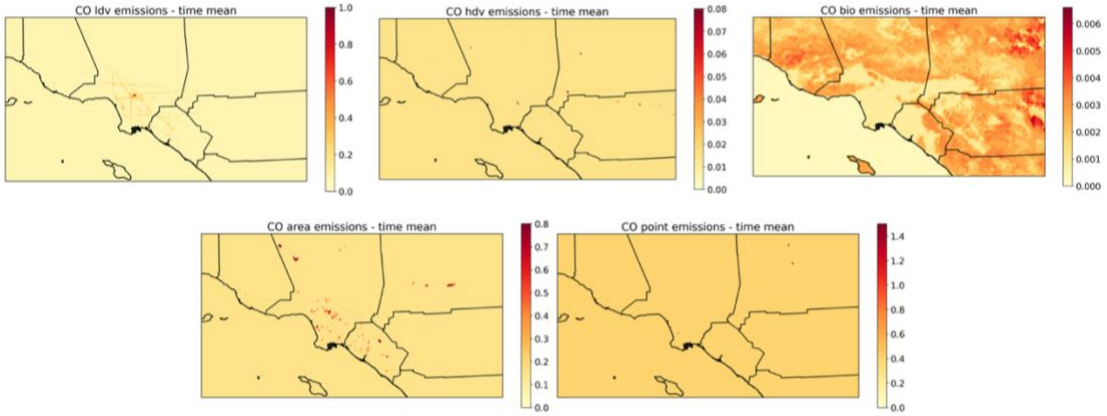

Figure 3.S3: Time-averaged (April, 2020) emission rate (tons/day) of CO from a) light duty onroad vehicles, b) heavy duty onroad vehicles, c) biogenic, d) area, and e) point sources.

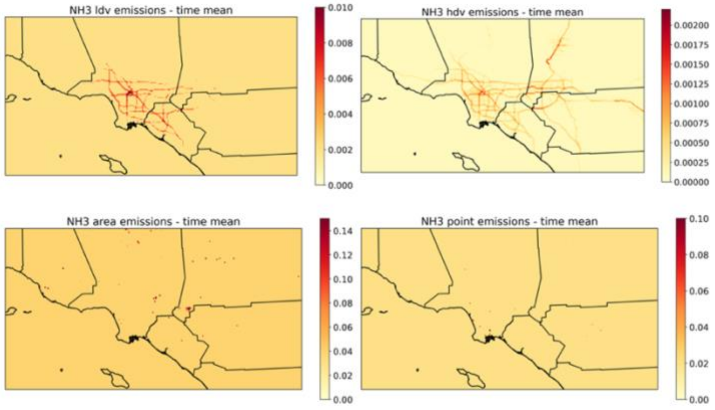

Figure 3.S4: Time-averaged (April, 2020) emission rate (tons/day) of NH_3 from a) light duty onroad vehicles, b) heavy duty onroad vehicles, c) area, and d) point sources.

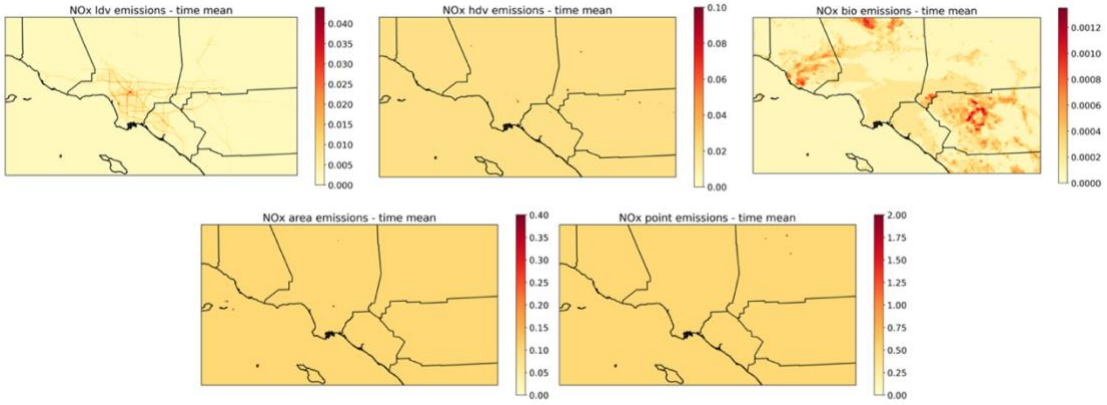

Figure 3.S5: Time-averaged (April, 2020) emission rate (tons/day) of NO_x from a) light duty onroad vehicles, b) heavy duty onroad vehicles, c) biogenic, d) area, and e) point sources.

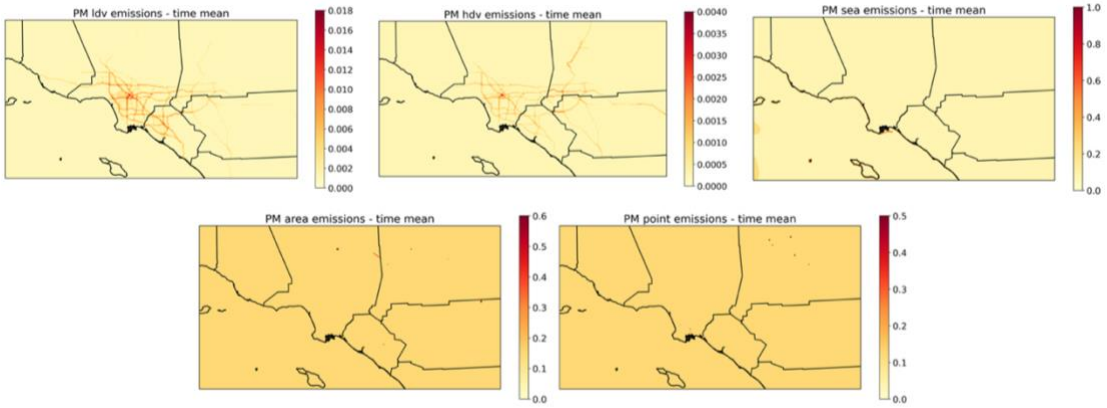

Figure 3.S6: Time-averaged (April, 2020) emission rate (tons/day) of PM from a) light duty onroad vehicles, b) heavy duty onroad vehicles, c) seaspray, d) area, and e) point sources.

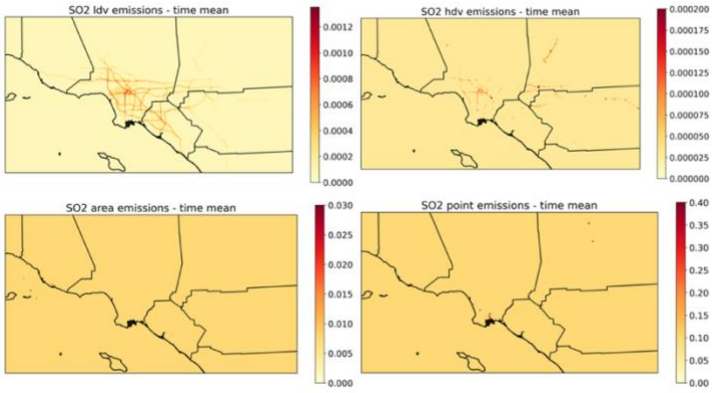

Figure 3.S7: Time-averaged (April, 2020) emission rate (tons/day) of SO_2 from a) light duty onroad vehicles, b) heavy duty onroad vehicles, c) area, and d) point sources.

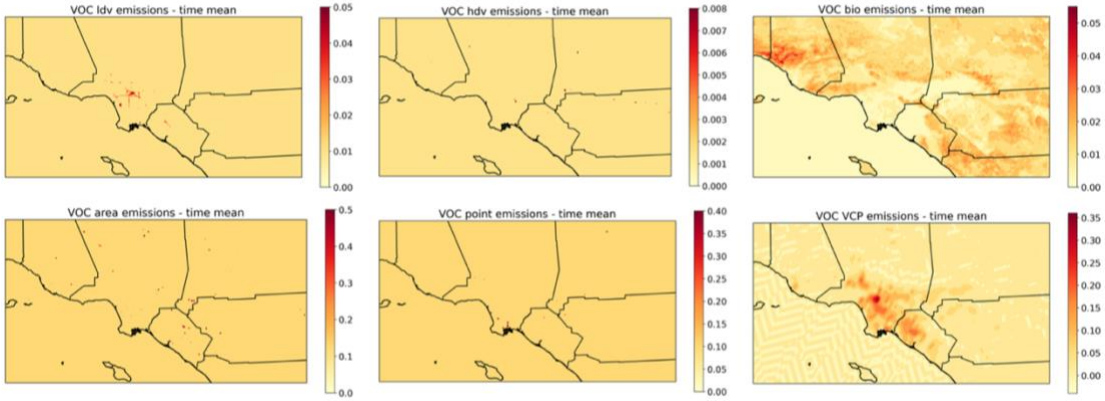

Figure 3.S8: Time-averaged (April, 2020) emission rate (tons/day) of VOCs from a) light duty onroad vehicles, b) heavy duty onroad vehicles, c) biogenic, d) area, e) point, and f) VCP sources.

Chapter 4

APPLICATION OF A NEW MODEL FRAMEWORK FOR LOS ANGELES METEOROLOGY AND AIR QUALITY IN LOS ANGELES IN 2020

This work is in progress and will be completed and submitted for publication within the next few months.

4.0 Abstract

The Los Angeles Basin has high anthropogenic emissions and unique meteorological phenomena which makes it an important study location for understanding the chemistry of atmospheric pollutants and impact of mitigation policies. Regional-scale models allow for an understanding of complex chemical and physical processes where measurements are not available. Using the model inputs and configuration options described in Chapter 3, we run the Community Multiscale Air Quality (CMAQ) model over the Los Angeles region in April, 2020. We quantify model accuracy and explain the chemistry of pollutant formation, including processes that the model must improve on. We investigate source apportionment of pollutants on gas- and aerosol-phase species and describe the impact of the COVID-19 pandemic on vehicle-derived pollutants. Investigating the response of the COVID-19 pandemic, we find that the urban core of the Los Angeles Basin displays NO_x-saturated behavior, but surrounding areas display NO_x-limited behavior. Ozone and PM reductions are greatest when VOC emissions are reduced, particularly from volatile chemical products.

4.1 Model Configuration and Analysis Methods

4.1.1 Model configuration

The model inputs and configuration options were described in Chapter 3.

4.1.2 Model simulations

Multiple simulations were performed to investigate the source apportionment and nonlinear chemistry occurring in the LA atmosphere, and these are listed in Table 4.1 along with the goal of each experiment.

Table 4.1: CMAQ simulations performed in this study.

Name	Simulation Description	Science Goal
VMT (a.k.a. Base)	All inputs and configuration options given in Chapter 3.	To represent the Los Angeles atmosphere using the inputs described in Chapter 3. Can be considered a "base case".
0xVCP	Remove all VCP emissions.	To investigate the impact of VCPs on gas- and aerosol-phase species.
0xonroad	Remove all onroad (LDV & HDV) emissions.	To investigate the impact of onroad sources on gas- and aerosol-phase species.
0xother	Remove all "other" source (i.e., area & point) emissions.	To investigate the impact of other sources on gas- and aerosol-phase species.
0xbio	Remove all biogenic emissions.	To investigate the impact of biogenic sources on gas- and aerosol-phase species.
0xsea	Remove all seaspray emissions.	To investigate the impact of seaspray aerosol on gas- and aerosol-phase species.
noVMT	Do not apply PeMS VMT scaling to onroad emissions.	To investigate the air quality in the absence of the COVID-19 pandemic.
hemiBC	Replace the initial and boundary conditions with 2016 seasonal-average hemispheric CMAQ output.	To investigate the impact of boundary conditions on gas- and aerosol-phase species.
75VOC	Scale all VOC emissions from anthropogenic sources by 0.75	To investigate the VOC-NO_x regime and the impact of VOC reductions on ozone, and to include the uncertainty associated with VCP emissions.

125VOC	Scale all VOC emissions from anthropogenic sources by 1.25	To investigate the VOC-NO_x regime and the impact of VOC increases on ozone, and to include the uncertainty associated with VCP emissions.

4.1.3 Observational data

Observational data throughout the modeling domain are provided by the EPA AQS monitoring system (US EPA, 2013). These sites include measurements of O_3, CO, NO, NO_2, NO_y, SO_2, $PM_{2.5}$, PM_{10}, temperature, relative humidity, wind speed, and wind direction (not all sites contain all species at all times) and their locations are shown in Figure 4.1. In addition, gas- and aerosol-phase measurements were collected concurrent to our modeling period in Pasadena at Caltech. The Caltech air quality system (CITAQS) site measures O_3, CO, NO, NO_2, NO_y, SO_2, and $PM_{2.5}$ (Parker et al., 2020). Aerosol mass spectrometer (AMS) measurements of PM_1 and its components (organic, NH_4, NO_3, SO_4, and Cl) as described in Schulze et al. (submitted, 2022). Primary matrix factorization (PMF) was performed to obtain the composition of the organic fraction of PM_1.

4.1.4 Spatial analysis

The model domain covers the region displayed in Figure 4.1 over 49 vertical layers. AQS measurement site locations are distributed throughout the full domain (black circles), and a few sites were studied in detail and were chosen to represent a variety of emission and meteorological qualities and to be consistent with the work of Parker et al. (2020). In addition, domain-wide averages were calculated using time- and space-averaged values using the masked, green region shown in Figure 4.1. The mask removes grid cells which contain water or lay above 600 m elevation. This elevation cutoff removes many rural or remote locations which are not representative of urban SOA, as well as many of the grid cells around the boundary which are more heavily impacted by boundary conditions.

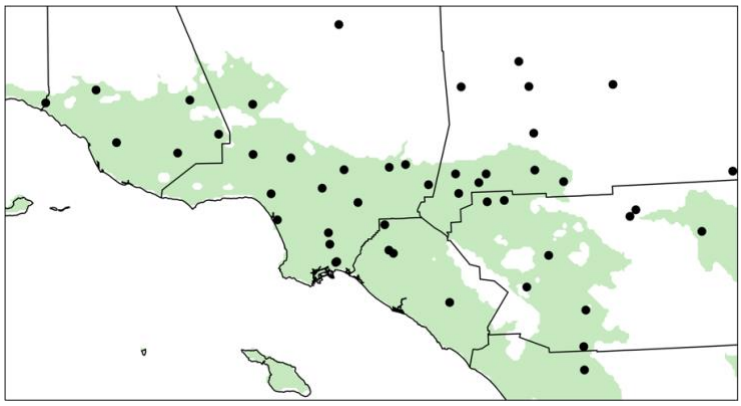

Figure 4.1: LA modeling domain with AQS measurement sites (black markers). Green shading represents the domain-average mask which excludes grid cells containing water or over 600 m elevation.

We primarily present surface concentrations since these are directly comparable to observations. However, many of the pollutants' diurnal trends can be understood by considering the impact of the planetary boundary layer (PBL) height. Pollutants tend to be well-mixed inside the PBL with concentrations sharply declining outside of the PBL. As the height of the PBL changes throughout the day (Figure 4.2), species are diluted or concentrated. Multiplying surface concentrations by PBL height can provide insight into the total mass of a species present in a column and available for mixing.

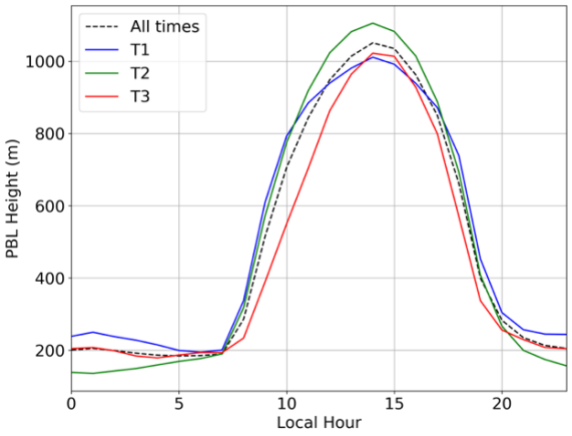

Figure 4.2: PBL height for the masked domain average for diurnal averages of T_1 (blue), T_2 (green), T_3 (red), and all times April 1–30, 2020 (dashed black).

4.1.5 Temporal analysis

The modeling period covers April 1–30, 2020. We separate the month into 3 8-day periods, which have markedly different meteorology (Figure 4.3). Time period 1 (T_1) runs from April 4 00:00 LT to April 12 00:00 LT and is uniquely cold with high precipitation. Time period 2 (T_2) runs from April 13 00:00 LT to April 21 00:00 LT and has moderate, average temperature and very little precipitation. Time period 3 (T_3) runs from April 22 12:00 LT to April 30 12:00 LT and is very warm and dry. VMT is at its lowest during all 3 time periods, with slightly higher COVID vehicle impacts (i.e., more negative) in T_1 and T_2 (Fig 4.S1). Most emissions are consistent through all time periods, except biogenic emissions which are temperature-dependent and high during T_3 and seaspray emissions, which depend on many factors (Figure 4.S2).

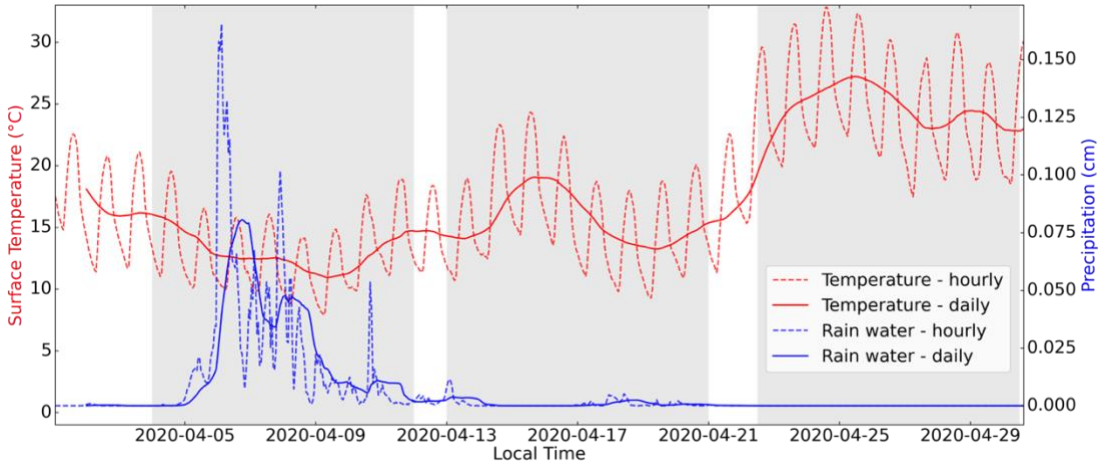

Figure 4.3: Hourly (dashed) and rolling daily average (solid) temperature (red) and precipitation (cm) averaged over the masked domain April 1–30, 2020. Gray shading represents T_1, T_2, and T_3.

4.2 Results and Discussion

4.2.1 Evaluation of model predictions

This section is forthcoming.

4.2.2 Source apportionment

To investigate the contribution of each emission source to pollutant concentrations, we ran 5 additional simulations in which a single emissions source was removed in each simulation: 0xVCP, 0xonroad, 0xother, 0xbio, and 0xsea (Table 4.1). We investigate the overall impact on important pollutants such as O_3 and $PM_{2.5}$ by quantifying the change over the entire domain (Section 4.2.2.1). We investigate the detailed impact on SOA and PM composition by evaluating the change of SOA and PM_1 composition in Pasadena, where concurrent AMS measurements were made (Section 4.2.2.2). We also consider the impact on SOA and PM_1 composition in other locations in Section 4.2.2.3, which have different emission profiles and meteorology compared to Pasadena.

4.2.2.1 Full domain

The impact of removing each emission source on O_3 (Figure 4.4), NO_x (Figure 4.5), VOC (Figure 4.6), OH (Figure 4.7), $PM_{2.5}$ (Figure 4.8), POA (Figure 4.9), and SOA (Figure 4.10) are presented alongside the concentration of each given species in the base (VMT) case.

The O_3 changes can be understood by investigating the changes in NO_x, VOC, and OH. Onroad vehicles emit NO_x, VOC, particles, and other inorganic gas-phase species. So when this emission source is removed, VOC and NO_x concentrations decrease everywhere. However, OH and O_3 do not have such clear impacts. In the urban core where VOC and NO_x concentrations are high, OH and O_3 increase in response to VOC and NO_x reductions. This is characteristic of NO_x-saturated conditions, which typically describe urban areas. In a NO_x-saturated regime, the ratio of VOC to NO_x concentrations is low, so that NO_2 competes with VOC for reaction with OH. When NO_2 concentration decreases, OH concentrations increase and more is available to react with VOCs to form peroxy radicals and O_3. This chemistry describes the regions in the urban core with OH and O_3 increases. In contrast, the outer regions display NO_x-limited (or NO_x-insensitive) behavior. In this case, the ratio of VOC to NO_x concentrations is higher (relative to the NO_x-saturated regime), so reaction with OH is dominated by VOCs. When VOC and NO_x concentrations

decrease, the formation of peroxy radicals and the subsequent reactions to form O_3 are stunted. The reduction of other sources of emissions, which emit VOC, NO_x, aerosol, and gas-phase inorganics, has a similar impact on O_3. There is an increase of OH and O_3 in the urban core, but a decrease of OH and O_3 in the outer regions.

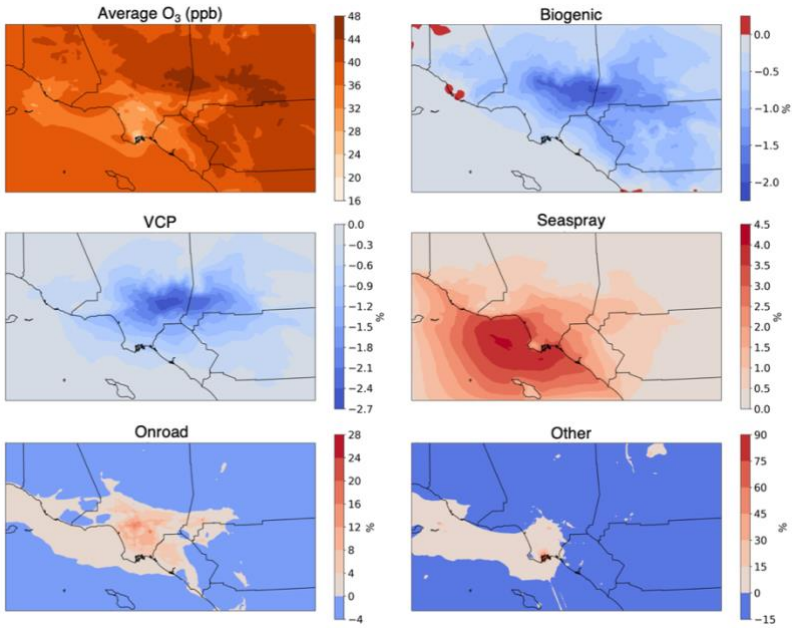

Figure 4.4: a) Average O_3 concentration predicted in base (VMT) case April 1–30, 2020. b-f) Percent change in average predicted O_3 concentration caused by removing each emission source.

O_3 decreased everywhere in response to the removal of VCP and biogenic emissions, in contrast to the removal of onroad and other emission sources. VCPs only emit VOCs, shown spatially by the decrease of VOC concentrations (Figure 4.6c). In response, OH and NO_x concentrations increase downwind of the primary emission region. When VOCs are removed, the reaction between VOCs and OH slows, increasing the concentration of OH. The importance of transport and secondary aging processes is evident by the downwind location of most of the OH increase. Decreased VOCs also means that there are fewer peroxy radicals reacting with HO_2 in HO_x-terminating reactions, further increasing OH. Fewer peroxy radicals also means slower reaction with NO to form NO_2, so there is a high ratio of NO to NO_2. This

leads to less NO_x termination via the OH + NO_2 reaction, and thus an increase in NO_x. Because of the increased NO_x and decreased peroxy radicals, O_3 preferentially reacts with NO, instead of NO reacting with peroxy radicals, and so the O_3 concentration decreases. This chemistry is consistent with NO_x-saturated behavior. The removal of biogenic emissions has a similar response, except biogenic sources emit NO, so there is a decrease of NO_x concentrations in the regions where biogenic emissions are high, e.g., over the mountains outside of the urban core. However, there is a slight increase of NO_x concentrations downwind of the urban core, and the same chemistry results here as with the VCP removal chemistry. In the outer region, the chemistry of the NO_x-limited regime results. In this case, removal of VOC and NO_x allows for an increase of OH because of the slowdown of HO_x-terminating reactions, but the increase of OH does little to impact O_3 because the necessary VOC and NO_x are not available for the O_3 forming reactions, and so O_3 decreases in this regime.

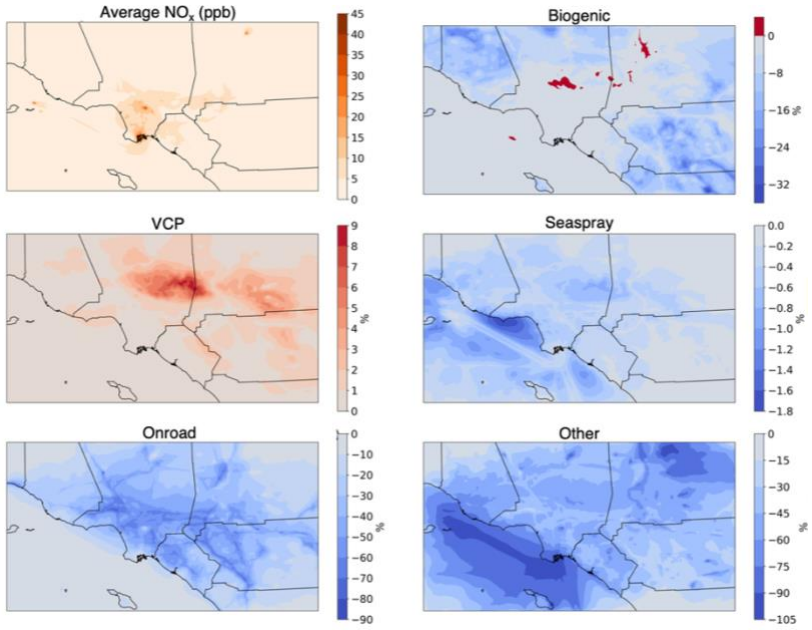

Figure 4.5: a) Average NO_x concentration predicted in base (VMT) case April 1–30, 2020. b-f) Percent change in average predicted NO_x concentration caused by removing each emission source.

Removing seaspray emissions has a small impact on gas-phase concentrations because seaspray only emits aerosol-phase particles. The impact on VOC and NO_x concentrations is near-zero because the seaspray emissions are only inorganic. The seaspray particles contain sulfate which can evaporate and react with OH, plus the particles themselves can react with OH. When all of these particles are removed, there is then more OH available in the system, as demonstrated by the ocean and coastal increase of OH.

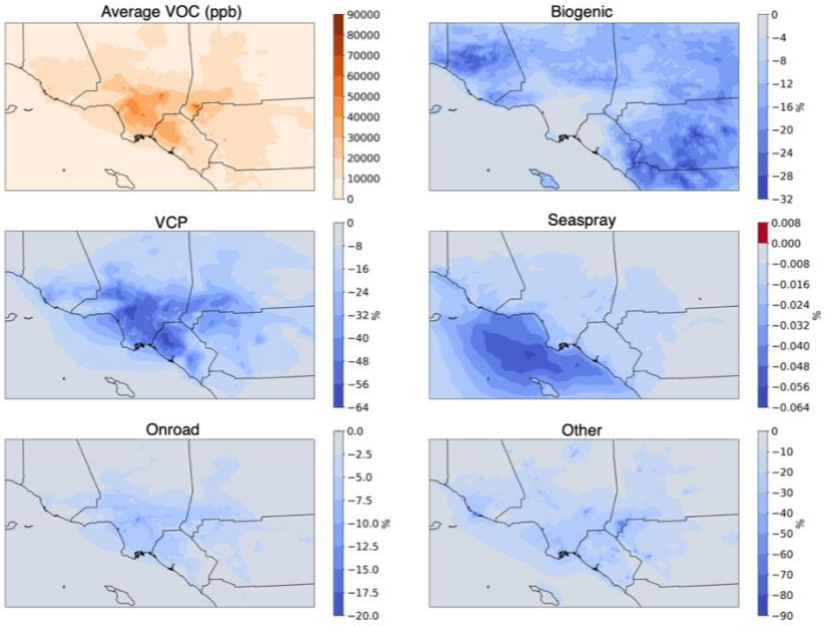

Figure 4.6: a) Average VOC concentration predicted in base (VMT) case April 1–30, 2020. b-f) Percent change in average predicted VOC concentration caused by removing each emission source.

We learn some important qualities about the LA atmosphere from this source apportionment study. The urban core of LA demonstrates NO_x-saturated behavior. When NO_x emissions are removed (while VOC concentrations are decreased to a smaller degree, as is the case when removing onroad and other emissions), O_3 increases. When VOC emissions are removed without NO_x removal (as is the case when VCP emissions are removed), O_3 decreases. Outside of the urban core, O_3 decreases in response to any level of either NO_x or VOC removal, characteristic of a

NO_x-limited regime, or at least a regime lying close to the O_3- NO_x-VOC ridgeline in the VOC-sensitive regime (Seinfeld & Pandis, 2016). The NO_x regime is explored further in Section 4.2.3. Reducing ozone is a consistent goal for policymakers, and this work shows that O_3 in Los Angeles is reduced by the removal of VOCs. NO_x emission decreases are still important, as these decreases will move the Basin from a NO_x-saturated regime closer to a NO_x-insensitive regime. However, without concurrent or larger reductions in VOC concentrations, O_3 pollution will become worse until the NO_x-insensitive regime is reached. It is particularly important for policymakers to consider reducing emissions from VCPs, since these sources emit the highest amount of VOCs from anthropogenic activities. It is also important to consider the spatial distribution of emissions and reduction policies. Reducing emissions in the NO_x-limited, outer regions of the domain will have a lesser impact than reductions in the urban core, or may have an opposite effect. Focusing on emissions in the urban core is critical and will effect downwind regions.

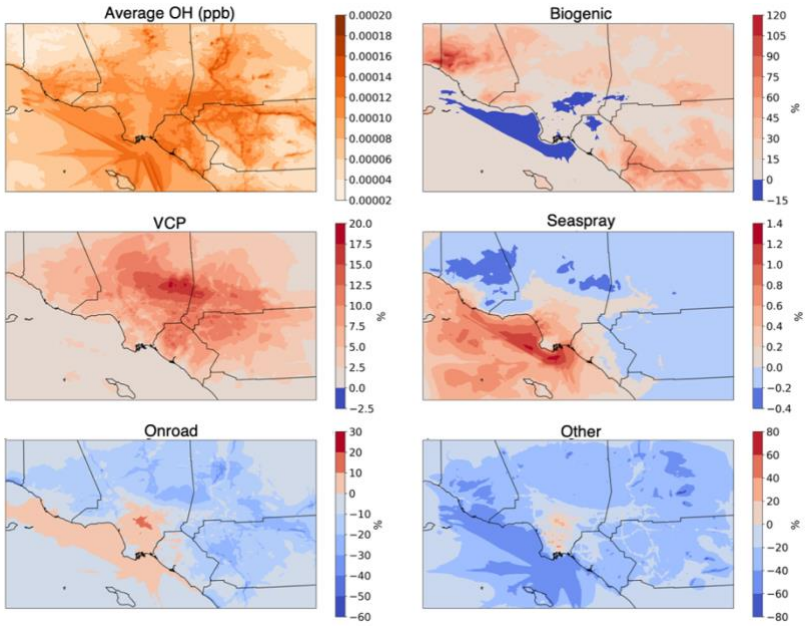

Figure 4.7: a) Average OH concentration predicted in base (VMT) case April 1–30, 2020. b-f) Percent change in average predicted OH concentration caused by removing each emission source.

$PM_{2.5}$ concentrations decrease everywhere in response to emission reductions (Figure 4.8). PM from onroad and other sources is mostly emitted directly, because most of the impact to $PM_{2.5}$ is located in high emission regions. VCPs and biogenic sources only emit gas-phase species, so PM is formed via secondary processes. Biogenic PM is formed mostly over high emission areas like mountains, while VCP-derived PM is found in downwind regions, highlighting the importance of secondary formation during transport. Seaspray particles are reduced along the coastline where waves break, as expected.

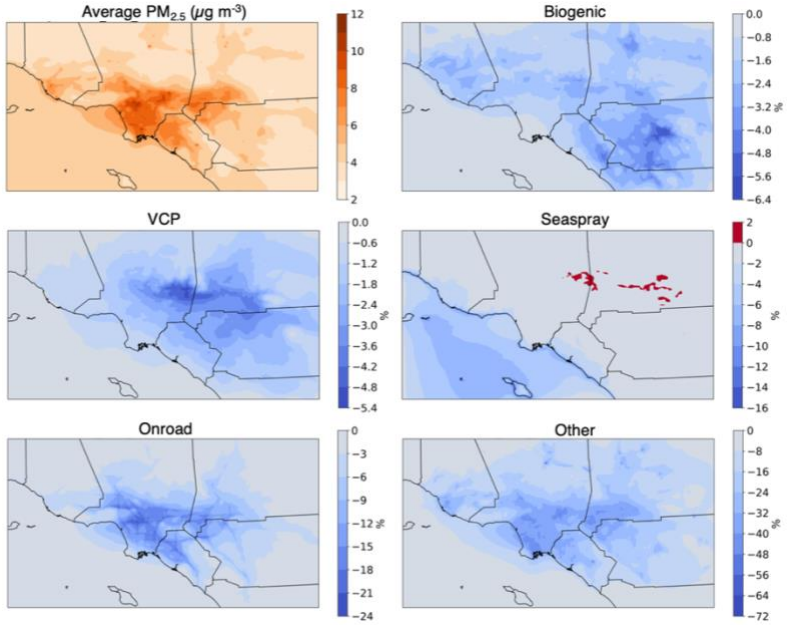

Figure 4.8: a) Average $PM_{2.5}$ concentration predicted in base (VMT) case April 1–30, 2020. b-f) Percent change in average predicted $PM_{2.5}$ concentration caused by removing each emission source.

POA and SOA changes are given in Figure 4.9 and Figure 4.10, respectively. Consistent with changes in $PM_{2.5}$, POA decreases in areas of high emissions from onroad and other sources. SOA decreases from these sources are witnessed downwind of high-emission regions, as are the SOA changes from VCPs. VCPs and biogenic sources effect POA by decreasing partitioning into OA by lowering SOA and total OA mass, so some of the POA evaporates. Seaspray emits only inorganic

aerosols, so the impact on OA is small. Figure 4.7 demonstrated that removing seaspray emissions increased OH, which speeds up VOC oxidation and leads to higher SOA and thus higher POA via partitioning into the aerosol phase.

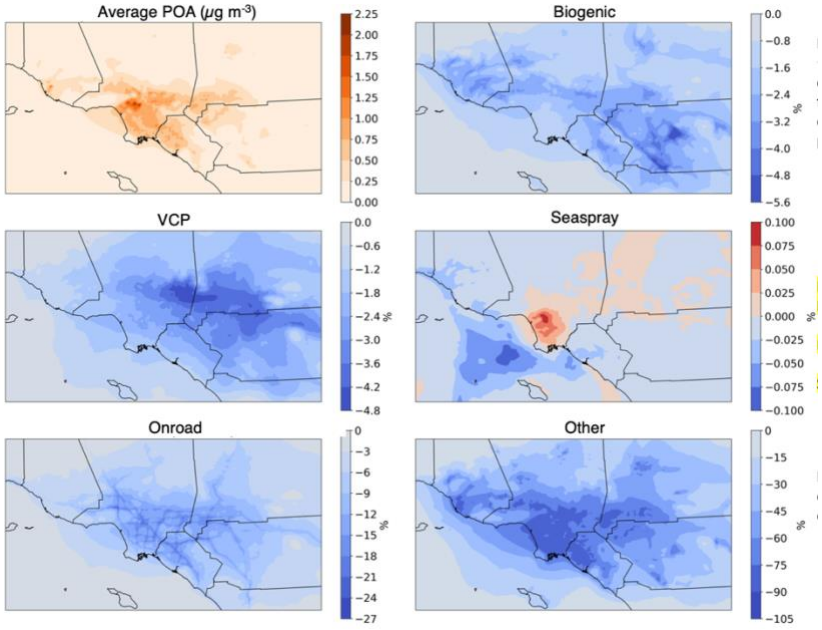

Figure 4.9: a) Average POA concentration predicted in base (VMT) case April 1–30, 2020. b-f) Percent change in average predicted POA concentration caused by removing each emission source.

In Chapter 3, we predicted that emissions from natural sources are too high while emissions from anthropogenic sources are often too low. So, the relative impact of these sources on pollutant concentrations may be over- or under-estimated. For example, VCPs and biogenic gases had an almost equal impact on O_3 concentrations (Figure 4.4), while in reality VCPs are likely more important than biogenic sources. Another source of this error could be the simplification of ozone chemistry used in the VCP chemical mechanism (Pennington et al., 2021). An updated mechanism which is developed with a focus on ozone may increase the ozone formation potential of VCPs. As another example, some emission sources in the "other" category may be underpredicted. Figure 3.S1 showed that most NO_x and SO_x emissions originate from boats, and this explains the large impact of removing other source emissions on

NO_x, OH, and O_3 in the ocean and near the Long Beach Port. NO_x from other sources (e.g., offroad, agriculture) and VOCs from other sources (e.g., oil and gas) may be higher than predicted by the inventories used here, which would increase the impact of other sources over the land. These specific factors will be investigated in future work.

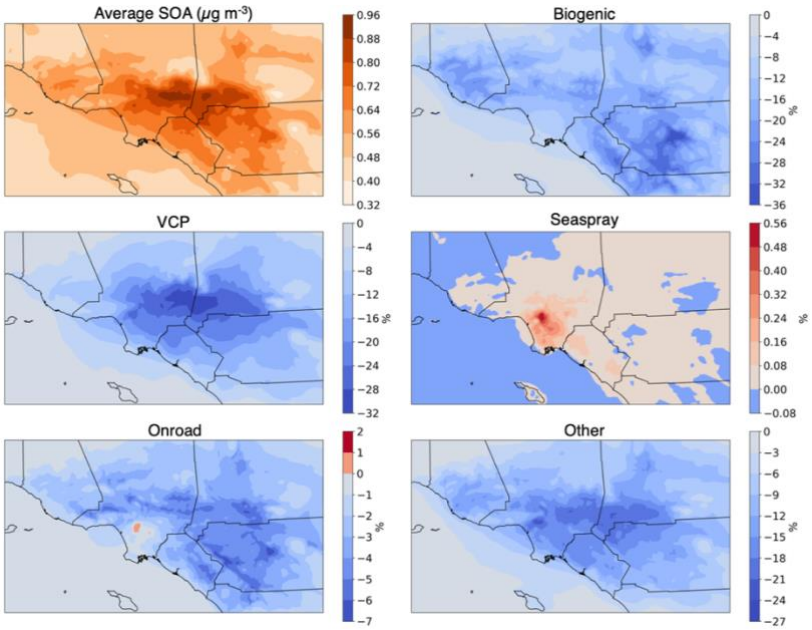

Figure 4.10: a) Average SOA concentration predicted in base (VMT) case April 1–30, 2020. b-f) Percent change in average predicted SOA concentration caused by removing each emission source.

4.2.2.2 Pasadena

This section is forthcoming.

4.2.2.3 Other locations

This section is forthcoming.

4.2.3 COVID-19 vehicle impacts

To understand the impacts of the COVID-19 pandemic, we compare the VMT (COVID) and noVMT (non-COVID) simulations (see Table 4.1).

4.2.3.1 Full domain

Figure 4.11 shows the percent change of some gas-phase pollutant concentrations between the COVID (VMT) and non-COVID (noVMT) cases throughout the domain averaged over April 1–30, 2020. NO_x and VOC concentrations decreased everywhere in response to emission decreases. The NO_x percent decrease is larger because onroad vehicles emit significant NO_x, but relatively little VOC compared to other sources (Figure 3.8). Despite the domain-wide decrease in emitted precursor gases, OH and O_3 both increased in the urban core. This is characteristic of a NO_x-saturated regime, as explained in Section 4.2.2.1. The spatial correlation between increased OH and increased O_3 (Figure 4.11a-b) is consistent with this logic. Also consistent with Section 4.2.2.1, the outer regions of the domain demonstrate NO_x-limited or NO_x-insensitive behavior, where small decreases in NO_x and VOC result in O_3 decrease.

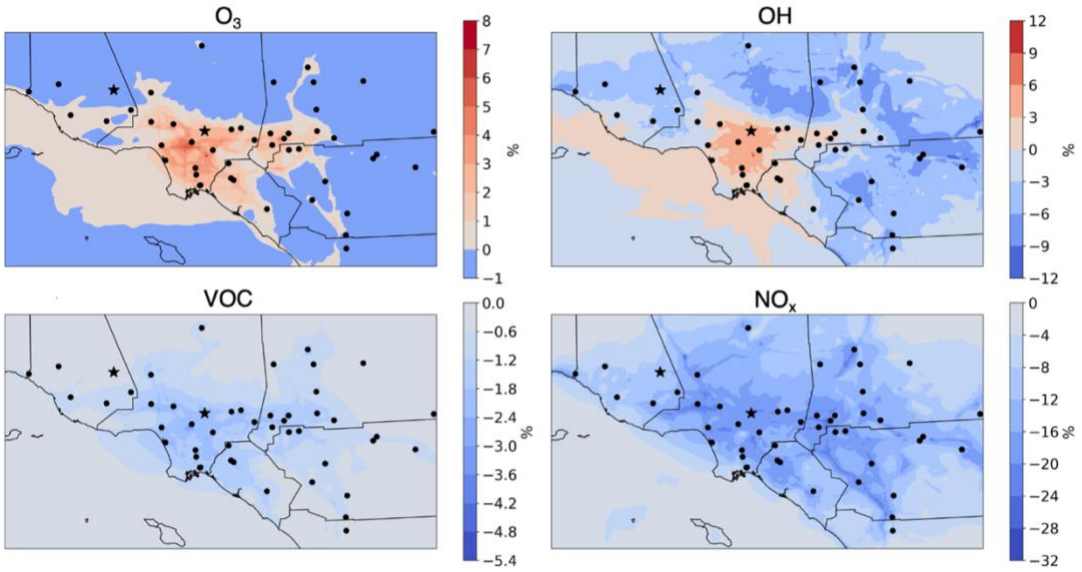

Figure 4.11: Percent change ([C_{COVID} - $C_{non\text{-}COVID}$] / $C_{non\text{-}COVID}$ * 100) averaged April 1–30, 2020 for a) O_3, b) OH, c) VOC, and d) NO_x. Black circles represent all EPA AQS measurement sites and black stars represent Pasadena and Fillmore.

The NO_x regimes can be compared to those investigated by Parker et al. (2020). In that work, COVID-impacted 2020 concentrations of O_3 and NO_2 were compared to historical trends of those concentrations at routine monitoring sites throughout the

LA Basin. They compared 2020 concentrations with concentrations predicted by extrapolating the historical trend, and determined whether O_3 and NO_2 either increased or decreased relative to the historical prediction. Based on the relative signs of the O_3 and NO_2 changes, they were able to classify each site as NO_x-saturated or NO_x-limited/insensitive. The sites investigated in Parker et al. (2020) are labeled on this study's April 1–30 average O_3 change predictions in Figure 4.12. In this work, we determine that all sites except Banning are NO_x-saturated, because the O_3 concentration increased in response to NO_x decreases. Parker et al. determined that Pasadena, Azusa, Glendora, Pomona, San Bernardino, and UCLA displayed NO_x-saturated behavior, consistent with our results. They found NO_x-limited or NO_x-insensitive behavior in Reseda, Upland, Fontana, Lake Elsinore, and La Habra, which is inconsistent with our findings. However, we note that the locations which were predicted in the prior study to have NO_x-limited behavior have small O_3 increases in our study. Taking the average O_3 change in only T_3 (Figure 4.12b), the O_3 change becomes even smaller. Therefore, while our work suggests that most of these regions are still NO_x-saturated, they are approaching NO_x-insensitivity. This is especially true at the high temperatures of T_3, which will become more prevalent as climate change worsens. T_3 also had the highest NO_x levels, so transitioning from NO_x-saturated to NO_x-limited is not simply dependent on reducing NO_x concentrations; it depends on decreasing VOC concentrations as well, since the NO_x regime is determined by the VOC-to-NO_x ratio.

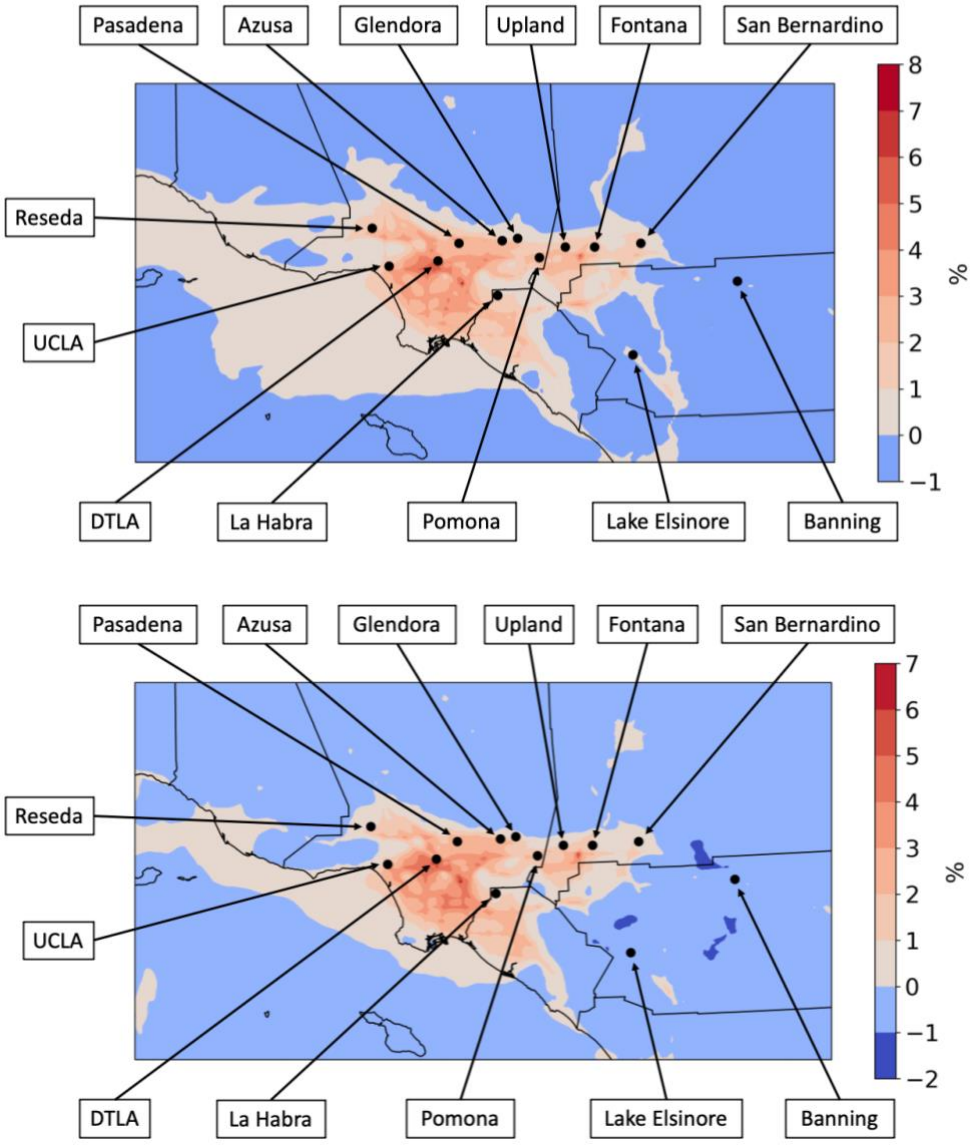

Figure 4.12: Percent change ([C_{COVID} - $C_{non\text{-}COVID}$] / $C_{non\text{-}COVID}$ * 100) of O_3 concentration averaged a) April 1–30, 2020 and b) T_3. Black circles and labels represent the sites studied in Parker et al. (2020).

Figure 4.13 shows the percent change of some aerosol-phase pollutant concentrations between the COVID (VMT) and non-COVID (noVMT) cases throughout the domain averaged over April 1–30, 2020. POA and $PM_{2.5}$ decrease everywhere, especially along freeways where vehicle particulate emissions are high. SOA decreases in most regions, but increases in the center of the urban core where emissions are highest.

The spatial distribution of SOA increase is consistent with the spatial distribution of OH increase (Figure 4.11). SOA is formed when OH reacts with gas- or aerosol-phase precursor species, so an increase in OH could increase SOA. Despite the decrease of POA and VOC precursor gases, the increase of OH was more important in terms of SOA formation. The ratio of SOA mass to POA mass increased everywhere (Figure 4.13c). This is due mostly to the decrease of POA concentrations. The increased ratio demonstrates the importance of considering secondary formation of pollutants when considering policy changes, as it is not enough to simply reduce the emissions of primary aerosols.

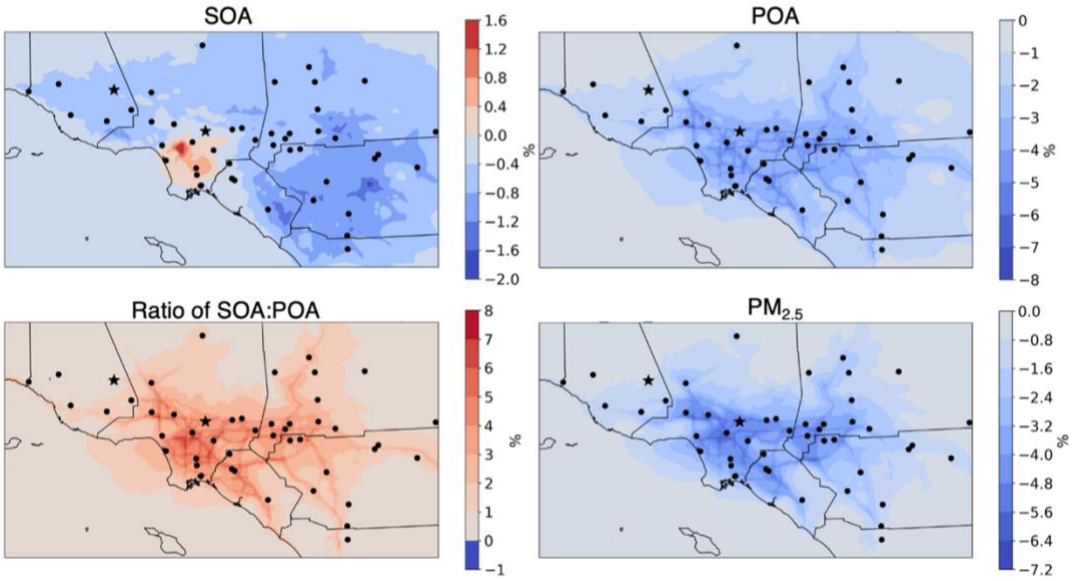

Figure 4.13: Percent change ([C_{COVID} - $C_{non\text{-}COVID}$] / $C_{non\text{-}COVID}$ * 100) averaged April 1–30, 2020 for a) SOA, b) POA, c) the ratio of SOA / POA, and d) $PM_{2.5}$. Black circles represent all EPA AQS measurement sites and black stars represent Pasadena and Fillmore.

The percent change of the main components of PM_1 are shown in Figure 4.14, and all components decrease. The importance of primary emissions on OM and SO_4 is clear by the visibility of specific freeways in those maps. Secondary production of NH_4 and NO_3 is evident by the spatial distribution of those species, i.e., the largest decreases existing downwind of the high-emissions regions.

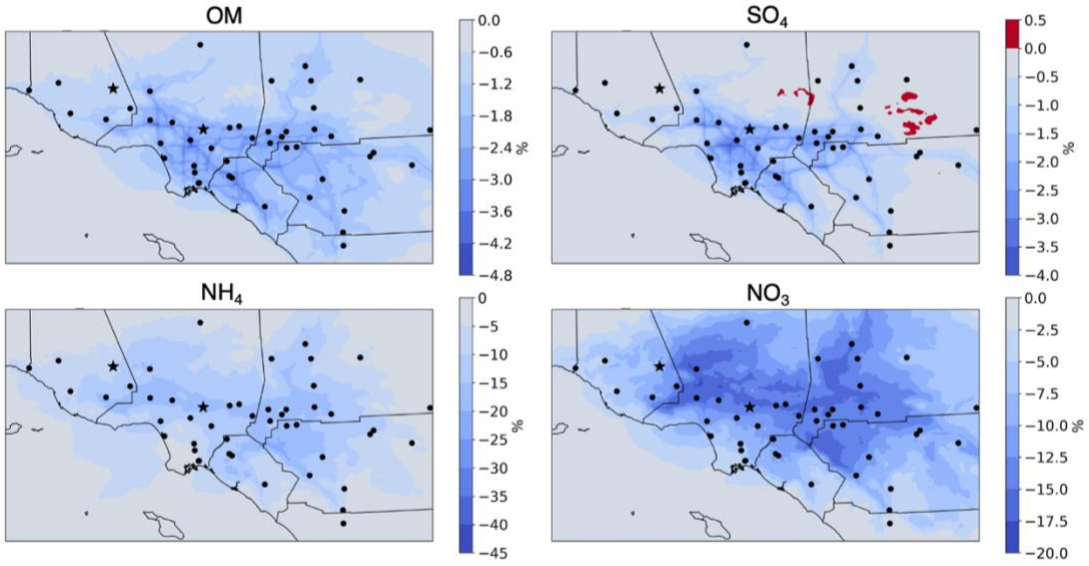

Figure 4.14: Percent change ([C_{COVID} - $C_{non\text{-}COVID}$] / $C_{non\text{-}COVID}$ * 100) averaged April 1–30, 2020 for PM_1 components: a) OM, b) SO_4, c) NH_4, and d) NO_3. Black circles represent all EPA AQS measurement sites and black stars represent Pasadena and Fillmore.

Next, we take a closer look at predicted pollutant concentrations in 2 locations with opposite NO_x regimes: Pasadena and Fillmore. These sites are labeled with stars in Figures 4.11, 4.12-14. We select Fillmore as the NO_x-limited region to investigate because it is contained within the masked domain which describes urban LA (Figure 4.1), as opposed to many of the other sites labeled in Figures 4.11 and 4.12-14 which are removed by the elevation mask.

4.2.3.2 Pasadena: NO_x-saturated

Pasadena is a polluted area that has its own emission sources in addition to being located downwind from heavily-polluted areas downtown, and our results show that it is in a NO_x-saturated regime (Figure 4.11). In response to COVID restrictions, emissions of CO, SO_2, NO_x, VOCs, and primary aerosols decreased, but OH and O_3 increased (Figure 4.15). The change in the nitrate radical (NO_3) is near zero when averaging over the entire month, but has variable behavior when averaged over T_1, T_2, and T_3 (Figure 4.15). NO_3 increases in response to the pandemic in T_1 and T_2, but

decreases in T_3, and the diurnal patterns are shown in Figure 4.S3. NO_3 is rapidly photolyzed during the day, so it only forms at night via the reaction of NO_2 and O_3. NO_3 then reacts with NO_2 to form dinitrogen pentaoxide (N_2O_5), which reacts with water particles to form nitric acid (HNO_3). HNO_3, unlike NO_3, does not photolyze during the daytime and so is a reservoir species which stores nitrogen and removes it from actively participating in reactions as NO_x. In T_3, NO_x concentrations are the highest, which increases the rate of NO_3 formation (Figure 4.S4) and subsequent N_2O_5 and HNO_3 formation. This means that less NO_x is available since more nitrogen is stored as daytime HNO_3. This explains why the difference in NO_x concentrations between the COVID and non-COVID simulations are the smallest in T_3, and why a smaller increase in O_3 is seen in T_3. NO_3 is an important overnight oxidant and contributes to the formation of inorganic NO_3 aerosol and organic nitrate aerosol. So, it is important to consider the potentially disparate impact of declining NO_x levels on NO_3 levels.

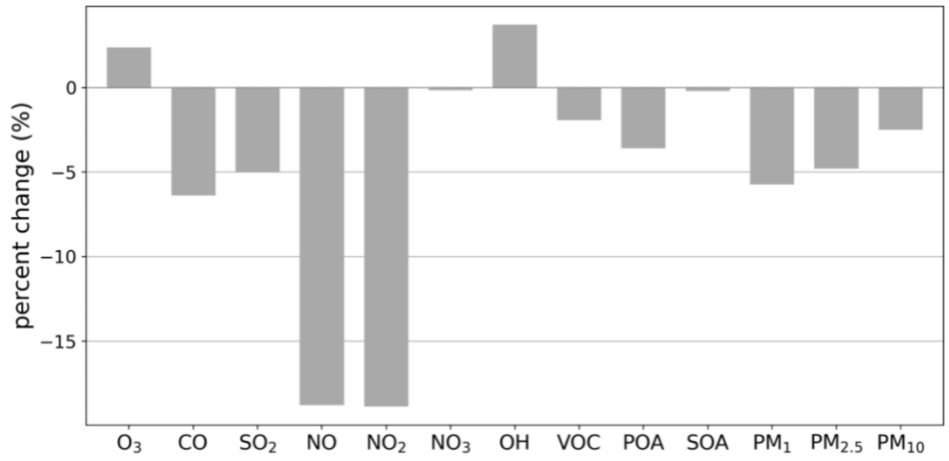

Figure 4.15: Percent change ($[C_{COVID} - C_{non\text{-}COVID}] / C_{non\text{-}COVID} * 100$) of pollutant concentrations in Pasadena averaged April 1–30, 2020.

SOA decreases during T_3, increases during T_2, and remains approximately unchanged during T_1. The decrease during T_3 is caused by a decrease in organic nitrate aerosol formation, explained by the decrease in the NO_3 radical (Figure 4.S4). The increase during T_2 is caused by increased daytime oxidation of precursors, as a

result of a slightly larger increase of the OH radical compared to other time periods (Figure 4.S3). However, this increase is very small, and almost negligible like the change seen in T_1. During all 3 time periods, total PM of all sizes (PM_1, $PM_{2.5}$, and PM_{10}) decreased (Figure 4.15). Despite increased oxidative capacity of the atmosphere, all components of PM (except SOA) decreased at all times due to decreased emissions of the aerosol components (e.g., NH_4, POA) as well as decreased emissions of the aerosol precursors gases (e.g., SO_2, NO_x, NH_3). Because SOA makes up a small fraction of PM as predicted by our model, the small changes in SOA had little impact on PM. In truth, SOA should make up a significant fraction of PM (Zhang et al., 2007; Jimenez et al., 2009), and so this is an inaccuracy in the model.

4.2.3.3 Fillmore: NO_x-limited

Our results suggest that Fillmore exists in a NO_x-limited or VOC-saturated regime, since O_3 concentrations decreased in response to decreased NO_x and VOC concentrations (Figure 4.11). In fact, the concentrations of most important pollutants decreased in response to the pandemic (Figure 4.16 and Figure 4.S5). The absolute percent reduction of NO_x is lowest in T_3 following the same reasoning as presented above for the reduced NO_x (via increased HNO_3) in Pasadena (Figure 4.S6), but to a lesser extent.

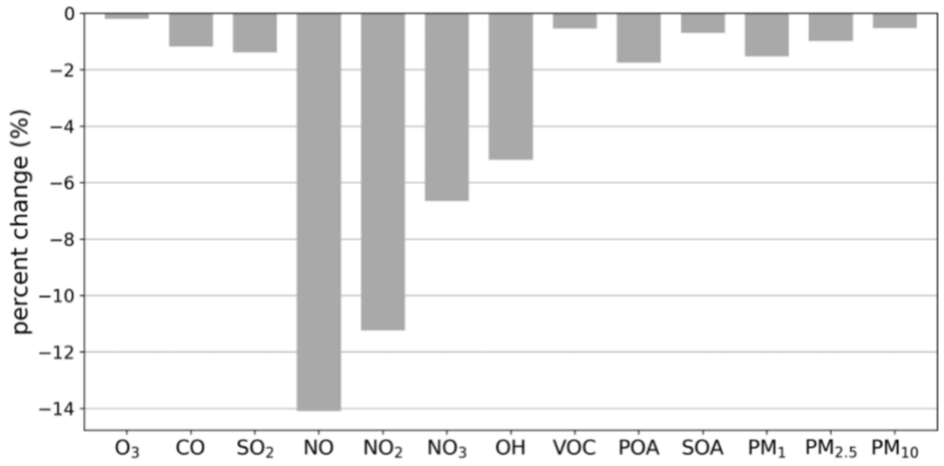

Figure 4.16: Percent change ($[C_{COVID} - C_{non\text{-}COVID}] / C_{non\text{-}COVID} * 100$) of pollutant concentrations in Fillmore averaged April 1–30, 2020.

4.2.4 Impact of boundary conditions

This section is forthcoming.

4.3 Conclusions

This section is forthcoming.

4.4 References

Caltrans. (2020). *Caltrans PeMS*. https://pems.dot.ca.gov/

Jimenez, J. L., Canagaratna, M. R., Donahue, N. M., Prevot, A. S. H., Zhang, Q., Kroll, J. H., DeCarlo, P. F., Allan, J. D., Coe, H., Ng, N. L., Aiken, A. C., Docherty, K. S., Ulbrich, I. M., Grieshop, A. P., Robinson, A. L., Duplissy, J., Smith, J. D., Wilson, K. R., Lanz, V. A., … Worsnop, D. R. (2009). Evolution of Organic Aerosols in the Atmosphere. *Science*, *326*(5959), 1525–1529. https://doi.org/10.1126/science.1180353

Parker, H. A., Hasheminassab, S., Crounse, J. D., Roehl, C. M., & Wennberg, P. O. (2020). Impacts of Traffic Reductions Associated With COVID-19 on Southern California Air Quality. *Geophysical Research Letters*, *47*(23), e2020GL090164. https://doi.org/10.1029/2020GL090164

Pennington, E. A., Seltzer, K. M., Murphy, B. N., Qin, M., Seinfeld, J. H., & Pye, H. O. T. (2021). Modeling secondary organic aerosol formation from volatile chemical products. *Atmospheric Chemistry and Physics*, *21*(24), 18247–18261. https://doi.org/10.5194/acp-21-18247-2021

Seinfeld, J. H., & Pandis, S. N. (2016). *Atmospheric Chemistry and Physics: From Air Pollution to Climate Change* (3rd ed.). John Wiley & Sons, Inc.

US EPA, O. (2013, August 1). *Air Quality System (AQS)* [Data and Tools]. US EPA. https://www.epa.gov/aqs

Zhang, Q., Jimenez, J. L., Canagaratna, M. R., Allan, J. D., Coe, H., Ulbrich, I., Alfarra, M. R., Takami, A., Middlebrook, A. M., Sun, Y. L., Dzepina, K., Dunlea, E., Docherty, K., DeCarlo, P. F., Salcedo, D., Onasch, T., Jayne, J. T., Miyoshi,

T., Shimono, A., … Worsnop, D. R. (2007). Ubiquity and dominance of oxygenated species in organic aerosols in anthropogenically-influenced Northern Hemisphere midlatitudes. *Geophysical Research Letters*, *34*(13). https://doi.org/10.1029/2007GL029979

4.5 Supporting Information

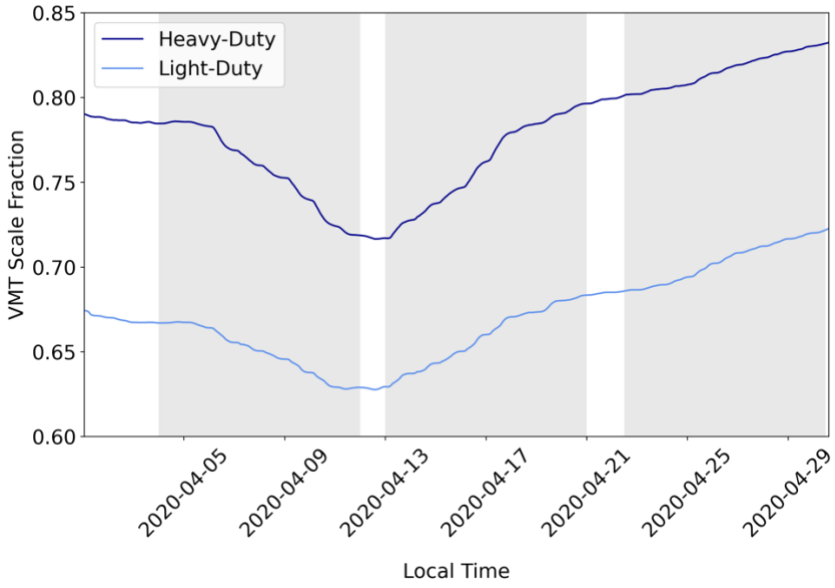

Figure 4.S1: Vehicle miles traveled (VMT) scale fractions for heavy-duty (dark blue) and light-duty (light blue) vehicles averaged over the masked domain April 1–30, 2020. Gray shading represents T_1, T_2, and T_3. VMT was scaled according to in situ PeMS data (Caltrans, 2020), described in Chapter 3.

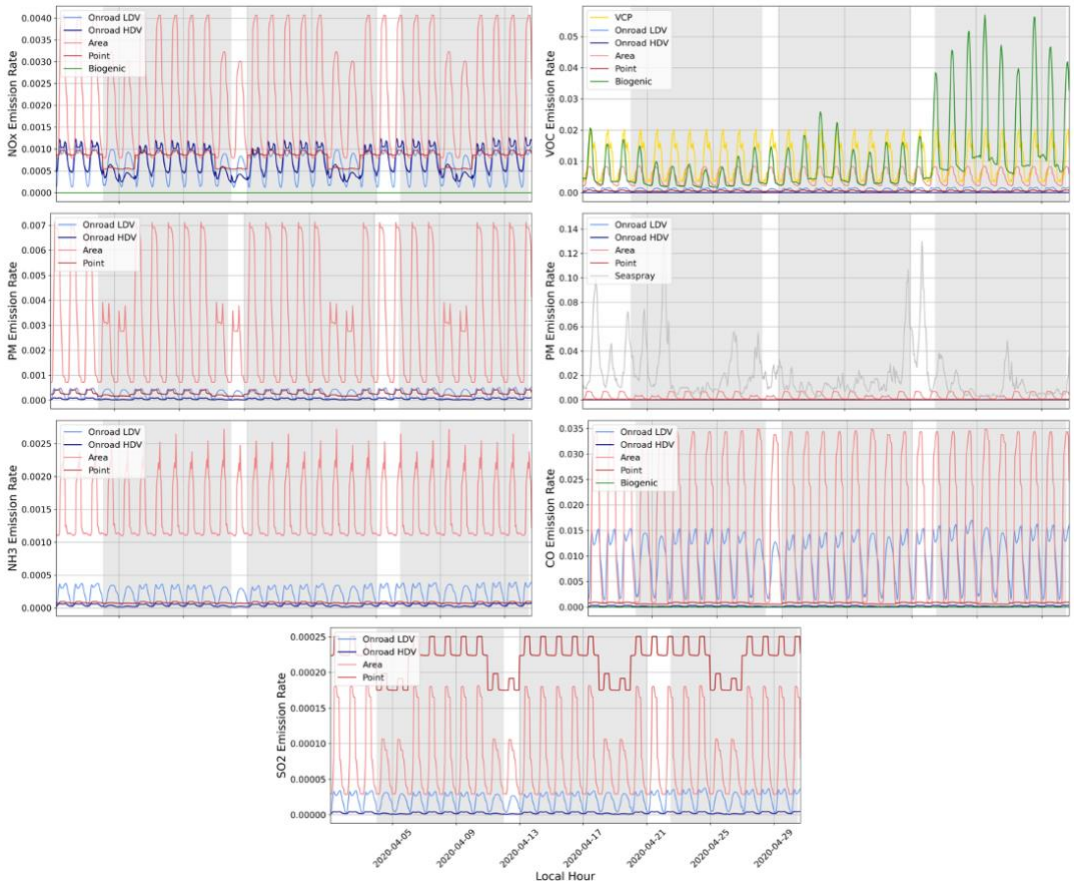

Figure 4.S2: Hourly emission rates from all sources averaged over the masked domain for a) NO_x, b) VOCs, c) PM with seaspray emissions excluded, d) PM, e) NH_3, f) CO, and g) SO_2. Gray shading represents T_1, T_2, and T_3.

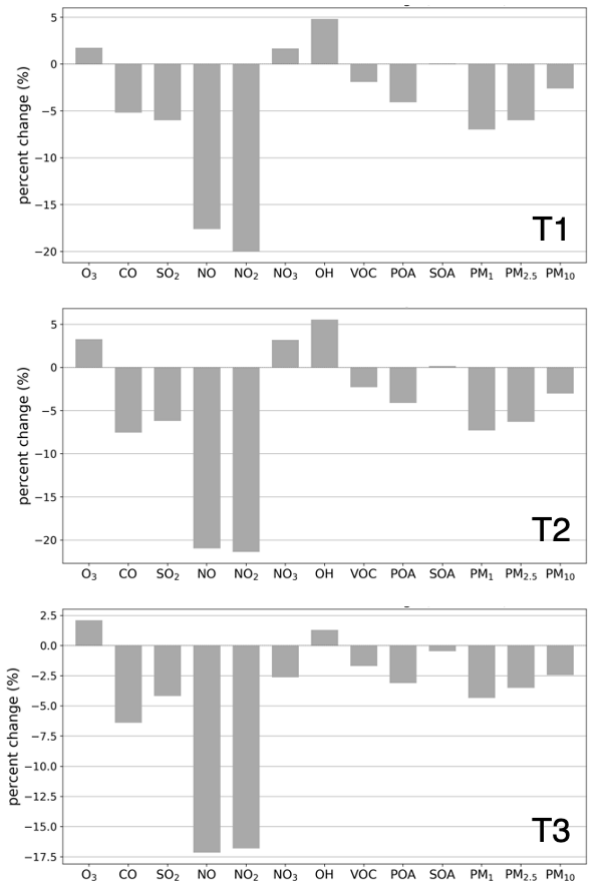

Figure 4.S3: Percent change ([C_{COVID} - $C_{non\text{-}COVID}$] / $C_{non\text{-}COVID}$ * 100) of pollutant concentrations in Pasadena averaged over T_1, T_2, and T_3.

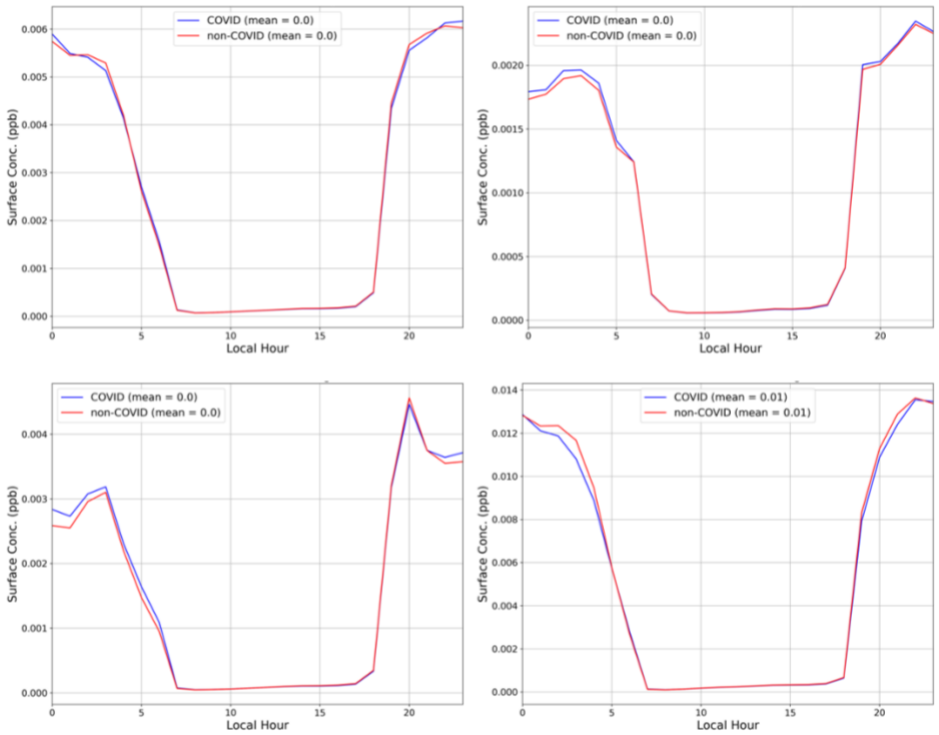

Figure 4.S4: Diurnally-averaged concentration of NO_3 in Pasadena for the COVID (VMT) simulation and non-COVID (noVMT) simulation using hourly data from a) all times, b) T_1, c) T_2, and d) T_3.

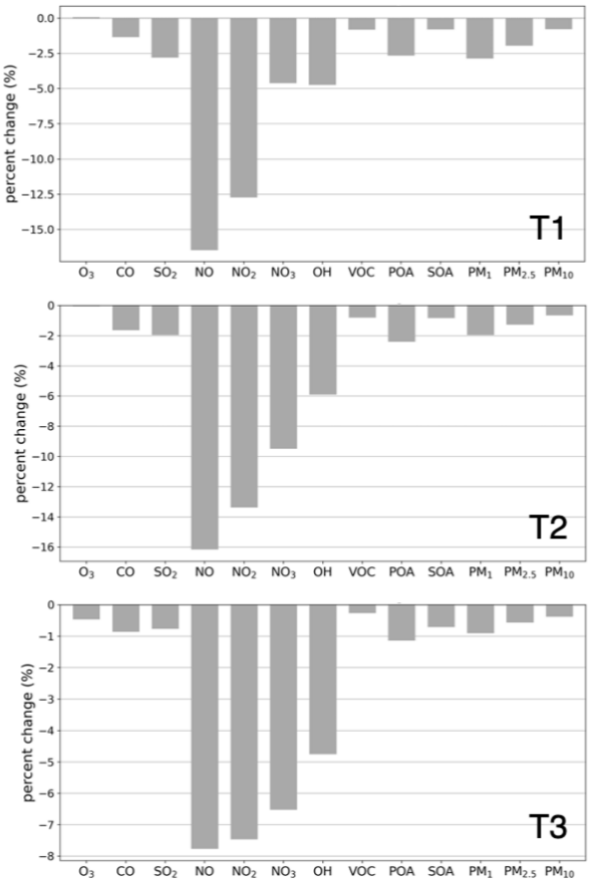

Figure 4.S5: Percent change ([C_{COVID} - $C_{non\text{-}COVID}$] / $C_{non\text{-}COVID}$ * 100) of pollutant concentrations in Fillmore averaged over T_1, T_2, and T_3.

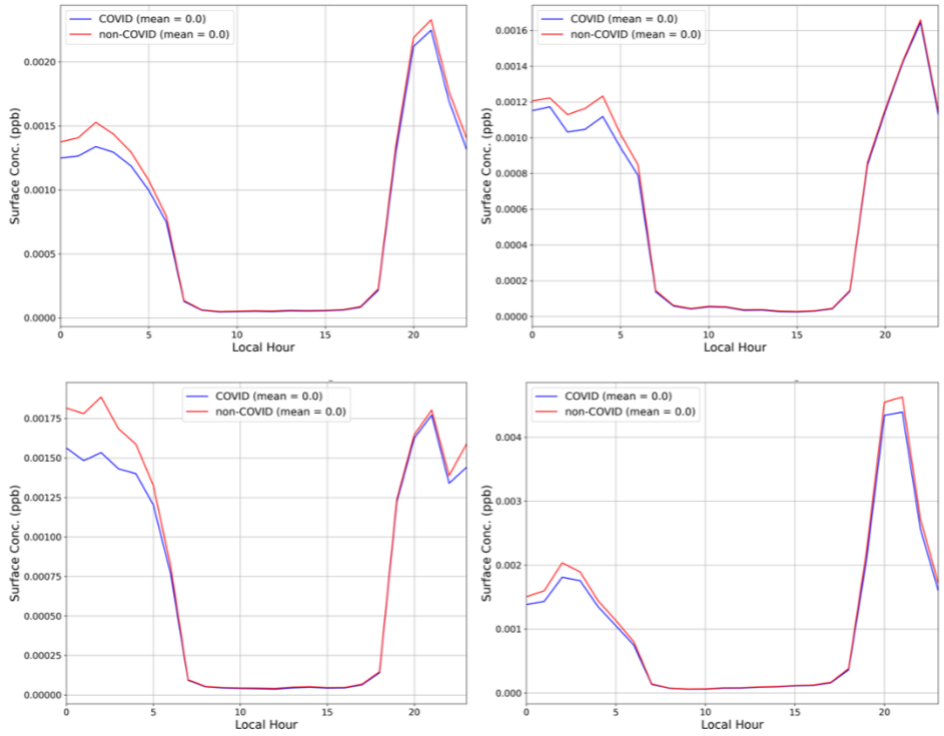

Figure 4.S6: Diurnally-averaged concentration of NO_3 in Fillmore for the COVID (VMT) simulation and non-COVID (noVMT) simulation using hourly data from a) all times, b) T_1, c) T_2, and d) T_3.

Appendix A

MODIFYING A CHEMICAL MECHANISM IN CMAQ

I wrote a section of the EPA's publicly available CMAQ documentation on Github.

The tutorial is available here:

https://github.com/USEPA/CMAQ/blob/main/DOCS/Users_Guide/Tutorials/CMAQ_UG_tutorial_chemicalmechanism.md.

Appendix B

VOLATILE CHEMICAL PRODUCT ENHANCEMENTS TO CRITERIA POLLUTANTS IN THE UNITED STATES

Seltzer, K. M., Murphy, B. N., Pennington, E. A., Allen, C., Talgo, K., & Pye, H. O. T. (2021). Volatile Chemical Product Enhancements to Criteria Pollutants in the United States. *Environmental Science & Technology*. https://doi.org/10.1021/acs.est.1c04298.

Volatile Chemical Product Enhancements to Criteria Pollutants in the United States

Karl M. Seltzer[1], Benjamin N. Murphy[2], Elyse A. Pennington[3], Chris Allen[4], Kevin Talgo[4], Havala O. T. Pye[2*]

[1]Oak Ridge Institute for Science and Education Postdoctoral Fellow in the Office of Research and Development, U.S. Environmental Protection Agency, 109 TW Alexander Dr, Research Triangle Park, NC 27711

[2]Office of Research and Development, U.S. Environmental Protection Agency, 109 TW Alexander Dr, Research Triangle Park, NC 27711

[3]Department of Chemical Engineering, California Institute of Technology, Pasadena, CA 91125

[4]General Dynamics Information Technology, Research Triangle Park, NC, 27711

*Correspondence to Havala O. T. Pye, pye.havala@epa.gov

Synopsis: Volatile chemical products are anthropogenic sources of reactive organic carbon emissions that enhance fine particulate matter and ozone throughout the United States.

Keywords: volatile chemical products, reactive organic carbon, secondary organic aerosol, ozone, PM2.5, air quality impacts.

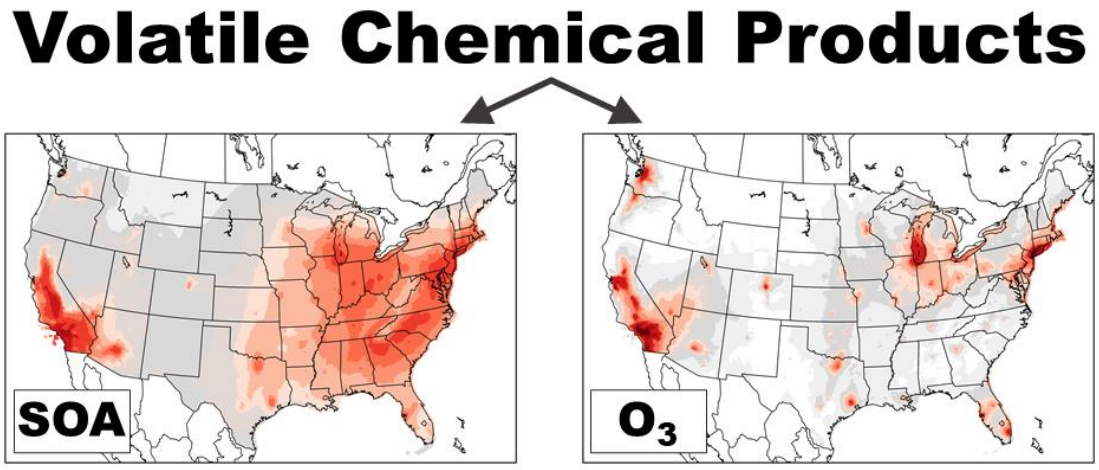

ABSTRACT

Volatile chemical products (VCPs) are a significant source of reactive organic carbon emissions in the United States, with a substantial fraction (>20% by mass) serving as secondary organic aerosol (SOA) precursors. Here, we incorporate a new nationwide VCP inventory into the Community Multiscale Air Quality (CMAQ) model, with VCP-specific updates to better model air quality impacts. Model results indicate that VCPs most enhance anthropogenic SOA in densely populated areas, with population-weighted annual average SOA increasing 15 – 30% in Southern California and New York City due to VCP emissions (contribution of 0.2 - 0.5 μg m^{-3}). Annually, VCP emissions enhance total population-weighted $PM_{2.5}$ by ~5% in California, ~3% in New York, New Jersey, and Connecticut, and 1 – 2% in most other states. While the maximum daily 8-hr ozone enhancements from VCP emissions are more modest, their influence can cause a several ppb increase on select days in major cities. Printing Inks, Cleaning Products, and Paints & Coatings product use categories contribute ~75% to the modeled VCP-derived SOA and Cleaning Products, Paints & Coatings, and Personal Care Products contribute ~81% to the modeled VCP-derived ozone. Overall, VCPs enhance multiple criteria pollutants throughout the United States, with the largest impacts in urban cores.

INTRODUCTION

Emissions of reactive organic carbon (ROC) are a critical component of atmospheric photochemistry (Heald et al., 2020). These emissions, which include all non-methane gas-phase and aerosol organic compounds (i.e. organic aerosol; OA), regulate the abundance of oxidants and gas-phase reactivity in the atmosphere (Heald et al., 2020; Safieddine et al., 2017). In addition, ROC contributes to the formation of fine particulate matter ($PM_{2.5}$) and tropospheric ozone (O_3). The influence of ROC on $PM_{2.5}$ can result from primary emission (i.e. primary organic aerosol; POA), secondary production via gas-phase oxidation of organics (i.e. secondary organic aerosol; SOA), or modulation of oxidants, which can influence the formation of inorganic $PM_{2.5}$ components (e.g. NH_4NO_3). Since $PM_{2.5}$ (Di et al., 2017), SOA (Pye et al., 2021), and O_3 (Turner et al., 2016) are all associated with adverse impacts to human health and welfare (U.S. EPA, 2020; U.S. EPA, 2019), understanding the sources and accurately modeling the evolution of ROC emissions in the atmosphere is important.

Volatile chemical products (VCPs) are used in residential, commercial, institutional, and industrial settings and lead to ROC emissions. These sources include, but are not limited to, cleaners, personal care products, adhesives, sealants, paints, coatings, pesticides, and printing inks, all of which partially evaporate on atmospherically relevant timescales. Collectively, VCPs are a major source of anthropogenic ROC emissions throughout the United States (Mc Donald et al., 2018; Seltzer et al., 2021) and the primary source of anthropogenic gas-phase ROC emissions in several urban regions (Gkatzelis et al., 2021; Khare & Gentner, 2018). In 2016, VCPs contributed ~3.1 Tg of ROC emissions in the United States (Seltzer et al., 2021), with ~20% of emissions by mass considered intermediate volatility organic compounds (IVOCs), which are efficient SOA precursors (Robinson et al., 2007; Zhao et al., 2014). As such, VCPs represent an emission source with considerable potential to affect urban $PM_{2.5}$ and O_3.

Despite their importance, adequate representation of VCP emissions in photochemical transport modeling is lacking (Qin et al., 2021). This partially stems

from the long-term focus on ROC emissions from combustion sources, which are largely non-oxygenated and have decreased dramatically in recent years due to targeted emission control efforts (Bishop & Stedman, 2008; McDonald et al., 2013), as well as the preeminent concern for reducing ozone in urban areas. As a result, the source attribution and chemical composition of ROC emissions has changed in the past few decades (Khare & Gentner, 2018). In addition, modeling urban SOA experiences continuing challenges (Baker et al., 2015; Ensberg et al., 2014; Woody et al., 2016) and representation of IVOC emissions and their multigenerational aging within chemical transport models (CTMs) is typically lacking (Murphy et al., 2017). Since VCPs have considerable SOA potential from their IVOC components (McDonald et al., 2018; Seltzer et al., 2021), representation of the complete volatility spectrum from VCP emissions is necessary to model their potential criteria pollutant impacts. These changes require updates to the chemical mechanisms within CTMs; which are used to predict air quality impacts from emissions.

Here, we incorporate a new VCP inventory (Seltzer et al., 2021) into the Community Multiscale Air Quality (CMAQ) model, with VCP-specific chemistry updates (Pennington et al., 2021), to better represent VCP emissions and subsequent air quality impacts throughout the contiguous United States. These updates include representation of secondary air pollutant formation pathways for alkane-like IVOCs, oxygenated IVOCs, and siloxanes. We then simulate air quality throughout the continental United States and quantify the national-level contributions of VCPs to criteria pollutants ($PM_{2.5}$ and O_3). Contributions from various categorical aggregations are assessed and the relative importance of VCP contributions to $PM_{2.5}$ and O_3 are quantified. We also evaluate the model's ability to simulate air quality following these updates and assess the potential burden that can result from additional assumptions related to VCP emissions, specifically marginal evaporation of potential semi-volatile organic compound (SVOC) ingredients.

METHODS

Regional Emissions

VCP emissions throughout the United States are estimated using VCPy.v1.1 (Seltzer et al., 2021). In VCPy, hundreds of individual VCPs (e.g. shampoo, glass cleaner, paint thinner) are aggregated into Product Use Categories (PUCs), which are split into sub-Product Use Categories (sub-PUCs) based on characteristic usage patterns. The methods of VCPy.v1.1 match the methods of VCPy.v1.0, as described in Seltzer et al. (2018). However, VCPy.v1.1 includes a substantial update to the organic composition of most sub-Product Use Categories (sub-PUCs), which incorporates the organic profiles reported in the latest California Air Resources Board (CARB) Consumer & Commercial Products survey (California Air Resources Board, 2020; Table S1). This update results in nearly no change to the estimated magnitude of VCP emissions, but some distinct variations in the volatility distribution and compound class make-up of emissions (Fig. S1). Notably, the proportion of IVOCs (3×10^2 μg $m^{-3} < C^* < 3 \times 10^6$ μg m^{-3}) and oxygenated compounds increase.

The emissions used here reflect 2016 conditions and yield a VCP national-average emission rate of 9.5 kg $person^{-1}$ $year^{-1}$. Prior analysis estimated that the sector-wide emission uncertainty, stemming from variables such as product usage and assigned product use timescale, is ±15% (Seltzer et al., 2021). Paints & Coatings contribute the largest fraction of ROC emissions and are predicted to be emitted at an average rate of ~3.1 kg $person^{-1}$ $year^{-1}$ nationally. Cleaning Products and Personal Care Products each contribute ~2.0 kg $person^{-1}$ $year^{-1}$, Adhesives & Sealants and Printing Inks both emit ~0.8 kg $person^{-1}$ $year^{-1}$, and pesticides emit ~0.6 kg $person^{-1}$ $year^{-1}$. Emissions from all other categories, including dry-cleaning, solvent usage in oil and gas operations, lighter fluids, and other miscellaneous products are estimated to emit ~0.1 kg $person^{-1}$ $year^{-1}$. VCPy currently assumes that all emissions occurring indoors are fully transported to the ambient atmosphere. A first-order approximation that includes chemical loss pathways and reduced characteristic timescales of evaporation

in indoor environments yields a reduction of ~12% for the complete sector. However, a comprehensive analysis of indoor termination pathways for VCP emissions, which can be particularly important for reactive species (Nazaroff & Weschler, 2004; Singer et al., 2007; Singer et al., 2004), will be the focus of future VCPy work and these approximations will not be included in the present analysis.

In VCPy, emissions are calculated at the national-level and allocated to the county-level using several proxies, including population, employment statistics, agricultural pesticides use, and oil and gas well counts. County-level emissions are further processed and gridded at 12-km scale within the continental United States for input into CMAQ. County-level data on the density of agricultural land and oil and gas wells are used to grid the agricultural pesticides and oil and gas solvent sub-PUCs. Population density is used to grid the remaining sub-PUCs within each county. Seasonal and diurnal emission variations are then applied to most sub-PUCs using profiles reported in Gkatzelis et al. (2021; Table S2). Sub-PUCs for which no applicable tracer from Gkatzelis et al. (2021) are available use a sinusoidal diurnal emissions profile with a peak at noon and no seasonal variation.

Other significant modeling updates include IVOC emissions and semi-volatile primary organic aerosol (SV-POA) profiles for all gasoline, diesel, and gas-turbine mobile sources (Lu et al., 2018). The implementation of mobile IVOC emissions follows the methodology of Lu et al. (2020). The remaining regional emission inputs come from the 2016 version 1 (U.S. EPA, 2021) emission modeling platform, which is built upon the U.S. Environmental Protection Agency's (U.S. EPA) 2014 National Emission Inventory (NEI) version 2 (2014NEIv2) and summarized in greater detail in Appel et al. (2021). The simulations performed here do not apply the approach of Murphy et al. (2017), which accounts for the estimated potential SOA contribution from combustion sources using an empirical relationship derived from southern California observations.

Using a near-field exposure model (Isaacs et al., 2021), prior research has indicated that non-negligible quantities of residential personal care products, household products, and coatings contain SVOC (0.3 $\mu g\ m^{-3} < C^* < 3 \times 10^2\ \mu g\ m^{-3}$) ingredients (Qin et al., 2021), which can evaporate on atmospherically relevant timescales (Khare & Gentner, 2018). To test the implications of marginal SVOC evaporation from VCPs on SOA potential, a simulation that assumes 2% of all non-evaporative organics (i.e. assumed non-volatile components of VCPs) evaporate is performed. This is within the bounds of near-field exposure modeling uncertainty for many VCP categories (Qin et al., 2021) and translates to ~0.355 kg $person^{-1}$ $year^{-1}$. In this sensitivity test, the additional emissions of SVOCs are given sinusoidal diurnal and seasonal emissions profiles, with peaks at noon and in summer, and are allocated to the county-level using population density as a spatial surrogate.

Chemical Transport Modeling

Air quality is simulated using CMAQv5.3.2 at 12-km resolution over the contiguous United States. The domain includes 299 rows, 459 columns, and 35 vertical layers spanning from the surface to 50 hPa, with the mid-point of the lowest layer typically ~10-m above ground level. All simulations include the complete 2016 calendar year with a 10-day spin-up beginning in December 2015 to minimize the influence of initial conditions. Additional modeling options largely follow the methods outlined in Appel et al. (2021), including: (1) no inline wind-blown dust, (2) the M3Dry deposition model with bi-directional NH_3 exchange enabled (Pleim et al., 2019), (3) inline calculation of biogenic emissions using the Biogenic Emission Inventory System (BEIS) v3.61 (Bash et al., 2016), (4) the AERO7 aerosol module, (5) inline lightning NO_x emissions calculated using the National Lighting Detection Network (Kang et al., 2019a; Kang et al., 2019b), (6) the CB6r3_AE7_AQ chemical mechanism (Yarwood et al., 2010), (7) ocean halogen chemistry and sea spray aerosol emissions (Sarwar et al., 2019), and (8) runtime emissions processing using the Detailed Emissions Scaling, Isolation, and Diagnostic (DESID) module (Murphy et al., 2020). Boundary conditions are generated from a 108-km Hemispheric CMAQ

simulation using CMAQv5.3 and meteorology inputs are generated from the Weather Research and Forecasting model v4.1.1 (see Appel et al. (2021) for more details).

Substantial updates to VCP-relevant chemistry were added to both the emissions processing for CB6r3_AE7_AQ and the chemistry of AERO7. In current and previous public, operational versions of CMAQ, lower-volatility, gas-phase anthropogenic ROC emissions were not represented in the chemical mechanism (Qin et al., 2021). As a result, much of the VCP mass (~30%; Pennington et al., 2021), often dominated by IVOCs, was not considered for SOA or radical chemistry. Recent work (Pennington et al., 2021; Lu et al., 2020) introduced several new chemical components to the AERO7 module within CMAQ to alleviate this issue, with an focus on alkane-like IVOCs, oxygenated IVOCs, SVOCs, and siloxanes, and modeled Los Angeles air quality during the 2010 California Nexus of Air Quality and Climate Change (CalNex) campaign (Ryerson et al., 2013).

Here, the mapping of all compounds emitted from VCPs are reviewed to ensure proper SOA and radical chemistry representation within CMAQ. For many VCP-relevant species emitted in high quantities (e.g. ethanol, acetone, toluene), no updates are necessary as they are explicitly considered within the chemical mechanism. For the compounds that are not explicitly included in the chemical mechanism, the order-of-operations for mapping explicit compounds to model species, with both SOA and radical chemistry considerations, is described in the Supporting Information.

To quantify the criteria pollutant enhancements resulting from VCP emissions, two main simulations are performed. The first incorporates all emission and chemical mechanism updates described above (i.e. the “base” simulation) and the second eliminates all VCP emissions (i.e. the “zero VCP” simulation). Thus, the difference of the two represents the enhancement of air pollution attributable to the VCP emissions in the modeling system. Seven additional zero-out simulations are performed to quantify the criteria pollutant enhancements from aggregations of different sub-PUCs. These simulations individually assess Cleaning Products,

Personal Care Products, Adhesives & Sealants, Paints & Coating, Printing Inks, Pesticides, and all other categories. For the SVOC evaporation simulation, additional emissions are treated as semi-volatile with a C* of 100 μg m^{-3}, undergo gas-phase oxidation chemistry, and have a SOA yield of ~65% at 10 μg m^{-3} (VSVPO3 model species; Murphy et al., 2017).

Air Quality Observations & Model Evaluation

Predictions of organic carbon (OC), total $PM_{2.5}$, and maximum daily 8-hour O_3 (MDA8 O_3) concentrations from the base simulation are compared with observations acquired from the U.S. Environmental Protection Agency's Air Quality System (AQS) to evaluate model performance. Since SOA is not routinely measured, organic carbon is the only organic fraction of $PM_{2.5}$ evaluated here. For OC and total $PM_{2.5}$, 24-hour filter samples are retrieved on a 1-in-3-day sampling schedule; whereas O_3 measurements are collected hourly, with the maximum daily 8-hour metric generated by the Atmospheric Model Evaluation Tool (AMET; Appel et al., 2011). Model predictions are paired in space and time with corresponding AQS observations using AMET. To assess model performance, the normalized mean bias (NMB) of daily model and observed pairings are sorted seasonally and regionally. We then evaluate whether the NMB from this study falls within the top 33rd percentile or the top 67th percentile of past evaluation applications, as reported by Emery et al. (2017). The top third of OC, $PM_{2.5}$, and MDA8 O_3, NMB are less than ±15%, ±10%, and ±5%, respectively, and the top two-thirds of NMB for OC, $PM_{2.5}$, and MDA8 O_3 are less than ±50%, ±30%, and ±15%, respectively.

RESULTS

Model Performance

The modeling configuration, emissions, and chemistry updates used here yield improved predictions of OC (Fig. AB.1 vs. Fig. S2) with bias metrics that often rank among the top, previously published model evaluations. Of the 24 seasonal and

regional aggregations evaluated, 10 had NMB values smaller than ±10% and the remaining 14 had NMB values smaller than ±50%. OC predictions were within ±15% of observations throughout most of the country in the winter and fall months, as well as the northeast in the spring and summer and the southeastern spring. Despite the inclusion of a state-of-science VCP inventory and improved SOA chemistry, CMAQ underpredicted OC in broad swaths of the country outside the East Coast in the spring and summer months (-44% ≤ NMB ≤ -16%). In addition, the model overpredicted OC in the southeastern U.S. during the summer (NMB = 39%) and was persistently low biased in the southwest, which is dominated by monitoring locations in California.

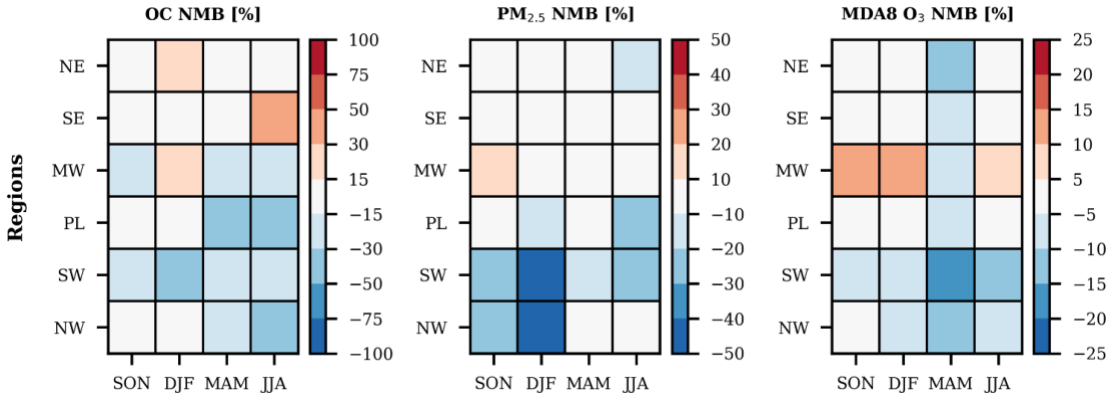

Figure *AB*.9. Modeling performance metrics for OC, $PM_{2.5}$, and maximum daily 8-hour O_3, disaggregated by season and region. Note: NE – U.S. EPA Regions 1, 2, 3; SE – U.S. EPA Region 4; MW – U.S. EPA Region 5; PL – U.S. EPA Regions 6, 7, 8; SW – U.S. EPA Region 9; NW – U.S. EPA Region 10; SON – fall months; DJF – winter months; MAM – spring months; JJA – summer months; NMB – normalized mean bias. See Table S3 in the supporting information for additional data related to the model evaluation.

Predictions of total $PM_{2.5}$ had a NMB smaller than ±10% in 14 seasonal and regional aggregations and smaller than ±30% in 8 others (Fig. AB.1). Model performance was generally good throughout the year and contiguous United States, except for a strong low bias along the West during cooler months. The cold season negative bias is

persistent in CMAQ (Appel et al., 2021) and has been attributed to biased predictions of nitrate during strong meteorological inversion episodes that could be alleviated using a finer modeling grid resolution (Appel et al., 2021; Kelly et al., 2019).

MDA8 O_3 was well predicted in all locations and seasons, with three notable exceptions. The model was persistently low biased throughout the United States in the spring, which has previously been attributed to underestimated ozone from the lateral boundary conditions (Appel et al., 2021; Sarwar et al., 2019). A separate possible mechanism for this bias could be the variability in the stomatal uptake of ozone, which is a major loss pathway for tropospheric ozone. This process initiates each year in the spring (Clifton et al., 2020), features year-to-year variability that is difficult to model (Clifton et al., 2017), and can perturb regional mean surface ozone concentrations by more than 5 ppb (Baublitz et al., 2020). Beyond this persistent springtime bias, the model results were also low biased in the southwest for all seasons, and generally high biased in the midwest for all non-springtime seasons. The correlation in low bias for OC and O_3 in the southwest year-round suggests a possible systematic error, such as missing emissions, oxidants, planetary boundary layer issues, or other transport errors.

Enhancements of Criteria Pollutants Attributable to VCP Emissions

VCPs generate a spatially variable increase in SOA concentrations throughout the contiguous United States, with notable peaks in California, along much of the East Coast, and in the Upper Midwest (Fig. AB.2). Enhancements were highest in Southern California, with Los Angeles County featuring a population-weighted annual average enhancement of ~0.5 μg m^{-3}. This translates to ~30% of the modeled, annual-average SOA mass in the county (Fig. S3). However, modeled organic carbon is still low biased in California (Fig. AB.1). This residual bias could be driven by additional missing emissions, inadequate process representations in the model, or systematic biases in meteorology. These factors can all influence the estimated increase in SOA attributable to VCPs found here. The greater New York City region

showed the second highest SOA enhancements attributable to VCPs, with annual increases generally spanning 0.2 – 0.3 µg m^{-3}, which accounts for ~17% of the modeled, annual-average SOA mass. Outside of heavily populated cities, VCP enhancements of SOA dropped precipitously throughout the Great Plains and Northwest. Nonetheless, VCPs were an important contributor to anthropogenic SOA throughout the United States with a nationwide, annual-average, population-weighted SOA enhancement of ~0.15 µg m^{-3}, or ~10% of the modeled, population-weighted SOA mass (Fig. S3).

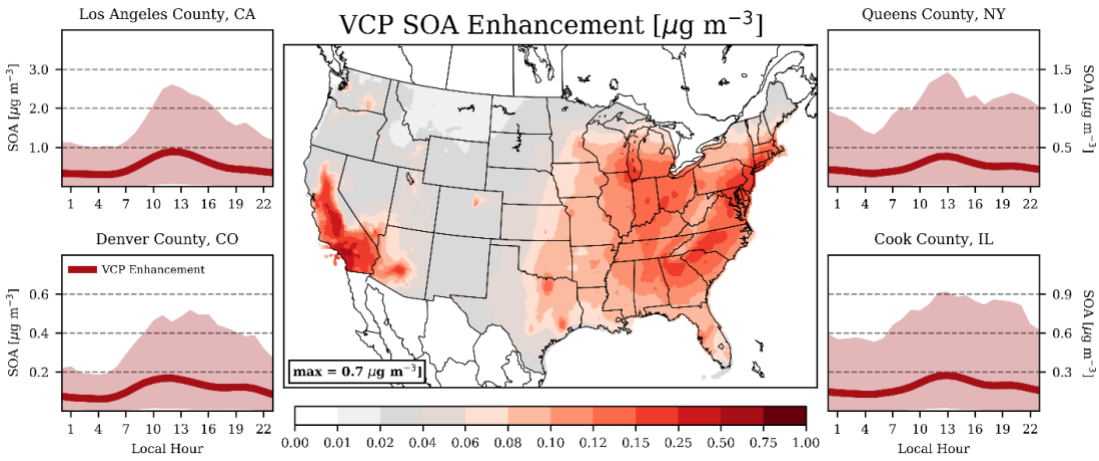

Figure *AB*.10. (Center) Annual-averge SOA enhancements attributable to VCP emissions. (Side Panels) Diurnal, population-weighted SOA enhancements attributable to VCP emissions for select counties. Line indicates the average VCP enhancements for each hour and shading represents the VCP enhancements for 95% of all days. Note: colormap is non-linear.

Seasonally, the magnitude of VCP-SOA enhancements was typically largest in the summer and fall months (Table S4), but the proportional contribution of VCPs to modeled SOA peaked in the cooler months (Table S5) when biogenic SOA is at a minimum. For example, the summer SOA enhancements in New York City (0.3 - 0.4 µg m^{-3}) were ~2.5x higher than the winter enhancements on an absolute basis, but VCPs contributed less on a relative basis in summer (~15%) than winter (~22%).

Diurnally, mean SOA enhancements peaked mid-afternoon along with photochemical intensity and fluctuated substantially from day-to-day (Fig. AB.2). In Los Angeles County, the population-weighted noontime-average SOA enhancement from VCPs was 0.9 μg m^{-3}, and 95% of the individual days fall within a range of 0.1 – 2.6 μg m^{-3}. Notably, these daily fluctuations were persistent during both the warmer and cooler months. Daily variation was pronounced in other major populations centers, as well (e.g. Denver, New York City, Chicago), suggesting the influence of VCPs on urban SOA could be a substantial component of $PM_{2.5}$ on select days throughout the United States.

While the ambient $PM_{2.5}$ enhancements from VCP emissions were dominated by SOA production, VCP chemistry can lead to the formation, or even reduction, of other $PM_{2.5}$ components (Fig. AB.2 vs. Fig. S4). These changes are driven by the effect of VCPs on local radical concentrations. VCP emissions serve as a sink of hydroxyl via reaction, which reduce the formation of nitric acid and cascaded into marginally lower ammonium nitrate concentrations (generally < 0.01 μg m^{-3}) throughout much of the United States. However, many urban cores are VOC-limited for O_3 production in cooler months (Simon et al., 2015). During the winter season, VCP emissions in these locations (e.g. Los Angeles, New York City, Detroit) generated O_3, which enhanced photochemistry and can produce up to ~0.3 μg m^{-3} of additional ammonium nitrate on select days. Annually, VCP emissions enhanced total $PM_{2.5}$ most in Southern California (Fig. S4) through the SOA formation pathway, with a net increase in the statewide population-weighted $PM_{2.5}$ of ~5%. Elsewhere, VCPs enhanced total $PM_{2.5}$ by ~3% in New York, New Jersey, and Connecticut, and 1 – 2% in most other states.

The spatial pattern of MDA8 O_3 enhancements from VCP emissions closely followed the SOA enhancements, but the relative effects were more localized and modest. Nationally, VCPs enhanced annual, population-weighted MDA8 O_3 by 0.4 ppb, which is ~1% of the modeled total (Fig. S5). The largest statewide enhancement in the population-weighted annual-average MDA8 O_3 was 1.2 ppb in California (~3%

of the modeled total; Table S4-S5). In the South Coast Air Basin (SoCAB) counties, annual-average enhancements were higher and spanned 1.6 – 3.0 ppb (4 – 6% of the modeled total). These average increases, however, do mask the relative importance of VCPs to O_3 on select days. For example, VCPs occasionally enhanced middle-of-the-day O_3 in Los Angeles County by 6-8 ppb (Fig. AB.3). Additionally, VCPs fractionally enhanced MDA8 O_3 to a greater degree on high ozone days in these urban centers. On average, VCPs enhanced MDA8 O_3 in SoCAB by ~4% when the daily MDA8 O_3 was less than 50 ppb and by ~7% when the daily MDA8 O_3 was greater than 60 ppb. MDA8 O_3 in the New York City region was also sensitive to VCP emissions. Annual enhancements of MDA8 O_3 averaged ~0.8 ppb in this region (2 – 3% of the modeled total), with larger contributions again on high ozone days. VCPs enhanced MDA8 O_3 in NYC by ~2% when the daily MDA8 O_3 was less than 50 ppb and by ~3% when the daily MDA8 O_3 was greater than 60 ppb. Outside California, the Northeast, and the upper Midwest, MDA8 O_3 enhancements from VCPs were minor, with most states indicating annual increases in population-weighted MDA8 O_3 of 0.1 – 0.2 ppb due to VCP usage.

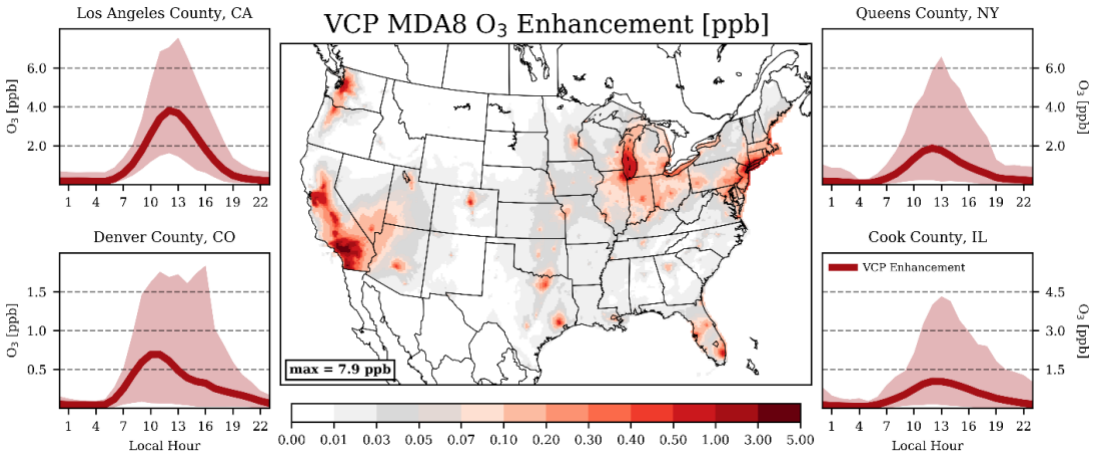

Figure *AB*.11. (Center) Summertime-averge MDA8 O_3 enhancements attributable to VCP emissions. (Side Panels) Diurnal, population-weighted O_3 enhancements attributable to VCP emissions for select counties. Line indicates the average VCP enhancements for each hour and shading represents the VCP enhancements for 95% of all days. Note: colormap is non-linear.

The influence of VCP emissions on O_3 peaked in the summer and in urban centers where NO_x emissions were highest (Fig. *AB.*3). Southern California again experienced the largest enhancement, with summer MDA8 O_3 increasing by 1.7 – 5.8 ppb (4 – 8%), on average, in the SoCAB counties. MDA8 O_3 in the New York City region was also sensitive to VCP emissions. Summertime enhancements in this region averaged ~1.5 ppb, which is 3 – 4% of the modeled total. While the magnitude of peak O_3 enhancements in the summertime were greater than in the winter, the effects of VCP emissions on O_3 were more widespread in the cooler months (Table S4). The peak county-level increase in MDA8 O_3 in the summer and winter season were 5.8 ppb (San Bernardino, California) and 1.5 ppb (Orange County, California), respectively. However, the median county-level increase of MDA8 O_3 in the winter was ~5x the median county-level increase in the summer, reflecting the localized nature of VCP impacts on summer O_3.

Product Use Category Contributions to SOA and MDA8 O_3

Variability in the chemical composition and subsequent speciated emissions of VCP categories generated considerable differences in contributions to SOA enhancements by PUC (Fig. AB.4). Annual average, population-weighted SOA enhancements were largely driven by emissions from Printing Inks, Cleaning Products, and Paints & Coatings, with smaller contributions from Pesticides, Adhesives & Sealants, and Personal Care Products. Printing Ink emissions contain large quantities of IVOC alkanes (C12-C16 hydrocarbons, represented by n-Tetradecane here) and toluene, Cleaning Products are rich in fragrances (represented by terpenes, such as limonene, here), and Paints & Coatings have an assortment of straight, branched, and cyclic IVOC alkanes, as well as toluene and xylenes in their composition. While Personal Care Products were responsible for ~20% of national VCP emissions, their contributions to SOA were predicted to be small (~6%). Siloxanes are a significant potential source of SOA in Personal Care Products, but oxidize slowly (k_{OH} = 1.55 x 10^{-12} cm^3 $molec.^{-1}$ s^{-1}) and thus generate little SOA in the source region.

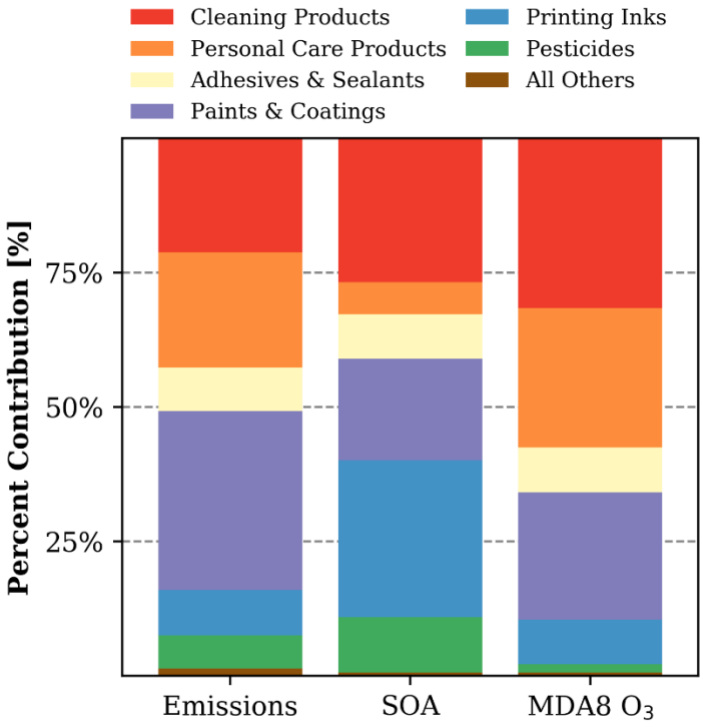

Figure *AB*.12. Percent contributions to national emissions, population-weighted, annual average SOA concentrations, and population-weighted, summertime average MDA8 O_3 concentrations by Product Use Category for the VCP sector.

In contrast, contributions to the summertime averaged, population-weighted MDA8 O_3 from each VCP category were closely correlated with emissions magnitude. Cleaning Products, Paints & Coatings, and Personal Care Products contributed ~76% of the total VCP emissions considered here and made up the bulk (~81%) of the MDA8 O_3 enhancements. The contributions from both Cleaning Products and Personal Care Products were driven by fragrances and glycols. Glycols and glycol ethers drove the response from architectural coatings, and toluene and xylene were the main contributors for aerosol and industrial coatings. The MDA8 O_3 contributions from both Adhesives & Sealants and Printing Inks were roughly proportional to their emissions magnitude. Lastly, emissions from pesticides and all other categories (i.e. dry-cleaning, solvent usage in oil and gas operations, lighter

fluids, and other miscellaneous products) together contribute ~2% of the MDA8 O_3 enhancement.

Possible Role of SVOC Evaporation on Ambient SOA

An emissions rate of ~0.355 kg person^{-1} year^{-1} of a SVOC model species with an effective SOA yield of 65% leads to ~114 Gg of ROC emissions and ~74 Gg of SOA potential. Following allocation of this SVOC using population density, the national-level, annual-average VCP-SOA increased ~8 – 17%, with the highest absolute increases over Southern California and New York City. These emissions led to non-negligible average SOA enhancements in urban centers (0.1 – 0.2 μg m^{-3} in summer months) and increased summer, county-level VCP-SOA by 13 – 27% (maximum of 34%). While these emissions might be a potentially important source of VCP-SOA, their inclusion did not systematically improve the predictions of OC (Fig. S6). The biggest improvements occurred in the southwestern summer and throughout the contiguous United States in the fall months. However, there was added high bias in the northeastern and midwestern winter (Fig. AB.1 vs. Fig. S6). Since VCP emissions are correlated with population density (Gkatzelis et al., 2021; Coggon et al., 2018) and low bias in modeled OC often manifests in locations with low population (i.e. the northwest and Great Plains), this suggests missing VCP sources that scale nationally cannot alone explain the remaining differences between model predictions and observations. Other drivers of modeled OC bias could include VCP sources that are regional in nature (e.g. agricultural pesticides, solvent usage in oil and gas operations; Seltzer et al., 2021), other sectors that are regional in nature (e.g. residential wood combustion; U.S. EPA, 2021), systematic biases in meteorological input, or missing SOA production pathways within CMAQ.

DISCUSSION

The results shown here indicate that VCPs enhance multiple criteria pollutants throughout the contiguous United States and are particularly impactful in populated

cities. Of the criteria pollutants and their sub-components, VCPs most enhance anthropogenic SOA, which has historically been low biased in CTMs unless empirical representations of missing emissions and chemistry are added. While modeled OC performance improves when VCP emissions and SOA formation pathways are added, additional work is needed to further enhance the robustness of SOA predictions from VCPs. For example, due to data limitations, several of the product composition profiles used here are older (i.e., Printing Inks and Industrial Coatings) and their assumed composition might not reflect present-day formulations. A separate, but equally old Printing Ink composite profile from CARB's organic profile database has an estimated effective SOA yield that is ~60% lower than what was used here. In addition, the alkane-like IVOC SOA parameterization implemented here was based on calculated precursor saturation concentration (C^*) and did not consider the effect of compound structure on SOA yield (Lim & Ziemann, 2009; Tkacik et al., 2012). Oxygenated-IVOCs, which contribute ~6.5% of VCP emissions, are understudied SOA precursors and represented with a simple parameterization. Some chamber studies suggest these compounds may have substantially higher yields (10 – 100%; Charan et al., 2021; Li et al., 2018) than what was assumed here (4.5%). The effects of chamber wall loss (Krechmer et al., 2016; Matsunaga & Ziemann, 2010) and NO_x-dependence (Chuang & Donahue, 2016) on estimated SOA yields could also modify the magnitude of the VCP-SOA response. Furthermore, field studies that deploy instrumentation capable of detecting VCP-tracer compounds (Gkatzelis et al., 2021) will help constrain the overall magnitude and trends of VCP emissions, as well as provide insight into additional seasonal and diurnal patterns of emission.

In the future, if emissions from the mobile sector continue their multi-decade decline, VCPs will inherit a growing proportion of the anthropogenic ROC emissions burden. Even at near-present emission conditions, the VCP IVOC emissions modeled here generate nearly double the population-weighted SOA concentrations that mobile IVOC emissions are predicted to produce. Future implications of VCP emissions on ozone air quality are less clear and thus are deserving of attention. Most summertime

O_3 production in the United States occurs under NO_x-limited conditions, except for a few major urban areas (Los Angeles, Chicago, and New York; Jin et al., 2020) where VCPs currently have large impacts. As NO_x emissions are further reduced, even these NO_x-saturated locations could become NO_x-limited. However, many urban regions shift to NO_x-saturated conditions during the winter (Jin et al., 2017). Several epidemiological studies have indicated that annual exposure to ozone can have deleterious impacts on human-health (Turner et al., 2016; Lim et al., 2019), which suggests ozone mitigation strategies could indicate an increasing effectiveness of controlling ROC from VCPs.

In addition to criteria pollutants, oxidation of VCP emissions in the atmosphere can lead to other toxic compounds, such as formaldehyde (Fig. S3). In southern California and the New York City region, VCP emissions enhance modeled formaldehyde by 5 – 7% and 3 – 4%, respectively. These multiphase pollution endpoints (i.e., particle-phase, SOA, and gas-phase, O_3 and HCHO), as well as the seasonal ammonium nitrate response previously discussed, underscore the need for chemical mechanisms that more tightly couple gas- and aerosol-phase chemistry, thus accommodating important but less recognized feedbacks. Such considerations will only increase in importance as additional chemistry updates (e.g. autoxidation, particulate organic nitrates, oligomerization) are incorporated into CTMs.

ASSOCIATED CONTENT

Supporting Information. The Supporting Information associated with this manuscript is available free of charge at https://pubs.acs.org/doi/10.1021/acs.est.1c04298.

Corresponding Author

*Havala O. T. Pye; pye.havala@epa.gov

Author Contributions

KMS and HOTP designed the research scope. All authors participated in data curation, model development, and/or analysis. KMS and HOTP drafted the initial

manuscript and all authors contributed to subsequent drafts. All authors have given approval to the final version of the manuscript.

Funding Sources

This research was supported in part by an appointment to the U.S. Environmental Protection Agency (EPA) Research Participation Program administered by the Oak Ridge Institute for Science and Education (ORISE) through an interagency agreement between the U.S. Department of Energy (DOE) and the U.S. Environmental Protection Agency. ORISE is managed by ORAU under DOE contract number DE-SC0014664. All opinions expressed in this paper are the author's and do not necessarily reflect the policies and views of US EPA, DOE, or ORAU/ORISE.

NOTES

The authors declare no competing financial interest.

Although this work was contributed by research staff in the Environmental Protection Agency and has been reviewed and approved for publication, it does not reflect official policy of the EPA. The views expressed in this document are solely those of authors and do not necessarily reflect those of the Agency. EPA does not endorse any products or commercial services mentioned in this publication.

ACKNOWLEDGEMENTS

The authors would like to thank Venkatesh Rao, Alison Eyth, Wyat Appel, Heather Simon, Norm Possiel, Art Diem, and George Pouliot at the U.S. EPA, Kyriacos Kyriacou at the California Air Resources Board, and Georgios Gkatzelis, Carsten Warneke, and Matthew Coggon at the National Oceanic and Atmospheric Administration Chemical Sciences Laboratory/Cooperative Institute for Research in Environmental Sciences at the University of Colorado, Boulder for helpful discussions and/or data acquisition. Comments by Heather Simon (EPA), Ivan Piletic (EPA), and three anonymous reviewers served to strengthen this manuscript.

REFERENCES

Appel, K. W.; Gilliam, R. C.; Davis, N.; Zubrow, A.; Howard, S. C., Overview of the atmospheric model evaluation tool (AMET) v1.1 for evaluating meteorological and air quality models. *Environ Modell Softw* **2011,** *26* (4), 434-443.

Appel, K. W.; Bash, J. O.; Fahey, K. M.; Foley, K. M.; Gilliam, R. C.; Hogrefe, C.; Hutzell, W. T.; Kang, D.; Mathur, R.; Murphy, B. N.; Napelnok, S. L.; Nolte, C. G.; Pleim, J. E.; Pouliot, G. A.; Pye, H. O. T.; Ran, L.; Roselle, S. J.; Sarwar, G.; Schwede, D. B.; Sidi, F. I.; Spero, T. L.; Wong, D. C., The Community Multiscale Air Quality (CMAQ) model versions 5.3 and 5.3.1: system updates and evaluation. *Geosci Model Dev* **2021,** *14*, 2867-2897.

Baker, K. R.; Carlton, A. G.; Kleindienst, T. E.; Offenberg, J. H.; Beaver, M. R.; Gentner, D. R.; Goldstein, A. H.; Hayes, P. L.; Jimenez, J. L.; Gilman, J. B.; de Gouw, J. A.; Woody, M. C.; Pye, H. O. T.; Kelly, J. T.; Lewandowski, M.; Jaoui, M.; Stevens, P. S.; Brune, W. H.; Lin, Y. H.; Rubitschun, C. L.; Surratt, J. D., Gas and aerosol carbon in California: comparison of measurements and model predictions in Pasadena and Bakersfield. *Atmos Chem Phys* **2015,** *15* (9), 5243-5258.

Bash, J. O.; Baker, K. R.; Beaver, M. R., Evaluation of improved land use and canopy representation in BEIS v3.61 with biogenic VOC measurements in California. *Geosci Model Dev* **2016,** *9* (6), 2191-2207.

Baublitz, C. B.; Fiore, A. M.; Clifton, O. E.; Mao, J. Q.; Li, J. Y.; Correa, G.; Westervelt, D. M.; Horowitz, L. W.; Paulot, F.; Williams, A. P., Sensitivity of Tropospheric Ozone Over the Southeast USA to Dry Deposition. *Geophys Res Lett* **2020,** *47* (7).

Bishop, G. A.; Stedman, D. H., A decade of on-road emissions measurements. *Environ Sci Technol* **2008,** *42* (5), 1651-1656.

California Air Resources Board *Organic Gas Speciation Profiles for Consumer Products (2020 Update)*; Air Quality Planning and Science Division: 2020.

Charan, S. M.; Buenconsejo, R. S.; Seinfeld, J. H., Secondary organic aerosol yields from the oxidation of benzyl alcohol. *Atmos Chem Phys* **2021,** *20* (21), 13167-13190.

Chuang, W. K.; Donahue, N. M., A two-dimensional volatility basis set - Part 3: Prognostic modeling and NOx dependence. *Atmos Chem Phys* **2016,** *16* (1), 123-134.

Clifton, O. E.; Fiore, A. M.; Munger, J. W.; Malyshev, S.; Horowitz, L. W.; Shevliakova, E.; Paulot, F.; Murray, L. T.; Griffin, K. L., Interannual variability in ozone removal by a temperate deciduous forest. *Geophys Res Lett* **2017,** *44* (1), 542-552.

Clifton, O. E.; Lombardozzi, D. L.; Fiore, A. M.; Paulot, F.; Horowitz, L. W., Stomatal conductance influences interannual variability and long-term changes in regional cumulative plant uptake of ozone. *Environ Res Lett* **2020,** *15* (11).

Coggon, M. M.; McDonald, B. C.; Vlasenko, A.; Veres, P. R.; Bernard, F.; Koss, A. R.; Yuan, B.; Gilman, J. B.; Peischl, J.; Aikin, K. C.; DuRant, J.; Warneke, C.; Li, S. M.; de Gouw, J. A., Diurnal Variability and Emission Pattern of Decamethylcyclopentasiloxane (D-5) from the Application of Personal Care Products in Two North American Cities. *Environ Sci Technol* **2018,** *52* (10), 5610-5618.

Di, Q.; Wang, Y.; Zanobetti, A.; Wang, Y.; Koutrakis, P.; Choirat, C.; Dominici, F.; Schwartz, J. D., Air Pollution and Mortality in the Medicare Population. *New Engl J Med* **2017,** *376* (26), 2513-2522.

Emery, C.; Liu, Z.; Russell, A. G.; Odman, M. T.; Yarwood, G.; Kumar, N., Recommendations on statistics and benchmarks to assess photochemical model performance. *J Air Waste Manage* **2017,** *67* (5), 582-598.

Ensberg, J. J.; Hayes, P. L.; Jimenez, J. L.; Gilman, J. B.; Kuster, W. C.; de Gouw, J. A.; Holloway, J. S.; Gordon, T. D.; Jathar, S.; Robinson, A. L.; Seinfeld, J. H., Emission factor ratios, SOA mass yields, and the impact of vehicular emissions on SOA formation. *Atmos Chem Phys* **2014,** *14* (5), 2383-2397.

Gkatzelis, G. I.; Coggon, M. M.; McDonald, B. C.; Peischl, J.; Gilman, J. B.; Aikin, K. C.; Robinson, M. A.; Canonaco, F.; Prevot, A. S. H.; Trainer, M.; Warneke, C., Observations Confirm that Volatile Chemical Products Are a Major Source of Petrochemical Emissions in U.S. Cities. *Environ Sci Technol* **2021,** *55* (8), 4332-4343.

Gkatzelis, G. I.; Coggon, M. M.; McDonald, B. C.; Peischl, J.; Aikin, K. C.; Gilman, J. B.; Trainer, M.; Warneke, C., Identifying Volatile Chemical Product Tracer Compounds in US Cities. *Environ Sci Technol* **2021,** *55* (1), 188-199.

Heald, C. L.; Kroll, J. H., The fuel of atmospheric chemistry: Toward a complete description of reactive organic carbon. *Sci Adv* **2020,** *6* (6).

Isaacs, K. K.; Glen, W. G.; Egeghy, P.; Goldsmith, M. R.; Smith, L.; Vallero, D.; Brooks, R.; Grulke, C. M.; Ozkaynak, H., SHEDS-HT: An Integrated Probabilistic Exposure Model for Prioritizing Exposures to Chemicals with Near-Field and Dietary Sources. *Environ Sci Technol* **2014,** *48* (21), 12750-12759.

Jin, X.; Fiore, A.; Boersma, K. F.; De Smedt, I.; Valin, L., Inferring Changes in Summertime Surface Ozone–NOx–VOC Chemistry over U.S. Urban Areas from Two Decades of Satellite and Ground-Based Observations. *Environ Sci Technol* **2020,** *54* (11), 6518-6529.

Jin, X. M.; Fiore, A. M.; Murray, L. T.; Valin, L. C.; Lamsal, L. N.; Duncan, B.; Folkert Boersma, K.; De Smedt, I.; Abad, G. G.; Chance, K.; Tonnesen, G. S., Evaluating a Space-Based Indicator of Surface Ozone-NOx-VOC

Sensitivity Over Midlatitude Source Regions and Application to Decadal Trends. *J Geophys Res-Atmos* **2017,** *122* (19), 10231-10253.

Kang, D. W.; Foley, K. M.; Mathur, R.; Roselle, S. J.; Pickering, K. E.; Allen, D. J., Simulating lightning NO production in CMAQv5.2: performance evaluations. *Geosci Model Dev* **2019a,** *12* (10), 4409-4424.

Kang, D. W.; Pickering, K. E.; Allen, D. J.; Foley, K. M.; Wong, D. C.; Mathur, R.; Roselle, S. J., Simulating lightning NO production in CMAQv5.2: evolution of scientific updates. *Geosci Model Dev* **2019b,** *12* (7), 3071-3083.

Kelly, J. T.; Koplitz, S. N.; Baker, K. R.; Holder, A. L.; Pye, H. O. T.; Murphy, B. N.; Bash, J. O.; Henderson, B. H.; Possiel, N. C.; Simon, H.; Eyth, A. M.; Jang, C.; Phillips, S.; Timin, B., Assessing PM2.5 model performance for the conterminous U.S. with comparison to model performance statistics from 2007-2015. *Atmos Environ* **2019,** *214* (1).

Khare, P.; Gentner, D. R., Considering the future of anthropogenic gas-phase organic compound emissions and the increasing influence of non-combustion sources on urban air quality. *Atmos Chem Phys* **2018,** *18* (8), 5391-5413.

Krechmer, J. E.; Pagonis, D.; Ziemann, P. J.; Jimenez, J. L., Quantification of Gas-Wall Partitioning in Teflon Environmental Chambers Using Rapid Bursts of Low-Volatility Oxidized Species Generated in Situ. *Environ Sci Technol* **2016,** *50* (11), 5757-5765.

Li, W. H.; Li, L. J.; Chen, C. L.; Kacarab, M.; Peng, W. H.; Price, D.; Xu, J.; Cocker, D. R., Potential of select intermediate-volatility organic compounds and consumer products for secondary organic aerosol and ozone formation under relevant urban conditions. *Atmos Environ* **2018,** *178*, 109-117.

Lim, Y. B.; Ziemann, P. J., Effects of Molecular Structure on Aerosol Yields from OH Radical-Initiated Reactions of Linear, Branched, and Cyclic Alkanes in the Presence of NOx. *Environ Sci Technol* **2009,** *43* (7), 2328-2334.

Lim, C. C.; Hayes, R. B.; Ahn, J.; Shao, Y. Z.; Silverman, D. T.; Jones, R. R.; Garcia, C.; Bell, M. L.; Thurston, G. D., Long-Term Exposure to Ozone and Cause-Specific Mortality Risk in the United States. *Am J Resp Crit Care* **2019,** *200* (8), 1022-1031.

Lu, Q. Y.; Zhao, Y. L.; Robinson, A. L., Comprehensive organic emission profiles for gasoline, diesel, and gas-turbine engines including intermediate and semi-volatile organic compound emissions. *Atmos Chem Phys* **2018,** *18* (23), 17637-17654.

Lu, Q. Y.; Murphy, B. N.; Qin, M. M.; Adams, P.; Zhao, Y. L.; Pye, H. O. T.; Efstathiou, C.; Allen, C.; Robinson, A. L., Simulation of organic aerosol formation during the CalNex study: updated mobile emissions and secondary organic aerosol parameterization for intermediate-volatility organic compounds. *Atmos Chem Phys* **2020,** *20* (7), 4313-4332.

Matsunaga, A.; Ziemann, P. J., Gas-Wall Partitioning of Organic Compounds in a Teflon Film Chamber and Potential Effects on Reaction Product and Aerosol Yield Measurements. *Aerosol Sci Tech* **2010,** *44* (10), 881-892.

McDonald, B. C.; Gentner, D. R.; Goldstein, A. H.; Harley, R. A., Long-Term Trends in Motor Vehicle Emissions in US Urban Areas. *Environ Sci Technol* **2013,** *47* (17), 10022-10031.

McDonald, B. C.; de Gouw, J. A.; Gilman, J. B.; Jathar, S. H.; Akherati, A.; Cappa, C. D.; Jimenez, J. L.; Lee-Taylor, J.; Hayes, P. L.; McKeen, S. A.; Cui, Y. Y.; Kim, S. W.; Gentner, D. R.; Isaacman-VanWertz, G.; Goldstein, A. H.; Harley, R. A.; Frost, G. J.; Roberts, J. M.; Ryerson, T. B.; Trainer, M., Volatile chemical products emerging as largest

petrochemical source of urban organic emissions. *Science* **2018,** *359* (6377), 760-764.

Murphy, B. N.; Woody, M. C.; Jimenez, J. L.; Carlton, A. M. G.; Hayes, P. L.; Liu, S.; Ng, N. L.; Russell, L. M.; Setyan, A.; Xu, L.; Young, J.; Zaveri, R. A.; Zhang, Q.; Pye, H. O. T., Semivolatile POA and parameterized total combustion SOA in CMAQv5.2: impacts on source strength and partitioning. *Atmos Chem Phys* **2017,** *17* (18), 11107-11133.

Murphy, B. N.; Nolte, C. G.; Sidi, F.; Bash, J. O.; Appel, K. W.; Jang, C.; Kang, D.; Kelly, J.; Mathur, R.; Napelnok, S.; Pouliot, G.; Pye, H. O. T., The Detailed Emissions Scaling, Isolation, and Diagnostic (DESID) module in the Community Multiscale Air Quality (CMAQ) Modeling System version 5.3. *Geoscientific Model Development Discussions* **2020**.

Nazaroff, W. W.; Weschler, C. J., Cleaning products and air fresheners: exposure to primary and secondary air pollutants. *Atmos Environ* **2004,** *38* (18), 2841-2865.

Pennington, E. A.; Seltzer, K. M.; Murphy, B. N.; Qin, M.; Seinfeld, J. H.; Pye, H. O. T., Modeling secondary organic aerosol formation from volatile chemical products. *Atmos Chem Phys Discuss* **2021**.

Pleim, J. E.; Ran, L. M.; Appel, W.; Shephard, M. W.; Cady-Pereira, K., New Bidirectional Ammonia Flux Model in an Air Quality Model Coupled With an Agricultural Model. *J Adv Model Earth Sy* **2019,** *11* (9), 2934-2957.

Pye, H. O. T.; Ward-Caviness, C. K.; Murphy, B. N.; Appel, K. W.; Seltzer, K. M., Secondary organic aerosol association with cardiorespiratory disease mortality in the United States. *in review.* **2021**.

Qin, M. M.; Murphy, B. N.; Isaacs, K. K.; McDonald, B. C.; Lu, Q. Y.; McKeen, S. A.; Koval, L.; Robinson, A. L.; Efstathiou, C.; Allen, C.; Pye, H. O. T., Criteria pollutant impacts of volatile chemical products informed by near-field modelling. *Nat Sustain* **2021,** *4*, 129–137.

Robinson, A. L.; Donahue, N. M.; Shrivastava, M. K.; Weitkamp, E. A.; Sage, A. M.; Grieshop, A. P.; Lane, T. E.; Pierce, J. R.; Pandis, S. N., Rethinking organic aerosols: Semivolatile emissions and photochemical aging. *Science* **2007,** *315* (5816), 1259-1262.

Ryerson, T. B.; Andrews, A. E.; Angevine, W. M.; Bates, T. S.; Brock, C. A.; Cairns, B.; Cohen, R. C.; Cooper, O. R.; de Gouw, J. A.; Fehsenfeld, F. C.; Ferrare, R. A.; Fischer, M. L.; Flagan, R. C.; Goldstein, A. H.; Hair, J. W.; Hardesty, R. M.; Hostetler, C. A.; Jimenez, J. L.; Langford, A. O.; McCauley, E.; McKeen, S. A.; Molina, L. T.; Nenes, A.; Oltmans, S. J.; Parrish, D. D.; Pederson, J. R.; Pierce, R. B.; Prather, K.; Quinn, P. K.; Seinfeld, J. H.; Senff, C. J.; Sorooshian, A.; Stutz, J.; Surratt, J. D.; Trainer, M.; Volkamer, R.; Williams, E. J.; Wofsy, S. C., The 2010 California Research at the Nexus of Air Quality and Climate Change (CalNex) field study. *J Geophys Res-Atmos* **2013,** *118* (11), 5830-5866.

Safieddine, S. A.; Heald, C. L.; Henderson, B. H., The global nonmethane reactive organic carbon budget: A modeling perspective. *Geophys Res Lett* **2017,** *44* (8), 3897-3906.

Sarwar, G.; Gantt, B.; Foley, K.; Fahey, K.; Spero, T. L.; Kang, D. W.; Mathur, R.; Foroutan, H.; Xing, J.; Sherwen, T.; Saiz-Lopez, A., Influence of bromine and iodine chemistry on annual, seasonal, diurnal, and background ozone: CMAQ simulations over the Northern Hemisphere. *Atmos Environ* **2019,** *213*, 395-404.

Seltzer, K. M.; Pennington, E.; Rao, V.; Murphy, B. N.; Strum, M.; Isaacs, K. K.; Pye, H. O. T., Reactive organic carbon emissions from volatile chemical products. *Atmos Chem Phys* **2021,** *21* (6), 5079-5100.

Simon, H.; Reff, A.; Wells, B.; Xing, J.; Frank, N., Ozone Trends Across the United States over a Period of Decreasing NOx and VOC Emissions. *Environ Sci Technol* **2015,** *49* (1), 186-195.

Singer, B. C.; Revzan, K. L.; Hotchi, T.; Hodgson, A. T.; Brown, N. J., Sorption of organic gases in a furnished room. *Atmos Environ* **2004,** *38* (16), 2483-2494.

Singer, B. C.; Hodgson, A. T.; Hotchi, T.; Ming, K. Y.; Sextro, R. G.; Wood, E. E.; Brown, N. J., Sorption of organic gases in residential rooms. *Atmos Environ* **2007,** *41* (15), 3251-3265.

Tkacik, D. S.; Presto, A. A.; Donahue, N. M.; Robinson, A. L., Secondary Organic Aerosol Formation from Intermediate-Volatility Organic Compounds: Cyclic, Linear, and Branched Alkanes. *Environ Sci Technol* **2012,** *46* (16), 8773-8781.

Turner, M. C.; Jerrett, M.; Pope, C. A.; Krewski, D.; Gapstur, S. M.; Diver, W. R.; Beckerman, B. S.; Marshall, J. D.; Su, J.; Crouse, D. L.; Burnett, R. T., Long-Term Ozone Exposure and Mortality in a Large Prospective Study. *Am J Resp Crit Care* **2016,** *193* (10), 1134-1142.

U.S. EPA *Integrated Science Assessment for Particulate Matter*; Office of Research and Development – Center for Public Health & Environmental Assessment – RTP: December 2019, 2019.

U.S. EPA *Integrated Science Assessment for Ozone and Related Photochemical Oxidants*; Office of Research and Development – Center for Public Health & Environmental Assessment – RTP: 2020.

U.S. EPA *Preparation of Emissions Inventories for the 2016v1 North American Emissions Modeling Platform, Technical Support Document (TSD)*; Office of Air Quality Planning and Standards, Air Quality Assessment Division, Emissions Inventory and Analysis Group: 2021.

U.S. EPA *2017 National Emissions Inventory: January 2021 Updated Release, Technical Support Document* Office of Air Quality Planning and Standards, Air Quality Assessment Division, Emissions Inventory and Analysis Group: 2021.

Woody, M. C.; Baker, K. R.; Hayes, P. L.; Jimenez, J. L.; Koo, B.; Pye, H. O. T., Understanding sources of organic aerosol during CalNex-2010 using the CMAQ-VBS. *Atmos Chem Phys* **2016,** *16* (6), 4081-4100.

Yarwood, G.; Whitten, G. Z.; Jung, J.; Heo, G.; Allen, D. T. *Development, Evaluation and Testing of Version 6 of the Carbon Bond Chemical Mechanism (CB6)*; ENVIRON International Corporation: 2010.

Zhao, Y. L.; Hennigan, C. J.; May, A. A.; Tkacik, D. S.; de Gouw, J. A.; Gilman, J. B.; Kuster, W. C.; Borbon, A.; Robinson, A. L., Intermediate-Volatility Organic Compounds: A Large Source of Secondary Organic Aerosol. *Environ Sci Technol* **2014,** *48* (23), 13743-13750.

Appendix C

REACTIVE ORGANIC CARBON EMISSIONS FROM VOLATILE CHEMICAL PRODUCTS

Seltzer, K. M., Pennington, E., Rao, V., Murphy, B. N., Strum, M., Isaacs, K. K., & Pye, H. O. T. (2021). Reactive organic carbon emissions from volatile chemical products. *Atmospheric Chemistry and Physics*, *21*(6), 5079–5100. https://doi.org/10.5194/acp-21-5079-2021.

Reactive Organic Carbon Emissions from Volatile Chemical Products

Karl M. Seltzer[1], Elyse Pennington[2,3], Venkatesh Rao[4], Benjamin N. Murphy[5], Madeleine Strum[4], Kristin K. Isaacs[5], Havala O.T. Pye[5]

[1]Oak Ridge Institute for Science and Education Postdoctoral Fellow in the Office of Research and Development, US Environmental Protection Agency, Research Triangle Park, NC 27711

[2]Oak Ridge Institute for Science and Education Fellow in the Office of Research and Development, US Environmental Protection Agency, Research Triangle Park, NC 27711

[3]California Institute of Technology, Pasadena, CA 91125

[4]Office of Air and Radiation, US Environmental Protection Agency, Research Triangle Park, NC 27711

[5]Office of Research and Development, US Environmental Protection Agency, Research Triangle Park, NC 27711

Correspondence to: Havala O.T. Pye (Pye.Havala@epa.gov)

Abstract. Volatile chemical products (VCPs) are an increasingly important source of anthropogenic reactive organic carbon (ROC) emissions. Among these sources are everyday items, such as personal care products, general cleaners, architectural coatings, pesticides, adhesives, and printing inks. Here, we develop VCPy, a new framework to model organic emissions from VCPs throughout the United States, including spatial allocation to regional and local scales. Evaporation of a species from a VCP mixture in the VCPy framework is a function of the compound specific physiochemical properties that govern volatilization and the timescale relevant for product evaporation. We introduce two terms to describe these processes: evaporation timescale and use timescale, respectively. Using this framework, predicted national, per-capita organic emissions from VCPs are 9.5 kg person^{-1} year^{-1} (6.4 kgC person^{-1} year^{-1}) for 2016, which translates to 3.05 Tg (2.06 TgC), making VCPs a dominant source of anthropogenic organic emissions in the United States. Uncertainty associated with this framework and sensitivity to select parameters were characterized through Monte Carlo analysis, resulting in a 95% confidence interval

of national VCP emissions for 2016 of 2.61 – 3.53 Tg (1.76 – 2.38 TgC). This nationwide total is broadly consistent with the US EPA's 2017 National Emission Inventory (NEI); however, county-level and categorical estimates can differ substantially from NEI values. VCPy predicts higher VCP emissions than the NEI for approximately half of all counties, with 5% of all counties having greater than 55% higher emissions. Categorically, application of the VCPy framework yields higher emissions for personal care products (150%) and paints/coatings (25%) when compared to the NEI, whereas pesticides (-54%) and printing inks (-13%) feature lower emissions. An observational evaluation indicates emissions of key species from VCPs are reproduced with high fidelity using the VCPy framework (normalized mean bias of -13% with r = 0.95). Sector-wide, the effective secondary organic aerosol yield and maximum incremental reactivity of VCPs are 5.3% by mass and 1.58 g O_3 g^{-1}, respectively, indicating VCPs are an important, and likely underrepresented to-date, source of secondary pollution in urban environments.

1 Introduction

Reactive organic carbon (ROC), which includes both non-methane organic gases and organic aerosol (OA), is central to atmospheric oxidant levels and modulates the concentration of all reactive species (Heald and Kroll, 2020; Safieddine et al., 2017). Gas-phase ROC features both biogenic and anthropogenic sources and, following oxidation, can lead to the formation of tropospheric ozone (O_3) and secondary organic aerosol (SOA). Organic aerosol is often the dominant component of total fine particulate matter ($PM_{2.5}$) throughout the world (Jimenez et al., 2009; Zhang et al., 2007), and SOA is often the dominant component of OA in both urban and rural settings (Jimenez et al., 2009; Volkamer et al., 2006; Williams et al., 2010; Xu et al., 2015). Since ozone and $PM_{2.5}$ are both associated with impacts on human health and welfare (U.S. Environmental Protection Agency, 2019a; U.S. Environmental Protection Agency, 2020) that are global in nature (Burnett et al., 2018; Mills et al., 2018) and persist at low concentrations (Di et al., 2017; Kazemiparkouhi et al., 2020), accurately understanding the sources, magnitude, and speciation of organic emissions is critical.

Historically, the leading source of anthropogenic organic emissions in the United States has been motor vehicles (Khare and Gentner, 2018; McDonald et al., 2013; Pollack et al., 2013). However, successful emission reduction strategies implemented over several decades have dramatically reduced mobile emissions (Bishop and Stedman, 2008; Khare and Gentner, 2018; McDonald et al., 2013), resulting in substantial declines in both ambient gas-phase non-methane volatile organic compounds (NMVOCs) and OA concentrations (Gentner et al., 2017; McDonald et al., 2015; Pollack et al., 2013; Warneke et al., 2012). Due to these changes, volatile chemical products (VCPs) are now viewed as the foremost source of anthropogenic organic emissions (Khare and Gentner, 2018; McDonald et al., 2018). The U.S. EPA has long accounted for VCPs in the National Emissions Inventory (NEI) as the "solvent sector." In 1990, the mobile and VCP sectors were the two highest emitters of volatile organic compounds (VOCs; a regulatory defined collection of organic species that excludes certain compounds, such as acetone) at the national level. Mobile and VCP sources emitted 7.2 Tg and 5.0 Tg of VOCs, respectively (U.S. Environmental Protection Agency, 1995). By 2017, EPA estimates of VOC emissions from both the mobile and VCP sectors each dropped to 2.7 Tg (U.S. Environmental Protection Agency, 2020). For VCPs, factors driving the emissions decrease over this period include, but are not limited to, reformulation of consumer products (Ozone Transport Commission, 2016) and implementation of National Emissions Standards for Hazardous Air Pollutants regulations for industrial processes (Strum and Scheffe, 2016). Potentially complicating the trend and assessment of relative roles of different sectors, new inventory methods have suggested that VCP emissions in the NEI could be biased low by a factor of 2-3 (McDonald et al., 2018).

The decades-long increasing relative contribution of VCPs to total anthropogenic organic emissions could have several important implications for modelling and improving air quality. First, modelling studies of SOA from anthropogenic VOCs have generally focused on combustion sources (Hodzic et al., 2010; Jathar et al., 2017; Murphy et al., 2017), which are typically rich in aromatics

and alkanes (Gentner et al., 2012; Lu et al., 2018). In contrast, emissions from VCPs occur through evaporation and contain large fractions of oxygenated species (e.g. glycol ethers, siloxanes), many of which feature uncertain SOA yields (McDonald et al., 2018). Second, adequate chemical mechanism surrogates for species common in VCPs (e.g. siloxanes) are lacking (Qin et al., 2020). As VCPs and their components could have significant SOA potential (Li et al., 2018; Shah et al., 2020), revisiting VCP emissions mapping to chemical mechanisms could help reduce modelled bias, which has historically been difficult to resolve (Baker et al., 2015; Ensberg et al., 2014; Lu et al., 2020; Woody et al., 2016). Third, VCPs feature substantial quantities of intermediate-volatility organic carbon (IVOC) compounds (CARB, 2019) and better representing their source strength could help resolve the high IVOC concentrations observed in urban atmospheres (Lu et al., 2020; Zhao et al., 2014). Fourth, if the VCP sector is systematically biased low in the NEI or select urban areas, there could be implications for ozone pollution (Zhu et al., 2019). Finally, reducing organic emissions from VCPs has traditionally been viewed through the lens of minimizing near-field chemical exposure (Isaacs et al., 2014) or mitigating ozone pollution (Ozone Transport Commission, 2018), both of which can be accomplished through product reformulation. For example, reducing the magnitude of regulatory VOC emissions from VCPs can be accomplished by reformulating a product with lower-volatility ingredients that are less likely to evaporate (Ozone Transport Commission, 2016). However, if these lower-volatility replacement ingredients eventually evaporate on atmospherically relevant timescales, they could be efficient SOA precursors (Li et al., 2018).

Given these implications, the need to understand and resolve differences among inventories becomes increasingly important. Here, we develop VCPy, a new framework to model organic emissions from VCPs throughout the United States, including spatial allocation to the county-level. In this framework, fate and transport assumptions regarding evaporation of a species in a product into ambient air are a function of the compound specific physiochemical properties that govern volatilization and the timescale available for a product to evaporate. We introduce

two terms to describe these processes: evaporation timescale and use timescale, respectively. Since product ingredients are considered individually, determination of emission composition is explicit. This approach also enables quantification of emission volatility distributions and the abundance of different compound classes. In addition, we test the sensitivity of predicted emission factors to uncertain parameters, such as evaporation timescale and use timescale, through Monte Carlo analysis, evaluate the VCPy inventory using published emission ratios, and estimate the effective SOA and ozone formation potential of both the complete sector and individual product use categories.

2 Methods

2.1 VCPy: A Framework for Estimating Reactive Organic Carbon Emissions from Volatile Chemical Products

The VCPy framework is based on the principle that the magnitude and speciation of organic emissions from VCPs are directly related to (1) the mass of chemical products used, (2) the composition of these products, (3) the physiochemical properties of their constituents that govern volatilization, and (4) the timescale available for these constituents to evaporate (Fig. 1). Since the VCP sector includes residential, commercial, institutional, and industrial sources, a consistent stream of data sources for all product categories is difficult. As such, this work implements a hybridized methodology that utilizes the best features of prior emission inventory methods, while introducing new methods to make improvements where necessary. The result produces national-level, per capita emission factors for all product categories in the VCP sector that can be further tailored for regional or localized analysis. The per capita basis is useful for comparison across frameworks and over time, but emissions can be recast in other units as needed. Briefly, survey data are used to generate a 1^{st}-order product composition profile for a composite of product types, which quantifies the fraction of organic, inorganic, and water components. The organic component is further divided into individual species (e.g. ethanol, isobutane, isopropyl alcohol). A variety of data sources are used to estimate the national-level product usage and each composite is assigned a use timescale,

reflecting the elapsed time between use and any explicit removal process. Finally, the characteristic evaporation timescale of each organic component is calculated using quantitative structure-activity relationship (QSAR) modelled physiochemical properties and compared to the assigned use timescale. If the characteristic evaporation timescale of the organic component is less than the assigned use timescale of the composite, it is assumed that the compound is emitted. Else, the compound is retained in the product or other condensed phase (e.g. water) and permanently sequestered.

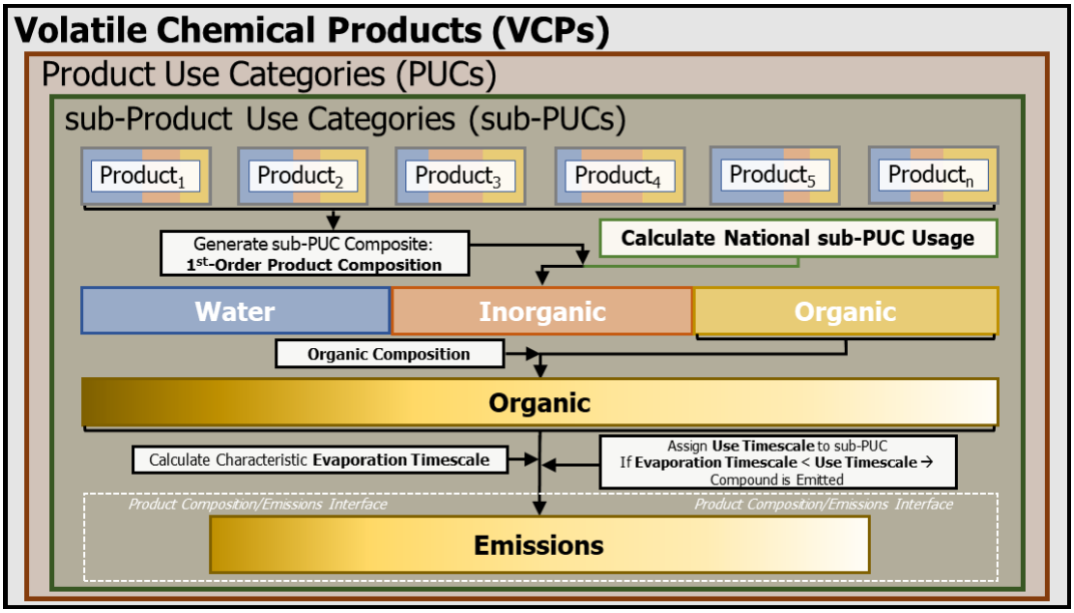

Figure 13: Conceptual overview of the VCPy framework. Note: PUC = Product Use Category.

2.1.1 Product Use Categories (PUCs) and sub-Product Use Categories (sub-PUCs)

VCPy disaggregates the VCP sector into several components called Product Use Categories (PUCs). An individual PUC is not exclusively used in a singular setting (e.g. residential vs. commercial) and examples include Personal Care Products, Cleaning Products, and Paints & Coatings. PUCs are further divided into sub-PUCs, which are composites of individual product types featuring similar use patterns. In addition to permitting tailored fate-and-transport assumptions, similar hierarchical product schema are also useful for models estimating near-field exposure to chemicals, through routes such as dermal contact and indoor inhalation (Isaacs et al., 2020). As an example, there are two sub-PUCs allocated to the Personal Care Product PUC: Short Use Products and Daily Use Products. These two sub-PUCs are differentiated by the length of use prior to removal (i.e. the use timescale). The mass of chemical products used and subsequent organic emission factors, which are the main output from VCPy, are calculated at the sub-PUC level (Fig. 1). Currently, there are ten PUCs and sixteen sub-PUCs implemented in VCPy (Table 1).

Table 5: Description of all PUCs and sub-PUCs currently implemented in VCPy, their estimated mass usage for 2016, and product examples of each. See Table S2 for a derivation of all product usage estimates.

Product Use Categories (PUCs)	**Sub-Product Use Categories (sub-PUCs)**	**2016 Annual Usage [kg person^{-1} year^{-1}]**	**Product Examples**
Cleaning Products	Detergents & Soaps	40.58	Soaps, Detergents, Metal Cleaners, Scouring Cleaners
	General Cleaners	28.47	Disinfectants, Air Fresheners, Glass & Bathroom Cleaners, Windshield Washer Fluid, Hand Sanitizer, Automotive & Floor Polishes, Bleaches, Surfactants
	Daily Use Products	8.83	Hair Products, Perfumes, Colognes, Cleansing &

Personal Care Products			Moisturizing Creams, Sunscreens, Hand & Body Lotion and Oils, Cosmetics, Deodorants
	Short Use Products	3.16	Shampoo, Conditioners, Shaving Cream, Aftershave, Mouthwashes, Toothpaste
Adhesives & Sealants	Adhesives & Sealants	15.23	Glues and Adhesives, Epoxy Adhesives, Other Adhesives, Structural and Nonstructural Caulking Compounds and Sealants
Paints & Coatings	Architectural Coatings	13.27	Exterior/Interior Flat/Gloss Paints, Primers, Sealers, Lacquers
	Aerosol Coatings	0.39	Paint Concentrates Produced for Aerosol Containers
	Allied Paint Products	1.26	Thinners, Strippers, Cleaners, Paint/Varnish Removers
	Industrial Coatings	7.42	Automotive, Appliance, Furniture, Paper, Electrical Insulating, Marine, Maintenance, and Traffic Marking Finishes and Paints
Printing Inks	Printing Inks	3.20	Letterpress, Lithographic, Gravure, Flexographic, Nonimpact/Digital Inks
Pesticides & FIFRA Products	FIFRA Pesticides	1.46	Lawn and Garden Pesticides and Chemicals, Household and Institutional Pesticides and Chemicals
	Agricultural Pesticides	10.32	Agricultural and Commercial Pesticides & Other Organic Chemicals
Dry Cleaning	Dry Cleaning	0.03	Dry Cleaning Fluids
Oil & Gas	Oil & Gas	1.32	Cleaners, Deicers

Misc. Products	Misc. Products	0.18	Pens, Markers, Arts and Crafts, Dyes
Fuels & Lighter	Fuels & Lighter	2.80	Lighter Fluid, Fire Starter, Other Fuels

2.1.2 National-Level Product Usage

To estimate VCP product use, some prior work has used national economic statistics, such as market sales or shipment values (e.g. U.S. Environmental Protection Agency, 2020; McDonald et al., 2018). Others have incorporated product usage statistics based on consumer habits and practices (e.g. Isaacs et al., 2014; Qin et al., 2020), but these statistics are generally unavailable for commercial and industrial chemical usage, which limits their application. To better ensure the capture of all chemical product usage, including usage in residential, commercial, institutional, and industrial settings, national economic statistics are utilized, where possible (Table S1).

Product usage from twelve sub-PUCs is estimated using national-level shipment statistics, commodity prices, and producer price indices. National-level economic statistics are retrieved from the U.S. Census Bureau's Annual Survey of Manufactures (ASM; U.S. Census Bureau, 2016a), which provides annual statistical estimates for all manufacturing establishments. Values are available for all 6-digit North American Industry Classification System (NAICS) codes, provided as product shipment values ($ year^{-1}), and are reported with associated relative standard errors (generally < 5%). To translate shipment values ($ year^{-1}) to usage (kg year^{-1}), we use commodity prices ($ kg^{-1}) from the U.S. Department of Transportation's 2012 Commodity Flow Survey (U.S. Department of Transportation, 2015). An exception is for all Paint & Coating sub-PUCs. Commodity prices for these sub-PUCs are taken from the U.S. Census Bureau's Paint and Allied Products Survey (U.S. Census Bureau, 2011a) and representative of 2010. To translate these commodity prices, which are from 2010 and 2012, to values reflective of 2016, we use producer price indices reported by the Federal Reserve Bank of St. Louis (U.S. Bureau of Labor Statistics, 2020). Commodity price indices from the Federal Reserve Bank are

updated for all NAICS manufacturing codes monthly, which we average to create annual price indices (Table S2). An implicit assumption in this methodology is that manufacturing and product usage are, on average, annually balanced.

We preferentially utilize product usage numbers derived from the above methodology, when possible, as all data sources have the following characteristics: (1) they are nationally derived and therefore less influenced by regional differences in manufacturing and formulation, and (2) all datasets are freely available to the public. However, due to data limitations, product usage for four sub-PUCs are estimated using other sources. The Dry Cleaning and Oil & Gas product usage estimates are derived from the national-level solvent mass usage reported by an industry study (The Freedonia Group, 2016). The Miscellaneous Products and Fuels & Lighter product usage estimates are derived from reported sales data, specific to California, from the California Air Resources Board's 2015 Consumer and Commercial Products Survey Data (CARB, 2019). These sales numbers are scaled upwards to a national-level by assuming equivalent per-capita product usage.

2.1.3 1st-Order and Organic Product Composition

Each sub-PUC features two composite profiles. The initial composite is the 1st-order product composition profile, which disaggregates the total mass of each sub-PUC into its water, inorganic, and organic fractions (Table 2). The organic component is further decomposed into non-evaporative and evaporative organics. The quantification and accounting of evaporative organics in this framework are necessary as CARB's organic profiles are processed to exclude organics that are not anticipated to evaporate on atmospherically relevant timescales. For ten sub-PUCS, the 1st-order product composition profile uses data from the California Air Resources Board's 2015 Consumer and Commercial Products Survey (CARB, 2019). Various product types are sorted into each sub-PUC and the 1st-order product composition profiles are calculated on a weighted basis using the reported sales from manufacturers and formulators in California. Due to omissions stemming from confidentiality concerns, not all sales and composition data from the survey are available. We utilize the publicly available portions of the data, which constitutes

most of the survey and includes over 330 product types. For example, 126 product types and 20 product types were sorted into the General Cleaners and Adhesives & Sealants (Table S3) sub-PUCs, respectively.

Table 6: 1st-Order product composition profiles and evaporative organics proportion for all sub-PUCs.

Product Use Categories (PUCs)	**Sub-Product Use Categories (sub-PUCs)**	**Water**	**Inorganic**	**Non-Evaporative Organics[a]**	**Evaporative Organics[a]**
Cleaning Products	Detergents & Soaps[b]	67.8%	13.9%	15.4%	2.9%
	General Cleaners[b]	73.3%	8.6%	11.1%	6.9%
Personal Care Products	Daily Use Products[b]	48.8%	10.7%	16.9%	23.7%
	Short Use Products[b]	72.2%	5.8%	17.7%	4.3%
Adhesives & Sealants	Adhesives & Sealants[b]	12.8%	53.2%	29.0%	5.0%
Paints & Coatings	Architectural Coatings[c]	45.5%	49.6%	0.0%	5.0%
	Aerosol Coatings[d]	12.7%	12.7%	0.0%	74.7%
	Allied Paint Products[b]	5.1%	3.5%	0.6%	90.8%
	Industrial Coatings[e]	15.0%	70.0%	0.0%	14.0%
Printing Inks	Printing Inks[f]	8.0%	67.0%	0.0%	25.0%
Pesticides & FIFRA Products	FIFRA Pesticides[b]	74.8%	4.9%	15.1%	5.1%
	Agricultural Pesticides[b]	74.8%	4.9%	15.1%	5.1%
Dry Cleaning	Dry Cleaning[g]	0.0%	0.0%	0.0%	100%

Oil & Gas	Oil & Gas[g]	0.0%	0.0%	0.0%	100%
Misc. Products	Misc. Products[b]	27.1%	14.6%	48.8%	9.5%
Fuels & Lighter	Fuels & Lighter[b]	0.0%	92.9%	0.0%	7.1%

[a]: "Non-Evaporative Organics" and "Evaporative Organics" sum to total product organics. "Evaporative Organics" represent the potentially evaporative organic fraction of the total product and excludes assumed "non-evaporative" (i.e. assumed non-volatile) organics, which are not included in the California Air Resource Board's organic profiles.

[b]: Source: California Air Resources Board 2015 Consumer and Commercial Products Survey Data (CARB, 2019).

[c]: Source: California Air Resources Board 2005 Architectural Coatings Survey (CARB, 2007). VOC + Exempts is used for both organic and evaporative organics. Non-evaporative organic proportions not provided. Sales proportions of water vs. solvent-based architectural coatings based on California Air Resource Board 2014 Architectural Coatings Survey (CARB 2014).

[d]: Source: California Air Resources Board 2010 Aerosol Coatings Survey (CARB, 2012). Only evaporative organics is provided. Remainder (~25%) is split evenly between water and inorganics.

[e]: Source: Industrial Maintenance composition data from California Air Resources Board 2005 Architectural Coatings Survey (CARB, 2007).

[f]: Source: Graphic Arts composition data from California Air Resources Board 2005 Architectural Coatings Survey (CARB, 2007).

[g]: All product usage is composed of organic functional solvents (The Freedonia Group, 2016). Therefore, all mass is assumed to be potentially evaporative.

For Architectural Coatings, Industrial Coatings, and Printing Inks, the 1st-order product composition profile is derived from data in the California Air Resources Board's 2005 Architectural Coatings Survey (CARB, 2007). The Architectural Coatings sub-PUC uses data from all profiles in the survey, which is dominated by flat paint, non-flat paints, and primers. Industrial Coatings and Printing Inks use the 1st-order product composition profiles of Industrial Maintenance coatings and Graphic Arts coatings, respectively. The 1st-order product composition profile for aerosol coatings uses data from the California Air Resources Board's 2010 Aerosol Coatings Survey (CARB, 2012), which includes more than 20 aerosolized product types. Only the evaporative organic composition of aerosol coating products was reported, so the remaining mass was evenly split between water and inorganics. For Dry Cleaning and Oil & Gas, as the product usage for these sub-PUCs were derived from the organic functional solvent mass usage, it is assumed that this mass is entirely evaporative organics.

The second composite is the organic composition profile. Again, the California Air Resources Board's 2015 Consumer and Commercial Products Survey (CARB, 2019) was used to derive a composite of product types for ten sub-PUCs (Table S4). These product types are then mapped to an associated organic profile (CARB, 2018; see Table S3) and weighted based on their evaporative organic contributions to the total sub-PUC. For Architectural Coatings, a 94% water-based and 6% solvent-based paint (CARB, 2014) composite is generated. Aerosol Coatings are calculated on a weighted basis using the potentially evaporative organic contributions reported by CARB's 2010 Aerosol Coatings Survey (CARB, 2012). The organic composition profiles for Industrial Coatings, Printing Inks, and Dry Cleaning all utilize profiles (3149, 2570, 2422, respectively) from EPA's SPECIATEv5.0 database (EPA, 2019b). Approximately 65% of the solvents used in the Oil & Gas sector are alcohols and the remainder are a broad range of hydrocarbons (The Freedonia Group, 2016). Since detailed composition data for Oil & Gas solvents are sparse, all Oil & Gas alcohols are assumed to be methanol, as it is widely used in and emitted from Oil & Gas operations (Lyman et al., 2018;

Stringfellow et al., 2017; Mansfield et al., 2018). The remaining 35% is allocated to naphtha, a blend of hydrocarbon solvents.

Several components within CARB profiles are lumped categories or complex mixtures. This includes naphtha, mineral spirits, distillates, Stoddard Solvent, fragrances, volatile methyl siloxanes, and a series of architectural coating and consumer product "bins." All naphtha, mineral spirits, distillates, and Stoddard Solvent occurrences in individual profiles are treated as a single mineral spirits profile (Carter, 2015). Volatile methyl siloxanes include several compounds (e.g. D_4, D_5, D_6), all of which are emitted in varying proportions (Janechek et al., 2017). Here, the lumped volatile methyl siloxane identity is preserved but the physiochemical properties of decamethylcyclopentasiloxane is applied to the surrogate. Fragrances are a diverse mixture of organic compounds that include many terpenes and alkenes (Nazaroff and Weschler, 2004; Sarwar et al., 2004; Singer et al., 2006b). However, since the proportion of these constituents are unknown, all fragrances are physically treated as d-limonene since it is the most prevalent terpene emitted from fragranced products (Sarwar et al., 2004; Singer et al., 2006b). Finally, for the architectural coating and consumer product "bins," we use the representative chemical compositions derived by Carter, 2015.

2.1.4 Controls

There are two methods for controlling organic emissions from VCPs. The first method is through product reformulation, which would occur prior to product usage. Strategies that fit this definition include switching from a hydrocarbon solvent-based ingredient to one that is water-based, replacing an organic component with a non-organic component, and reformulating a product with lower-volatility ingredients that are less likely to evaporate (Ozone Transport Commission, 2016). VCP emissions that stem from residential, commercial, and institutional settings rely on these pre-use controls to reduce emissions. Regulators often set VOC content limits for chemical products (e.g. national standards: Section 183(e) of the Clean Air Act; 40 CFR 59), with California (e.g. CARB – Title 17 CCR) typically setting some of the most stringent limits in the country (Ozone Transport Commission, 2016). As

the 1st-order and organic composition profiles utilized here are almost exclusively derived from product composition data, pre-use controls are implicitly represented. In fact, since the product composition data is from manufacturers and formulators in California, where product VOC content limits are typically more stringent than national regulations, applying these profiles nationally likely results in conservative assumptions.

The second pathway of controlling organic emissions from VCPs is through post-use controls. Strategies that fit this definition include add-on controls, manufacturing process modifications, and disposal techniques. Add-on control strategies and manufacturing process modifications are limited to industrial and commercial emission sources, such as Industrial Coating (U.S. EPA, 2007; U.S. EPA, 2008) and Printing Ink (U.S. EPA, 2006a; U.S. EPA, 2006b) facilities. Since adoption of these technologies vary widely in space and time, assigning post-use controls via these strategies is not considered here. As several of these industrial sources (e.g. coatings, printing inks, dry cleaning) feature controls, as required by Section 112 of the Clean Air Act (40 CFR 63), this assumption could lead to localized high bias and will be refined in future work. Here, we only consider post-use controls through disposal techniques for the Oil & Gas and Fuels & Lighter sub-PUCs. For Oil & Gas, we assume that the solvents used in these processes become entrained in the produced water at these sites. Since produced water is largely (~89-98%) reinjected for enhanced oil and gas recovery or disposal (Lyman et al., 2018; Liden et al., 2018), we apply a post-use control efficiency of 94% (i.e. average of reported reinjection rates) to this sub-PUC. However, it should be noted that reinjection frequency and solvent usage can vary regionally. For Fuels & Lighters, we assume 90% of the organics are destroyed through combustion upon use (CARB, 2019).

2.1.5 Evaporation Timescale and Use Timescale

Fate-and-transport in the VCPy framework is a function of the predicted compound specific evaporation timescale and the assigned use timescale of each sub-PUC. It should be noted that this methodology explicitly results in the organic speciation of emissions differing from the organic composition of products from

which they volatilize. For example, the composition of organics within a product may differ from the speciation of emitted organics if the product contains low-volatility compounds that do not evaporate on relevant timescales.

The evaporation timescale is the compound specific (i.e. independent of the sub-PUC of interest), characteristic timescale of emission from a surface layer and is calculated using previously published methods (Khare and Gentner, 2018; Weschler and Nazaroff, 2008). This timescale is defined as a relationship between the mass of a compound applied and the rate of its emission, which can be expressed by:

$$Evaporation\ Timescale\ [hr] = {M_{applied}}/{R_{emission}} = {K_{OA} \times d}/{v_e} \quad (1)$$

where K_{OA} is the octanol-air partitioning coefficient of the compound, d [m] is the assumed depth of the applied product layer, and v_e [m/hr] is the mass transfer coefficient of the compound from the surface layer into the bulk air, which is a function of aerodynamic and boundary layer resistances. Median values for d [0.1 mm] and v_e [30 m/hr] from Khare and Gentner (2018) are selected here. It should be noted that v_e can vary substantially based on outdoor vs. indoor atmospheric conditions and future work will incorporate a two-box model to better account for such differences. A compound's K_{OA} it is the ratio of an organic chemical's concentration in octanol to the organic chemical's concentration in air at equilibrium. It is often used to quantify the partitioning behaviour of an organic compound between air and a matrix. As experimental values of K_{OA} are sparse, modelled estimates from the quantitative structure-activity relationship (QSAR) model OPERA (Mansouri et al., 2018) are used here. All physiochemical properties, including OPERA results, are retrieved from the U.S. EPA's CompTox Chemistry Dashboard (https://comptox.epa.gov/dashboard; last access: August 31, 2020).

Use timescale is the timescale available for a sub-PUC to evaporate and is based on the length of its direct use phase (i.e. the elapsed time between application and any explicit removal process). As this value is subjective, broad values are

applied to each sub-PUC (Table S5). For example, it is assumed that all products used in the bath and shower are quickly sequestered and washed down the drain, thus largely unavailable for emission (Shin et al., 2015). As such, Short Use Personal Care Products are assigned a "Minutes" use timescale. In contrast, it is also assumed that each person bathes once a day and associated Daily Use Personal Care Products are therefore assigned a "Days" use timescale.

Emissions are determined by comparing the calculated evaporation timescale for each component with the assigned use timescale for the sub-PUC. If the use timescale for the sub-PUC is greater than the evaporation timescale for a compound, the compound is emitted. Else, the compound is retained in the product or other condensed phase and permanently sequestered. Overall, organic emissions (E) for the complete sector are calculated as a summation over all organic compounds, *i*, and sub-PUCs, *j*, as follows:

$$E = \sum_{i,j} \begin{cases} 0 & if\ Use\ Timescale_j < Evaporation\ Timescale_i \\ U_j \times f_{E_j} \times f_{S_{i,j}} \times \left(1 - f_{C_j}\right) & if\ Use\ Timescale_j \geq Evaporation\ Timescale_i \end{cases} \quad (2)$$

where U is the product usage (Table 1), f_E is the evaporative organic fraction (Table 2), f_S is the fraction of an organic compound in the evaporative organics portion of a sub-PUC (Table S4), and f_C is the fraction of emissions that feature post-use controls on a mass basis. Application of Eqn. 2 determines the difference between organic product composition and organic emissions speciation.

2.2 Uncertainty Analysis

The sensitivity of emission estimates to a variety of input variables are tested through a systematic Monte Carlo analysis. We perform 10,000 simulations where product usage, evaporative organic proportions, variables associated with the characteristic evaporation timescale, the assigned use timescale, and post-use control assumptions are tested, both individually and collectively. For product usage, the

primary sources of uncertainty are shipment values provided by the ASM, commodity prices, the balance of imports (including tourism) and exports, and unused product disposal. The ASM provides standard error estimates for most shipment values and are typically less than 5%. Uncertainty estimates are not provided for commodity prices and national-level exports generally outweigh traditional imports for most sub-PUCs (~2-15%; U.S. Census Bureau, 2016), but there are also imports of personal care products through tourism. Therefore, we assume there is a ±25% uncertainty (95% CI) for all product usage estimates. CARB does not provide uncertainty estimates associated with the composition of product types or sales proportions. To account for these uncertainties, as well as the uncertainties associated with generating composites, we assume there is a ±25% uncertainty (95% CI) for all "Evaporative Organic" (Table 2) proportions. For the characteristic evaporation timescale, there are several layers of uncertainty. Application patterns vary by product type, which impacts assumptions regarding the depth of the chemical layer. In addition, indoor vs. outdoor product use and application of products to variable surface types (e.g. absorbing vs. non-absorbing) can impact mass transfer rates. As such, we apply broad uncertainties for variables associated with the characteristic evaporation timescale. We assume d (i.e. the depth of the applied chemical layer) is lognormally distributed with a median value of 0.1 mm (95% CI ~ [0.01 mm – 1 mm]) and v_e (i.e. the mass transfer coefficient) is normally distributed with a mean value of 30 m/hr (95% CI = [10 m/hr – 50 m/hr]). Since use timescales are categorical (e.g. minutes, days, years), we apply uncertainty by assuming the 95% CI of the assigned use timescale features a ±1 categorical uncertainty (e.g. mean: minutes; 95% CI = [seconds – hours]). Finally, for non-zero, post-use controls, we assume a ±25% uncertainty (95% CI) in the post-use control efficiency. It should be noted that additional avenues of uncertainty likely persist but are difficult to quantify and therefore not included here. For example, due to the scarcity of large-scale product surveys, many of the 1st-order product composition profiles (e.g. Architectural Coatings) and organic profiles (e.g. Printing Inks) used in this analysis are more than a decade old. As a result, the proportion of organics in

these product types and their organic components (i.e. the mean values applied here) may have changed in the interim period. Furthermore, the uncertainty associated with the evaporative organic composition of individual product types is not known or provided by the source data.

2.3 Spatial Allocation of National-Level Emissions

Emissions are calculated at the national-level and spatially allocated to the county-level using several proxies. Ten sub-PUCs, including all Cleaning Products and Personal Care Products, are allocated using population (Table S6; U.S. Census Bureau, 2020). Four sub-PUCs (Industrial Coatings, Allied Paint Products, Printing Inks, Dry Cleaning), all typically industrial in nature, are allocated using county-level employment statistics from the U.S. Census Bureau's County Business Patterns (U.S. Census Bureau, 2018). The employment mapping scheme for these four sub-PUCs utilize the methods from the 2017 NEI (U.S. EPA, 2020). On occasion, data in the County Business Patterns (CBP) is withheld due to confidentiality concerns. In those instances, we take the mid-point of the range associated with each data suppression flag. For Agricultural Pesticides, emissions are allocated based on county-level agricultural pesticide use and again taken from the 2017 NEI (U.S. EPA, 2020). Oil & Gas emissions are allocated using oil and gas well counts (U.S. EIA, 2019).

2.4 Inventory Evaluation

Previously published emission ratios from the Los Angeles basin during the summer of 2010 (de Gouw et al., 2018; de Gouw et al., 2017) are used to evaluate the VCPy emissions inventory (Table S7). Emissions ratios are generated by post-processing observed concentrations of organic gases, typically normalized to carbon monoxide (CO) or acetylene, to a period of "no chemistry" (Borbon et al., 2013; de Gouw et al., 2005; Warneke et al., 2007). As the air parcel is not photochemically aged (i.e. "no chemistry"), it is an ideal tool for evaluating an emissions inventory. An important caveat is that this method assumes the species being used for normalization (e.g. CO) is accurately inventoried and measured.

Since the emission ratios are not specific to a sector and represent total emissions, all other sectors must be quantified and speciated. For this purpose, all

non-VCP anthropogenic emissions from the 2017 NEI (U.S. EPA, 2020) are collected and speciated using EPA's SPECIATEv5.0 database (EPA, 2019b; Table S8). This includes all on road, nonroad, nonpoint, and point sources. All VCP emission from the 2017 NEI are also collected and speciated for supplementary evaluation. In addition, biogenic emissions of ethanol, methanol, and acetone for May and June of 2016, as simulated by the Biogenic Emission Inventory System (Bash et al., 2016), were included to capture non-anthropogenic sources of these compounds. May and June were selected to coincide with the observational sampling months (de Gouw et al., 2018; de Gouw et al., 2017). As the observed emission ratios are specific to the Los Angeles basin, we derive all VCPy inventory emission ratios using data for Los Angeles County. Total CO emissions, including all on-road, non-road, non-point, and point sources, for Los Angeles County in 2017 are ~320 Gg. While the observed and VCPy inventory emission ratios are separated by 6-7 years, the ambient non-methane hydrocarbon to CO concentration ratio in Los Angeles has been consistent for several decades, indicating changes in emission controls feature similar improvements for both pollutants over time (McDonald et al., 2013). In addition, the magnitude of observed emission ratios for a given region do not appreciably change over marginal time horizons (Warneke et al., 2007).

2.5 Air Quality Impact Potential

Each organic compound is assigned a SOA yield and Maximum Incremental Reactivity (MIR) to facilitate an approximation of the potential air quality impacts of VCPs. For SOA, a wide collection of published yields, including both chamber results and prediction tools, were utilized (Fig. S1). These include: (1) all linear alkanes use a quadratic polynomial fit to the volatility basis set (VBS) data from Presto et al., 2010 at 10 $\mu g/m^3$; (2) all cyclic alkanes use linear alkane yields that are three carbons larger in size (Tkacik et al., 2012); (3) all branched alkanes use yields obtained from the Statistical Oxidation Model (SOM; Cappa and Wilson, 2012), as reported in McDonald et al. (2018); (4) benzene and xylenes use the average yields from Ng et al., 2007 under high-NO_x conditions; (5) toluene uses the average from Ng et al., 2007 under high-NO_x conditions and the VBS data from Hildebrant et al.,

2009 at 10 μg/m^3; (6) all alkenes use yields obtained from SOM, as reported in McDonald et al. (2018); (7) volatile methyl siloxanes use the two-product model parameters from Janecheck et al., 2019, which includes additional SOA yields from Wu and Johnson 2017, at 10 μg/m^3; (8) all glycol ethers use chamber results and molecular structure relationships from Li and Cocker 2018 for reported and unreported glycol ethers, respectively; (9) benzyl alcohol uses the average of the lower-bound yields reported by Charan et al., 2020; (10) all remaining non-cyclic oxygenates, where available, use the arithmetic average of SOM results and a 1-D VBS approach, as reported by McDonald et al., 2018; (11) all remaining cyclic oxygenates, where available, use yields obtained from SOM, as reported by McDonald et al., 2018; (12) all halocarbons and compounds with less than five carbons are assigned a yield of zero; and (13) all remaining species are conservatively assigned a yield of zero if the effective saturation concentration (i.e. $C^* = (P^{vap} \times MW)/(R \times T)$) is $\geq 3 \times 10^6\ \mu g/m^3$ and assigned the same yield as n-dodecane if the effective saturation concentration is $< 3 \times 10^6\ \mu g/m^3$. The MIR of each compound, which measures the formation potential of ozone under various atmospheric conditions where ozone is sensitive to changes in organic compounds (Carter, 2010b), is calculated using the SAPRC-07 chemical mechanism (Carter, 2010a) and expressed as a mass of additional ozone formed per mass of organic emitted (Carter, 2010b).

3 Results and Discussion

3.1 National-Level PUC and sub-PUC Emissions

National-level, per-capita organic emissions from VCPs are 9.5 kg person^{-1} year^{-1} (6.4 kgC person^{-1} year^{-1}) for 2016 (Table 3), which translates to 3.05 Tg (2.06 TgC). When filtered to remove regulatory exempt organics, total emissions from VCPs are 2.6 Tg of VOC. In comparison, the 2017 NEI reports a combined total of 2.6 Tg of VOC emissions for on-road mobile, non-road mobile, and other mobile (i.e. aircraft, commercial marine vessels, and locomotives) sources, respectively. Therefore, when measured as VOC, the VCP sector is equal in magnitude to the sum of all mobile sources nationally, which is broadly consistent with the national-level

emissions estimate from the 2017 NEI. Categorically, emission factors are largest for Paints & Coatings, which total 3.1 kg person^{-1} year^{-1} (2.2 kgC person^{-1} year^{-1}) and are approximately 33% of the total sector (Table 3). The next largest PUCs are Personal Care Products and Cleaning Products, which contribute 2.1 kg person^{-1} year^{-1} (22%) and 2.0 kg person^{-1} year^{-1} (21%), respectively. Printing Inks, Adhesives & Sealants, and Pesticides each account for 6-9% each, and the remaining PUCs contribute less than 2% in total.

Table 7: National-level emissions, volatilization fraction, and proportion of all usage that is emitted for all sub-PUCs.

Product Use Categories (PUCs)	**Sub-Product Use Categories (sub-PUCs)**	**ROC Emissions**		**Organic Volatilization Fraction [%][a]**	**Total Product Emitted [%]**
		[kg person^{-1} year^{-1}]	**[kgC person^{-1} year^{-1}]**		
Cleaning Products	Detergents & Soaps	0.12	0.06	1.6%	0.3%
	General Cleaners	1.85	1.25	36.0%	6.5%
Personal Care Products	Daily Use Products	2.04	1.12	56.9%	23.1%
	Short Use Products	0.02	0.01	3.3%	0.7%
Adhesives & Sealants	Adhesives & Sealants	0.76	0.56	14.7%	5.0%
Paints & Coatings	Architectural Coatings	0.67	0.37	100%[b]	5.0%
	Aerosol Coatings	0.29	0.22	100%[b]	74.7%
	Allied Paint Products	1.14	0.80	99.2%	90.6%
	Industrial Coatings	1.04	0.79	100%[b]	14.0%
Printing Inks	Printing Inks	0.80	0.65	100%[b]	25.0%
Pesticides & FIFRA Products	FIFRA Pesticides	0.07	0.06	25.2%	5.1%
	Agricultural Pesticides	0.53	0.41	25.2%	5.1%

Dry Cleaning	Dry Cleaning	0.01	0.01	34.5%	34.5%
Oil & Gas	Oil & Gas	0.08	0.04	6.0%	6.0%
Misc. Products	Misc. Products	0.02	0.01	16.3%	9.5%
Fuels & Lighter	Fuels & Lighter	0.02	0.02	10.0%	0.7%
Total		9.45	6.38	31.5%	6.9%

[a]: Volatilization fraction represents the fraction of the total organic content of products that volatilize/emit to ambient air.

[b]: The "Organic" portion of these sub-PUCs is entirely composed of "Evaporative Organics" (see Table 2). Only data from the California Air Resources Board's 2015 Consumer and Commercial Products Survey featured the disaggregation of evaporative and non-evaporative organics. Prior surveys typically combined the non-evaporative organic portion of each profile with solids/inorganics.

For the complete sector (Fig. 2), the most abundantly emitted compound classes were oxygenated species (53%), followed by alkanes (31%; including straight-chained, branched, and cyclic), aromatics (8%), alkenes (5%), and halocarbons (3%). Individually, organic emissions are dominated by ethanol (Daily Use Products, General Cleaners), acetone (Paints & Coatings, General Cleaners), isopropyl alcohol (Daily Use Products, General Cleaners), toluene (Paints & Coatings, Adhesives & Sealants), n-tetradecane (Printing Inks), fragrances (Daily Use Products, General Cleaners), propane (Aerosol Coatings, Industrial Coatings), and volatile methyl siloxanes (Daily Use Products, Adhesives & Sealants). Each of these species compose > 3% of total VCP organic emissions (see Table S9 for the top-200 emitted compounds).

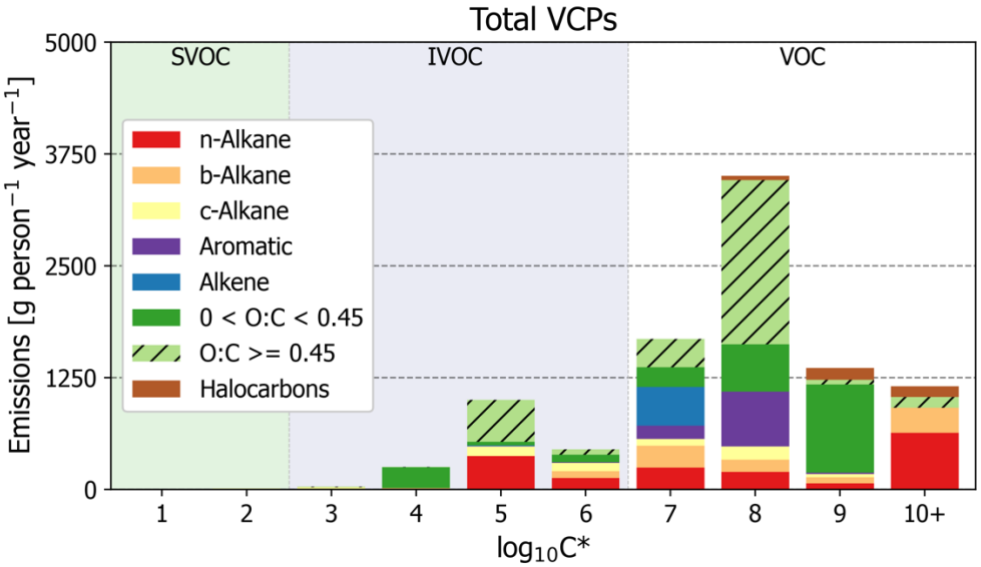

Figure 14: Sector-wide volatility distribution of emissions by compound class.

In terms of volatility classification (Donahue et al., 2012), as determined by the effective saturation concentration (i.e. C^*), total emissions are predominately VOCs ($C^* > 3 \times 10^6$ μ$g\ m^{-3}$), but there are also considerable contributions from IVOCs (3×10^2 μ$g\ m^{-3} < C^* < 3 \times 10^6$ μ$g\ m^{-3}$; Fig. 2-3). IVOC emissions, which are efficient SOA precursors (Chan et al., 2009; Presto et al., 2010), are approximately 20% of total emissions. Of this 20% that are IVOCs, 52% are oxygenated compounds (e.g. Texanol™, propylene glycol, ethylene glycol, siloxanes, benzyl alcohol, and glycol ethers), 30% are n-alkanes, and the rest are largely branched and cyclic alkanes. The prominence of oxygenated IVOC emissions from VCPs is noteworthy, as SOA yields from these compounds have not historically been evaluated nor included as SOA precursors in model chemical mechanisms (Qin et al., 2020). However, work has been undertaken in recent years to better understand these compounds (e.g. Wu and Johnson 2017; Li and Cocker 2018; Janechek et al., 2019; Charan et al., 2020). Overall, Paints & Coatings is the largest source of IVOC emissions (~760 g person^{-1} year^{-1}; Fig. 3), followed by Printing Inks (~350 g person^{-1} year^{-1}), Cleaning Products (~180 g person^{-1} year^{-1}), and Pesticides (~170 g person^{-1} year^{-1}). While Paints & Coatings emit more IVOCs by mass than all other PUCs,

Printing Ink and Pesticide emissions both feature greater proportions of IVOCs to their total emissions (~44% and ~28%, respectively).

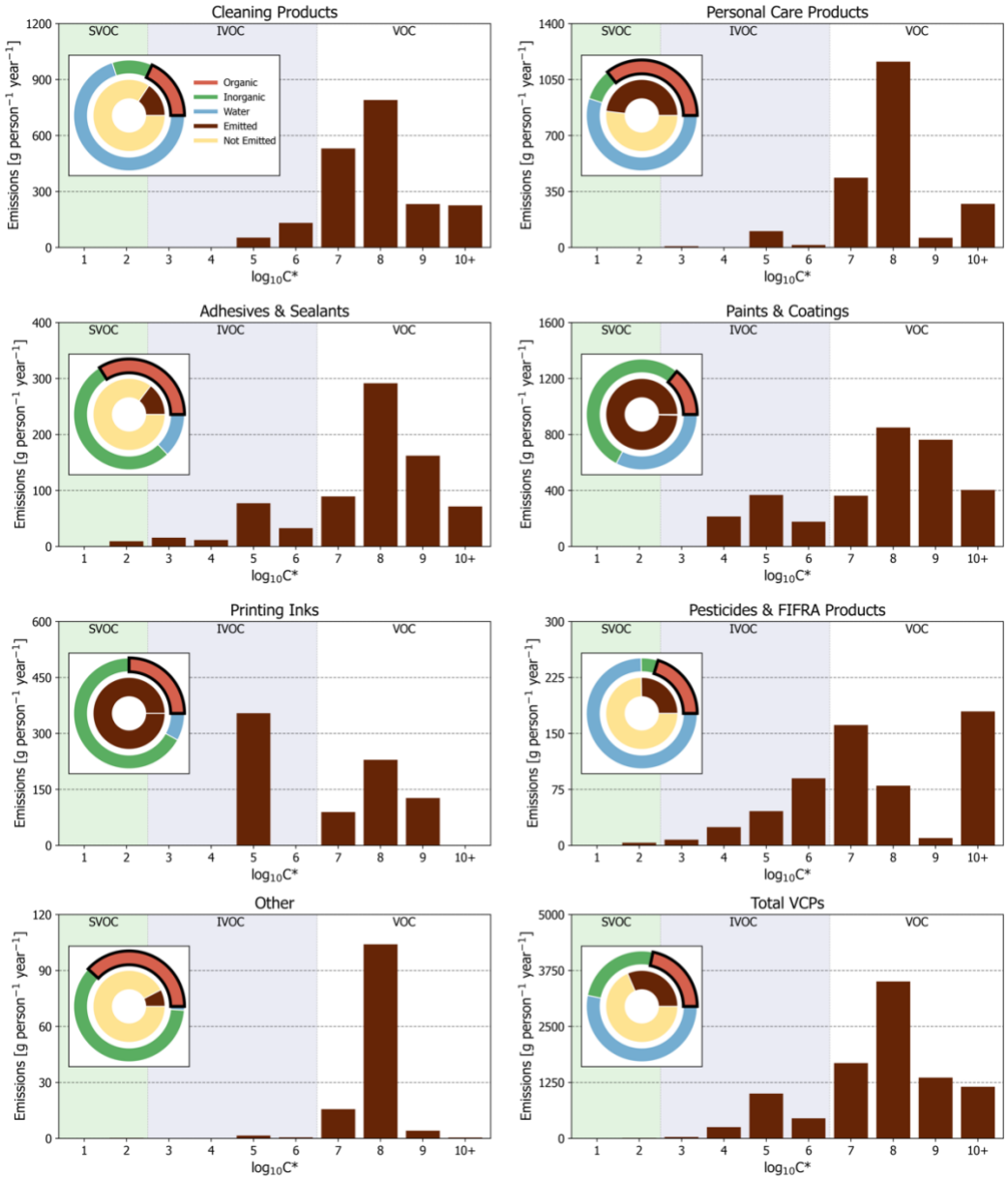

Figure 15: PUC and sector-wide volatility distribution of organic emissions. Other is summation of Dry Cleaning, Oil & Gas, Misc. Products, and Fuels & Lighter. Pie charts are 1st-order product composition and organic emission proportions for PUCs and the complete sector. Note: The "Organic" portion of all Paints & Coatings and

Printing Inks pie charts is entirely composed of "Evaporative Organics" (see Table 2).

These results also highlight how emissions from each PUC and sub-PUC are uniquely driven by mass of products used, organic composition, and use timescale. For example, the two largest sub-PUC sources are Daily Use Products and General Cleaners. Both are assigned a use timescale of 24-hr, but 40.6% of Daily Use Products are organic while General Cleaners are overwhelming composed of water (Table 2) and the annual mass usage of General Cleaners is ~3x higher than Daily Use Products (Table 1). As a result, net emissions of General Cleaners are within 10% of those from Daily Use Products (1.85 kg person^{-1} year^{-1} and 2.04 kg person^{-1} year^{-1}, respectively). The emissions of Short Use Products, which is assigned a "Minutes" use timescale, can further illustrate the importance of considering fate-and-transport. Under these use timescale assumptions, only high volatility compounds (i.e. $C^* > 3 \times 10^7\ \mu g/m^3$) are emitted and a majority (~97%) of its organics are retained (Table 3). Besides Daily Use Products and General Cleaners, all remaining sub-PUCs emit ≤ 1.14 kg person^{-1} year^{-1}, with six emitting less than 0.1 kg person^{-1} year^{-1} (Table 3). Generally, sub-PUCs with low emissions stem from minimal use (e.g. Misc. Products), short use timescales (e.g. Short Use Products), or high control assumptions (e.g. Oil & Gas, Fuels & Lighter).

3.2 Uncertainty Analysis of National-Level Emission Factors

Uncertainty associated with product usage, proportion of evaporative organics, assumptions related to evaporation and use timescale, and post-use controls, where applicable, result in a total sector-wide emission uncertainty of ±15% (Fig. 4; 9.5 kg person^{-1} year^{-1} [95% CI: 8.1 – 10.9]). Interestingly, the interaction of evaporation and use timescales can result in a threshold effect, where small changes in either do not necessarily translate into changes in the magnitude of emissions for a given sub-PUC (Fig. S2). For many PUCs, such as Paints & Coatings, Adhesives & Sealants, and Printing Inks, the use timescale is sufficiently long (i.e. years) for all evaporative organics to evaporate, regardless of the uncertainty associated with the evaporation and use timescales. Under such conditions, only uncertainty in product

usage and product composition affect uncertainty in the emission magnitude. As a result, these two variables are the largest drivers of uncertainty for the complete sector (Fig. S2). However, uncertainties associated with evaporation and use timescale assumptions can be important for certain sub-PUCs with moderate to low use timescales (see Cleaning Products in Fig. S2). For example, Detergents & Soaps is assigned a "Minutes" use timescale, which results in a 0.12 kg person^{-1} year^{-1} emission factor (Table 3). If the use timescale for this sub-PUC was changed "Hours," the emission factor would increase by a factor of 5.

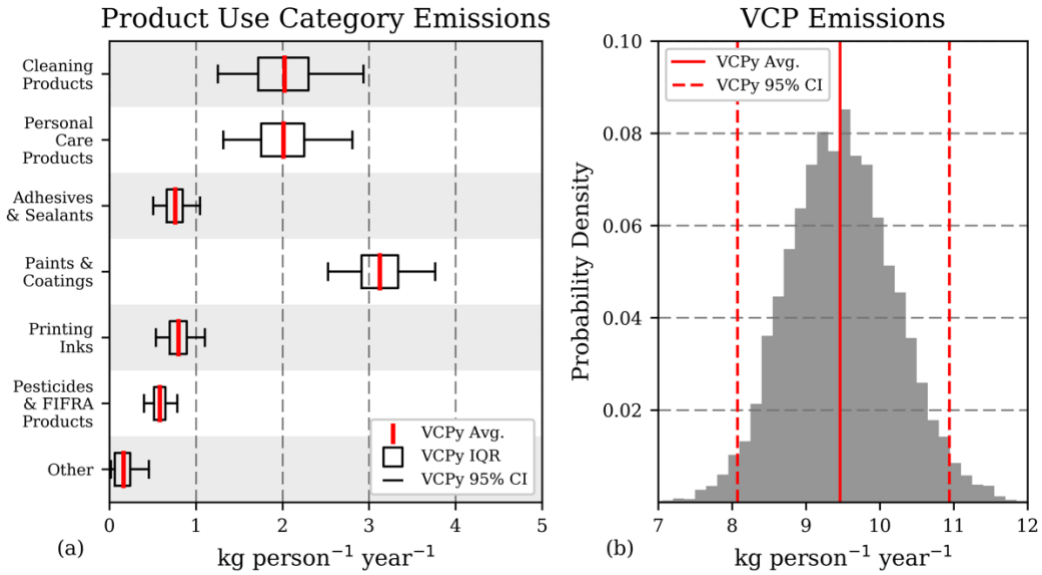

Figure 16: Monte Carlo sensitivity results for organic emissions. (a) Mean, interquartile range, and 95% confidence intervals for six PUCs and a combination of the remaining four (Dry Cleaning, Oil & Gas, Misc. Products, and Fuels & Lighter). (b) Probability distribution of sector-wide emission estimates. See Table S10 for a tabulation of this figure.

From a national emissions perspective, these Monte Carlo results contain several important results. First, as mentioned above, the largest drivers of uncertainty are associated with a sub-PUC's usage and composition, not assumptions related to fate-and-transport (i.e. evaporation and use timescales). Second, the most uncertain PUCs are Cleaning Products, Personal Care Products, and Paints & Coatings, and their uncertainty generates a significant amount of

emissions potential. The 95% confidence interval for all three span > 1.24 kg person^{-1} year^{-1}, which is equivalent to > 400 Gg of organic emissions per year. Finally, the 95% confidence interval for the national-level emissions from the complete sector for 2016 is 2.6 – 3.5 Tg (1.8 – 2.4 TgC), which is broadly consistent with the US EPA's 2017 NEI (2.8 Tg) and, largely due to differences in predicted evaporation, approximately half the emissions magnitude reported elsewhere (McDonald et al., 2018).

3.3 State- and County-Level Emissions Allocation

The magnitude of VCP emissions varies substantially throughout the country, with the most populated states and counties featuring the highest ROC emissions (Fig. 5). California (349 Gg), Texas (247 Gg), and Florida (173 Gg) are the largest state-level emitters and contribute ~25% of all VCP emissions. In contrast, the 30 smallest state-level emitters (plus Washington, DC) together emit ~780 Gg. At the county-level, Los Angeles County, Cook County (Chicago), and Harris County (Houston) are the largest emitters. However, after normalizing by population, these three counties all feature per-capita emissions (8.21, 8.88, and 8.76 kg person^{-1} year^{-1}, respectively) less than the national average (9.45 kg person^{-1} year^{-1}) due to less industrial activity.

National spatial variability in per-capita emissions are largely driven by sub-PUCs tied to industrial and commercial activity (Fig. 5c). These sub-PUCs include Allied Paint Products (1.14 kg person^{-1} year^{-1}), Industrial Coatings (1.04 kg person^{-1} year^{-1}), Printing Inks (0.80 kg person^{-1} year^{-1}), Agricultural Pesticides (0.53 kg person^{-1} year^{-1}), and Oil & Gas (0.08 kg person^{-1} year^{-1}). The employment proxies for Allied Paint Products, Industrial Coatings, and Printing Inks are usually consistent with the underlying population (Fig. S3), with peaks in California, Texas, Florida, New York, and the industrial Midwest. In contrast, emissions from Agricultural Pesticides and Oil & Gas drive the large per-capita emissions in the Midwest and Great Plains (Fig. 5c). Emissions from these two sub-PUCs are heavily concentrated in the central United States (Fig. S3), including North Dakota, South Dakota, Iowa, Nebraska, Kansas, and Oklahoma. Collectively, these States contain < 4.5 % of the

United States population but 24.1% and 17.5% of the Agricultural Pesticides and Oil & Gas VCP emissions, respectively. Both sub-PUCs also contribute to atypically high per-capita emissions in other States, such as Texas, Colorado, Idaho, and Wyoming.

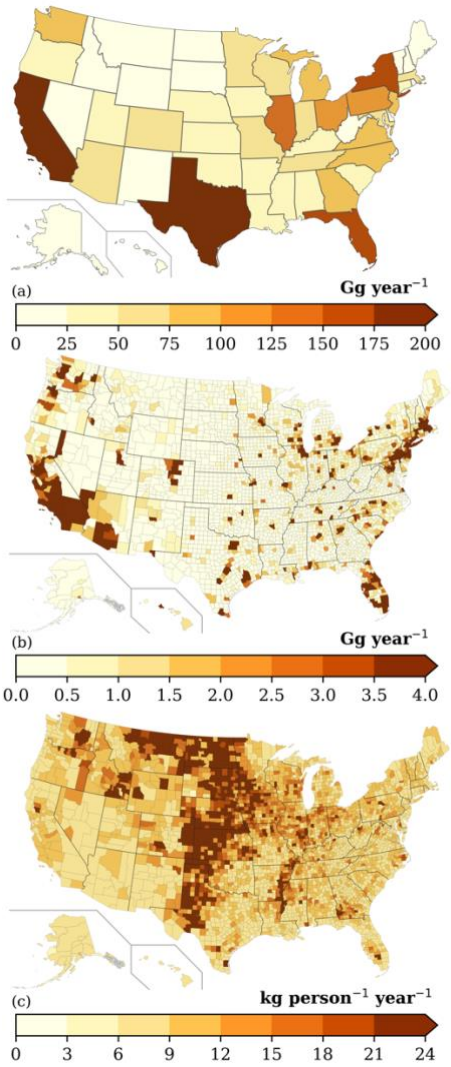

Figure 17: (a) State-level, (b) County-level, and (c) County-level per-capita VCP emissions.

While national VCP emissions from the 2017 NEI and the VCPy inventory are broadly consistent, county-level and categorical estimates can differ substantially between the two (Fig. S4). For example, VCPy reports > 35% lower emissions for 5% of all counties and > 55% higher emissions for another 5% of all counties. When

compared to the 2017 NEI, the States with the greatest emissions increases were Delaware, California, and Colorado, and the States with the greatest emissions decreases were North Dakota and South Dakota. There are also many spatial similarities between the two inventories. Both feature peaks in per-capita emissions over the Midwest and Great Plains (Fig. S4) and approximately half of all county-level emissions in the VCPy inventory are within 15% of their value in the 2017 NEI. To compare the two inventories categorically, all product use categories are mapped to individual Source Classification Codes (SCCs; Table S11). Categorically, VCPy reports higher emissions for Personal Care Products (150%) and Paints & Coatings (25%), whereas Pesticides (-54%) and Printing Inks (-13%) feature emission decreases. The VCPy inventory also includes marginal increases in Cleaning Products and Adhesives & Sealants emissions, while also quantifying solvent-borne emissions in Oil & Gas operations (included as "Other" in Fig. S5).

3.4 Evaluation of Inventory Using Emission Ratios

Predicted per-capita VCP emissions in Los Angeles County are 8.21 kg person^{-1} year^{-1} and consist of 250+ organic compounds. Observed emission ratios were available for 30 species (Table S7), including some of the most abundantly emitted (e.g. ethanol, acetone, isopropyl alcohol, toluene). In fact, of the 30 available emission ratios, 24 were for compounds that contributed more than 0.1% to total VCP emissions (Fig. 6), providing the opportunity to evaluate important markers. For most compounds, the VCPy estimate was well within a factor of 2 when compared to observations. Some important markers were marginally low biased (e.g. ethanol, isopropyl alcohol), while others were marginally high biased (e.g. acetone, methyl ethyl ketone, isobutane), illustrating the difficulty in precisely speciating organic emissions and uncertainties introduced by compositing. However, when considered as a whole, the complete VCPy inventory performs remarkably well with a correlation of 0.95. In total, the observed emission ratio for all 30 compounds was 0.259 g (g CO)$^{-1}$ and the inventory estimate is 0.226 g (g CO)$^{-1}$, indicating a 13% low bias. In addition, the VCPy inventory shows a marked improvement over the 2017 NEI, which reports 3.28 kg person^{-1} year^{-1} of VCP emissions in Los Angeles County.

For the 30 compounds considered here, the 2017 NEI reports 0.143 g (g CO)$^{-1}$, which is 45% lower than observations (Fig. S6). Most notably, the emissions ratio of ethanol, acetone, isopropyl alcohol, and propane, all of which are emitted by VCPs in substantial quantities, were low by a factor of 2-3.

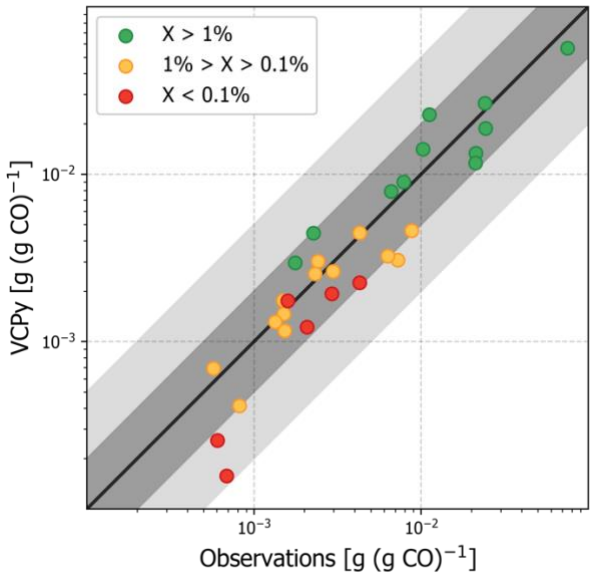

Figure 18: Evaluation of organic emission ratios in Los Angeles County using observed emission ratios from summer 2010. VCPy inventory ratios utilize VCPy predicted emissions for VCPs and the 2017 NEI for all other sources. The scatter point colors represent the relative abundance of each compound (represented as "X" in the figure legend) in the complete VCP sector. For example, all green points represent compounds that are > 1% of the total VCP emissions in Los Angeles County. Black line – 1:1; Dark grey shading – 2:1; Light grey shading – 5:1. Values available in Table S7.

While the residual, 13% low bias could suggest that additional organic emissions might be missing from the VCPy inventory, several other factors could explain discrepancies. First, emission ratios are equally sensitive to both organic and CO emissions. While CO appears to be represented and modelled well in current inventories (Lu et al., 2020), a marginal, systematic bias in CO can affect the results presented here. For example, if the CO inventory were systematically high bias by 10%, the bias in the VCPy inventory emission ratios would be nearly eliminated. Second, since emission ratios are not sector-specific but reflect total emissions, missing organic emissions might be from other sources. Mobile sources, especially gasoline exhaust, is rich in small ($\leq C_6$) hydrocarbons, including ethene, n-butane, n-pentane, isopentane, methylpentanes, propene, and methylhexanes (Gentner et al., 2013). Except for n-butane, none of the remaining compounds appreciably come from VCP sources and all are low biased in the complete inventory (Fig. S6). Finally, while the ambient NMVOC to CO concentration ratio in Los Angeles has been consistent for several decades (McDonald et al., 2013), it is possible that trends for these two pollutants could have diverged in recent years.

3.5 Effective SOA Yields, O3 MIR, and Air Pollution Potential

Nationally, the effective SOA yield of the complete sector is 5.3% by mass (Table 4) and the most abundantly emitted SOA precursors are IVOC alkanes, aromatics, volatile methyl siloxanes, and fragrances. On a sub-PUC basis, the effective yield spans more than two-orders of magnitude, with Short Use Products and Printing Inks featuring an effective yield of 0.05% and 14.8%, respectively. For O_3, the effective MIR of the complete sector is 1.6 (g O_3) g^{-1} and, when compared to SOA yields, there is considerably less sub-PUC variability. While VCPs do emit aromatics and alkenes, both of which are photochemically reactive compound classes with high ozone potential, emissions are usually dominated by oxygenated compounds and alkanes, such as acetone, isopropyl alcohol, propane, and isobutane, which are minimally reactive. In fact, of the top fifteen highest emitting VCP compounds, seven feature a MIR < 1.0 (g O_3) g^{-1}.

Table 8: The national effective SOA yield and MIR for all sub-PUCs. These results are plotted in Fig. S7.

Product Use Categories (PUCs)	**Sub-Product Use Categories (sub-PUCs)**	**Effective SOA Yield [%]**	**Effective MIR [(g O_3) g^{-1}]**
Cleaning Products	Detergents & Soaps	0.00	1.48
	General Cleaners	4.74	1.88
Personal Care Products	Daily Use Products	3.26	1.38
	Short Use Products	0.05	1.27
Adhesives & Sealants	Adhesives & Sealants	6.19	1.51
Paints & Coatings	Architectural Coatings	1.92	1.92
	Aerosol Coatings	3.26	1.66
	Allied Paint Products	6.56	1.27
	Industrial Coatings	2.94	1.71
Printing Inks	Printing Inks	14.81	1.93
Pesticides & FIFRA Products	FIFRA Pesticides	8.10	1.01
	Agricultural Pesticides	8.10	1.01
Dry Cleaning	Dry Cleaning	3.47	1.13
Oil & Gas	Oil & Gas	2.21	1.03
Misc. Products	Misc. Products	1.94	2.26
Fuels & Lighter	Fuels & Lighter	5.35	1.15
Total		5.29	1.58

While a sub-PUC may be a large source of organic emissions, this does not necessarily translate to a high potential impact on $PM_{2.5}$ and ozone. This is best highlighted by Industrial and Architectural Coatings. Together, these two sub-PUCs constitute ~20% of all VCP emissions (Table 3), but only ~10% of the total SOA potential due to their low effective yields (2.9% and 1.9%, respectively). Architectural Coatings emissions feature significant quantities of Texanol™ (a highly branched oxygenate) and small glycols, such as propylene and ethylene glycol. A < 1% and 0% SOA yield is assigned to Texanol™ and both glycols, respectively. Though, it should be noted that this may be a lower bound as Li et al., 2018 report moderate aerosol formation from propylene glycol. Similarly, Printing Inks contribute ~8% of all VCP emissions, which is nearly 2.5x less than Daily Use Products and General Cleaners nationally (Table 3). However, Printing Ink emissions are dominated by IVOC alkanes (C12-C16 hydrocarbons, represented by n-

tetradecane here) and aromatics, resulting in a high effective SOA yield (14.8%). As a result, Printing Inks contribute significantly to the total SOA potential nationally (Fig. 7). Paints & Coatings are nonetheless the dominant contributor to SOA potential, but this is more so due to the high emissions of the component sub-PUCs rather than their modest effective SOA yields (1.9 – 6.6%). Both General Cleaners and Daily Use Products also have moderate quantities of SOA precursors and high emissions, which translates to 17.5% and 13.3% of the national VCP SOA potential, respectively. Since the effective MIR of each sub-PUC is not highly variable, O_3 potential is highly correlated with emissions magnitude. Overall, the three highest emitting PUC, Paints & Coatings, Cleaning Products, and Personal Care Products, are also the highest contributors to O_3 potential (Fig. 7).

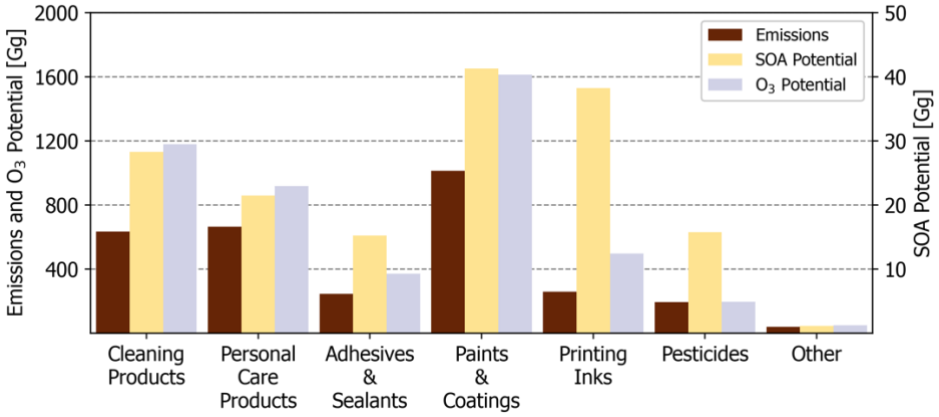

Figure 19: National-level emissions, SOA potential, and O_3 potential by PUC. Other is summation of Dry Cleaning, Oil & Gas, Misc. Products, and Fuels & Lighter.

These results also demonstrate how fate-and-transport assumptions can impact estimates of SOA production. For example, a prior study reported that both laundry detergent and a general-purpose spray cleaner can form appreciable quantities of SOA (Li et al., 2018). Here, the VCPy inventory reports an effective yield of 0.0% by mass of organic emitted for Detergents & Soaps and 4.7% for General Cleaners (Table 4). While the organic content of both sub-PUCs, by mass, is $\geq$ 18% (Table 2), Detergents & Soaps feature a dramatically smaller use timescale (Minutes vs. Days). As a result, not only is the total mass of organic emissions from

Detergents & Soaps smaller than General Cleaners, but the collection of compounds that are emitted feature systematically smaller evaporation timescales. Such compounds are highly volatile (i.e. $C^* > 1 \times 10^8\ \mu g\ m^{-3}$) and not SOA precursors. In contrast, General Cleaners are assigned a longer use timescale, which provides time for lower volatility organics (i.e. IVOCs) to evaporate and subsequently contribute to the formation of SOA.

3.6 Non-Evaporative Organic Assumptions

The composition and volatility distribution of the organics assumed to be non-evaporative, which is ~60% of all organics (Fig. S8), is unidentified and assumed to be entirely non-volatile for the main analysis. However, there is evidence that a non-negligible portion of this mass may be SVOCs ($0.3\ \mu g\ m^{-3} < C^* < 300\ \mu g\ m^{-3}$), which can evaporate on atmospherically relevant timescales (Khare and Gentner, 2018). SHEDS-HT, a near-field model used to prioritize human exposure to chemicals (Isaacs et al., 2014), reports that > 15%, > 5%, and > 2% of all organics found in residential personal care product, household product, and coatings, respectively, are composed of SVOCs (Qin et al., 2020). The treatment of non-evaporative organics and their potential emission can have a substantial impact on the modulation of SOA potential from VCPs. For example, if the assumption regarding evaporation of these organics is relaxed by assuming 1% of all non-evaporative organics eventually do evaporate, sector-wide emissions would increase by 0.18 kg person^{-1} year^{-1} (i.e. < 2% of the VCP emissions). Such a scenario is possible for products featuring long use timescales (e.g. paints, pesticides), if SVOCs are considered non-evaporative, or if products featuring shorter use timescales (e.g. Daily Use Products, Cleaning Products) are not fully sequestered. Since this increase in emissions is minor (i.e. < 2%), there would be negligible impacts on the total emission magnitude and O_3. However, these compounds, by definition, feature low vapor pressures, which makes them prime SOA precursor candidates. If these compounds were permitted to form SOA with 100% efficiency, the effective yield from the complete sector would increase from 5.3% to 7.0% by mass (Fig. S8). Correspondingly, if 2% of all non-evaporative organics were assumed to evaporate

with similar SOA formation assumptions, the effective yield from the complete sector would increase to 8.7% by mass.

4 Additional Uncertainties

The current VCPy framework assumes all evaporated organics reach the ambient atmosphere, regardless of origin. However, VCP emissions occur both indoors and outdoors (Farmer et al., 2019; Nazaroff and Weschler, 2004; Singer et al., 2006a). In fact, the indoor concentration of prevalent VCP markers and secondary pollutants often exceeds outdoor concentrations (Farmer et al., 2019; Patel et al., 2020). For ambient air emissions, consideration of VCP emissions indoors is important if there is a gas-phase loss mechanism occurring at a scale that is comparable to typical indoor air exchange rates (~0.5 hr^{-1}; Murray and Burmaster, 1995). Indeed, sorption of gas-phase organics (e.g. terpenes) into typical residential furnishing and dust has been shown to occur on relevant timescales (Singer et al., 2007; Singer et al., 2004; Weschler and Nazaroff, 2008). Organics emitted indoors can also react with oxidants, leading to the formation of lower-volatility organics that can form particulates (Nazaroff and Weschler, 2004; Singer et al., 2006b). These particulates can deposit before outdoor exhaust occurs due to the high surface-to-volume ratio of indoor settings (Abbatt and Wang, 2020; Farmer et al., 2019). Planned future VCPy functionality includes the incorporation of a two-box model to capture these possible termination mechanisms and distinguish between near-field and far-field exposure pathways.

In addition, the efficiency of post-use controls for several sub-PUCs can be highly uncertain and vary both in space and time. In particular, this includes Oil & Gas, which is assigned a post-use control based on average reported reinjection rates of produced water (Liden et al., 2018; Lyman et al., 2018), as well as Industrial Coatings and Printing Inks, which occur at facilities capable of add-on controls (U.S. Environmental Protection Agency, 2006a; 2006b; 2007; 2008). Here, post-use controls are not assigned for Industrial Coatings or Printing Inks. As such, emissions from these sub-PUCs could feature localized high bias, depending on regional control requirements for facilities that use associated products. Similarly, the spatial

allocation of nonpoint emissions features unique difficulties. For example, even if the allocation of nonpoint emissions was precisely matched to a quantifiable proxy, variation in the emission strength of individuals within that proxy (e.g. humans or employees) is often neglected (Li et al., 2020).

5 Conclusions

VCPy is a new framework to model organic emissions from volatile chemical products throughout the United States, including spatial allocation to regional and local scales. In VCPy, product volatilization is a function of the characteristic evaporation timescale of individual components and the use timescale for product-use categories. National, per-capita organic emissions from VCPs are 9.5 kg person^{-1} year^{-1} (6.4 kgC person^{-1} year^{-1}) for 2016, which translates to 3.05 Tg (2.06 TgC) for the U.S. Paints & Coatings, Personal Care Products, and Cleaning Products contribute most to these emissions. When filtered to remove regulatory exempt organics, total emissions from VCPs are 2.6 Tg of VOC and equal in magnitude to the sum of all mobile sources nationally, thus highlighting the growing importance of the VCP sector. Organic emissions featured substantial (~20%) contributions from IVOCs, which are likely SOA precursors. Of this 20%, 52% are oxygenated compounds, 30% are n-alkanes, and the rest are largely branched and cyclic alkanes. Nationally, the effective SOA yield and O_3 MIR, two metrics that facilitate an approximation of the potential air quality impacts, of VCPs is 5.3% by mass and 1.58 (g O_3) g^{-1}, respectively. This effective SOA yield indicates VCPs are likely a significant source of SOA in urban environments (Qin et al., 2020).

Uncertainty associated with this framework was tested through Monte Carlo analysis. Notably, the dominant drivers of uncertainty were associated with estimated product usage and the composition of products, and not assumptions related to fate-and-transport. SOA formation from VCP emissions is especially sensitive to assumptions regarding evaporation of low volatility species. If 1% of all non-evaporative organics eventually do evaporate, sector-wide emissions would increase by 0.18 kg person^{-1} year^{-1} and the effective SOA yield from the complete sector could increase by > 1.5%. The 95% confidence interval for the national-level

emissions from the complete sector for 2016 is 2.61 – 3.53 Tg (1.76 – 2.38 TgC). This is broadly consistent with the 2017 National Emission Inventory (2.84 Tg) and half the emissions magnitude reported elsewhere (McDonald et al., 2018).

While the national-level emissions from the VCPy framework and the 2017 NEI are comparable, regional and localized differences can be significant. This is most clear when evaluating the VCPy inventory to published emission ratios. For Los Angeles County, the VCPy inventory performs well (normalized mean bias of -13% with r = 0.95) and is significantly improved over the reported 2017 NEI VCP emissions. Planned future work includes adoption of variable emission settings (indoor vs. outdoor) to account for loss mechanisms indoors (e.g. gas-phase sorption to surfaces), revisited mapping of VCP emissions to common chemical mechanisms for ease of research use in the chemical transport modelling community, estimation of SOA and ozone formation from VCPs using a chemical transport model and VCPy emissions inputs, and understanding the evolution of VCP emissions over time.

Data Availability

VCPy.v1.0 is available on data.gov (doi: 10.23719/1520157). All data presented in this manuscript can be retrieved and/or generated by downloading VCPy.v1.0. Guidance on using VCPy.v1.0 can be requested by contacting the corresponding author.

Author Contributions

KMS and HOTP designed the research scope. All authors participated in data curation and/or analysis. KMS and HOTP drafted the initial manuscript and all authors contributed to subsequent drafts.

Competing Interests

The authors declare that they have no conflicts of interest.

Disclaimer

Although this work was contributed by research staff in the Environmental Protection Agency and has been reviewed and approved for publication, it does not reflect official policy of the EPA. The views expressed in this document are solely those of

authors and do not necessarily reflect those of the Agency. EPA does not endorse any products or commercial services mentioned in this publication.

Acknowledgements

The authors would like to thank Janice Godfrey, Art Diem, Jennifer Snyder, Rich Mason, Caroline Farkas, Claudia Toro, Alison Eyth, Luke Valin, Mohammed Jaoui, Jim Szykman, Donna Schwede, Christian Hogrefe, Kristen Foley, Jesse Bash, Marc Houyoux, and Cindy Beeler at the U.S. EPA and Kyriacos Kyriacou and Jose Gomez at the California Air Resources Board for helpful discussions and/or data acquisition. Comments by Marc Houyoux (EPA), Jim Szykman (EPA), and two anonymous reviewers served to strengthen this manuscript.

Financial Support

Karl Seltzer and Elyse Pennington were supported by the Oak Ridge Institute for Science and Education (ORISE) Research Participation Program for the U.S. Environmental Protection Agency (EPA).

References

Abbatt, J. P. D., and Wang, C.: The atmospheric chemistry of indoor environments, Environ Sci-Proc Imp, 22, 25-48, 10.1039/c9em00386j, 2020.

Baker, K. R., Carlton, A. G., Kleindienst, T. E., Offenberg, J. H., Beaver, M. R., Gentner, D. R., Goldstein, A. H., Hayes, P. L., Jimenez, J. L., Gilman, J. B., de Gouw, J. A., Woody, M. C., Pye, H. O. T., Kelly, J. T., Lewandowski, M., Jaoui, M., Stevens, P. S., Brune, W. H., Lin, Y. H., Rubitschun, C. L., and Surratt, J. D.: Gas and aerosol carbon in California: comparison of measurements and model predictions in Pasadena and Bakersfield, Atmos Chem Phys, 15, 5243-5258, 10.5194/acp-15-5243-2015, 2015.

Bash, J. O., Baker, K. R., and Beaver, M. R.: Evaluation of improved land use and canopy representation in BEIS v3.61 with biogenic VOC measurements in California, Geosci Model Dev, 9, 2191-2207, 10.5194/gmd-9-2191-2016, 2016.

Bishop, G. A., and Stedman, D. H.: A decade of on-road emissions measurements, Environ Sci Technol, 42, 1651-1656, 10.1021/es702413b, 2008.

Borbon, A., Gilman, J. B., Kuster, W. C., Grand, N., Chevaillier, S., Colomb, A., Dolgorouky, C., Gros, V., Lopez, M., Sarda-Esteve, R., Holloway, J., Stutz, J., Petetin, H., McKeen, S., Beekmann, M., Warneke, C., Parrish, D. D., and de Gouw, J. A.: Emission ratios of anthropogenic volatile organic compounds in northern mid-latitude megacities: Observations versus emission inventories in Los Angeles and Paris, J Geophys Res-Atmos, 118, 2041-2057, 10.1002/jgrd.50059, 2013.

Burnett, R., Chen, H., Szyszkowicz, M., Fann, N., Hubbell, B., Pope, C. A., Apte, J. S., Brauer, M., Cohen, A., Weichenthal, S., Coggins, J., Di, Q., Brunekreef, B., Frostad, J., Lim, S. S., Kan, H. D., Walker, K. D., Thurston, G. D., Hayes, R. B., Lim, C. C., Turner, M. C., Jerrett, M., Krewski, D., Gapstur, S. M., Diver, W. R., Ostro, B., Goldberg, D., Crouse, D. L., Martin, R. V., Peters, P., Pinault, L., Tjepkema, M., Donkelaar, A., Villeneuve, P. J., Miller, A. B., Yin, P., Zhou, M. G., Wang, L. J., Janssen, N. A. H., Marra, M., Atkinson, R. W., Tsang, H., Thach, Q., Cannon, J. B., Allen, R. T., Hart, J. E., Laden, F., Cesaroni, G., Forastiere, F., Weinmayr, G., Jaensch, A., Nagel, G., Concin, H., and Spadaro, J. V.: Global estimates of mortality associated with long-term exposure to outdoor fine particulate matter, P Natl Acad Sci USA, 115, 9592-9597, 10.1073/pnas.1803222115, 2018.

California Air Resources Board (CARB): 2005 Architectural Coatings Survey – Final Report, 2007.

California Air Resources Board (CARB): 2010 Aerosol Coatings Survey Results, 2012.

California Air Resources Board (CARB): 2014 Architectural Coatings Survey - Draft Data Summary, 2014.

California Air Resources Board (CARB): ORGPROF - Organic chemical profiles for source categories, 2018. https://ww2.arb.ca.gov/speciation-profiles-used-carb-modeling (last access: August 28, 2020)

California Air Resources Board (CARB): Final 2015 Consumer & Commercial Product Survey Data Summaries, 2019. https://ww2.arb.ca.gov/sites/default/files/2020-08/2015_CP_Survey_Summary_data_2019-12-09%20%28Autosaved%29.xlsx (last access: August 28, 2020)

Cappa, C. D., and Wilson, K. R.: Multi-generation gas-phase oxidation, equilibrium partitioning, and the formation and evolution of secondary organic aerosol, Atmos Chem Phys, 12, 9505-9528, 10.5194/acp-12-9505-2012, 2012.

Carter, W. P. L.: Development of the SAPRC-07 chemical mechanism, Atmos Environ, 44, 5324-5335, 10.1016/j.atmosenv.2010.01.026, 2010a.

Carter, W. P. L.: Updated Maximum Incremental Reactivity Scale and Hydrocarbon Bin Reactivities for Regulatory Applications, Prepared for California Air Resources Board Contract 07-339, 2010b.

Carter, W. P. L.: Development of a database for chemical mechanism assignments for volatile organic emissions, J Air Waste Manage, 65, 1171-1184, 10.1080/10962247.2015.1013646, 2015.

Chan, A. W. H., Kautzman, K. E., Chhabra, P. S., Surratt, J. D., Chan, M. N., Crounse, J. D., Kurten, A., Wennberg, P. O., Flagan, R. C., and Seinfeld, J. H.: Secondary organic aerosol formation from photooxidation of naphthalene and alkylnaphthalenes: implications for oxidation of intermediate volatility organic compounds (IVOCs), Atmos Chem Phys, 9, 3049-3060, 10.5194/acp-9-3049-2009, 2009.

Charan, S. M., Buenconsejo, R. S., and Seinfeld, J. H.: Secondary Organic Aerosol Yields from the Oxidation of Benzyl Alcohol, Atmospheric Chemistry Physics Discussions, 10.5194/acp-2020-492, 2020.

de Gouw, J. A., Middlebrook, A. M., Warneke, C., Goldan, P. D., Kuster, W. C., Roberts, J. M., Fehsenfeld, F. C., Worsnop, D. R., Canagaratna, M. R.,

Pszenny, A. A. P., Keene, W. C., Marchewka, M., Bertman, S. B., and Bates, T. S.: Budget of organic carbon in a polluted atmosphere: Results from the New England Air Quality Study in 2002, J Geophys Res-Atmos, 110, 10.1029/2004jd005623, 2005.

de Gouw, J. A., Gilman, J. B., Kim, S. W., Lerner, B. M., Isaacman-VanWertz, G., McDonald, B. C., Warneke, C., Kuster, W. C., Lefer, B. L., Griffith, S. M., Dusanter, S., Stevens, P. S., and Stutz, J.: Chemistry of Volatile Organic Compounds in the Los Angeles basin: Nighttime Removal of Alkenes and Determination of Emission Ratios, J Geophys Res-Atmos, 122, 11843-11861, 10.1002/2017jd027459, 2017.

de Gouw, J. A., Gilman, J. B., Kim, S. W., Alvarez, S. L., Dusanter, S., Graus, M., Griffith, S. M., Isaacman-VanWertz, G., Kuster, W. C., Lefer, B. L., Lerner, B. M., McDonald, B. C., Rappengluck, B., Roberts, J. M., Stevens, P. S., Stutz, J., Thalman, R., Veres, P. R., Volkamer, R., Warneke, C., Washenfelder, R. A., and Young, C. J.: Chemistry of Volatile Organic Compounds in the Los Angeles Basin: Formation of Oxygenated Compounds and Determination of Emission Ratios, J Geophys Res-Atmos, 123, 2298-2319, 10.1002/2017jd027976, 2018.

Di, Q., Wang, Y., Zanobetti, A., Wang, Y., Koutrakis, P., Choirat, C., Dominici, F., and Schwartz, J. D.: Air Pollution and Mortality in the Medicare Population, New Engl J Med, 376, 2513-2522, 10.1056/NEJMoa1702747, 2017.

Donahue, N. M., Kroll, J. H., Pandis, S. N., and Robinson, A. L.: A two-dimensional volatility basis set - Part 2: Diagnostics of organic-aerosol evolution, Atmos Chem Phys, 12, 615-634, 10.5194/acp-12-615-2012, 2012.

Ensberg, J. J., Hayes, P. L., Jimenez, J. L., Gilman, J. B., Kuster, W. C., de Gouw, J. A., Holloway, J. S., Gordon, T. D., Jathar, S., Robinson, A. L., and Seinfeld, J. H.: Emission factor ratios, SOA mass yields, and the impact of

vehicular emissions on SOA formation, Atmos Chem Phys, 14, 2383-2397, 10.5194/acp-14-2383-2014, 2014.

Farmer, D. K., Vance, M. E., Abbatt, J. P. D., Abeleira, A., Alves, M. R., Arata, C., Boedicker, E., Bourne, S., Cardoso-Saldana, F., Corsi, R., DeCarlo, P. F., Goldstein, A. H., Grassian, V. H., Hildebrandt Ruiz, L., Jimenez, J. L., Kahan, T. F., Katz, E. F., Mattila, J. M., Nazaroff, W. W., Novoselac, A., O'Brien, R. E., Or, V. W., Patel, S., Sankhyan, S., Stevens, P. S., Tian, Y., Wade, M., Wang, C., Zhou, S., and Zhou, Y.: Overview of HOMEChem: House Observations of Microbial and Environmental Chemistry, Environ Sci-Proc Imp, 21, 1280-1300, 10.1039/c9em00228f, 2019.

Gentner, D. R., Isaacman, G., Worton, D. R., Chan, A. W. H., Dallmann, T. R., Davis, L., Liu, S., Day, D. A., Russell, L. M., Wilson, K. R., Weber, R., Guha, A., Harley, R. A., and Goldstein, A. H.: Elucidating secondary organic aerosol from diesel and gasoline vehicles through detailed characterization of organic carbon emissions, P Natl Acad Sci USA, 109, 18318-18323, 10.1073/pnas.1212272109, 2012.

Gentner, D. R., Worton, D. R., Isaacman, G., Davis, L. C., Dallmann, T. R., Wood, E. C., Herndon, S. C., Goldstein, A. H., and Harley, R. A.: Chemical Composition of Gas-Phase Organic Carbon Emissions from Motor Vehicles and Implications for Ozone Production, Environ Sci Technol, 47, 11837-11848, 10.1021/es401470e, 2013.

Gentner, D. R., Jathar, S. H., Gordon, T. D., Bahreini, R., Day, D. A., El Haddad, I., Hayes, P. L., Pieber, S. M., Platt, S. M., de Gouw, J., Goldstein, A. H., Harley, R. A., Jimenez, J. L., Prevot, A. S. H., and Robinson, A. L.: Review of Urban Secondary Organic Aerosol Formation from Gasoline and Diesel Motor Vehicle Emissions, Environ Sci Technol, 51, 1074-1093, 10.1021/acs.est.6b04509, 2017.

Heald, C. L., and Kroll, J. H.: The fuel of atmospheric chemistry: Toward a complete description of reactive organic carbon, Science Advances, 6, 10.1126/sciadv.aay8967, 2020.

Hildebrandt, L., Donahue, N. M., and Pandis, S. N.: High formation of secondary organic aerosol from the photo-oxidation of toluene, Atmos Chem Phys, 9, 2973-2986, DOI 10.5194/acp-9-2973-2009, 2009.

Hodzic, A., Jimenez, J. L., Madronich, S., Canagaratna, M. R., DeCarlo, P. F., Kleinman, L., and Fast, J.: Modeling organic aerosols in a megacity: potential contribution of semi-volatile and intermediate volatility primary organic compounds to secondary organic aerosol formation, Atmos Chem Phys, 10, 5491-5514, 10.5194/acp-10-5491-2010, 2010.

Isaacs, K. K., Glen, W. G., Egeghy, P., Goldsmith, M. R., Smith, L., Vallero, D., Brooks, R., Grulke, C. M., and Ozkaynak, H.: SHEDS-HT: An Integrated Probabilistic Exposure Model for Prioritizing Exposures to Chemicals with Near-Field and Dietary Sources, Environ Sci Technol, 48, 12750-12759, 10.1021/es502513w, 2014.

Isaacs, K. K., Dionisio, K., Phillips, K., Bevington, C., Egeghy, P., and Price, P. S.: Establishing a system of consumer product use categories to support rapid modeling of human exposure, J Expo Sci Env Epid, 30, 171-183, 10.1038/s41370-019-0187-5, 2020.

Janechek, N. J., Hansen, K. M., and Stanier, C. O.: Comprehensive atmospheric modeling of reactive cyclic siloxanes and their oxidation products, Atmos Chem Phys, 17, 8357-8370, 10.5194/acp-17-8357-2017, 2017.

Janechek, N. J., Marek, R. F., Bryngelson, N., Singh, A., Bullard, R. L., Brune, W. H., and Stanier, C. O.: Physical properties of secondary photochemical aerosol from OH oxidation of a cyclic siloxane, Atmos Chem Phys, 19, 1649-1664, 10.5194/acp-19-1649-2019, 2019.

Jathar, S. H., Woody, M., Pye, H. O. T., Baker, K. R., and Robinson, A. L.: Chemical transport model simulations of organic aerosol in southern California: model evaluation and gasoline and diesel source contributions, Atmos Chem Phys, 17, 4305-4318, 10.5194/acp-17-4305-2017, 2017.

Jimenez, J. L., Canagaratna, M. R., Donahue, N. M., Prevot, A. S. H., Zhang, Q., Kroll, J. H., DeCarlo, P. F., Allan, J. D., Coe, H., Ng, N. L., Aiken, A. C.,

Docherty, K. S., Ulbrich, I. M., Grieshop, A. P., Robinson, A. L., Duplissy, J., Smith, J. D., Wilson, K. R., Lanz, V. A., Hueglin, C., Sun, Y. L., Tian, J., Laaksonen, A., Raatikainen, T., Rautiainen, J., Vaattovaara, P., Ehn, M., Kulmala, M., Tomlinson, J. M., Collins, D. R., Cubison, M. J., Dunlea, E. J., Huffman, J. A., Onasch, T. B., Alfarra, M. R., Williams, P. I., Bower, K., Kondo, Y., Schneider, J., Drewnick, F., Borrmann, S., Weimer, S., Demerjian, K., Salcedo, D., Cottrell, L., Griffin, R., Takami, A., Miyoshi, T., Hatakeyama, S., Shimono, A., Sun, J. Y., Zhang, Y. M., Dzepina, K., Kimmel, J. R., Sueper, D., Jayne, J. T., Herndon, S. C., Trimborn, A. M., Williams, L. R., Wood, E. C., Middlebrook, A. M., Kolb, C. E., Baltensperger, U., and Worsnop, D. R.: Evolution of Organic Aerosols in the Atmosphere, Science, 326, 1525-1529, 10.1126/science.1180353, 2009.

Kazemiparkouhi, F., Eum, K. D., Wang, B. Y., Manjourides, J., and Suh, H. H.: Long-term ozone exposures and cause-specific mortality in a US Medicare cohort, J Expo Sci Env Epid, 30, 650-658, 10.1038/s41370-019-0135-4, 2020.

Khare, P., and Gentner, D. R.: Considering the future of anthropogenic gas-phase organic compound emissions and the increasing influence of non-combustion sources on urban air quality, Atmos Chem Phys, 18, 5391-5413, 10.5194/acp-18-5391-2018, 2018.

Li, W. H., Li, L. J., Chen, C. L., Kacarab, M., Peng, W. H., Price, D., Xu, J., and Cocker, D. R.: Potential of select intermediate-volatility organic compounds and consumer products for secondary organic aerosol and ozone formation under relevant urban conditions, Atmos Environ, 178, 109-117, 10.1016/j.atmosenv.2017.12.019, 2018.

Li, L. J., and Cocker, D. R.: Molecular structure impacts on secondary organic aerosol formation from glycol ethers, Atmos Environ, 180, 206-215, 10.1016/j.atmosenv.2017.12.025, 2018.

Li, Y., Rodier, C., Lea, J. D., Harvey, J., and Kleeman, M. J.: Improving spatial surrogates for area source emissions inventories in California, Atmos Environ, 10.1016/j.atmosenv.2020.117665, 2020.

Liden, T., Santos, I. C., Hildenbrand, Z. L., and Schug, K. A.: Treatment modalities for the reuse of produced waste from oil and gas development, Sci Total Environ, 643, 107-118, 10.1016/j.scitotenv.2018.05.386, 2018.

Lu, Q. Y., Zhao, Y. L., and Robinson, A. L.: Comprehensive organic emission profiles for gasoline, diesel, and gas-turbine engines including intermediate and semi-volatile organic compound emissions, Atmos Chem Phys, 18, 17637-17654, 10.5194/acp-18-17637-2018, 2018.

Lu, Q. Y., Murphy, B. N., Qin, M. M., Adams, P., Zhao, Y. L., Pye, H. O. T., Efstathiou, C., Allen, C., and Robinson, A. L.: Simulation of organic aerosol formation during the CalNex study: updated mobile emissions and secondary organic aerosol parameterization for intermediate-volatility organic compounds, Atmos Chem Phys, 20, 4313-4332, 10.5194/acp-20-4313-2020, 2020.

Lyman, S. N., Mansfield, M. L., Tran, H. N. Q., Evans, J. D., Jones, C., O'Neil, T., Bowers, R., Smith, A., and Keslar, C.: Emissions of organic compounds from produced water ponds I: Characteristics and speciation, Sci Total Environ, 619, 896-905, 10.1016/j.scitotenv.2017.11.161, 2018.

Mansfield, M. L., Tran, H. N. Q., Lyman, S. N., Bowers, R. L., Smith, A. P., and Keslar, C.: Emissions of organic compounds from produced water ponds III: Mass-transfer coefficients, composition-emission correlations, and contributions to regional emissions, Sci Total Environ, 627, 860-868, 10.1016/j.scitotenv.2018.01.242, 2018.

Mansouri, K., Grulke, C. M., Judson, R. S., and Williams, A. J.: OPERA models for predicting physicochemical properties and environmental fate endpoints, J Cheminformatics, 10, 10.1186/s13321-018-0263-1, 2018.

McDonald, B. C., Gentner, D. R., Goldstein, A. H., and Harley, R. A.: Long-Term Trends in Motor Vehicle Emissions in US Urban Areas, Environ Sci Technol, 47, 10022-10031, 10.1021/es401034z, 2013.

McDonald, B. C., Goldstein, A. H., and Harley, R. A.: Long-Term Trends in California Mobile Source Emissions and Ambient Concentrations of Black Carbon and Organic Aerosol, Environ Sci Technol, 49, 5178-5188, 10.1021/es505912b, 2015.

McDonald, B. C., de Gouw, J. A., Gilman, J. B., Jathar, S. H., Akherati, A., Cappa, C. D., Jimenez, J. L., Lee-Taylor, J., Hayes, P. L., McKeen, S. A., Cui, Y. Y., Kim, S. W., Gentner, D. R., Isaacman-VanWertz, G., Goldstein, A. H., Harley, R. A., Frost, G. J., Roberts, J. M., Ryerson, T. B., and Trainer, M.: Volatile chemical products emerging as largest petrochemical source of urban organic emissions, Science, 359, 760-764, 10.1126/science.aaq0524, 2018.

Mills, G., Sharps, K., Simpson, D., Pleijel, H., Frei, M., Burkey, K., Emberson, L., Uddling, J., Broberg, M., Feng, Z. Z., Kobayashi, K., and Agrawal, M.: Closing the global ozone yield gap: Quantification and cobenefits for multistress tolerance, Global Change Biol, 24, 4869-4893, 10.1111/gcb.14381, 2018.

Murphy, B. N., Woody, M. C., Jimenez, J. L., Carlton, A. M. G., Hayes, P. L., Liu, S., Ng, N. L., Russell, L. M., Setyan, A., Xu, L., Young, J., Zaveri, R. A., Zhang, Q., and Pye, H. O. T.: Semivolatile POA and parameterized total combustion SOA in CMAQv5.2: impacts on source strength and partitioning, Atmos Chem Phys, 17, 11107-11133, 10.5194/acp-17-11107-2017, 2017.

Murray, D. M., and Burmaster, D. E.: Residential Air Exchange Rates in the United States: Empirical and Estimated Parametric Distributions by Season and Climatic Region, Risk Analysis, 15, 459-465, 10.1111/j.1539-6924.1995.tb00338.x, 1995.

Nazaroff, W. W., and Weschler, C. J.: Cleaning products and air fresheners: exposure to primary and secondary air pollutants, Atmos Environ, 38, 2841-2865, 10.1016/j.atmosenv.2004.02.040, 2004.

Ng, N. L., Kroll, J. H., Chan, A. W. H., Chhabra, P. S., Flagan, R. C., and Seinfeld, J. H.: Secondary organic aerosol formation from m-xylene, toluene, and benzene, Atmos Chem Phys, 7, 3909-3922, DOI 10.5194/acp-7-3909-2007, 2007.

Ozone Transport Commission, OTC Model Regulations for Nitrogen Oxides (NOx) and Photo-reactive Volatile Organic Compounds (VOCs), Technical Support Document, 2016.

Ozone Transport Commission, OTC Regulatory and Technical Guideline for Reduction of Ozone Precursor Emissions from Consumer Products – Phase V, 2018.

Patel, S., Sankhyan, S., Boedicker, E. K., DeCarlo, P. F., Farmer, D. K., Goldstein, A. H., Katz, E. F., Nazaroff, W. W., Tian, Y. L., Vanhanen, J., and Vance, M. E.: Indoor Particulate Matter during HOMEChem: Concentrations, Size Distributions, and Exposures, Environ Sci Technol, 54, 7107-7116, 10.1021/acs.est.0c00740, 2020.

Pollack, I. B., Ryerson, T. B., Trainer, M., Neuman, J. A., Roberts, J. M., and Parrish, D. D.: Trends in ozone, its precursors, and related secondary oxidation products in Los Angeles, California: A synthesis of measurements from 1960 to 2010, J Geophys Res-Atmos, 118, 5893-5911, 10.1002/jgrd.50472, 2013.

Presto, A. A., Miracolo, M. A., Donahue, N. M., and Robinson, A. L.: Secondary Organic Aerosol Formation from High-NOx Photo-Oxidation of Low Volatility Precursors: n-Alkanes, Environ Sci Technol, 44, 2029-2034, 10.1021/es903712r, 2010.

Qin, M. M., Murphy, B. N., Isaacs, K. K., McDonald, B. C., Lu, Q. Y., McKeen, S. A., Koval, L., Robinson, A. L., Efstathiou, C., Allen, C., and Pye, H. O.

T.: Criteria pollutant impacts of volatile chemical products informed by near-field modelling, Nat Sustain, 10.1038/s41893-020-00614-1, 2020.

Safieddine, S. A., Heald, C. L., and Henderson, B. H.: The global nonmethane reactive organic carbon budget: A modeling perspective, Geophys Res Lett, 44, 3897-3906, 10.1002/2017gl072602, 2017.

Sarwar, G., Olson, D. A., Corsi, R. L., and Weschler, C. J.: Indoor fine particles: The role of terpene emissions from consumer products, J Air Waste Manage, 54, 367-377, Doi 10.1080/10473289.2004.10470910, 2004.

Shah, R. U., Coggon, M. M., Gkatzelis, G. I., McDonald, B. C., Tasoglou, A., Huber, H., Gilman, J., Warneke, C., Robinson, A. L., and Presto, A. A.: Urban Oxidation Flow Reactor Measurements Reveal Significant Secondary Organic Aerosol Contributions from Volatile Emissions of Emerging Importance, Environ Sci Technol, 54, 714-725, 10.1021/acs.est.9b06531, 2020.

Singer, B. C., Revzan, K. L., Hotchi, T., Hodgson, A. T., and Brown, N. J.: Sorption of organic gases in a furnished room, Atmos Environ, 38, 2483-2494, 2004.

Singer, B. C., Coleman, B. K., Destaillats, H., Hodgson, A. T., Lunden, M. M., Weschler, C. J., and Nazaroff, W. W.: Indoor secondary pollutants from cleaning product and air freshener use in the presence of ozone, Atmos Environ, 40, 6696-6710, 2006a.

Singer, B. C., Destaillats, H., Hodgson, A. T., and Nazaroff, W. W.: Cleaning products and air fresheners: emissions and resulting concentrations of glycol ethers and terpenoids, Indoor Air, 16, 179-191, 10.1111/j.1600-0668.2005.00414.x, 2006b.

Singer, B. C., Hodgson, A. T., Hotchi, T., Ming, K. Y., Sextro, R. G., Wood, E. E., and Brown, N. J.: Sorption of organic gases in residential rooms, Atmos Environ, 41, 3251-3265, 2007.

Stringfellow, W. T., Camarillo, M. K., Domen, J. K., and Shonkoff, S. B. C.: Comparison of chemical-use between hydraulic fracturing, acidizing, and routine oil and gas development, Plos One, 12, 2017.

Strum, M., and Scheffe, R.: National review of ambient air toxics observations, J Air Waste Manage, 66, 120-133, 10.1080/10962247.2015.1076538, 2016.

The Freedonia Group: Solvents, Industry Study #3429, 2016.

Tkacik, D. S., Presto, A. A., Donahue, N. M., and Robinson, A. L.: Secondary Organic Aerosol Formation from Intermediate-Volatility Organic Compounds: Cyclic, Linear, and Branched Alkanes, Environ Sci Technol, 46, 8773-8781, 2012.

U.S. Bureau of Labor Statistics, Producer Price Index by Industry, retrieved from FRED, Federal Reserve Bank of St. Louis, 2020. https://fred.stlouisfed.org/categories/31 (last access: August 21, 2020)

U.S. Census Bureau: Paint and Allied Products - 2010, MA325F(10), 2011. https://www.census.gov/data/tables/time-series/econ/cir/ma325f.html (last access: August 20, 2020)

U.S. Census Bureau: Manufacturing and International Trade Report (MITR): 2016, Washington D.C., USA, 2016a. https://www.census.gov/foreign-trade/Press-Release/MITR/2016/index.html (last access: August 28, 2020)

U.S. Census Bureau: 2016 Annual Survey of Manufacturers (ASM), Washington D.C., USA, 2016b. https://www.census.gov/data/tables/2016/econ/asm/2016-asm.html (last access: August 20, 2020)

U.S. Census Bureau, Economy Wide Statistics Division: County Business Patterns, 2018. https://www.census.gov/programs-surveys/cbp/data/datasets.html (last access: August 20, 2020)

U.S. Census Bureau, Population Division: Annual Resident Population Estimates, Estimated Components of Resident Population Change, and Rates of the Components of Resident Population Change for States and Counties, 2020.

https://www.census.gov/data/datasets/time-series/demo/popest/2010s-counties-total.html (last access: August 21, 2020)

U.S. Department of Transportation and the U.S. Department of Commerce, 2012 Commodity Flow Survey, EC12TCF-US, 2015. https://www.census.gov/library/publications/2015/econ/ec12tcf-us.html (last access: August 21, 2020)

U.S. Energy Information Administration: The Distribution of U.S. Oil and Natural Gas Wells by Production Rate, Washington, DC, 2019. https://www.eia.gov/petroleum/wells/ (last access: August 21, 2020)

U.S. Environmental Protection Agency: Study of Volatile Organic Compound Emissions from Consumer and Commercial Products, Research Triangle Park, NC, EPA 453/R-94-066, 1995.

U.S. Environmental Protection Agency: Control Techniques Guidelines for Offset Lithographic Printing and Letterpress Printing, Research Triangle Park, NC, EPA 453/R-06-002, 2006a. https://www3.epa.gov/airquality/ctg_act/200609_voc_epa453_r-06-002_litho_letterpress_printing.pdf (last access: August 20, 2020)

U.S. Environmental Protection Agency: Control Techniques Guidelines for Flexible Package Printing, Research Triangle Park, NC, EPA 453/R-06-003, 2006b. https://www3.epa.gov/airquality/ctg_act/200609_voc_epa453_r-06-003_flexible_package_printing.pdf (last access: August 20, 2020)

U.S. Environmental Protection Agency: Control Techniques Guidelines for Large Appliance Coatings, Research Triangle Park, NC, EPA 453/R-08-003, 2007. https://www3.epa.gov/airquality/ctg_act/200709_voc_epa453_r-07-004_lg_appliance_coating.pdf (last access: August 20, 2020)

U.S. Environmental Protection Agency: Control Techniques Guidelines for Automobile and Light-Duty Truck Assembly Coatings, Research Triangle Park, NC, EPA 453/R-08-006, 2008a. https://www3.epa.gov/airquality/ctg_act/200809_voc_epa453_r-08-006_auto_ldtruck_assembly_coating.pdf (last access: August 20, 2020)

U.S. Environmental Protection Agency: Integrated Science Assessment for Particulate Matter, Office of Research and Development – Center for Public Health & Environmental Assessment – RTP, 2019a.

U.S. Environmental Protection Agency: Final Report, SPECIATE Version 5.0, Database Development Documentation, Research Triangle Park, NC, EPA/600/R-19/988, 2019b. https://www.epa.gov/air-emissions-modeling/speciate-51-and-50-addendum-and-final-report (last access: August 21, 2020)

U.S. Environmental Protection Agency: Integrated Science Assessment for Ozone and Related Photochemical Oxidants, Office of Research and Development – Center for Public Health & Environmental Assessment – Research Triangle Park, NC, 2020a.

U.S. Environmental Protection Agency: 2017 National Emissions Inventory (NEI), Research Triangle Park, NC, 2020b. https://www.epa.gov/air-emissions-inventories/2017-national-emissions-inventory-nei-data (last access: August 20, 2020)

Volkamer, R., Jimenez, J. L., San Martini, F., Dzepina, K., Zhang, Q., Salcedo, D., Molina, L. T., Worsnop, D. R., and Molina, M. J.: Secondary organic aerosol formation from anthropogenic air pollution: Rapid and higher than expected, Geophys Res Lett, 33, 2006.

Warneke, C., McKeen, S. A., de Gouw, J. A., Goldan, P. D., Kuster, W. C., Holloway, J. S., Williams, E. J., Lerner, B. M., Parrish, D. D., Trainer, M., Fehsenfeld, F. C., Kato, S., Atlas, E. L., Baker, A., and Blake, D. R.: Determination of urban volatile organic compound emission ratios and comparison with an emissions database, J Geophys Res-Atmos, 112, 10.1029/2006jd007930, 2007.

Warneke, C., de Gouw, J. A., Holloway, J. S., Peischl, J., Ryerson, T. B., Atlas, E., Blake, D., Trainer, M., and Parrish, D. D.: Multiyear trends in volatile organic compounds in Los Angeles, California: Five decades of decreasing emissions, J Geophys Res-Atmos, 117, 2012.

Weschler, C. J., and Nazaroff, W. W.: Semivolatile organic compounds in indoor environments, Atmos Environ, 42, 9018-9040, 2008.

Williams, B. J., Goldstein, A. H., Kreisberg, N. M., Hering, S. V., Worsnop, D. R., Ulbrich, I. M., Docherty, K. S., and Jimenez, J. L.: Major components of atmospheric organic aerosol in southern California as determined by hourly measurements of source marker compounds, Atmos Chem Phys, 10, 11577-11603, 2010.

Woody, M. C., Baker, K. R., Hayes, P. L., Jimenez, J. L., Koo, B., and Pye, H. O. T.: Understanding sources of organic aerosol during CalNex-2010 using the CMAQ-VBS, Atmos Chem Phys, 16, 4081-4100, DOI 10.5194/acp-16-4081-2016, 2016.

Xu, L., Suresh, S., Guo, H., Weber, R. J., and Ng, N. L.: Aerosol characterization over the southeastern United States using high-resolution aerosol mass spectrometry: spatial and seasonal variation of aerosol composition and sources with a focus on organic nitrates, Atmos Chem Phys, 15, 7307-7336, 10.5194/acp-15-7307-2015, 2015.

Zhang, Q., Jimenez, J. L., Canagaratna, M. R., Allan, J. D., Coe, H., Ulbrich, I., Alfarra, M. R., Takami, A., Middlebrook, A. M., Sun, Y. L., Dzepina, K., Dunlea, E., Docherty, K., DeCarlo, P. F., Salcedo, D., Onasch, T., Jayne, J. T., Miyoshi, T., Shimono, A., Hatakeyama, S., Takegawa, N., Kondo, Y., Schneider, J., Drewnick, F., Borrmann, S., Weimer, S., Demerjian, K., Williams, P., Bower, K., Bahreini, R., Cottrell, L., Griffin, R. J., Rautiainen, J., Sun, J. Y., Zhang, Y. M., and Worsnop, D. R.: Ubiquity and dominance of oxygenated species in organic aerosols in anthropogenically-influenced Northern Hemisphere midlatitudes, Geophys Res Lett, 34, 10.1029/2007gl029979, 2007.

Zhao, Y. L., Hennigan, C. J., May, A. A., Tkacik, D. S., de Gouw, J. A., Gilman, J. B., Kuster, W. C., Borbon, A., and Robinson, A. L.: Intermediate-Volatility Organic Compounds: A Large Source of Secondary Organic

Aerosol, Environ Sci Technol, 48, 13743-13750, 10.1021/es5035188, 2014.

Zhu, S. P., Mac Kinnon, M., Shaffer, B. P., Samuelsen, G. S., Brouwer, J., and Dabdub, D.: An uncertainty for clean air: Air quality modeling implications of underestimating VOC emissions in urban inventories, Atmos Environ, 211, 256-267, 10.1016/j.atmosenv.2019.05.019, 2019.

Appendix D

FROM COVID-19 TO FUTURE ELECTRIFICATION: ASSESSING TRAFFIC IMPACTS ON AIR QUALITY BY A MACHINE-LEARNING MODEL

Yang, J., Wen, Y., Wang, Y., Zhang, S., Pinto, J. P., Pennington, E. A., Wang, Z., Wu, Y., Sander, S. P., Jiang, J. H., Hao, J., Yung, Y. L., & Seinfeld, J. H. (2021). From COVID-19 to future electrification: Assessing traffic impacts on air quality by a machine-learning model. *Proceedings of the National Academy of Sciences*, *118*(26). https://doi.org/10.1073/pnas.2102705118.

From COVID-19 to Future Electrification: Assessing Traffic Impacts on Air Quality in a Megacity

Jiani Yang[1], Yifan Wen[2], Yuan Wang[1,3,*], Shaojun Zhang[2,*], Joseph Pinto[4], Elyse A. Pennington[5], Zhou Wang[6], Ye Wu[2], Stanley P. Sander[3], Johnathan H. Jiang[3], Jiming Hao[2], John H. Seinfeld[5], Yuk L. Yung[1,3]

[1]Division of Geological and Planetary Sciences, California Institute of Technology, Pasadena, CA, USA.

[2]School of Environment, Tsinghua University, Beijing, China.

[3]Jet Propulsion Laboratory, California Institute of Technology, Pasadena, CA, USA.

[4]Gillings School of Global Public Health, University of North Carolina at Chapel Hill, NC, USA.

[5]Division of Chemistry and Chemical Engineering, California Institute of Technology, Pasadena, CA, USA.

[6]Department of Geography, University of Mainz, Mainz, Germany.

J.Y. and Y.Wen. contributed equally to this work

*To whom correspondence may be addressed

Email: yuan.wang@caltech.edu, zhsjun@tsinghua.edu.cn

Keywords: COVID-19; Air Pollution; Traffic Emissions; Machine Learning; Vehicular Electrification.

Abstract

The large fluctuations in traffic during the COVID-19 pandemic provide an unparalleled opportunity to assess motor vehicle emission control efficacy. Here we develop a machine-learning (ML) model, based on the large volume of real-time observational data during COVID-19, to predict surface-level NO_2, O_3, and fine particle concentration in the Los Angeles mega-city. Our ML model exhibits high fidelity in reproducing pollutant concentrations in the Los Angeles basin and identifies major factors controlling each species. During the strictest lockdown period, the traffic reduction led to decreases in NO_2 and $PM_{2.5}$ by –27.8% and –17.5%, respectively, but a 6% increase in O_3. Heavy-duty truck emissions contribute primarily to these variations. Future traffic emissions controls are estimated to impose similar effects as observed during the COVID-19 lockdown, but with smaller magnitude. Vehicular electrification will achieve further alleviation of NO_2 levels.

Significance Statement

We capitalize on large variations of urban air quality during the COVID-19 pandemic and real-time observations of traffic, meteorology, and air pollution in Los Angeles to develop a machine-learning air pollution prediction model. Such a novel model can adequately account for the nonlinear relationships between emissions, atmospheric chemistry, and meteorological factors. Moreover, this model enables us to identify the key drivers of air quality variations during the COVID-19 pandemic in a megacity like Los Angeles and assess the effect of future traffic emissions control on air quality. We unambiguously demonstrate that the full benefit from fleet electrification cannot be attained if focused only on mitigation of on-road emissions. To continue to improve air quality in Los Angeles, off-road emissions and those of volatile chemical products need to be more strictly regulated.

Main Text

Introduction

In the urban environment, vehicular traffic is a principal source of air pollutants, including nitrogen oxides (NO_x=NO+NO_2), carbon monoxide (CO), and carbonaceous particles. Secondary ozone (O_3) and particulate matter (PM) have profoundly adverse impacts on human health (1), by inducing dysfunction and deterioration of cardiovascular, respiratory, and immune systems (2). The COVID-19 pandemic led to unprecedented decreases in traffic-related emissions in mega-cities worldwide (3–5). Owing to the short chemical lifetime of NO_x and the pandemic-induced emission changes, the well-defined and abrupt decrease in NO_2 has been captured by satellites as well as ground-based observations (6–8). However, changes in secondary pollutants like O_3 and a major portion of $PM_{2.5}$ (PM with aerodynamic diameters < 2.5 micrometers) during the pandemic were diverse in different regions (7, 9), for which the major drivers remain unclear. Atmospheric chemical reactions serve as essential nonlinear links between emissions and atmospheric composition. Moreover, local meteorological factors, such as air temperature and humidity, also strongly regulate photochemical formation of ozone and multiphase chemistry of secondary PM (6, 9, 10). The response of secondary pollutants to COVID-19 induced emission changes remains poorly understood; existing studies provide limited insight into the consequent chemistry (7). Here, we disentangle the complex factors involving emissions, chemical reactions, pollutant transport, and meteorology to evaluate the effect of pandemic-induced or other dramatic emission changes on air quality.

Los Angeles (LA) has long been one of the most polluted cities in the U.S. (11). Surrounded by mountains on three sides and bounded by the Pacific Ocean, ideal conditions exist for pollutant build-up over the LA Basin and downwind areas (12, 13). Owing to the strict sulfur oxides (SO_x) emission control program established in 1978 and major improvements of motor vehicle engines, SO_2 and black carbon levels have significantly declined (14). However, organic aerosol concentrations, contributing to more than half of $PM_{2.5}$, have not declined as significantly as primary emissions (15, 16). The COVID-19

induced variability of air quality provides an opportunity to evaluate the efficacy of traffic mitigation strategies.

Diesel-powered heavy-duty vehicles (HDVs) and medium-duty vehicles (MDVs) comprise only a modest fraction of the total numbers of the on-road fleet in Los Angeles but disproportionately contribute to a large fraction of overall vehicle emissions (*17*, *18*, *19*). Even with installation of diesel particle filters (DPFs) and selective catalytic reduction (SCR) systems, unusually high emissions of NO_x and lower SCR efficiency are still reported (19). In 2017, The California Air Resources Board (CARB) adopted a series of regulations including reduction of NO_x emissions by 90% for new heavy-duty diesel trucks (20), requiring truck manufacturers to transition from diesel trucks and vans to electric zero-emission trucks beginning in 2024, aiming for an all zero-emission short-haul drayage fleet in ports and railyards by 2035, and zero-emission "last-mile" delivery trucks and vans by 2040 (21). An assessment of the air quality related benefit of the zero-emission delivery truck plan is lacking.

Atmospheric chemical transport models have been widely used to examine the response of air pollutant concentrations to the changes of emissions and meteorological conditions. However, the challenge in preparing high-temporal-resolution emission profiles has limited a long-term, dynamic analysis of the air quality impacts resulting from the abrupt emission changes through the pandemic period. Recent studies have demonstrated the capability of predictive machine learning (ML) models to capture the timing, magnitude, and major factors influencing real-time atmospheric responses to emission control measures (22–24). Compared with traditional chemical transport modeling, the ML technique has more flexibility in leveraging real-world data and possesses higher computational efficiency. Here, real-time data including traffic information from the California Department of Transportation (Caltrans) and in situ pollutant concentrations and surface level meteorology from the California Air Resources Board (CARB), population density and points of interest (physical location of compressed natural gas stations, power plants, landfills etc.) at the city level are used with a machine learning framework to develop a model that can directly link atmospheric composition with societal factors (Methods). We use this model to assess the sensitivity of NO_2, O_3 and $PM_{2.5}$ in the Los Angeles Basin to traffic emission changes at different stages of the COVID-19 lockdown by comparing predicted concentration levels

under different traffic emission scenarios. Moreover, by considering future climate changes and traffic emissions, we assess the possible benefits of future traffic evolution, including vehicular electrification, in 2035 and 2050 (SI Appendix, Fig. S1).

Results

Identifying Key Factors Using ML Models

Machine-learned geostatistical models are developed here to predict the concentrations of three major pollutants: NO_2, O_3 and, $PM_{2.5}$ in the Los Angeles basin, using traffic information, meteorological conditions, and other socio-economic factors as inputs (SI Appendix, Fig. S1). The models account for the nonlinear relationships among traffic emissions, atmospheric chemistry, and meteorological conditions. Additional model descriptions can be found in the Method and SI Appendix. To evaluate the performance of the ML models, a commonly used 5-fold cross validation method is used. As shown in Figure 1, the models exhibit high fidelity in reproducing the observed NO_2 and O_3 concentrations, with coefficients of determination (R^2) of 0.91 and 0.87, respectively. The root-mean-square error (RMSE) of the predicted NO_2 and O_3 concentrations are 3.0 and 5.1 ppb, respectively. The predicted $PM_{2.5}$ concentrations also show reasonable agreement with the ground-based observations, but with a smaller R^2 of 0.65. An underestimation of $PM_{2.5}$ starts to emerge when the $PM_{2.5}$ concentrations exceed 20 $\mu g/m^3$ corresponding to the 90th percentile in the $PM_{2.5}$ probability distribution function over LA. It is noted that ML models tend to have larger biases in predicting the extreme values due to fewer training data samples (25).

An important output of the ML model is a ranking of the relative importance of all input parameters. For NO_2, the three major governing factors are wind direction, non-truck VMT, and relative humidity (RH). The prominent rank of wind direction reflects the prevailing role of northwesterly and onshore winds in determining the spatially variable flow of pollutants received in the LA basin (26). The concentration of NO_2 which is a short-lived species closely follows that of the traffic emission patterns. The high correlation between NO_2 and RH is partly a result of their individual diurnal cycles, in which NO_2 peaks in the afternoon while RH peaks at night. In contrast to NO_2, ozone variations are largely regulated by meteorological conditions. Moreover, the top 7 factors are all

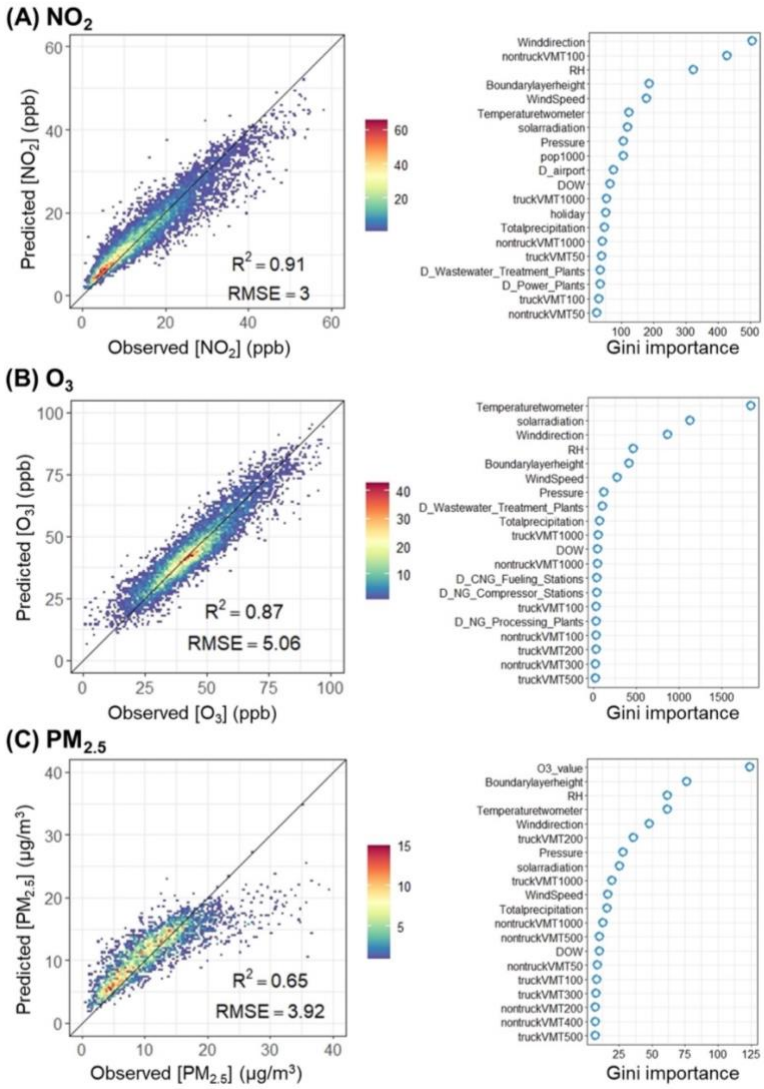

Figure 1. Model performance and variable importance for three species. (A) NO_2, (B) O_3 and (C) $PM_{2.5}$. Cross-validated model R^2 and root mean squared error (RMSE) are calculated by using a 5-fold cross-validation modeling performance for 24-h average concentrations. The color indicates the sample size for each dot. The variables are listed in order of importance from top to bottom. The horizontal axis represents the Gini index from the Random Forest model. A larger value represents higher importance. The definitions of all predictors are provided in Table S2.

meteorology related. Among them, the near-surface temperature (T_{2m}) exerts the largest influence through the photochemical reactions to form ozone (27) and biogenic volatile organic compound (VOC) emission rates (28). Solar irradiance is a limiting factor that influences ozone-related photochemistry. For $PM_{2.5}$ prediction, ozone ranks as the most prominent, indicating the secondary source of aerosols in LA. Boundary layer height is the most relevant meteorological factor with $PM_{2.5}$ in the Gini importance ranking (see Methods in SI Appendix), followed by RH, T_{2m}, and wind direction. Such a ranking of meteorological influence on $PM_{2.5}$ in Los Angeles is consistent with current understanding (9). Notably, a recent study on eight-year ground-based observations in Beijing, China showed the same importance ranking of meteorological factors (29). By using the points of interest (SI Appendix, Fig. S2) in the ML model, the influence of spatial contribution from crucial industrial locations (e.g., airport, wastewater treatment plants, power plants, natural gas compressor stations) on air quality is identified. The model-predicted importance of airport emissions for NO_2 corroborates that air quality impacts of major airports need to be addressed for emission control (30). Volatile consumer and industrial chemical products are estimated to be a significant source of reactive VOCs and SOA formation in the LA Basin (31). To test the importance of different predictors on a time scale longer than hours, we rebuild the ML models using the daily means of the input data. The results from those models show the generally similar ranking of predictors. The daily mean models retain 80%, 100%, and 80% of the top 5 most important predictors for NO_2, O_3, and $PM_{2.5}$, respectively, compared with the hourly models (SI Appendix, Fig. S3).

Role of Traffic Emission during COVID-19

During the COVID-19 pandemic, traffic was abruptly reduced in late March and early April, and then gradually recovered to the pre-COVID-19 level (SI Appendix, Fig. S4). The time series of NO_2 generally followed the temporal variation of traffic in LA during the COVID-19 period. O_3 and $PM_{2.5}$ concentrations remained at a relatively low level in March and early April due to rainy and windy weather conditions. We compare the observations and the ML model predictions with COVID-19 meteorology and pre-COVID-19 traffic information from on-road sensors (VMT, automobile type, etc.), to assess the influence of the COVID-19 induced traffic emission reductions (Figure 2A). During the strictest lockdown period (6 April - 12 April), traffic reduction led to decreases in NO_2 and $PM_{2.5}$ by

2.6 ppb and 1.1 $\mu g/m^3$, corresponding to fractional changes of –27.8% and –17.5%, respectively. In the later recovery period (08 May - 30 June), the all-traffic induced fractional changes of NO_2 and $PM_{2.5}$ decrease to –17.0% and –6.0%, respectively. The traffic impacts on ozone differ from those of NO_2 and $PM_{2.5}$. A 2.1 ppb (6.0%) increase in maximum daily 8-h average (MDA8) O_3 by all traffic occurred during the strictest lockdown period. This is a result of the fact that ozone production in LA is in the NO_x-saturated/VOC-limited regime under the traffic-as-usual scenario. Excessive NO_x can serve as a sink for OH radicals thus retarding the oxidation of VOC, sequestering ozone, or suppressing its production (7). We further differentiate the impacts from truck and non-truck vehicles by altering only the on-road truck activities according to the observations from different time periods (Figure 2B). During the strictest lockdown period, truck emission reductions account for 61.0%, 79.4%, and 70.4% of all-traffic induced changes in NO_2, MDA8 O_3, and $PM_{2.5}$, respectively. This result reinforces the fact that diesel trucks are a major source in the entire traffic sector.

To build a direct linkage between pollutant concentrations and traffic activity, we also develop an emulator for each species based on our ML model results. The emulator can predict the relative changes of emissions as a function of the fractional changes in truck and non-truck VMT relative to the year 2019 level. NO_2 monotonically decreases along with the reduction in either truck or non-truck VMT (Figure 3A). The reduction slope is steeper for trucks, indicating the larger emission factor of NO_x for diesel engines. MDA8 O_3 generally increases with the reduction of truck traffic in a monotonic manner (Figure 3B), while an overall decrease in MDA8 O_3 is found for the reduction of non-trucks. The distinctive impacts on ozone are likely explained by the fact that diesel trucks emit higher levels of NO_x than non-trucks (32), but they share the similar non-methane VOC emission factor (33, 34). Therefore, truck and non-truck emissions fall in NO_x-saturated and NO_x-limited regimes, respectively. This is also consistent with larger NO_2 susceptibility to reductions of truck than non-truck emissions. The $PM_{2.5}$ linkage with traffic is more complicated, especially with regard to non-truck emissions. In contrast with the monotonic decrease of $PM_{2.5}$ in response to the reduction in truck VMT, the bended-curve (Figure 3C)

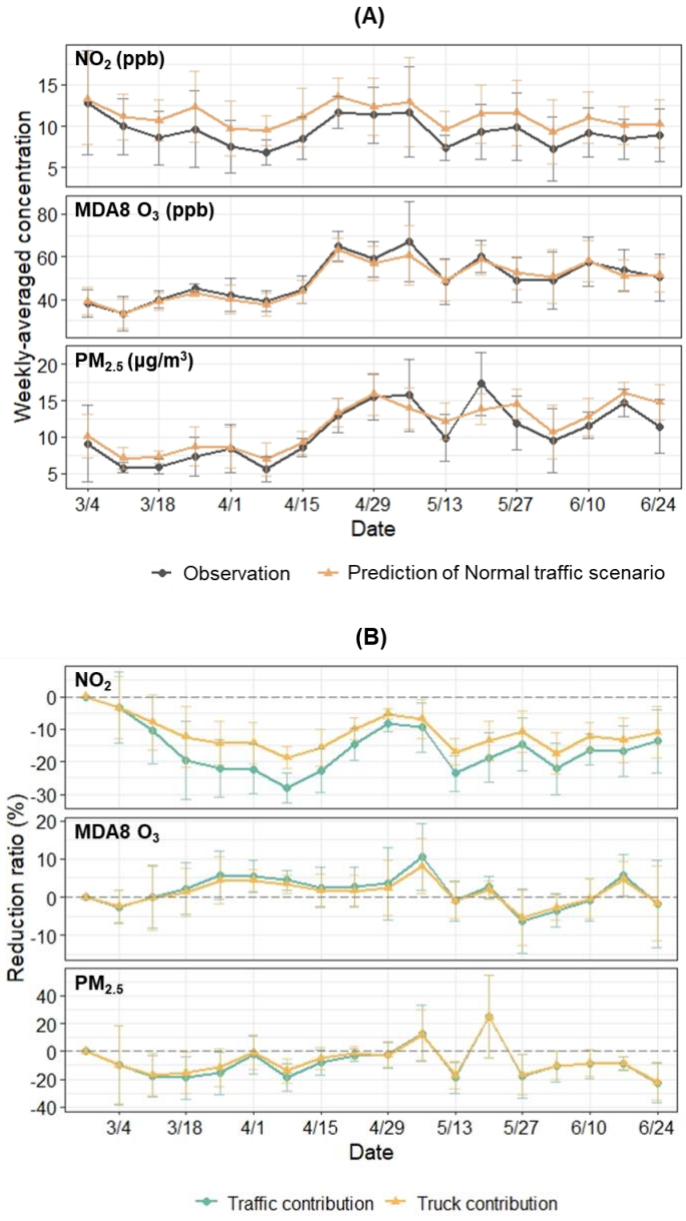

Figure 2. Comparison of observations and predictions. (A) Comparison of observations and predictions of normal traffic scenario and (B) the impact of traffic reduction from total fleet and truck fleet on NO_2, O_3 and $PM_{2.5}$ concentrations during the lockdown period of the COVID-19 pandemic in Los Angeles. Each data point represents a weekly mean. The error bars are standard deviations for daily results in each week.

response of $PM_{2.5}$ is found along with the non-truck VMT reduction. Similar to MDA8 O_3, the overall magnitude of fluctuation of $PM_{2.5}$ is also smaller for non-truck (less than 0.1 $\mu g/m^3$) than that for truck. In general, regulation of trucks can be a more efficient way to lower $PM_{2.5}$ concentration than other vehicles.

Air quality benefit for future on-road traffic decarbonization

The Paris Agreement aims to increase the percentage of zero emission vehicles to 25% by 2025, 80% by 2035, and 100% by 2050. Under the "Green New Deal" (GND), Los Angeles would build a clean and reliable power grid to empower the next generation of green transportation. The baseline future traffic emission changes are provided by the 2017 version of EMission FACtor (EMFAC), a model that estimates the official emission inventories of on-road mobile sources in California from 2000 to 2050 (35). Here we introduce three degrees of fleet electrification (also including other zero-emission vehicles like hydrogen fuel cell vehicles) based on the EMFAC emission inventories (SI Appendix, Methods and Table S1). All the fractional changes in the truck or non-truck vehicles for the future scenarios are within their ranges in our ML training dataset, i.e. hourly observations during 2019 and 2020.

The EMFAC model assumes that non-truck emissions will decrease by 54% in 2035 and 58% in 2050 as compared with 2019 (SI Appendix, Fig. S5). For truck emissions, CARB recently estimated that the low-NO_x omnibus regulation would lead to 29% of NO_x emission reduction in 2050 as compared with the original EMFAC results, which have been used as the baseline truck emissions without additional electrification (36). On the other hand, the EMFAC inventories assume greater truck activity caused by increases in intensity of consumer goods delivery in 2050 than 2035. Therefore, compared to 2019, truck emissions would have comparable decreasing ratios in 2035 (by 55%) and 2050 (by 54%). The impacts of the future traffic emission reduction are pronounced: compared to 2019, NO_2 would be reduced by 11.0% ± 1.2% in 2035 and 11.8% ± 0.8% in 2050, and $PM_{2.5}$ would be reduced by 3.1% ± 0.4% in 2035 and 2.9% ± 0.4% in 2050 (Figure 4 A and F). Similar to its behavior during the lockdown period of COVID-19, MDA8 O_3 is predicted to exhibit a reverse trend with a 0.6% ± 0.4% increase in 2035 and a 0.4% ± 0.3% increase in 2050. Of note, the reduction ratios of NO_2 and $PM_{2.5}$ concentrations increase

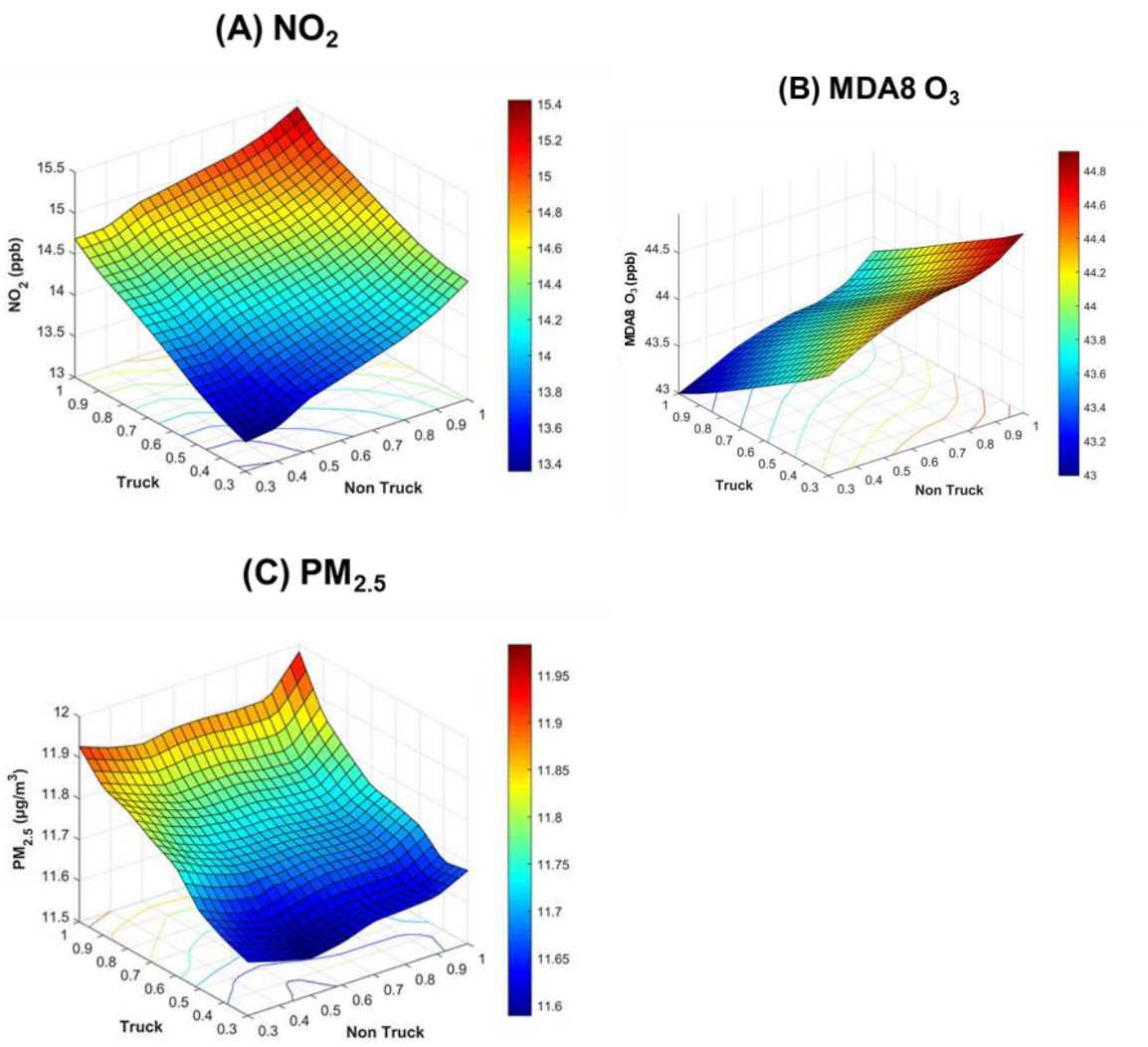

Figure 3. Predicted annual-average concentrations. (A to **C)** Distribution of (A) NO_2, (B) MDA8 O_3 and (C) $PM_{2.5}$ with different combinations of non-truck and truck activity fractional changes relative to the annual average level of 2019.

significantly from 2020 to 2035 due to the efficient reduction of traffic emissions, while the reductions slow down and even slightly rebound from 2035 to 2050 with the relatively limited emission reductions (SI Appendix, Fig. S6).

To further assess the impacts of fleet electrification on air quality, we alter independently electrification rates of total fleet mileage from the remaining parameters in EMFAC. Three scenarios are assessed here, representing moderate to aggressive electrification rates (SI Appendix, Table S1 and Fig. S7). Our first electrification scenario

(E1) assumes moderate electrification rates, i.e., 10% and 5% for non-trucks and trucks in 2035. The 2035 electrification rate of the truck fleet is close to the Advanced-Clean-Trucks regulation benefit estimated by CARB, because more than 60% of Class 8 trucks operating in California are registered as out-of-state vehicles that will not be mandatory to be electrified according to current federal plans (36). In 2035, as compared with 2019, E1 corresponds to emission reduction rates of 57% for non-truck and 57% for truck. In 2050, the electrification rates of E1 are 20% for non-truck and 10% for truck, corresponding to emission reduction rates of 65% for non-truck and 59% for truck. As shown in Fig. 4B, G, the ML model predicts that NO_2 will decrease by 12.0 % ± 1.0% in 2035 and 12.9% ± 0.6% in 2050 under E1. Also, $PM_{2.5}$ will drop by 3.0% ± 0.3% in 2035 and 2.9% ± 0.4% in 2050. MDA8 O_3 is predicted to increase by 0.6% ± 0.4% in 2035 and 0.4% ± 0.3% in 2050. The other two future scenarios (E2 and E3) are more aggressive in electrifying vehicles than E1. Therefore, the magnitudes of the NO_2 reduction are enlarged in E2 and E3, and the reduction ratio achieves 17.9% ± 1.1% in 2050 under E3 with the most aggressive electrification ratios (i.e., 80% for non-trucks, which is close to the estimated electrification rate from California's Advanced Clean Cars program (37), and 40% for trucks). The increasing ratio of MDA8 O_3 shrinks with higher electrification rates in both 2035 and 2050 (Figure 4 H and I). Such a change in MDA8 O_3 reveals that Los Angeles would be evolving to less NO_x-saturated conditions with further reduction of NO_X. However, $PM_{2.5}$ levels are less sensitive to progressive electrification. One possible reason is the unbalanced emission reduction in truck and non-truck fleets for future electrification. According to Figure 3, $PM_{2.5}$ is more sensitive to trucks than non-trucks. The relative higher emission contribution of trucks in the total fleet from E1 to E3 may explain the decrease in $PM_{2.5}$ reduction.

Future regional climate change on LA air quality

The effect of climate change on meteorological conditions is a key factor in modulating urban pollution. The responses of different pollutants to four key meteorological variables are probed here via idealized perturbation experiments (SI Appendix, Fig. S8). The model shows that $PM_{2.5}$ is enhanced by RH via the promotion of heterogeneous chemistry to form secondary aerosols in aerosol water (9) , while NO_2 and O_3 concentrations tend to be lower with larger RH. Increasing photochemistry via solar radiance tends to increase $PM_{2.5}$ and O_3 at the expense of NO_2. Both NO_2 and $PM_{2.5}$ concentrations are elevated by a lower

boundary layer height. O_3 shows the opposite responses due to concurrent O_3 titration and lower boundary layer height at nighttime. Higher surface temperature fosters ozone production and further promotes secondary aerosol formation.

Additional model predictions were performed to assess the impacts of future regional climate change on air quality in Los Angeles. Future meteorological variables near 2035 and 2050 are projected from the multi-model ensemble simulations of the Climate Model Inter-comparison Project Phase 6 (CMIP6, see Method in SI Appendix and Fig.S9), while the same traffic level as 2019 will be adopted. Our ML models predict that annual-average concentrations of NO_2 and MDA8 O_3 will decrease while $PM_{2.5}$ will increase at different rates around 2035 and 2050 (Figure 4 E and J). The different changing trends for three pollutants are possibly dominated by increasing relative humidity, according to the responses of different pollutants to key meteorological variables (SI Appendix, Fig. S8). The rates of change for the three species in 2050 are not in proportion with the changes in 2035, reflecting the highly nonlinear climate change over a few decades. Future climate changes are estimated to exert a higher influence on O_3 and $PM_{2.5}$ concentrations than traffic amount and type in 2035, demonstrating the impacts of meteorology on these two species. This result is consistent with the ranking of variable importance in the ML models (Figure 1). The uncertainty of future climate change is estimated by the spread among different CMIP6 models and different ensemble members.

In summary, we leverage the unprecedented large variations of road traffic spanning a few months in Los Angeles during the COVID-19 pandemic to probe the impacts of future decarbonization policies. A machine-learning model is developed for Los Angeles to predict NO_2, O_3, and $PM_{2.5}$ concentrations based on real-time traffic data and meteorological measurements. Capitalizing on the high fidelity and computing efficiency of this predictive ML model, we demonstrate the significant contribution of traffic, especially from heavy-duty trucks, to pollutant variations in the first few months of the COVID-19 pandemic. Future decarbonization policies are estimated to impose similar effects on air quality as COVID-19, but with smaller magnitude. Large-scale fleet

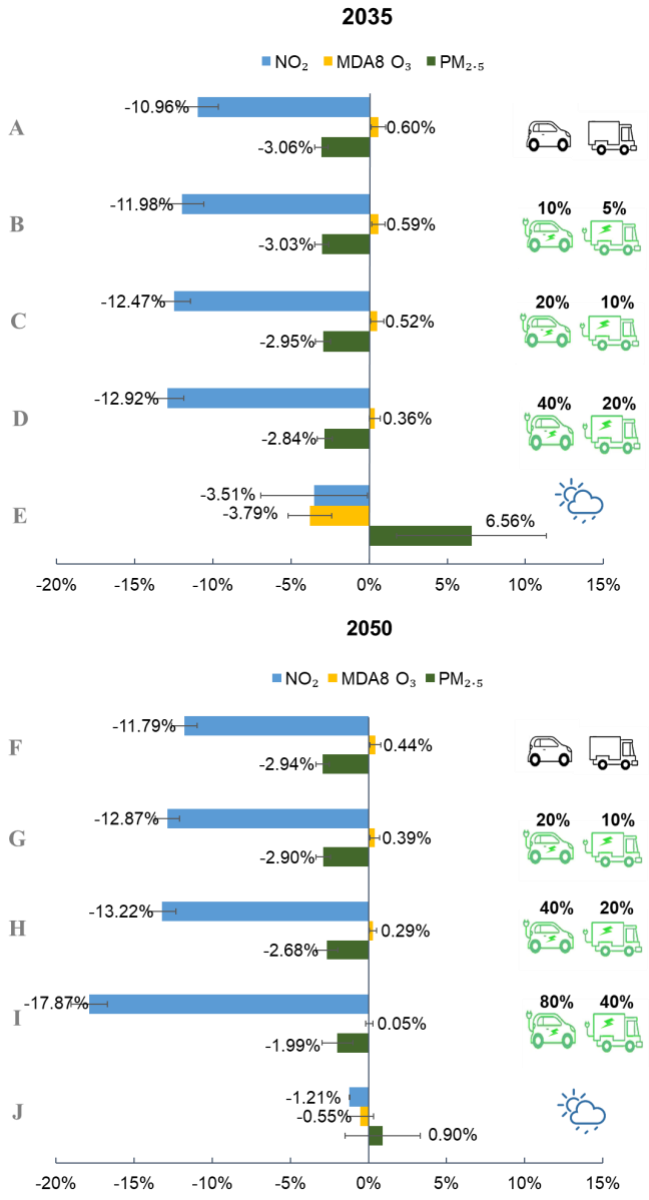

Figure 4. Reduction ratios of NO_2, MDA8 O_3 and $PM_{2.5}$ concentrations under different traffic scenarios in 2035 and 2050 relative to 2019. (A-E) and (F-J) represents baseline traffic emission scenario from EMFAC, three electrification scenarios and future climate change scenario in 2035 and 2050, respectively. The error bars represent uncertainty of model predictions calculated by the Monte Carlo method. Random sampling was repeated for 100 times considering uncertainty of each variable in prediction of each scenario.

electrification will achieve further alleviation of NO_2 levels and is likely to transition Los Angeles to a less NO_x-saturated regime of O_3 formation. However, the benefit from fleet electrification on $PM_{2.5}$ may be not attained if focused only on mitigation of on-road emissions. Moreover, emission standards of out-of-state vehicles should be aligned with those of the local fleet under federal efforts, and off-road emissions and those of volatile chemical products need to be more strictly regulated.

Methods

A supervised ML algorithm, the random forest model, is employed to account for the nonlinear interactions between different input parameters without specifying any form of their relationships. Hourly data over 1.5 years (01/2019 - 06/2020) serve as input to the model. Key input parameters include processed traffic activity (truck/non-truck vehicle miles traveled, short as VMT), meteorology (wind speed/direction, near-surface temperature, boundary layer height, precipitation, solar radiation, pressure, relative humidity), temporal information (day of the week, holiday), population density, distance to nearby points of interest (POI), etc. Complete information can be found in the Supplementary Material. A wide range of temporal variability is explicitly considered, from diurnal, daily, weekly, to seasonal timescales. The hourly temporal resolution of the training data is sufficiently high to capture the lifetimes of the three targeted species. The predictive capability is separately developed at 11 sites for $PM_{2.5}$, 18 sites for O_3, and 22 sites for NO_2, covering the populous urban areas in the LA basin (SI Appendix, Fig. S2). Additional data description and experiment designs can be found in SI Appendix.

Acknowledgments: Y.W., S.P.S., J.H.J. and Y.L.Y. acknowledge the support by the Jet Propulsion Laboratory, California Institute of Technology, under contract with NASA. S.Z acknowledges the support by the National Key Research and Development Program of China (grant 2017YFC0212100) and the National Natural Science Foundation of China (grant 41977180). We thank Leo Gallagher and Daniel Kitowski at the California Department of Transportation, Thomas E. Morrell at the Caltech Library, Jin Tao for helpful information of data inputs and Yu Zhou at Tsinghua University for useful discussions.

Author Contributions: J.Y., Y.Wang, and S.Z. designed the research. J.Y. conducted the observational data mining, processing, and analysis. Y.Wen, S.Z., and J.Y. developed the

ML model. Y.Wang led the manuscript writing. All authors discussed the results and contributed to the manuscript writing.

Competing Interest Statement: The authors declare no competing interest.

References

Near-road air pollutant concentrations of CO and PM2.5: A comparison of MOBILE6.2/CALINE4 and generalized additive models (November 8, 2019).

D. Liang, *et al.*, Urban Air Pollution May Enhance COVID-19 Case-Fatality and Mortality Rates in the United States. *Innovation* **1** (2020).

F. Pomponi, J. Hart, J. H. Arehart, B. D'Amico, Buildings as a Global Carbon Sink? A Reality Check on Feasibility Limits. *One Earth* **3**, 157–161 (2020).

Z. Liu, *et al.*, Near-real-time monitoring of global CO 2 emissions reveals the effects of the COVID-19 pandemic. *Nature Communications* **11**, 5172 (2020).

C. Le Quéré, *et al.*, Temporary reduction in daily global CO 2 emissions during the COVID-19 forced confinement. *Nature Climate Change* **10**, 647–653 (2020).

M. Bauwens, *et al.*, Impact of Coronavirus Outbreak on NO2 Pollution Assessed Using TROPOMI and OMI Observations. *Geophysical Research Letters* **47**, e2020GL087978 (2020).

J. H. Kroll, *et al.*, The complex chemical effects of COVID-19 shutdowns on air quality. *Nature Chemistry* **12**, 777–779 (2020).

F. Liu, *et al.*, Abrupt decline in tropospheric nitrogen dioxide over China after the outbreak of COVID-19. *Science Advances* **6**, eabc2992 (2020).

T. Le, *et al.*, Unexpected air pollution with marked emission reductions during the COVID-19 outbreak in China. *Science* **369**, 702–706 (2020).

Y. Zhao, *et al.*, Substantial Changes in Nitrogen Dioxide and Ozone after Excluding Meteorological Impacts during the COVID-19 Outbreak in Mainland China. *Environ. Sci. Technol. Lett.* **7**, 402–408 (2020).

R. Gottlieb, M. Vallianatos, R. Freer, P. Dreier, *The Next Los Angeles: The Struggle for a Livable City* (University of California Press, 2006).

K. W. Wong, *et al.*, Mapping CH_4 : CO_2 ratios in Los Angeles with CLARS-FTS from Mount Wilson, California. *Atmos. Chem. Phys.* **15**, 241–252 (2015).

D. Wunch, P. O. Wennberg, G. C. Toon, G. Keppel-Aleks, Y. G. Yavin, Emissions of greenhouse gases from a North American megacity: GREENHOUSE GAS EMISSIONS IN LA. *Geophys. Res. Lett.* **36**, n/a-n/a (2009).

S. Sonwani, P. Saxena, Identifying the Sources of Primary Air Pollutants and their Impact on Environmental Health: A Review. **6**, 20 (2016).

C. S. Christoforou, L. G. Salmon, M. P. Hannigan, P. A. Solomon, G. R. Cass, Trends in Fine Particle Concentration and Chemical Composition in Southern California. *Journal of the Air & Waste Management Association* **50**, 43–53 (2000).

A. C. Lloyd, T. A. Cackette, Diesel Engines: Environmental Impact and Control. *Journal of the Air & Waste Management Association* **51**, 809–847 (2001).

M. J. Haugen, G. A. Bishop, A. Thiruvengadam, D. K. Carder, Evaluation of Heavy- and Medium-Duty On-Road Vehicle Emissions in California's South Coast Air Basin. *Environ. Sci. Technol.* **52**, 13298–13305 (2018).

M. Kelp, *et al.*, Sensitivity analysis of area-wide, mobile source emission factors to high-emitter vehicles in Los Angeles. *Atmospheric Environment* **223**, 117212 (2020).

C. V. Preble, R. A. Harley, T. W. Kirchstetter, Control Technology-Driven Changes to In-Use Heavy-Duty Diesel Truck Emissions of Nitrogenous Species and Related Environmental Impacts. *Environ. Sci. Technol.* **53**, 14568–14576 (2019).

Heavy-Duty Omnibus Regulation | California Air Resources Board (January 4, 2021).

California takes bold step to reduce truck pollution | California Air Resources Board (October 27, 2020).

Y. Wang, *et al.*, Four-Month Changes in Air Quality during and after the COVID-19 Lockdown in Six Megacities in China. *Environ. Sci. Technol. Lett.* **7**, 802–808 (2020).

S. K. Grange, *et al.*, COVID-19 lockdowns highlight a risk of increasing ozone pollution in European urban areas. *Atmospheric Chemistry and Physics Discussions*, 1–25 (2020).

M. Lovrić, *et al.*, Understanding the true effects of the COVID-19 lockdown on air pollution by means of machine learning. *Environmental Pollution*, 115900 (2020).

M. C. Robinson, R. C. Glen, A. A. Lee, Validating the validation: reanalyzing a large-scale comparison of deep learning and machine learning models for bioactivity prediction. *J Comput Aided Mol Des* **34**, 717–730 (2020).

C. K. Wong, *et al.*, Monthly trends of methane emissions in Los Angeles from 2011 to 2015inferred by CLARS-FTS observations. *Atmos. Chem. Phys.* **16**, 13121–13130 (2016).

H. A. Parker, S. Hasheminassab, J. D. Crounse, C. M. Roehl, P. O. Wennberg, Impacts of Traffic Reductions Associated With COVID-19 on Southern California Air Quality. *Geophysical Research Letters* **47**, e2020GL090164 (2020).

S. E. Pusede, *et al.*, On the temperature dependence of organic reactivity, nitrogen oxides, ozone production, and the impact of emission controls in San Joaquin Valley, California. *Atmospheric Chemistry and Physics* **14**, 3373–3395 (2014).

T. Su, Z. Li, Y. Zheng, Q. Luan, J. Guo, Abnormally Shallow Boundary Layer Associated With Severe Air Pollution During the COVID-19 Lockdown in China. *Geophysical Research Letters* **47**, e2020GL090041 (2020).

N. Hudda, T. Gould, K. Hartin, T. V. Larson, S. A. Fruin, Emissions from an International Airport Increase Particle Number Concentrations 4-fold at 10 km Downwind. *Environ. Sci. Technol.* **48**, 6628–6635 (2014).

B. C. McDonald, *et al.*, Volatile chemical products emerging as largest petrochemical source of urban organic emissions. *Science* **359**, 760–764 (2018).

R. O'Driscoll, M. E. J. Stettler, N. Molden, T. Oxley, H. M. ApSimon, Real world CO2 and NOx emissions from 149 Euro 5 and 6 diesel, gasoline and hybrid passenger cars. *Sci Total Environ* **621**, 282–290 (2018).

B. C. McDonald, D. R. Gentner, A. H. Goldstein, R. A. Harley, Long-Term Trends in Motor Vehicle Emissions in U.S. Urban Areas. *Environ. Sci. Technol.* **47**, 10022–10031 (2013).

U. E. N. C. for E. Assessment, Gas- and particle-phase primary emissions from in-use, on-road gasoline and diesel vehicles (2009) (December 29, 2020).

P. Samson, EMFAC2017 Volume III Technical Documentation V1.0.2 July 20, 2018. 253.

Appendix D - Emissions Inventory Methods and Results for the Proposed Amendments. 20 (2020).

Vision Scenario Planning | California Air Resources Board (January 4, 2021).